THE DEVELOPMENT OF WOUND-ON-TENSION

IN WEBS WOUND INTO ROLLS

By

BALAJI KOVIL KANDADAI

Bachelor of Engineering in Mechanical Engineering
University of Madras
Chennai, Tamilnadu, India
1999

Master of Science in Mechanical Engineering
Oklahoma State University
Stillwater, Oklahoma
2001

Submitted to the Faculty of the
Graduate College of the
Oklahoma State University
in partial fulfillment of
the requirements for
the Degree of
DOCTOR OF PHILOSOPHY
December, 2006

THE DEVELOPMENT OF WOUND-ON-TENSION

IN WEBS WOUND INTO ROLLS

Dissertation Approved:

<div style="text-align:center;">

Dr. J. K. Good
Dissertation Advisor

Dr. G. S. Gipson

Dr. C. E. Price

Dr. H. Lu

Dr. A. Gordon Emslie
Dean of the Graduate College

</div>

Acknowledgements

My stay in Stillwater, Oklahoma for the past seven years has been fruitful for me for I have successfully accomplished what I came to Stillwater for in the first place; an advanced degree in engineering. During these years, many people have provided inspiration, ideas, assistance, and support and I am obliged to thank all of them.

Firstly, I express sincere thanks and appreciation to my advisor Dr. J. K. Good. He has been a great source of inspiration for me and I am thankful for his guidance, moral and financial support and more importantly, his friendship. There have been times when disappointment and frustration were the order of the day. During those times, if not for his patience, constant encouragement and measured criticism, this thesis would not have been completed. For that I am forever thankful to him.

Secondly, I would like to thank my thesis committee for their suggestions and help. During the coursework I undertook under every one of them, I had the opportunity to learn some interesting engineering fundamentals. For that I am thankful to each one of them.

Thirdly, I would like to extend my special appreciation to Mr. Ron Markum for his help during experimental studies and for his friendship. I would like to thank Joe

Beisel, Paul Hoffecker, Cagri Mollamahmutoglu and Angela Welch for their friendship and for all the interesting group discussions we have had. I would also like to thank the sponsors of the WHRC and the school of Mechanical and Aerospace Engineering, OSU.

Finally, I thank my parents, my brother and sister for their constant love, support and guidance.

I sincerely hope that this research will be useful to someone else.

<div align="right">

Balaji Kovil Kandadai
Stillwater, Oklahoma, July 2006.

</div>

Table of Contents

Table of Figures

Nomenclature

a	half-width of contact or inner radius or acceleration (context)
a^n	acceleration at time step 'n'
$A(t)$	loading amplitude as a function of time
A_s, A_f	starting, final amplitude values
b	composite layer thickness or outer radius (context)
b_1, b_2	linear, quadratic bulk viscosity coefficients
c_d	dilatational wave speed
CW, SW	center, surface winding
dr, dV, dS	incremental radius, volume, surface integral
d^n	displacements at time step 'n'
E_1, E_2, E_3	modulus of the web in 1, 2, 3 directions respectively
E, E_c	Young's modulus, modulus of the core
E_k	kinetic energy
E_{layer}, E_{nip}	modulus of the layer, nip roller respectively
EMD	machine direction modulus of the web
E_r, E^*, E_t	radial, equivalent, tangential modulus of the web
$f^T, f^{ext}, f^{int}, F_{ext}, F_{int}$	body, external, internal, external, internal forces
G_{12}, G_{13}, G_{23}	shear modulus in 12, 13, 23 directions respectively
g^2	nonlinearity factor in Hakiel's model
g_I	boundary conditions
h	web thickness (caliper)
I	integer
K_1, K_2	constants in Pfeiffer's equation (Eqn 5.9)
L^e, L_{min}	element length, smallest element dimension
m, M	mass
MD, CMD, ZD	machine direction, cross machine direction, thickness direction
n, n_c, N	integer, number of boundary conditions, nip load
N_s, N_f	start, final nip load
NIT	nip-induced-tension
P	nip load per unit width
$p(x)$	normal pressure
P_i, P_o	internal, external pressure
p_l, p_q	linear, bulk viscosity
P_θ	circumferential load
q	tangential traction
Q	integrated net traction (a.k.a total traction)
q_{Top}	tangential traction in the top surface of a given layer
q_{Bot}	tangential traction in the bottom surface of a given layer

q_{Net}	net traction in a given layer obtained as a sum of q_{Top} and q_{Bot}
r, R, R^*	radius, equivalent radius
$s, \acute{s}_x$	radial location (or) surface, micro-slip velocity
t^T	traction forces
T_1, T_2	tension upstream, downstream of the roller
$T_{cap}(x)$	torque capacity
T_{in}, T_{out}	incoming, outgoing web tension (upstream, downstream of nip)
t, t_s, t_f	time or thickness (context), start, final step time
T_s, T_f	start, final tension
T_w	web tension
$u_2, \ddot{u}$	displacement in '2' direction, acceleration
v, v_i	volume or velocity (context), velocity at time t_i
v_{x1}, v_{x2}	surface velocities at contacting points
$v_{i\text{-}j}$	surface velocity (i-layer number, j-surface (1-top, 2-bottom))
v^n	velocities at time step 'n'
V_1, V_2	velocity upstream, downstream of the nip roller
V_d	drum/nip roller velocity
V_s, V_f	start, final velocity
W_{ext}, W_{int}	total external, internal energies respectively
WOT	wound-on-tension
x	co-ordinate location along x-axis
δ	indentation depth
$\delta P, \delta v$	incremental pressure, measure of strain
$\delta\sigma_r$	incremental radial stress
Δt	stable time increment
ε_0	small constant
$\varepsilon_{11}, \varepsilon_{22}, \varepsilon_{33}$	web normal strain in 1, 2, 3 directions respectively
ε_{vol}	volumetric strain
γ	slip
$\gamma_{12}, \gamma_{13}, \gamma_{23}$	web shear strain in 12, 13, 23 directions respectively
λ	Lame's constants
μ, μ_k	coefficient of friction, kinetic coefficient of friction
$\mu_{k\ base/web}$	web/base kinetic coefficient of friction
$\mu_{k\ w/r}, \mu_{k\ nip/web}$	web/roller kinetic coefficient of friction
$\mu_{k\ w/w}, \mu_{k\ web/web}$	web/web kinetic coefficient of friction
$\nu, \nu_{12}, \nu_{13}, \nu_{23}$	Poisson's ratio, Poisson's ratio in 12, 13, 23 directions respectively
$\nu_{r\theta}, \nu_{\theta r}$	Poisson's ratio in rθ, θr directions respectively
ρ	web density
$\sigma, \sigma(x)$	stress, machine direction stress as a function of x
$\sigma_{11}, \sigma_{22}, \sigma_{33}$	web normal stress in 1, 2, 3 directions respectively
τ_{crit}	critical shear stress
σ_r, σ_t (or σ_θ)	radial, tangential (or circumferential) stress
$\tau_{12}, \tau_{13}, \tau_{23}$	web shear stress in 12, 13, 23 directions respectively
θ	wrap angle
$\xi(t)$	incremental time function
ω_{max}	maximum frequency of a stress wave

1 Introduction

The wound roll is a convenient form of storage for web materials. A web is material usually made in a continuous process. The length and width of a web is many times greater than its thickness. Webs are wound into rolls using winders. Winders are typically classified into single drum, multiple drum and belt-reel winders and in this dissertation, the focus will be on single drum winders. Different types of single drum winders fall into the following categories:

- Center winders

- Center winders with an undriven nip (rider or drum) roller

- Surface winders

- Differential torque winders (surface winders with center torque assist)

The main difference between the different types of single drum winders lies in how the torque is applied to the nip roller and/or the core during the winding process. A schematic of the different types of single drum winders is shown in Fig. 1.1. In center winders, winding is accomplished by providing torque to the core. An undriven nip roller may be employed in cases where air entrainment is an issue or tighter rolls need to be wound. In surface winders, the driven nip roller transmits torque to the winding roll due to the contact pressure and the friction between the nip roller and the winding roll.

Differential torque winders are similar to surface winders, but with additional torque provided at the core. Thus most of the winders use an impinged nip roller for some purpose.
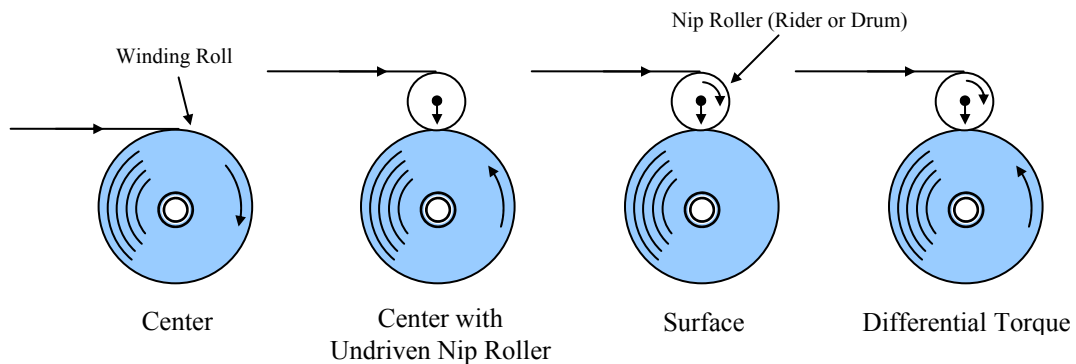
Figure 1.1: Types of Single Drum Winders.

Whatever may be the form of the winder employed, if the incoming web upstream of the winder is free of wrinkles, the wound roll structure, in many cases, determines the quality of the roll. The wound roll structure is a term that describes the finished state of a wound roll of web. Macroscopically, the roll appears to be a homogenous structural cylinder.   At the microscopic level, the roll is comprised of many layers (often thousands). The internal stresses which resulted from winding are responsible for giving the roll some integrity as a wound roll structure. The integrity of the wound roll must be sufficient to prevent defects during winding, transport, and subsequent unwinding operations.

Wound roll models (for example [1]) which predict the internal wound roll stresses have been developed ranging from linear models considering isotropic and

orthotropic webs to non-linear models involving orthotropic state dependent webs. The early models all focused on center winders where it was assumed that the tension in the web upstream of the winder was equal to the tension in the outer layer of the winding roll. These earlier models did not account for the effect of nip load on the tension in the outer layer of a winding roll. This effect of nip is referred to as the nip-induced tension (NIT).

Pfeiffer [2] and, later, Rand and Eriksson [3] studied the effect of nip roller in winding paper rolls. They observed that the nip roller increased the tension in the outer layer beyond the web line tension. Using a finite element model, Good and Wu [4] showed that the NIT is developed as a result of an elongating machine direction strain that exists beneath the surface of the incoming web layer and the winding roll. They modified the outer boundary condition in Hakiel's model [1] to include the component of NIT. In rolls of light weight coated paper (LWC) and polypropylene wound in a center winder with an undriven nip roller, Good et al [5] observed that all of the web tension summed with a NIT component becomes the final tension in the outer layer. The final level of tension in the outer layer of a winding roll, regardless of the winder type, is called the Wound-On-Tension (WOT). In surface wound rolls of newsprint, Rand and Eriksson [3] observed that the tension in the web drops to a minimum value before entering the nip roller and becoming the outermost wrap of the winding roll.

Initial models [5] that computed the value of the NIT component of the WOT were based on Amontons-Coulomb law of friction ($F=\mu N$) and relied on the values of

coefficient of friction ($\mu_{k \, web/web}$ and $\mu_{k \, nip/web}$) measured according to ASTM D 1894 [6]. Theorists [7-9] have agreed that the mechanics of slippage at the contact zone determine the behavior of the NIT and the WOT. Simple equations determined from Amontons-Coulomb law may work well in limiting cases, but the inability to predict the micro-slip and the actual friction that exists in the contact zone requires sophisticated solutions to predict the WOT. Good [8] hypothesized an algorithm to compute the NIT based on the assumptions of slip and stick zones at the entry point of web into the wound roll and friction between the web surfaces to be greater than the friction between the web and nip roller. Based on the traction capacity (which is the ability to resist slip) and extensional strains in the web as a result of Poisson expansion due to the contact compressive stresses, he was able to compute NIT. The theory was verified with experimental results. Jorkama [10] developed a model founded on the principles of contact mechanics of the nip roller and wound roll. His results show that the shear tractions in the contact zone control the slippage between the top two layers and hence the NIT.

Though both Good's and Jorkama's theories are different, their theories show that the NIT is limited by the frictional forces between the layers. Both Good and Jorkama treat the wound roll and the nip roller as a solid structural cylinder and not as a layered structure with multiple contacting interfaces. Hence, it is not very clear from the literature as to how exactly the NIT and WOT is developed and what parameters dictate their behavior. To answer these questions, one has to model the nip mechanics thoroughly and only a numerical solution that incorporates proper definition of the boundary conditions

and loads can determine where the stick and slip zones are and how the WOT is produced.

A thorough investigation of the nip mechanics in winding processes needs addressing and this dissertation documents a numerical approach to the analysis of the development of the wound-on-tension (WOT) in webs wound into rolls. The approach explored in this research will remove many of the underlying assumptions imposed by Good and Jorkama and will permit a thorough analysis of the resulting zones of stick and slip in the contact zone in a winding process and its effect on the development of the WOT. The effect of physical, material and winding parameters on the WOT has also been investigated. The numerical analyses needs to be verified experimentally and all the relevant details are discussed herein.

2   Literature Review

2.1   Wound Roll Mechanics and Models

Analysis of the wound roll structure has been carried out since the 1960s. Theoretical investigations on the wound roll structure and the wound roll models can broadly be classified into the following categories based on the solution approach

- Closed form solutions based on linear elastic small deformation theory

- Approximate solutions based on energy methods

- Numerical solutions based on linear elastic small deformation theory, viscoelastic and thermoelastic formulation and large deformation continuum approach

- Numerical solutions based on accretive axi-symmetric finite element formulations

- Numerical solutions with the use of commercial finite element (FE) codes

A review on most of these methods has been made by Good [11] and the author intends to focus primarily on the literature in the analysis of wound roll structure using finite element methods. Axisymmetric finite element accretive formulations have been used by Hoffecker and Good [12] to determine the stress distribution inside a wound roll. This model also predicts widthwise variations in wound roll stresses. Using

multi-point constraints the stresses in each lap due to addition of the incoming layer is computed. The problem of pressure fit between two cylinders is an analogy to the above concept. Lee and Wickert [13] used a similar approach to predict the wound roll stresses. The difference between Hoffecker's and Lee's model lies in the allocation of the web tension in the incoming web layer. In Hoffecker's model, the web tension is allocated based upon the widthwise variation in radius of the previous lap that was added to the roll. Lee's model does not allow any variation in radius across the width to impact the allocation of tension.

Commercial FE codes have been used to study the effect of roll weight, gravity, etc on the wound roll structure. Smolinski et al [14] used Altmann's model [15] and finite element methods to model the collapse of a coiled material. A jointed material model involving large deformation was used for this purpose [16]. A jointed material model provides a simple continuum model for a material containing a high density of parallel joint surfaces where each system of parallel joints is associated with a particular orientation, such as sedimentary rock. The jointed material model is intended primarily for applications where the stresses are mainly compressive such as in wound rolls. The collapse analysis was performed in two stages. In the first step, the initial stresses calculated from the winding model were specified with boundary conditions simulating a coil resting on a flat surface. A nonlinear static analysis was used to compute the deformation and the stresses. In the second step, a vertical gravitational body force was applied to the coil to simulate the collapse due to the roll weight.

Li and Cao [17] published a material model to compute sheet coil deformations. Using thin pressure vessel theory and simplified forms for radial and tangential strain by omitting the Poisson terms, they assumed a displacement function similar to Altmann's [15] to compute the radial and tangential stresses in wound rolls. The model results agreed with Benson's plane strain continuum model [18]. Li and Cao also used finite element methods to account for coil deformation under gravity load. This was accomplished by using a multilayer model in which the equivalent shear modulus of each layer was set to a different value in order to model the nonlinear behavior of the radial pressure inside the roll. The layers were designed according to the residual pressure distribution obtained using their analytical formulation for the wound roll stresses. Each layer was modeled by plane strain solid elements and the layer to layer interaction was modeled using Coulomb's friction law. The shear modulus was calculated as 'μP', where 'P' was calculated as the average radial pressure in that layer and the radial modulus was calculated based on stack compression experiments.

Be it a classical or a numerical approach, all the authors have assumed that the wound roll is a set of concentric hoops. Although models like Hakiel's [1] predict the stresses in a center wound roll accurately when the webs are not so compressible that tension loss in the outermost layer due to radial deformation is not exhibited, very few production winders operate in center winding mode without a nip roller. In most cases, some form of a nip roller is used. In the case of winding with a nip roller (driven or idling), additional stresses are introduced and the following sections deal with literature on experimental and theoretical investigations in nip mechanics.

2.2   Experimental Nip Mechanics

The tension in the outermost layer of a winding roll is commonly referred to as Wound-On-Tension (WOT). The WOT has two components; one due to incoming web tension and the other due to the nip, called the nip-induced-tension (NIT). Studies of wound roll structure based on the WOT measurement started with investigations by Pfeiffer [2, 19]. He observed that the rolls wound in either center or surface wound condition with an impinging nip roller produced harder rolls, as compared to those wound without any nip loading. He used a flat bed rolling nip test bed to understand the nip mechanics in the winding process. The tester consisted of a rigid base on top of which a stack of sheets clamped to a load cell at one end were placed. A rigid nip roller traversed across these sheets inducing additional tension in the web. It is common in these tests for the tension on the exit side of the rolling nip to rise exponentially to a nearly constant level of tension called the 'saturated' value. The saturated value of this tension is commonly referred to as the NIT. Based on the micro-photographs that observed the micro kinetics of a rolling nip, the instant center of rotation was observed a few sheets beneath the rolling contact interface. The instant center of rotation is the point about which all motions rotate at a given instant of time. Identifying the instant center meant that the sheets above the instant center moved in the direction of the rolling nip while the sheets below moved in the opposite direction of the rolling nip. This indicated that the sheets above the instant center were in tension while those below the instant center were in compression. The position of the instant center during paper winding was found to be regulated by the tension developed. If little or no tension developed, the instant center

existed several layers deep. As the tension increased, the instant center moved closer to the roll surface.

Rand and Eriksson [3] studied the behavior of the WOT in different winders using strain gages. Strain gages were attached to the webs to record the strain during the motion of the web around an impinging nip roller in a center winder with an undriven nip roller. They observed that the largest increase in circumferential stress occurred in the outermost layer directly under the nip and as more layers were wound, the circumferential stresses decreased as shown in Fig. 2.1. The increase in tension beyond the web tension under the nip roller is referred to as the WOT. This leads to the conclusion that the effect of nip on the wound roll pressures and stresses occur due to the slippage beneath the outermost layer that is under the nip roller. The pressure which is increasing beneath the successive layers below the outer layer acts to inhibit slippage beneath those layers.
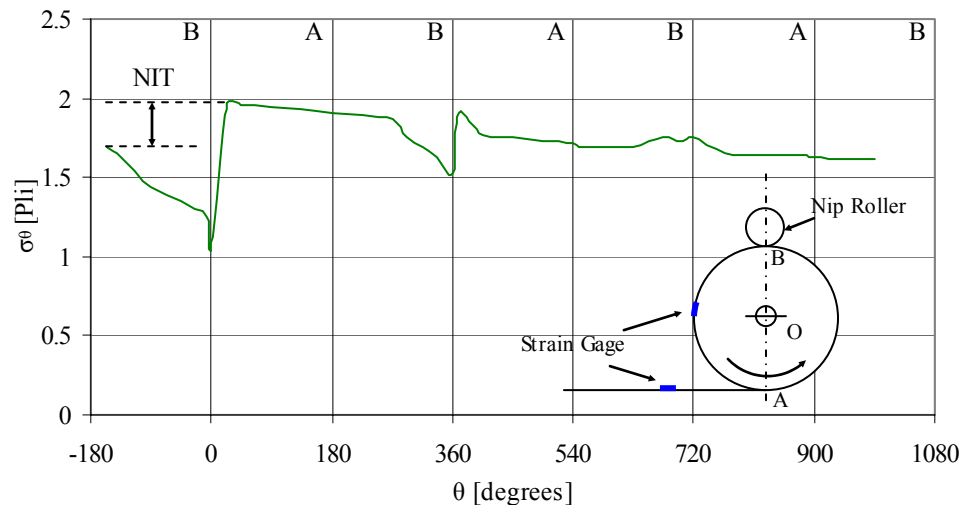
Figure 2.1: Circumferential stress in a paper web wound into a roll in a center winder with an undriven nip roller (a line curve using selected data points from the original publication is shown here).

10

Pfeiffer [19-21] developed a specialized winder, shown in Fig. 2.2, to measure the WOT. In a production winder, the incoming layer becomes the outermost layer of the winding roll. In the WIT-WOT winder, the outermost layer is peeled off of the winding roll, passed through a roller mounted on a load cell before returning the layer back to the winding roll. The roller mounted on the load cell serves to measure the WOT. Pfeiffer observed that the WOT increased with increase in nip load, as shown in Fig. 2.3. Also, the experimental data suggested that below certain nip loads in surface winding, the frictional force between the nip roller and the winding roll was not sufficient to overcome the web tension and the rolling resistance of the winding roll, resulting in a winder stall (the inability to wind material). The winder stall is represented by the region in Fig. 2.3 where the WOT is less than that predicted by the slope indicated in the figure.
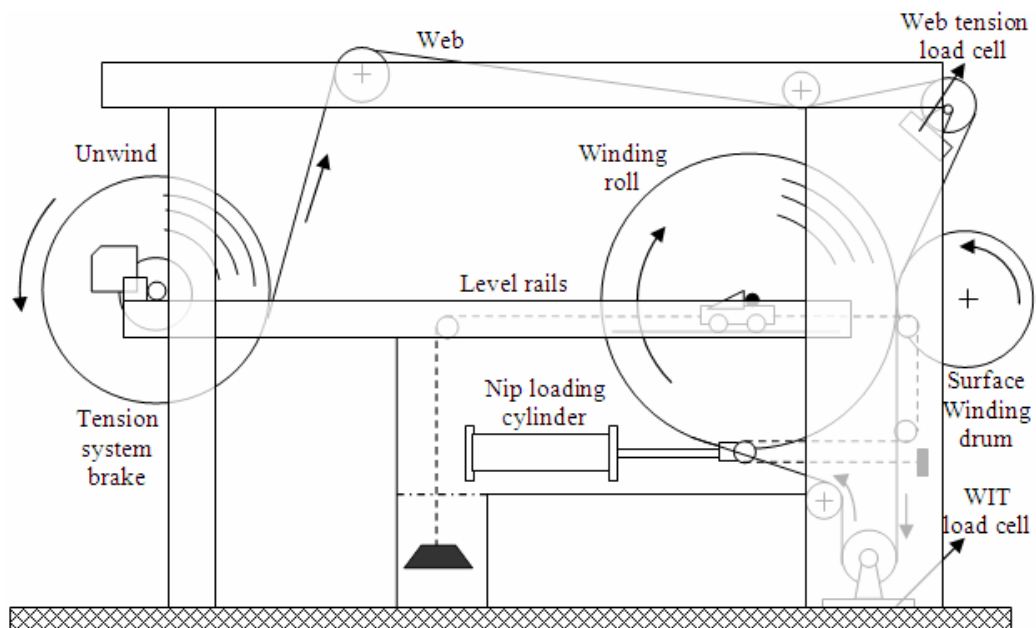
Figure 2.2: A schematic of the Pfeiffer's WOT apparatus.
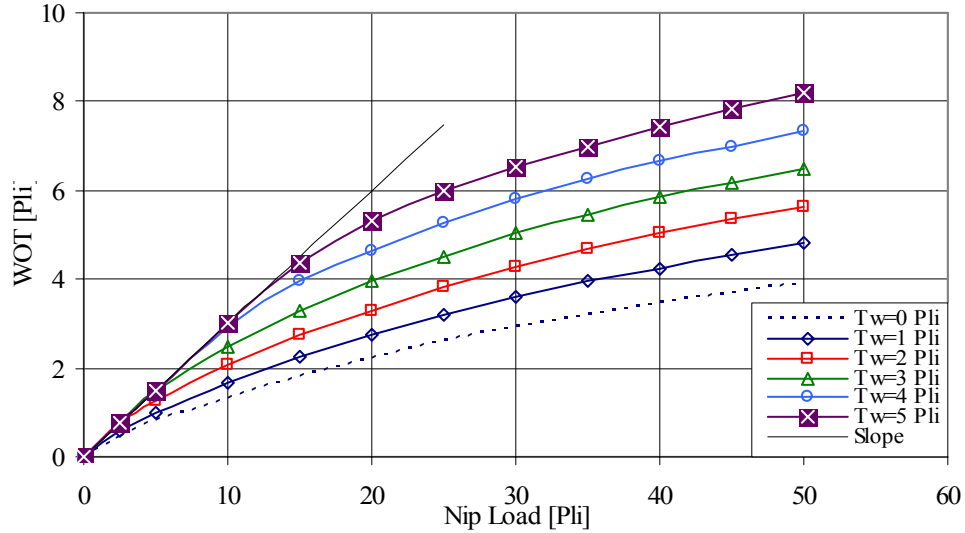
Figure 2.3: Pfeiffer's WOT curves for Canadian newsprint at different web tensions and nip loads (selected points from the original publication are shown here).

Good and Fikes [22] investigated the internal stresses in the wound roll with the presence of a nip roller. They measured the radial pressure inside the roll using force sensitive resistors (FSR). In Hakiel's model [1], the tension in the outermost layer of the winding roll is equal to the incoming web tension and hence the WOT. Thus, using a computer model similar to that of Hakiel's, by iterating on the tension that produced radial pressure profiles comparable to that obtained experimentally using FSRs, the WOT values were obtained. When the WOT was computed for different nip loads in this manner, the data showed that the WOT was directly affected by web tension prior to the winder and through a constant of proportionality for nip load. This constant appeared to be similar in magnitude proportional to the kinetic coefficient of friction. Based on these findings, a new boundary condition was formulated for wound roll stress models that incorporated the NIT as given in Eqn. 2.1, 2.2. This formulation was verified experimentally in wound rolls of Light Weight Coated paper (LWC) and Polypropylene at different nip loads and is shown in Fig. 2.4.

12

$$\delta\sigma_r\big|_{r=s} = \left\{T_w\big|_{r=s}\right\}\frac{h}{s} \qquad (2.1)$$

$$\delta\sigma_r\big|_{r=s} = \left[\left\{T_w\big|_{r=s}\right\} + \frac{\mu N}{h}\right]\frac{h}{s} \qquad (2.2)$$

Cai [23] studied the effects of nip roller compliancy upon center and surface winding. Based on the experimental data at a given nip load, the nip-induced tension was observed to be the same in both center and surface winding of webs. He showed that at low nip loads, and high wrap angles (in his case the wrap angle was greater than 180°), the rubber coverings on the nip roller had little or no impact on WOT inferred from pull-tab measurements. The WOT values in center and surface wound rolls were calculated using Eqn. 2.3, 2.4 respectively. Equations 2.3, 2.4 were based on simplistic assumptions and the derivations were based on Amontons-Coulomb law and band-brake expressions. They depend only on the nip load and the kinetic coefficient of friction and hence the effect of web and nip cover properties could not be predicted.
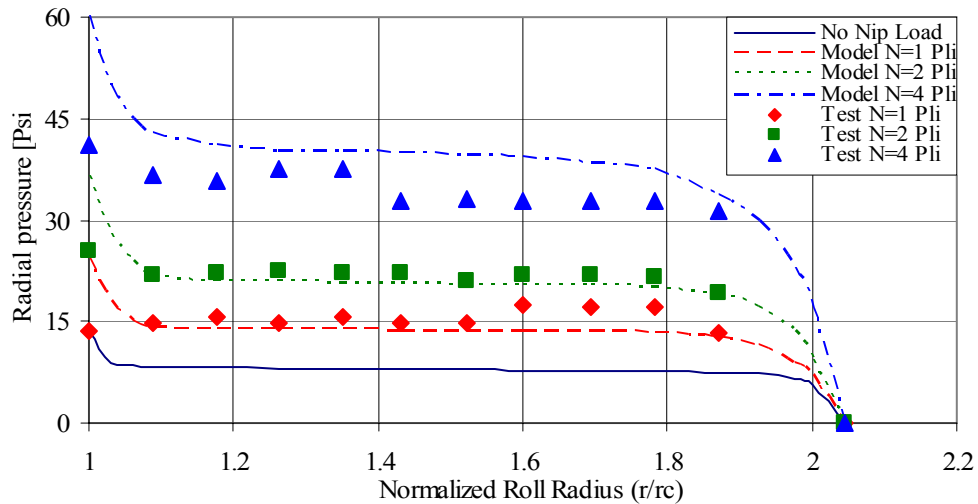
Figure 2.4: Pressures within wound rolls of Light Weight Coated paper at various load levels (selected data points from the original publication is reprinted here).

13

$$WOT_{CW} = T_w + \mu_k N \qquad\qquad (2.3)$$

$$WOT_{SW} = \frac{T_w}{e^{\mu_{kw/R}\theta}} + \mu_{kw/w} N \qquad\qquad (2.4)$$

Steves [24] studied the effects of nip load on the WOT in surface winding. He inserted pull-tabs while winding the rolls in order to document the wound roll pressures as a function of wound roll radius. A pull-tab is a piece of steel shim encased in a brass envelope. The use of dissimilar metals exhibits a low coefficient of friction between the two. After winding, a force gage is used to measure the pull force required to dislodge the steel shim and with the knowledge of the coefficient of friction between the shim and the envelope, the pressure can be inferred. Using a wound roll model like Hakiel's, the WOT was iterated to match the radial pressure profile obtained using pull-tabs. The results showed that the qualitative behavior of the WOT data agreed with Pfeiffer's results. In addition, the WOT was found to be independent of the winding torque in surface winding condition. He inferred that the slippage ceased to exist at high nip loads, with the measured WOT being lower than that calculated using the Eqn. 2.4. Velocity measurements showed that at higher nip loads, above 10 pli for newsprint, the wound roll velocity was greater than the nip velocity.

Good, Hartwig and Markum [25] conducted a series of experiments to study how the WOT differed in a center winder with an undriven nip roller and a surface winder. A new WOT apparatus as shown in Fig. 2.5. was developed wherein the web tension and the nip load were independent winding parameters. In Pfeiffer's WOT apparatus (shown in Fig. 2.2) the nip loading was affected by the level of the WOT and the new design

shown in Fig. 2.5 prevented this dependency. They found that the WOT method was an interfering test and that the measurement could be corrected to yield the true value of WOT that was inferred from pull-tab data. The WOT in center winding case was found to be dependent more on the web tension than the nip load. For example, the results from the center winding tests on newsprint are shown in Fig. 2.6. The corrected results were obtained by using a capstan band-brake type expression (Eqn. 2.6) for the slippage through the arc beyond the nip roller and the WOT load cell.

$$\frac{T_1}{T_2} = e^{\mu\theta} \qquad (2.5)$$
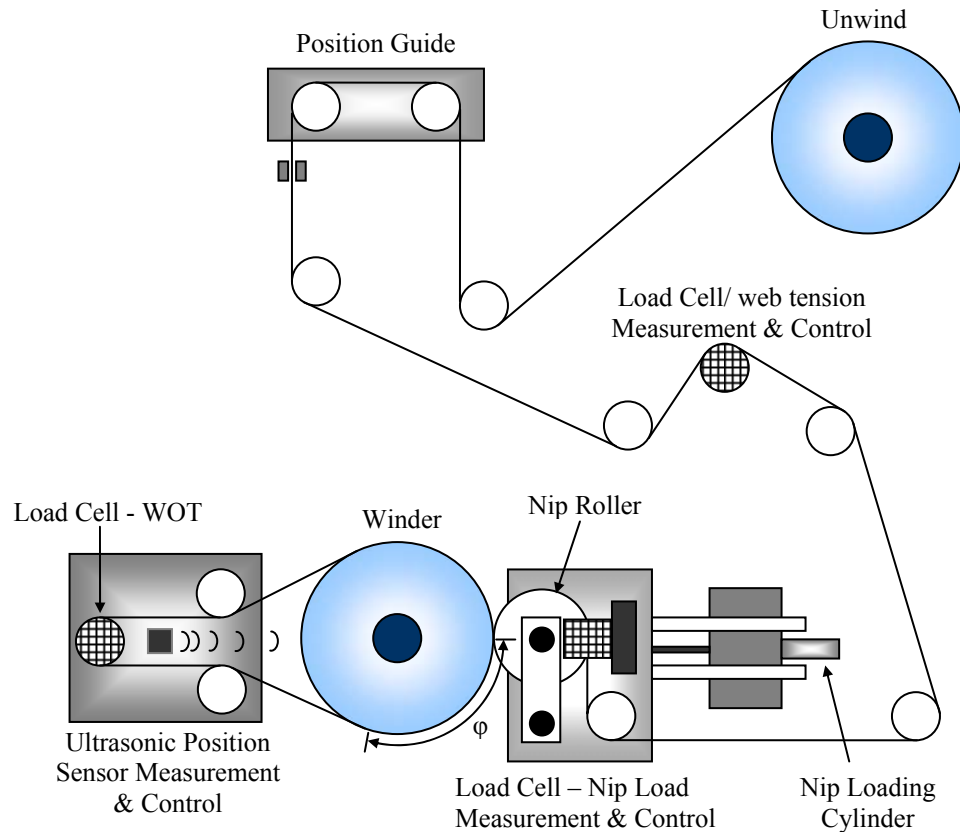
Figure 2.5: Schematic of the WOT apparatus used by Good et al [25].
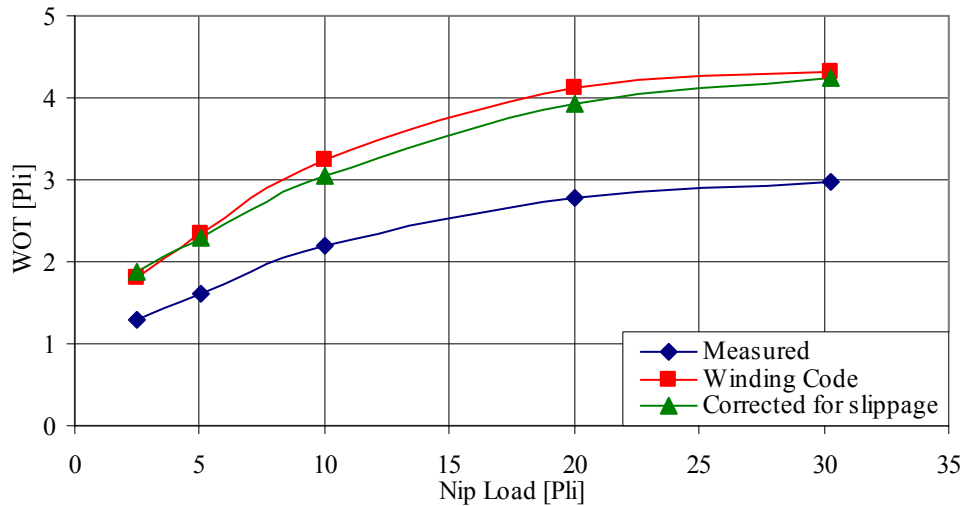
Figure 2.6: Effect of nip load on WOT in center winding Newsprint with an undriven nip roller (selected data points from the original publication is reprinted here).

In surface winding, they observed that the dependence of the WOT on web tension increased with increase in nip load. The qualitative behavior of the WOT in surface winding was similar to what Pfeiffer [19] observed in his case. They also found that the NIT was independent of the method of winding.

Welp and Gueldenberg [26] used a digital image processing technique to analyze the NIT. The procedure employed combined the principle of the J-Line technique [27] and digital imaging technique that captured strain in each layer through photographs. J-Line technique is a method of studying the deformations in the wound rolls by striking a straight line and observing for deflection of the line due to further addition of the incoming layers. As the roll was wound, an ink jet printer shoots an ink jet at the incoming layer and at the same instant, a CCD camera captured the image. With the help of a counter/timer board and LabVIEW® data acquisition system this process was carried

out as each layer was being wound. The purpose of the digital photograph is to determine the two dimensional displacement field of the observed objects in an image relative to a reference image. The marks on the edge of the layers are the observed objects in this case. By comparing the marks in two images, the displacement vectors can be calculated. Based on the strain fields, the tangential stresses due to nip were calculated. In addition, the total displacement of each layer was calculated.

Kandadai [28] observed the effect of nip loads and web tension on a nonwoven polyethylene web in surface winding. The proportionality between the WOT and the nip load at lower nip loads has been shown to approach the kinetic coefficient of friction between web layers for webs [25]. But, for the nonwoven web that was tested, the proportionality was much less than the kinetic coefficient of friction. Although the first statement is true, the method of measurement of friction coefficient is very important as WOT is a result of slippage between the top two layers, which in turn is dependent on the coefficient of friction in the contact zone. Kandadai and Good [29] showed that the flat bed nip mechanics tests can yield representative values of the friction coefficient that will be closer to the actual friction coefficient in the nip contact zone than those measured using ASTM standard tests [6].

Santhanakrishnan [30] studied the effects of rubber covered nip rollers on both center and surface winding and observed that the Poisson's ratio of the nip cover was an important factor. He also showed that at high nip loads, hard rubber covers produced higher WOT than rigid rollers for the same web tension and nip load. The results of this

17

work agreed with the results of Cai [23] for the cases where the angle of wrap of the web about the nip roller was high. He also studied the effect of grooved rubber covered nip rollers on WOT and observed that the grooved rollers produced a lower WOT compared to both rigid and solid rubber covered nip rollers.

2.3   Theoretical Nip Mechanics

Jalkanen [31] proposed a theoretical model for the NIT based on the velocity differences that exists between the nip roller and the winding roll. The velocity of the incoming sheet was assumed to be equal to that of the nip roller from the leading edge of the contact to the center of the contact and equal to the speed of the wound roll thereafter. He computed NIT based on the Eqn. 2.6.

$$NIT = E_t t \frac{\delta}{R}$$
(2.6)

The nip models including that of Good [8] (discussed in the preceding section) and Jalkanen [31] were based on the kinetics and kinematics of the nip respectively. Their intuition coupled with experimental observations led them to propose simple models based on analytical closed form solutions. Experimental studies carried out by Good [25] proved that these simple equations may work only in limiting cases. The inability to predict the micro-slip and the actual friction that exists in the contact zone requires sophisticated NIT models. The mechanics of the slippage at the contact zone determines the behavior of NIT.

Although numerous studies on rolling contact of cylinders can be found in the literature, only a few can be related to the nip mechanics that occurs in winding. These studies fall under two categories; calendaring and winding. Bentall and Johnson [32, 33] investigated the rolling contact of an elastic layer between elastic rollers. Closed form solutions were obtained for both the frictionless case and the case where the coefficient of friction was infinite. They realized that the occurrence of micro-slip was inevitable for cases when the value of friction was between the extremities. They studied the rolling contact involving micro-slip using a numerical technique that solved the contact problem at discrete number of points. The contact zone was divided into N discrete points and conditions of equilibrium were satisfied at each of these points. Since the tangential tractions have very little or no effect on the normal load the numerical technique resulted in a one step solution by matrix inversion. The results of the numerical simulation provided a general pattern to the behavior of the micro-slip. Five distinct regions were identified within the zone of contact; two slip zones at either ends of contact, a slip zone in the middle of contact, and two stick zones between the each of the three slip zones.

Kalker [34] employed a strip theory similar to that of Johnson and automated the solution scheme. The most important contribution in solution schemes of these types of contact problems involving micro-slip was by Panagiotopoulos [35]. An iterative procedure was utilized to solve the problem at the discrete points. In the first step, with the assumption of zero tangential traction throughout the contact zone, the normal stress was calculated. Assuming stick through the entire contact zone, the tangential tractions were then evaluated. If the traction exceeded the coefficient of friction multiplied by the

normal stresses at any point, a slip equation replaced the stick equation at that point. This process was repeated till a convergence of the order of 1% or less was obtained for the desired parameters.

Soong and Li [36-38] analyzed the rolling contact of two elastic cylinders with an elastic sheet between the rollers and including the tension in the sheet. They used a Fourier-series form for the displacements and stresses in the contact zone and used a solution process similar to that employed by Johnson. They used a collocation method wherein they derived a set of matching equations that were linear at discrete points in the contact zone and solved for the unknown coefficients called influence coefficients. These coefficients were the coefficients used in the Fourier-series. All the bodies involved were treated as isotropic materials. Although, the contact mechanics was properly described, the use of cylindrical coordinates for the solution meant that thousands of terms were needed for the convergence of Fourier-series solution. The above referenced papers describe the contact mechanics in a calendaring process. Calendaring is a process where the webs are crushed in the contact between two opposing rollers which results in densification of the web and burnishing of the web surfaces. This type of calendaring problem is the closest to the winding nip mechanics problem.

Good and Wu [4] studied the mechanism of the NIT in wound rolls in an investigation utilizing finite element and experimental analysis. They used finite element methods to understand the contact mechanics of a rolling nip and a stack of sheets. They observed that an elongating machine direction strain existed beneath the nip roller on the

20

lower side of the web, which is in contact with the wound roll. It was found that the strain was due to a compressive Hertzian-like [39] contact stress that exists through the depth of the web beneath the nip roller. As this elongating strain advances with the rolling nip, the web material attempts to advance in front of the rolling nip, and contact in towards the nip in back of the rolling nip. They proved that a net increase in tension could result when the web material in back of the nip is constrained. They also determined that the NIT could not exceed the kinetic coefficient of friction between the outer wrap and the layer beneath it multiplied by the nip load.

Welp and Gueldenberg [7] proposed a coupled contact mechanical model for nip mechanics. Two partial models were created; one for the wrapped roller and the other for the nip with the incoming web included. A capstan type formula with the assumptions that Coulomb friction was still valid through the contact interface was developed for the wrapped roller. For the nip and the web, with the assumptions of zero strain gradients and Coulomb's law for contact interaction at the stick and the slip zones, frictional forces were calculated. These two partial models were then coupled to model the entire nip mechanics. However, the contact conditions were not modeled accurately due to strong assumptions in the behavior of stick-slip zone.

Jorkama and von Hertzen [9] developed a contact mechanical computer model for the NIT based on an elasticity formulation similar to that described by Lekhinitski [40]. A linear orthotropic material model was used for the description of all the elastic bodies involved. Fourier-series solutions were derived for an orthotropic half space, cylinder and

the web and in most cases the half space solution was used to reduce the computational difficulty. In a purely elastic calendaring process, the nip does not introduce any additional tension beyond the web tension. This is due to the boundary conditions involved in the process, wherein the free sheet is under no stress or that of the web line stress on either side of the nip. In a winding process, the sheet enters the wound roll beyond the nip. This results in the tension beyond the nip being higher than the incoming web tension.

Jorkama [10] introduced a wound-on-condition (WOC) that ensured the velocity of the sheet 180° away from the contact zone and into the wound roll is the same as that of the wound roll. In his numerical procedure, he relaxed this condition and assumed that the velocity of the sheet was equal to that of the wound roll beyond the nip contact zone owing to the complexity of the contact mechanics calculation. The Panagiotopoulos [35] process was utilized in the solution scheme and an initial guess of contact width was required to solve the numerical problem. With this model, the WOT can be studied as a function of nip and wound roll diameter, web material properties, friction characteristics, winder operating parameters such as nip load and web tension, and whether one was center winding with a nip or surface winding. Their results show that the contact tractions due to the slippage between the nip/web and the web/wound roll interfaces result in the NIT. An example of the traction behavior at the contact zone for one of the cases studied by Jorkama is shown in Fig. 2.7. One of the shortcomings of their model is the inability of the model to accommodate the slippage between layers within the wound roll as the wound roll was assumed to be a solid cylindrical body. Also, their results were compared

to the WOT values measured using the load cell method which can be an interfering method and thus in error [25].
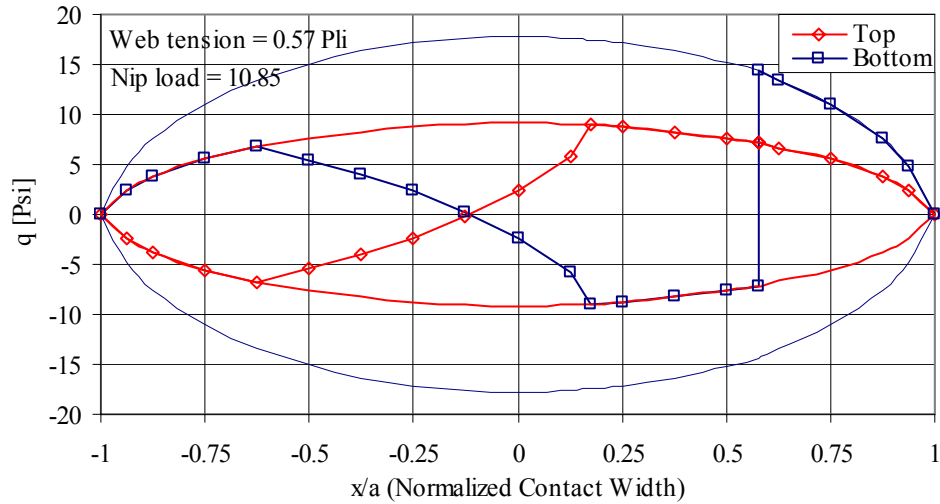
Figure 2.7: Tangential tractions in the contact zone in center winding (selected data points from the original publication are shown here)(Legend: Light shaded, dotted lines indicated the friction limits, Blue squares indicate the traction in bottom surface and Red Diamonds indicate the traction in the top surface).

Good [8] came up with a closed-form solution for NIT based on the assumptions of slip and stick zones in the contact zone. He defined traction capacity (the ability to resist slip) as an integral sum of the value of coefficient of friction multiplied by the normal pressure at any point in the contact zone. The strain in the machine direction was assumed to be caused due to the Poisson effect caused by the normal stress similar to that given by Johnson [41]. The NIT was defined as the value that exists at the intersection of the traction capacity and MD stress curve as shown in Fig. 2.8. Good was able to verify his NIT theory using experimental measurements as shown in Fig. 2.9. Since the stresses and strains were computed based on Poisson's effect using equations obtained by Johnson [41] at the rolling contact interface, the NIT algorithm was sensitive to the out-

of-plane Poisson's ratio ($\nu_{r\theta}$). Though both Good's and Jorkama's theories are different, it is apparent from their theories that NIT is limited by the frictional forces between the layers.
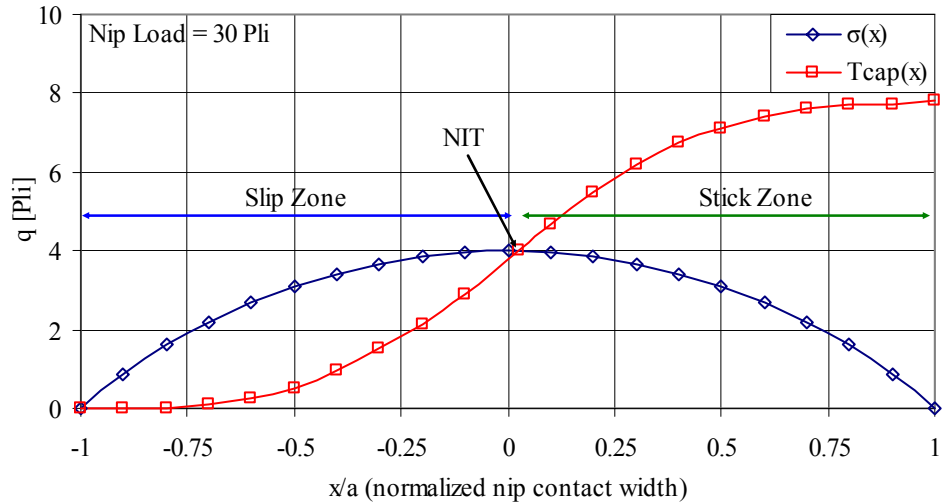
Figure 2.8: Stress behavior in the contact zone in center winding (Legends: $\sigma(x)$ represents the MD stress developed in the layer and Tcap(x) represents the traction capacity due to the nip) (selected data points from the original publication are shown here).
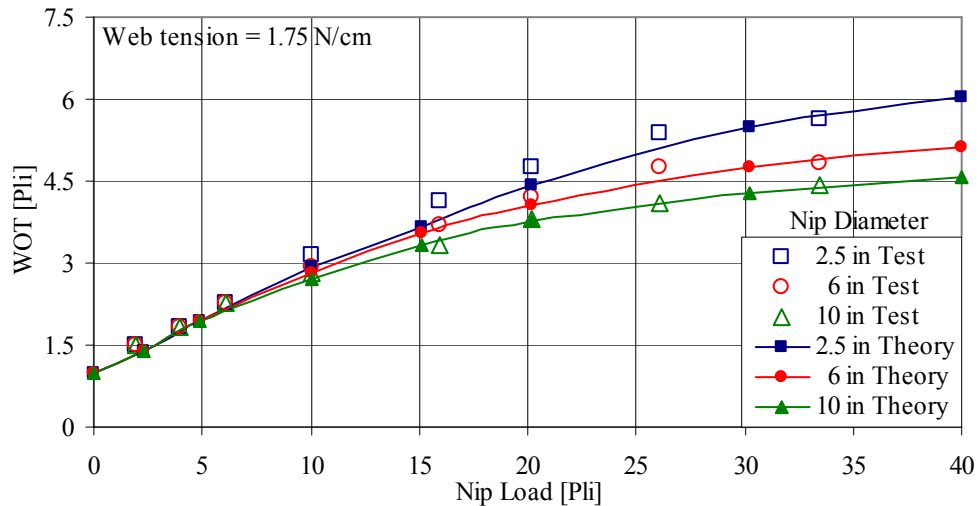
Figure 2.9: Effect of nip roller diameter on WOT in center winding Newsprint (selected data points from the original publication are shown here).

In all the cases described above, the wound roll was treated as a solid body instead of an Archimedean spiral. In reality, each layer being wound interacts with the

24

winding roll and within the winding roll, each layer slips or sticks relative to each other. This behavior is not accounted for in any of the models.

Äröla and von Hertzen [42] studied the rolling contact problem of a cylindrical drum on a stack of paper sheets using the finite element method. A two-dimensional model under plane strain conditions was considered and the paper sheets were modeled using linear orthotropic constitutive law. The friction between the various contacting surfaces was modeled using the conventional Coulomb's law. A comparison of the stick-slip behavior that existed in the nip area was made between solid elastic block and a layered stack. The net contact traction that existed in the top layer was found to be the cause of the NIT in the case studied. They reported three distinct zones in the behavior of both the top and bottom surface tractions in the top layer, namely, slip zones at the leading and trailing edges of contact and a stick zone in the middle of the contact. However, some of their observations were incorrect and will be discussed later.

Although, various models and theories that describe the nip mechanics exist, analysis of nip mechanics that treats the spiral nature of the wound roll does not exist. Hence, further analysis is needed to determine how the WOT is developed without any of the limiting assumptions that were imposed by Good and by Jorkama.

3 Research Objective

Wound roll models incorporating nip mechanics that currently exist do not sufficiently treat the winding problem to accurately describe the stick and slip conditions in the nip contact zone. If the focus is on obtaining a closed form solution for the WOT that can be used with a winding model to provide rapid solutions for internal roll stresses then one has to simplify the contact mechanics of the winding nip with many assumptions, like that reported by Good [8]. With complex numerical contact mechanics approach such as Jorkama's [10], one can study the slippage and the resulting tension within a single layer in the contact zone but the solution procedure is tedious and convergence can sometimes be a problem due to the type of solution scheme. Pseudo-closed form solutions like that of Welp [7] are based on coupling of partial models with high degree of idealization of the contact zone. Each of these models can be made to output values of internal stresses that can be measured experimentally, but are sensitive to input parameters like $v_{r\theta}$ and $G_{r\theta}$ that are extremely difficult to measure. Also, all these models assume the wound roll as a solid body. In reality it is a layered structure.

The objective of this research is to investigate the contact mechanics of a winding nip and analyze the development of wound-on-tension using a numerical

tool like finite element methods. A commercial finite element software (ABAQUS®) will be used in this effort and this research will determine:

- How the WOT is developed in a web wound into a roll?

- How do the winding parameters affect the behavior of the WOT?

- How do the material properties affect the development of the WOT? and

- What is the effect of a compliant nip roller cover on the WOT?

The analysis will be carried out without imposing any of the assumptions used by Good and by Jorkama. As a part of the objective, the numerical results shall be verified using experimental measurements of the WOT. Also, some of the qualitative observations will be compared with experimental results obtained by previous researchers.

4   Modeling Nip Mechanics in Winding Processes

4.1   Mechanics of Winding: A contact mechanics problem

One of the most effective treatments of wound roll stress analysis was performed by Hakiel [1]. The wound roll was assumed to be made up of concentric hoops of web layers and the webs were assumed to behave as an orthotropic material with nonlinearity in the radial direction. The plane stress equilibrium equation in cylindrical coordinates for this problem is given in Eqn. 4.1 and the stress state represented as shown in Fig. 4.1.

$$r \frac{d\sigma_r}{dr} + \sigma_r - \sigma_t = 0 \tag{4.1}$$
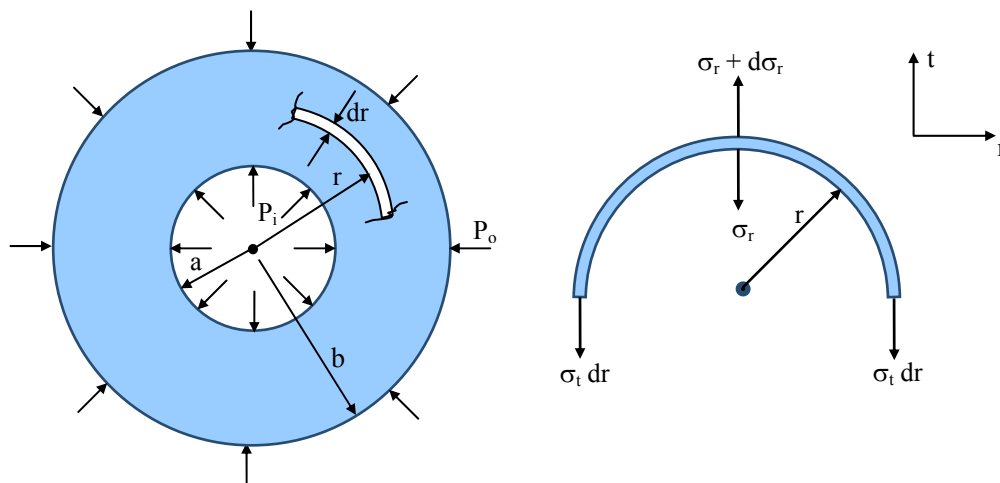
Figure 4.1: Representation of state of stress in Cylindrical Coordinates.

Equation 4.1 is a result of force equilibrium and is obtained by summing the forces in the vertical direction. Using constitutive relations and strain compatibility relations for a linear orthotropic material under plane stress conditions, the equilibrium equation can be expressed as given in Eqn. 4.2.

$$r^2 \frac{d^2\sigma_r}{dr^2} + 3r \frac{d\sigma_r}{dr} - \left(g^2 - 1\right)\sigma_r = 0; \; P = -\sigma_r \tag{4.2}$$

where,

$$g^2 = \frac{E_t}{E_r} \tag{4.3}$$

Equation 4.2 is solved for increments in pressure instead of the total radial pressure. The increments in pressure are due to the addition of more layers of web to the winding roll. After each solution, the total pressure is updated in each layer and the radial modulus is updated at all radial locations since it is state dependent on pressure. This second order differential equation requires two boundary conditions when solving for incremental pressures. The inner boundary condition is obtained based on the displacement continuity between the inside of the first layer of web and the outside of the core. The outer boundary condition is based on the tension in the outermost lap. The inner and outer boundary conditions are given in Eqn. 4.4 and Eqn. 4.5 respectively. These equations (4.1-4.4) form the boundary value problem that is linear yet analytically not solvable due to 'E_r' being a function of pressure, making 'g^2' nonlinear. Thus this problem has to be solved using a numerical formulation.

A central difference method is used to estimate the derivatives in Eqns. 4.2 and 4.5 at 'n-1' solution points throughout the roll After including Eqn. 4.4, a set of 'n' equations can be solved to yield the increments in pressure due to the addition of the most recent lap. Though the results obtained using this formulation has been found to compare well with experimental results, this model has strong shortcomings in its lack of ability to incorporate nip mechanics.

$$\delta P\big|_{r=b} = \frac{T_w\big|_{r=b}}{b} dr \qquad (4.4)$$

$$\frac{d\delta P}{dr}\bigg|_{r=a} = \left\{\frac{E_t}{E_c} - 1 + \upsilon\right\} \delta P\bigg|_{r=a} \qquad (4.5)$$

Rolls of webs are rarely wound without nips being applied to them. Nips introduce additional stresses inside the wound roll. The increase in the stresses inside the wound roll is due to the increase in the WOT due to the nip. Compliancy and differing Poisson's ratio of the nip roller cover introduces an additional variable in the winding process. Santhanakrishnan [30] studied the effect of different types of nip cover on the WOT in center and surface wound rolls of several grades of paper at different nip loads and the results of one of the cases he studied is shown in Fig. 4.2. In this case, observe that a 41 durometer foam covered nip roller produces lower levels of WOT at different nip loads compared to a 30 durometer rubber covered nip roller. When the WOT produced by the two foam covered nip rollers are compared, the lower durometer foam cover produces lower levels of WOT at different nip loads. Also, the rubber covered nip

roller produces approximately the same levels of WOT compared to that of a rigid nip roller. This indicates that both the Poisson's ratio and the compliancy of the nip roller can affect the WOT.

In other cases, wherein the material was Newsprint (not shown here), WOT higher than that produced by a rigid nip was produced. At high nip loads, hard rubber covers become nearly incompressible and when indented due to the nip contact, local speeding in circumferential direction occurs and increased WOT is observed. Kaya [43] also observed a similar behavior, but only at the highest nip loads. The foam covers have low Poisson's ratio which helps prevent or negate the local speed up resulting in a low or no WOT. This indicates that the relative velocities between the nip roller and wound roll and the angle of wrap of the web about the nip roll can become important in determining WOT. Johnson [41] shows that the micro-slip in the contact zone and the resulting relative velocities can be affected by both the shear modulus and the Poisson's ratio.

Figure 4.2 shows the importance of the mechanics at the contact zone of the nip roller and the winding roll in determining the amount of nip-induced tension. However, the existing theories are not accurate, as discussed in chapter 2. A closed form solution that determines the NIT based on the contact mechanics of the winding nip is difficult to arrive at, given the complexity of the problem. In order to handle the multiple contact interactions that occur in a winding problem and to predict the micro-slip behavior, a numerical solution is the only alternative. Before choosing a numerical approach, the

mechanics in the contact zone needs to be understood and the following section deals with the equilibrium of forces in the contact zone.
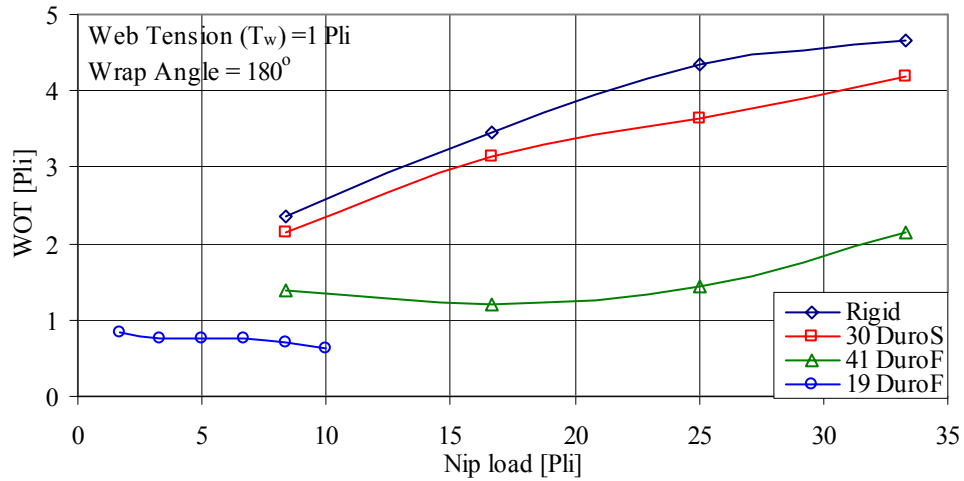
Figure 4.2: Effect of different nip covers on WOT in center wound rolls of Fine Coated Paper (Legend: Duro – Shore Hardness measurement [44], S – Solid Urethane Cover, F - Foam Urethane Cover, Numbers indicate the hardness value in Durometer).

4.2   Mechanics in the contact zone of a winding nip

Consider a winding process and the forces of interaction between the incoming web layer, the nip roller and the winding roll as shown in Fig 4.3. A free body diagram of the forces acting on the incoming web layer is also shown in the same figure. Based on the equilibrium of forces, the total tension in the web at the exit zone of the nip can be written as a function of the tractions in the contact zone as given in Eqn. 4.6. The surface shear stress is commonly referred to as the tangential traction. In a winding process, the incoming layer becomes a part of the winding roll past the nip. Due to frictional rolling contact between the surfaces involved and the boundary conditions of the winding process, a net tangential traction also referred to as the net traction arises. The net traction

is equal to the sum of the top and bottom surface tractions of the incoming web layer. The net traction varies through the contact zone and is dependent on the conditions of slip and stick within the rolling contact zone. The integrated value of the net traction is commonly referred to as the total traction (also referred to as the 'integrated net traction') and is given in Eqn. 4.7.

$$T_{out} = T_{in} + \int_{-a}^{a} \left[q_{top}(x) - q_{bot}(x) \right] dx \tag{4.6}$$

$$Q = \int_{-a}^{a} q_{net}(x)\,dx \; ; \; q_{net}(x) = q_{top}(x) - q_{bot}(x) \tag{4.7}$$
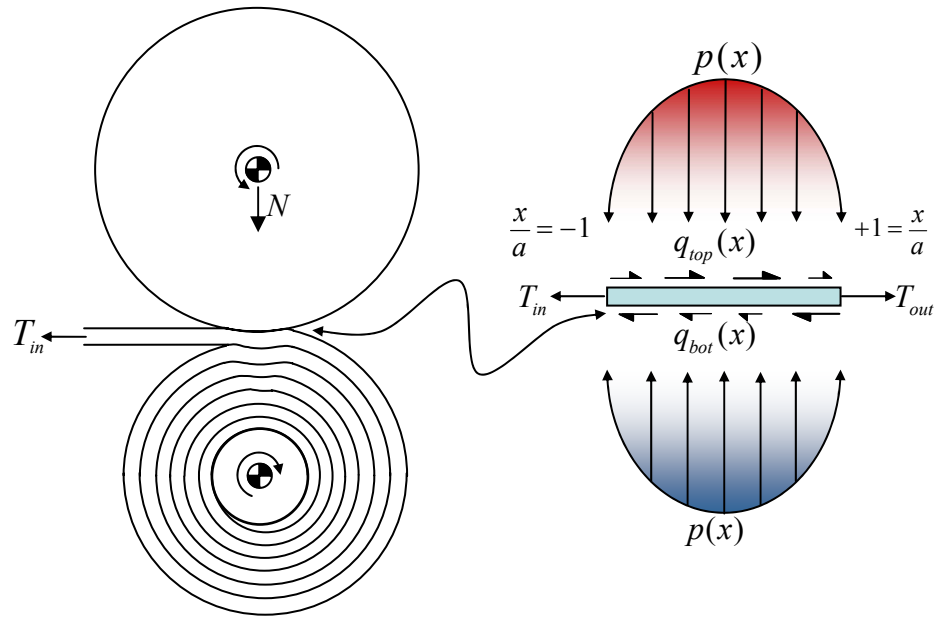
Figure 4.3: Equilibrium of forces acting in the contact zone in a winding process.

If the total traction 'Q' and the incoming web tension 'T_{in}' is known then the WOT can be computed using Eqn 4.6. Thus, the chosen numerical method should be capable of calculating the traction between the various surfaces involved as well as providing the nature of the stick and slip behavior.

4.3   Modeling Approach

The first step in the analysis of the winding problem is to understand the mechanics of contact between the different objects involved in the contact zone. In order to understand the contact mechanics, the following studies have been carried out and the details of each of these studies are in the sections 4.3.1 and 4.3.2 respectively.

- the rolling contact problem between a nip roller and a stack of sheets

    The mechanics at the contact zone in the rolling contact of a nip roller on a flat bed of sheets is very similar to that observed in a winding problem and hence the modeling will be similar. This type of modeling allows for much easier verification of the results in the lab compared to the winding contact problem.

- the Winding contact problem

    In this type of problem the spiral nature of the wound roll is accounted for. Although the mechanics at the contact zone remains similar to that observed in a flat bed model, this model accounts for the pressures within the wound roll.

4.3.1 Flat Bed Nip Mechanics

Rolling contact of cylinders with elastic covers has been studied by approximating the problem as a contact problem between an elastic roller and an elastic halfspace, with the help of St.Venant's principle [41]. Similarly, researchers like Pfeiffer [2] have studied the winding contact problem by approximating it to a rolling contact problem between a nip roller and a stack of webs using flat bed rolling nip test beds. The flat bed approximates a winding process by treating the wound roll as a roll of infinite radius in which the layers are uncoupled. The finite element analysis of the problem of the rolling nip on a web stack on top of a flat bed can provide significant insight into the mechanics of winding nip. As will be discussed later, finite element (FE) analysis of flat bed rolling contact mechanics is computationally advantageous compared to the winding case and for the same reason, the effect of compliancy of the rolling nip shall be studied using flat bed FE simulations. Pfeiffer [2] and Good and Wu [4] restrained several layers with load cells so that the NIT could be studied throughout their stack.

Flat bed tests resemble calendaring processes more than the winding processes. In a calendaring process the web is forced through two rolling nips. The primary difference between a calendaring process and a winding process is the boundary condition of the elastic layer that exits the contact zone. The exiting layer becomes part of the wound roll in a winding process. In a calendaring process, if the cylinders are identical, it does not matter which cylinder is the driver and which is the driven. However, in a winding process, whether the winding roll is being driven or being the driver matters (center or surface winding). In order to represent the winding problem, the layers at trailing edge of

35

the nip have to be constrained in a flat bed. This enables one to study the increase in tension in the topmost layer due to the nip.

4.3.2 Winding Contact Problem

Winding is a stress accretion problem as each new lap laid onto the winding roll increases the radial stresses inside the wound roll. Although, the geometry of the contact is constantly changing due to the growing nature of a winding roll, the WOT is still produced in a manner similar to that occurs in a flat bed rolling contact scenario. Thus, the underlying mechanics in both winding and flat bed rolling situations are similar except for the radial and tangential stresses that are present in the layers underlying the top layer of a wound/winding roll. These stresses are not present in a free stack of web. In a winding process, during the start of the process, the incoming sheet is tied to a rigid core and is impinged by a rigid nip. As each additional lap is laid, the contacting interfaces grow and thus the potential for stick or slip occurs at multiple points within the winding roll as well as between the winding roll and the nip roller. Analysis of this type of winding contact of problem, wherein slippage is allowed at multiple interfaces should provide insight into how the stresses are developed inside the wound roll as well as providing the knowledge of the slippage within the wound roll.

4.3.3 Solution Method

The finite element method is a numerical procedure and is one of the most used tools in the field of structural and mechanical engineering. ABAQUS® is a commercial

36

FE code capable of handling very complex contact mechanics problems and can be used to study transient and quasi-static problems. Modern codes like ABAQUS/Explicit$^{®}$ can analyze the contact between different bodies and output variables that can help understand the stick-slip behavior in the contact zone. This is essential for the analysis of a winding contact problem. However modeling of the winding problem in ABAQUS$^{®}$ requires the knowledge of finite element methods and the following chapter briefly describes the theory of dynamic FEM, the solution schemes that can be employed to solve dynamic problems and numerical models used for solving the winding problem.

5   Finite Element Modeling of Nip Mechanics

Finite element methods have been applied to solve a variety of problems. In order to solve the winding mechanics class of problems an explicit solution scheme is ideal for it can be used to solve both transient and quasi-static problems. Many researchers have applied explicit dynamic FEM procedures to rolling and forming processes (for example, [45-47]. However, the procedure is yet to be utilized in analyzing the winding contact problems and this section discusses about the theory and advantages of using an explicit FEM solution scheme.

5.1   Theory of dynamic FEM

When nonlinearities in the form of geometry, material and boundary are involved, direct integration must be used in order to study the dynamic response of the structure due to the loading condition [48]. The equilibrium equation in finite element methods is typically written as the principle of virtual work as given in Eqn. 5.1.

$$\int_V \sigma : \left(\frac{\partial \delta v}{\partial x} \right) dV - \int_V f^T \cdot \delta v \, dV - \int_S t^T \cdot \delta v \, dS = 0 \qquad (5.1)$$

In dynamic FEM, this principle of virtual work is changed by including the inertial forces effect in the d'Alembert sense and is given in Eqn. 5.2.

$$\int_V \sigma : \left(\frac{\partial \delta v}{\partial x} \right) dV - \int_V \left(f^T - \rho \ddot{u} \right) \cdot \delta v \, dV - \int_S t^T \cdot \delta v \, dS = 0 \tag{5.2}$$

The corresponding finite element equation is expressed as

$$F_{ext} - F_{int} = M \ddot{u} \tag{5.3}$$

This equation at a given time step 'n' is represented as

$$Ma^n = f^n = f^{ext}(d^n, t^n) - f^{int}(d^n, t^n) \tag{5.4}$$

subject to

$$g_I(d^n) = 0, \quad I = 1 \ to \ n_c \tag{5.5}$$

Equation 5.4 represents ordinary differential equations of second order in time and is semi-discrete (discrete in space but not in time). Equation 5.5 is a generalized representation of the 'n_c' displacement boundary conditions and other constraints on the model. These constraints are linear or nonlinear algebraic functions of the nodal displacements. Also, the internal and external nodal forces are functions of nodal displacements and the time. Given this, the time integration of the equations of motion is performed by using implicit or explicit integration methods. In the case of non-linear

dynamics that involves quasi-static or transient systems with multiple contacting interfaces, explicit integration scheme is better suited.

5.1.1 Explicit Scheme

The most popular of the explicit schemes is using a central difference method to perform the time integration of the equations of motion (ABAQUS/Explicit$^{®}$ uses central difference method). Using the central difference method, if the time increments are expressed as shown in Eqn. 5.6, the velocity and acceleration quantities are calculated as shown in Eqn. 5.7.

$$\Delta t^{n+\frac{1}{2}} = t^{n+1} - t^n, t^{n+\frac{1}{2}} = \frac{1}{2}(t^{n+1} + t^n), \Delta t^n = t^{n+\frac{1}{2}} - t^{n-\frac{1}{2}} \tag{5.6}$$

$$d^{n+1} = d^n + \Delta t^{n+\frac{1}{2}} v^{n+\frac{1}{2}} \quad ; \quad v^{n+\frac{1}{2}} = v^{n-\frac{1}{2}} + \Delta t^n a^n \tag{5.7}$$

The equations for updating the nodal velocities and displacements are obtained by substituting Eqn. 5.4 in Eqn. 5.7. and is given in Eqn. 5.8.

$$v^{n+\frac{1}{2}} = v^{n-\frac{1}{2}} + \Delta t^n M^{-1} f^n \tag{5.8}$$

At any time step 'n', the displacements 'd^n' are known. The nodal forces 'f^n' can be determined by sequentially evaluating the strain-displacement equations, the constitutive equation and the nodal external forces. Thus the right hand side of Eqn. 5.8

can be evaluated to get '$v^{n+\frac{1}{2}}$'. The displacements 'd^{n+1}' can then be determined from Eqn. 5.7. Hence, the update of the nodal velocities and the nodal displacements can be accomplished without solving any equations if the mass matrix 'M' is diagonal. Thus in an explicit method, the time integration of discrete momentum equations (Eqn. 5.4) does not require the solution of any equations and hence the computational cost per time increment is relatively small. The avoidance of solution of equations hinges on the use of a diagonal mass matrix.

5.1.2 Advantages of Explicit schemes

Explicit methods require a small time increment size that depends solely on the highest natural frequencies of the model and is independent of the type and duration of loading. Simulations generally take on the order of 10,000 to 1,000,000 increments, but the computational cost per increment is relatively small. Implicit methods do not place an inherent limitation on the time increment size; increment size is generally determined from accuracy and convergence considerations. Implicit simulations typically take orders of magnitude fewer increments than explicit simulations. However, since a global set of equations must be solved in each increment, the cost per increment of an implicit method is far greater than an explicit method. The analysis cost in explicit procedures rises only linearly with problem size, whereas the cost of solving the nonlinear equations associated with implicit integration rises more rapidly than linearly with problem size. Therefore, ABAQUS/Explicit$^{\circledR}$ is attractive for very large problems.

5.2 FEM Model – General Set Up

As mentioned in the previous chapter, the nip mechanics problem will be studied by studying the winding contact problem in steps. In this context, both the static and rolling contact of a nip on a stack of sheets and rolling contact of the nip and a winding roll will be modeled and analyzed separately. The problem set up of these two models is described in the following sections.

5.2.1 Static and rolling contact of a nip and a stack of sheets

Consider a winding problem wherein the wound roll radius is infinite. In such a case, the problem can be studied by approximating the wound roll as a flat stack of sheets. To get a basic understanding of the mechanics of contact and development of the wound on tension and to keep the computational cost lower, a stack of 10 sheets is considered here. The sheets are placed on a rigid plate that does not allow for any vertical rigid body motion. Except for the case wherein the effect of a compliant nip cover is sought, the nip roller is modeled as an analytical rigid body. Each layer is modeled as an individual entity made of a linear elastic material and is allowed to interact with other layers. The whole problem is analyzed in 2D plane strain conditions and a schematic of the model is shown in Fig. 5.1. In the case of static contact between the nip roller and the sheets, a known level nip load is prescribed at the center of rotation of the nip roller and the resulting deformations, stresses and the contact behavior are studied.
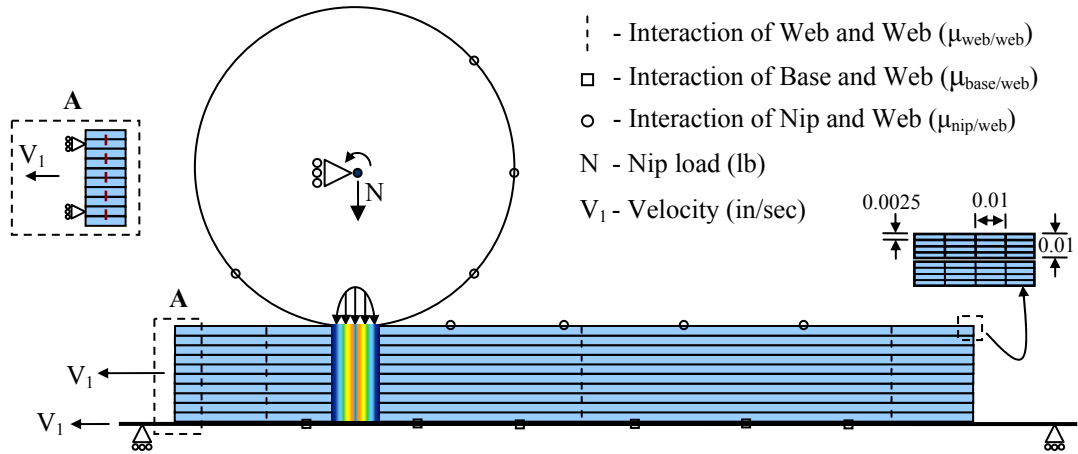
Figure 5.1: A Schematic of the problem set up for the flat bed rolling nip contact problem.

In the case of rolling contact, in addition to prescribing a nip load at the center of rotation of the nip roller, a velocity boundary condition is applied. Let us consider a case in which the nip roller starts rolling with a translational velocity 'V_1' to the right on a stack of 10 sheets clamped at the left end. If one were to observe the rolling process from a coordinate system translating with the center of the nip roller, the rigid base and the left end of the sheets are moving with a velocity 'V_1' to the left. In this case, the center of the nip roller is at rest and the nip roller will be idling about the center of rotation. Hence in the rolling contact case, a constant linear velocity is prescribed to both the rigid base and the left end of the sheets in addition to the prescribing a constant nip load at the center of rotation of the nip roller. The application of the boundary conditions in this way permits easier post processing of the results.

Depending on the nip load, the prescribed translational velocity 'V_1' induces a negligible horizontal force (reaction force opposite to the direction of motion of the sheets at the center of the nip) at the center of rotation of the nip roller due to frictional

losses suffered to overcome the rolling resistance that was caused as a result of the deformation of the sheets. A gravity load is applied to the stack to ensure that the sheets remain in position. The physical and geometrical properties of the bodies used in the model are shown in Table. 5.1.

Property	Value
Number of layers	10
Web length	Variable (Depending on nip load)
Web thickness (Caliper)	0.01 in
Rigid base length	11 in
Rigid nip roller diameter	4 in
Velocity (V_1)	4 in/sec

Table 5.1: Flat bed rolling nip model properties.

5.2.2 Winding contact problem

In a typical winding process, the incoming web under a known tension is fastened to a rigid core and the web is wound on top of the core by applying torque to either the core or the impinged nip roller. A typical wound roll is made up of many layers (often thousands). However winding an entire roll in ABAQUS/Explicit[®] is computationally expensive. In order to study the development of the WOT in a winding roll and get a basic understanding of the contact mechanics of a wound roll, the incoming web layer and a nip roller, the wound roll finite element model is run till five layers are wound onto a rigid core. The whole problem is analyzed in 2D plane strain conditions and a schematic of the model is shown in Fig. 5.2.

44
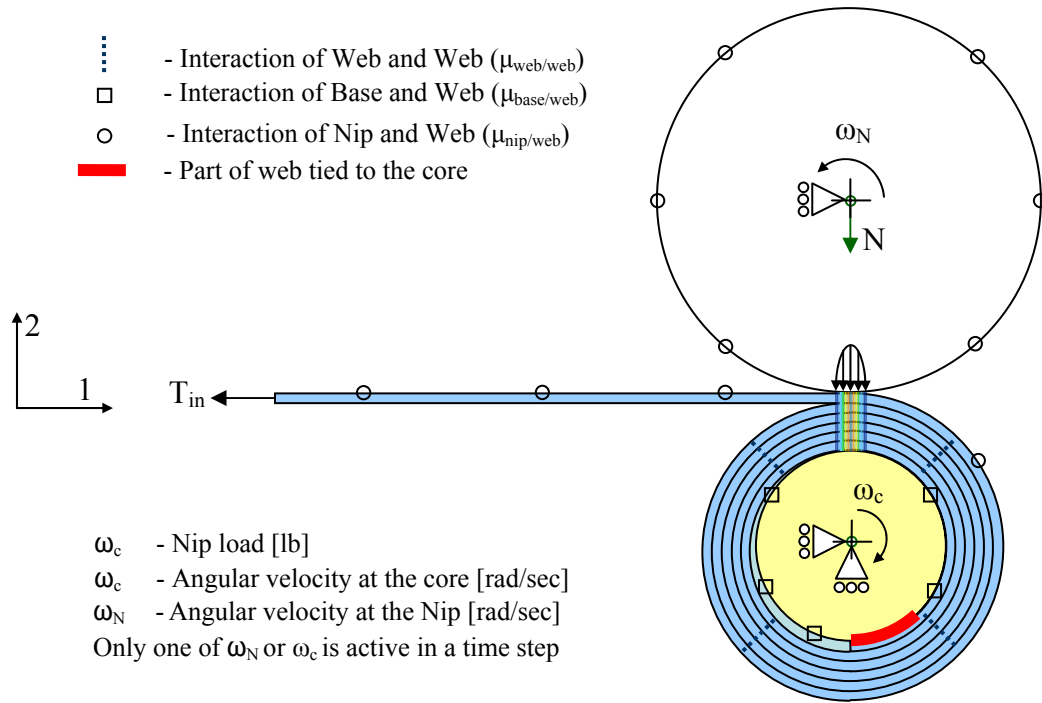
Figure 5.2: A schematic of the problem set up for winding contact problem.

Consider a free sheet of web wrapping a rigid core for 180° and is fastened to the core at its tail end (22.5°) as shown in Fig. 5.2. The web is modeled as a linear elastic material. Given this initial state, the winding process is accomplished in 3 different time steps in the simulation model. In the first step, a known value of load (distributed load 'T$_{in}$' at the end of the sheet) is prescribed at the left end of the sheet. This simulates the web tension in the incoming sheet. In this time step, the center of rotation of the core is fixed in all degrees of freedom while the nip roller is pinned. In the second time step, the nip roller contacts the incoming web under a prescribed nip load 'N'. In this time step the boundary conditions are modified such that the center of rotation of the nip roller is fixed only in the horizontal degree of freedom and is free to move vertically as well as rotate about its axis. This facilitates the application of nip load vertically. In the third step, winding of the roll is accomplished by prescribing an angular velocity to either the nip

roller or the core depending on the type of winding that has to be accomplished. Also, the rotational constraint on the rigid core is removed during this step to facilitate the winding process. The physical and geometric properties of the bodies in the winding model are listed in Table. 5.2. The angular velocity is chosen such that the surface velocity of either the nip or core (depending on the center or surface winding method) is fixed at 6 in/sec.

Property	Value
Web length	55.34 in
Web thickness (Caliper)	0.01 in
Rigid core diameter	3.4 in
Rigid nip roller diameter	4 in (or) 10 in
Angular velocity (ω_N or ω_c)	3 (4 in nip) or 3.53 rad/sec 1.2 (10 in nip) or 3.53 rad/sec

Table 5.2: Winding model properties.

5.2.3 Element Behavior

ABAQUS/Explicit$^®$ has four-noded isoparametric quadrilateral elements for two-dimensional explicit dynamic analysis. ABAQUS/Explicit$^®$ also offers these elements in both full and reduced integration types. For the first-order elements, the single-point reduced-integration scheme is based on the "uniform strain formulation": the strains are not obtained at the first-order Gauss point but are obtained as the (analytically calculated) average strain over the element volume. The uniform strain method, first published by Flanagan and Belytschko [49] ensures that the first-order reduced-integration elements pass the patch test and attain the accuracy when elements are skewed. A patch test is a

test of mesh convergence for a set of elements that are arbitrarily oriented. The results are compared with exact solutions for a set of displacement boundary conditions applied at the nodes. The element shall pass the patch test if the two results match exactly.

Reduced integration means that an integration scheme that is one order less than the full scheme is used to integrate the element's internal forces and stiffness. Superficially this appears to be a poor approximation, but it has proved to offer significant advantages. For first-order elements the uniform strain method yields the exact average strain over the element volume. Not only is this important with respect to the values available for output, it is also significant when the constitutive model is nonlinear, since the strains passed into the constitutive routines are a better representation of the actual strains. Also, the reduced integration lowers the cost of forming an element.

The deficiency of the reduced integration is that, except in one dimension and in axisymmetric geometries modeled with higher than first-order elements, the element stiffness matrix will be rank deficient. This most commonly exhibits itself in the appearance of singular modes ("hourglass modes") in the response. These are nonphysical response modes that can grow in an unbounded way unless they are controlled. In ABAQUS® the artificial stiffness method and the artificial damping method given by Flanagan and Belytschko [49] are used to control the hourglass modes in these elements. These methods help the reduced integration elements from exhibiting spurious energy modes. The use of reduced integration elements reduce the total computational time of a given problem as there are not as many integration points to compute the

deformations and stresses at. However, this also means that, if a single element is used to model the thickness of a layer, the strains and stresses through the depth of the layer would be uniform. If bending of the layer is to be simulated it is necessary to use at least two elements through the depth of the web. The stresses and strains obtained at integration points (same as the centroid for reduced integration elements) will have to be extrapolated in order to compute the surface strains and stresses. It should be noted that, in both the flat bed nip mechanics and winding nip mechanics models, a uniform meshing technique is used for meshing the web layers. The rigid bodies are modeled as analytical rigid objects within the model.

5.3   Material constants and constitutive behavior

Webs, typically, are strongly anisotropic and past researchers have made the assumption of orthotropic material behavior for materials like paper, films, etc. A 1000 gage (0.01 inches) PET (Polyethylene terapthalate) film with a density of 0.06 lb/in^3 was chosen for this research. The following sections discuss the material properties of this PET film.

5.3.1   In-Plane Modulus (E_{11}, E_{33})

For most webs, the in-plane moduli of the web are much higher than the out-of-plane modulus. Typically, the in-plane modulus of a material is measured based on ASTM D882 [50]. The in-plane moduli 'E_{11}' and 'E_{33}' measured per ASTM standards for PET film was 700,000 Psi and 740,000 Psi respectively (as quoted by the manufacturer).

However, the modulus measurements [51] made using a stretch test is much more representative of the in-plane modulus of the web in the wound rolls than those measured using ASTM tests. In a stretch test, a 50 ft sample of web is stretched and the load and deformation or simultaneously recorded and the modulus is calculated as the slope of the stress-strain curve. One of the advantages of the stretch test is that it eliminates the end effects. The results of the stretch test for this web is shown in Fig. 5.3 and the in-plane modulus (E_{11}) is calculated to be 710,000 Psi. The other in-plane modulus (E_{33}) was set at 740,000 Psi. (Material orientation is shown in Fig. 5.3)
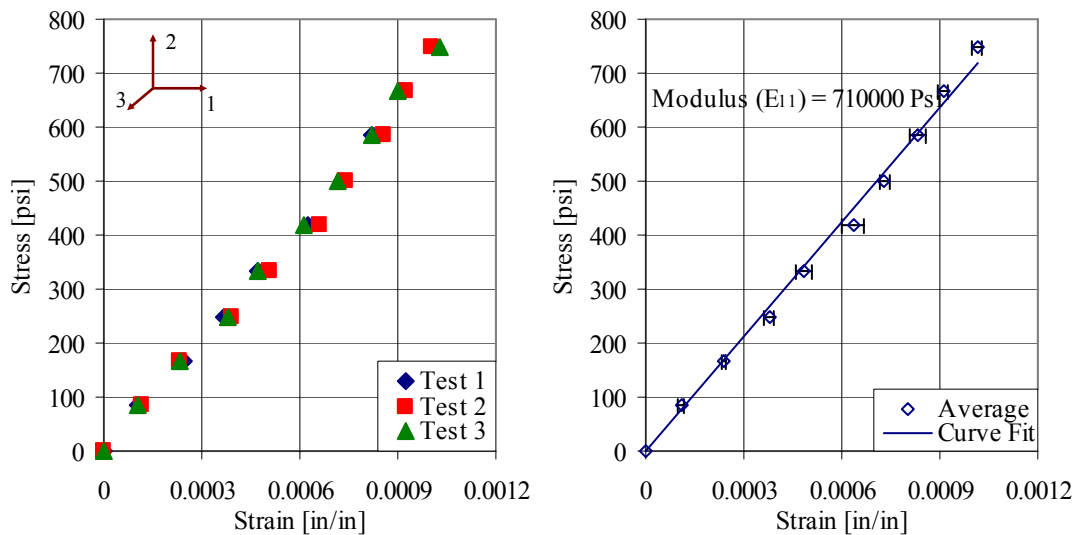
Figure 5.3: In-plane modulus (E_{11}) measurement by stretch test.

5.3.2 Out-of-plane Modulus (E_{22} or E_r)

The behavior of the out-of-plane modulus (modulus in the radial direction of a wound roll, also known as radial modulus) of webs has been shown to be non-linear [52]. The compressive strain varies exponentially with increase in compressive load and

49

Pfeiffer [52] showed this behavior in stacks of different grades of paper. Pfeiffer approximated the behavior of compressive strain for a web stack using Eqn. 5.9. 'K_2' is referred to as the '*springiness factor*'. The advantage of using this type of curve-fit for radial modulus is the ability to compare different webs when values of 'K_2' are known. The radial modulus is estimated as the slope of the pressure-strain curve and is given in Eqn. 5.10. Compression tests were conducted on a one inch high stack of PET webs that were cut into 6 X 6 in^2 coupons and stacked on top of each other. The stress-strain behavior is shown in Fig. 5.4. The estimated value of radial modulus (per Eqn. 5.10) is also shown in Fig. 5.4. Curve fit using Pfeiffer's expression results in a value of 120 for K_2.

$$P = K_1 \left[e^{K_2 \varepsilon_2} - 1 \right] \tag{5.9}$$

$$E_2(P) = \frac{dP}{d\varepsilon_2} = K_1 K_2 e^{K_2 \varepsilon_2} = K_2 (K_1 + P) \tag{5.10}$$
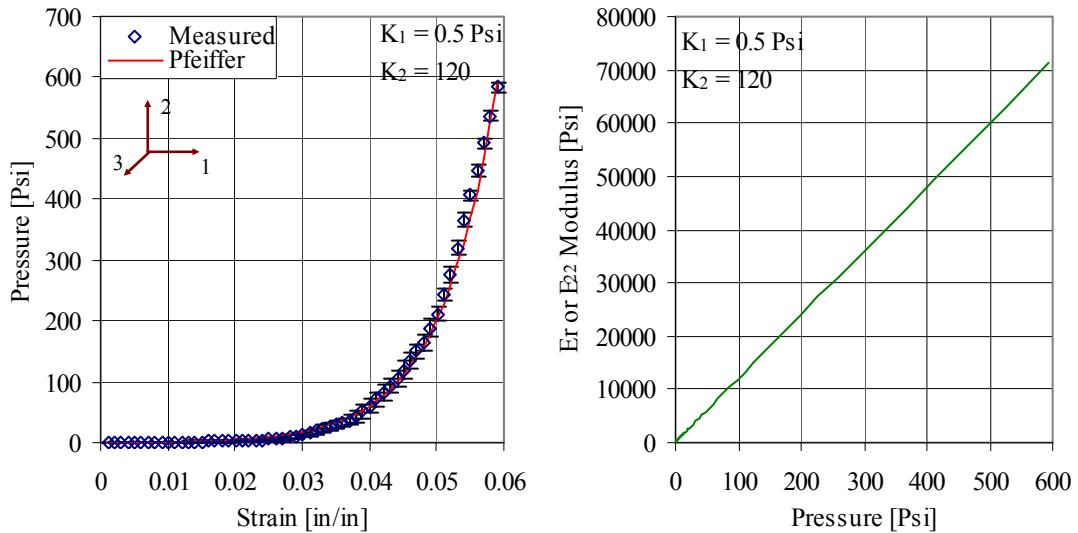
Figure 5.4: Stress-strain behavior during compression of a web stack.

5.3.3 Poisson's ratio and Shear Modulus (v_{13}, v_{12}, v_{23} and G_{12})

From various references [53-55], the in-plane Poisson's ratio 'v_{13}' was found to be between 0.29 and 0.39 and a value of 0.36 was chosen for this analysis. Choosing values for out-of-plane Poisson's ratio (v_{12}) and out-of-plane shear modulus (G_{12}) was not a straightforward task as these properties are extremely difficult to measure (for example, [11],[56]). The out-of-plane Poisson's ratio (v_{12}) governs the thinning of the web when the web is subjected to a tensile load in the machine direction (11). Generally, the value of 'v_{12}' is assumed to be a constant for film webs and is in the range of 0.3-0.4. Feng and Farris [53] measured a value of 0.41 for 'v_{12}' for PET film. However this value was measured for a single film. For wound roll modeling this parameter has to be measured in a web stack. Jorkama [57] assumes this value to be 0.25 for paper webs.

In this research, a value of 0.3 will be used for 'v_{12}'. Good [11] measured the out-of-plane Poisson's ratio and found it to be state dependent. He showed that the ratio asymptotically approached values near 0.01 for increasing values of pressure. Maxwell's relation (Eqn. 5.11) is automatically enforced by ABAQUS/Explicit$^{®}$ and hence, 'v_{21}' is calculated based on the values of E_{11}, v_{12}, and E_{22}. Since 'E_r' increases linearly with pressure, 'v_{21}' also varies linearly with pressure and this will be discussed in section 5.3.5.

$$\frac{v_{12}}{E_1} = \frac{v_{21}}{E_2} \quad or \quad \frac{v_{r\theta}}{E_\theta} = \frac{v_{\theta r}}{E_r} \tag{5.11}$$
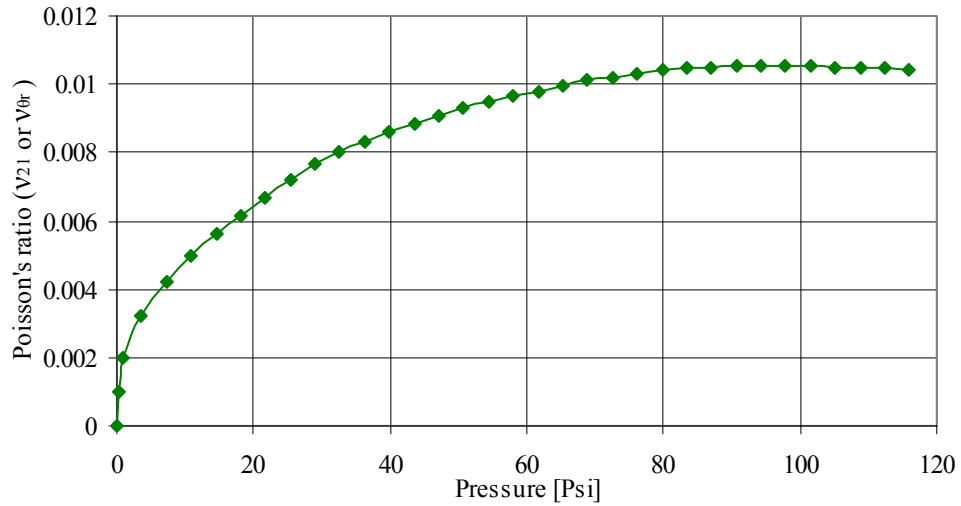
Figure 5.5: State dependency of Poisson's ratio (ν_{21} or $\nu_{r\theta}$) on pressure (a line curve using selected data points from the original publication is shown here).

The most difficult property to establish was the out-of-plane shear modulus 'G_{12}'. In a two dimensional analysis only one value of shear modulus is required and it is the out-of-plane shear modulus 'G_{12}'. For paper webs, Jorkama [10] chose the value of 'G_{12}' based on winding test results. In his case, he iterated on 'G_{12}' in his WOT model such that the model results for the WOT matched with experimental results at the highest nip load level. He retained this value for all the other nip load cases. Feng and Farris [53] measured this value at 23000 Psi and Okabe et al [54] measured this value at 145000 Psi. However they both measured this value for a single film and they recognize that this property was measured with the least accuracy.

Cheng and Cheng [58] state two different formulations to empirically predict the in-plane shear modulus from elastic moduli and Poisson's ratio. These formulations were originally used by St. Venant and are given in Eqns. 5.12 and 5.13 respectively. Saliklis

[59] compared experimental measurements of shear modulus measurements in plywood panels an expression similar to that shown in Eqn. 5.13. For PET film used in this research, Eqn. 5.12 predicts a value of 2367 Psi and Eqn. 5.13 predicts a value of 20000 Psi when used to compute the value out-of-plane shear modulus 'G_{12}'. Since the radial modulus is state dependent on pressure, Eqns 5.12, 5.13 indicate that 'G_{12}' will also be state dependent on pressure. However, the values of 'G_{12}' given above were calculated for a nip load value of ≈20 Pli. At this value of nip load the average pressure in the contact zone is 19.8 Psi and the radial modulus calculated from this average pressure value is equal to 2382 Psi.

In this dissertation, a constant value of 2367 Psi will be used for 'G_{12}' unless otherwise stated to keep the independent variables to a minimum. All the material constants are summarized in Table. 5.3 and any deviation from this data will be mentioned wherever they occur. Note that the values of G_{13}, G_{23} and v_{23} are set arbitrarily to 1000 Psi, 1000 Psi and 0.01 respectively as they do not affect the 2-D plane strain equations.

$$G_{12} = \frac{E_1 E_2}{E_1(1+v_{21}) + E_2(1+v_{12})} \tag{5.12}$$

$$G_{12} = \frac{\sqrt{E_1 E_2}}{2\left(1+\sqrt{v_{12}v_{21}}\right)} \tag{5.13}$$

Material Constant	Value
E_1, E_3	710000, 740000 Psi
E_2 (Pfeiffer Representation)	120 (0.01 + P) Psi, P-Pressure [Psi]
ν_{13}, ν_{12}, ν_{23}	0.36, 0.3, 0.01
G_{13}, G_{12}, G_{23}	1000, 2367, 1000 Psi

Table 5.3: Material properties of 1000 gage PET film.
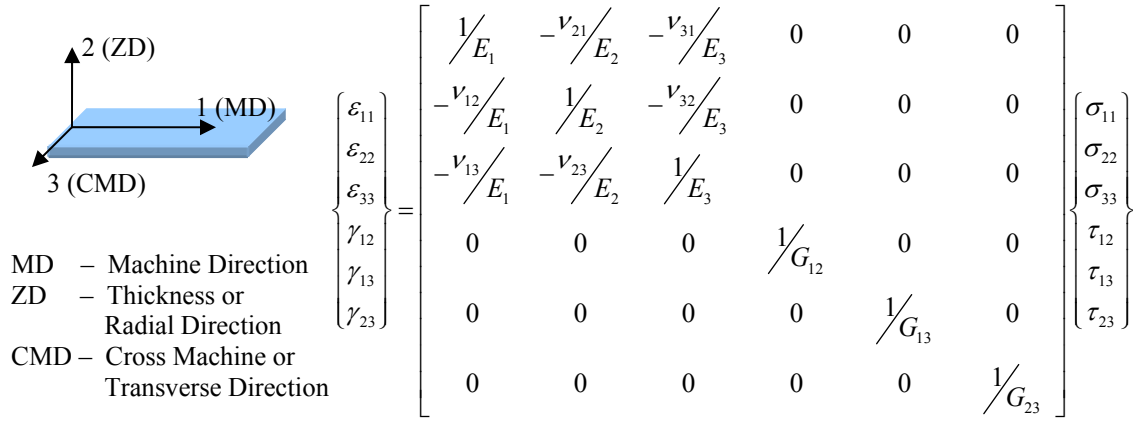
5.3.4 Material Constitutive Behavior

In the analysis, a linear orthotropic constitutive relationship is used to model the material behavior and the material orientation and the compliance matrix is shown in Fig. 5.6. In the preceding section the non-linearity of the radial modulus 'E_r' was presented. If this behavior is to be included in ABAQUS/Explicit[®], a material subroutine has to be written. On the other hand, if one can estimate an average 'E_r' through the contact zone for different nip loads, this average value can be set for the out-of-plane modulus 'E_{22}' in the constitutive relationship. Setting an average value of 'E_r' greatly reduces the computational time in comparison to executing a material subroutine for each element. The estimation of 'E_r' based on the average pressure in the nip contact zone that occurs due to the contact mechanics of the nip roller and web stack is presented in the following section. The estimated value of 'E_r' satisfies the material stability criterion given in Eqns. 5.14-5.16.

$$E_1, E_2, E_3, G_{12}, G_{13}, G_{23} > 0 \tag{5.14}$$

$$|v_{ij}| < \sqrt{\frac{E_i}{E_j}} \; ; \; \frac{v_{ij}}{E_i} = \frac{v_{ji}}{E_j} \; \forall \; i,j = 1,2,3 \; and \; i \neq j \qquad (5.15)$$

$$1 - v_{12}v_{21} - v_{23}v_{32} - v_{13}v_{31} - 2v_{21}v_{32}v_{13} > 0 \qquad (5.16)$$

2 (ZD)

1 (MD)

3 (CMD)

MD – Machine Direction
ZD – Thickness or
      Radial Direction
CMD – Cross Machine or
      Transverse Direction

$$
\begin{Bmatrix} \varepsilon_{11} \\ \varepsilon_{22} \\ \varepsilon_{33} \\ \gamma_{12} \\ \gamma_{13} \\ \gamma_{23} \end{Bmatrix} =
\begin{bmatrix}
1/E_1 & -v_{21}/E_2 & -v_{31}/E_3 & 0 & 0 & 0 \\
-v_{12}/E_1 & 1/E_2 & -v_{32}/E_3 & 0 & 0 & 0 \\
-v_{13}/E_1 & -v_{23}/E_2 & 1/E_3 & 0 & 0 & 0 \\
0 & 0 & 0 & 1/G_{12} & 0 & 0 \\
0 & 0 & 0 & 0 & 1/G_{13} & 0 \\
0 & 0 & 0 & 0 & 0 & 1/G_{23}
\end{bmatrix}
\begin{Bmatrix} \sigma_{11} \\ \sigma_{22} \\ \sigma_{33} \\ \tau_{12} \\ \tau_{13} \\ \tau_{23} \end{Bmatrix}
$$

Figure 5.6: Linear orthotropic constitutive relationship used in the model.

5.3.5 Estimation of an radial modulus in the contact zone

Consider a two-dimensional static contact of cylinders wherein one of the cylinders is rigid and the other is rigid with an elastic cover on top. This can be modeled by approximating the problem into a contact problem of a rigid cylinder with an elastic layer resting on a rigid base as shown in Fig. 5.7. When the contact width is much greater than the cover thickness, it is reasonable to assume that the deformation through the layer is homogenous, i.e. plane sections remain plane after compression, so that the 'σ_{11}' is uniform through the thickness. Since in both the flat bed and the winding models only a few layers are modeled, the thickness of the elastic layer (combined thickness of all the layers) 'b' is much less compared to the half width of contact 'a'.
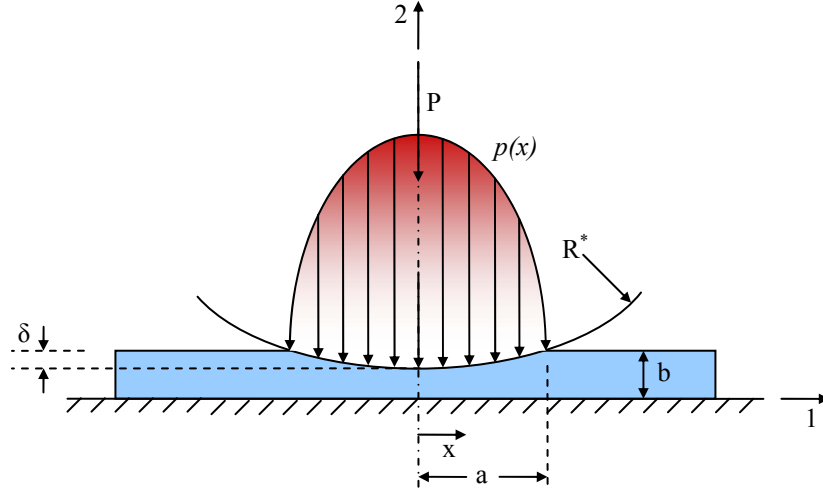
Figure 5.7: Static contact between a rigid cylinder and an elastic half-space.

Typically the effect of friction on normal pressure in the contact zone is minimal [41]. Assuming a frictionless contact between the rigid nip roller and the elastic layer results in '$\sigma_{11}(x)$' being zero in the contact zone. Hence the compressive strain in the contact zone shall be expressed as given in Eqn. 5.17.

$$\varepsilon_2(x) = -\frac{1-v^2}{E^*}\sigma_2(x) = \frac{1-v^2}{E^*}p(x) \tag{5.17}$$

Based on the geometry of the deformation, the compressive strain shall be written as

$$\varepsilon_2(x) = \frac{\delta - \dfrac{x^2}{2R^*}}{b} \tag{5.18}$$

In the above equations, the composite values for moduli and radii are used as given in Eqn. 5.19.

$$E^* = \left[\frac{1}{E_{layer}} + \frac{1}{E_{nip}} \right]^{-1} \quad , \quad R^* = \left[\frac{1}{R_{layer}} + \frac{1}{R_{nip}} \right]^{-1} \qquad (5.19)$$

Since the pressure must fall to zero at the edges of contact (x = ±a), Eqn. 5.17 and Eqn. 5.18 shall be used to express the indentation 'δ' as a function of half width of contact 'a' and hence, the compressive strain as expressed in Eqn. 5.20.

$$\delta = \frac{a^2}{2R^*} \quad \text{and} \quad \varepsilon_2(x) = \frac{a^2}{2R^* b} \left(1 - \frac{x^2}{a^2} \right) \qquad (5.20)$$

Substitution of Eqn. 5.20. in Pfeiffer's Eqn. 5.9 leads to

$$p(x) = K_1 \left[e^{\left[K_2 \left[\frac{a^2}{2R^* b} \left(1 - \frac{x^2}{a^2} \right) \right] \right]} - 1 \right] \qquad (5.21)$$

Integration of Eqn. 5.21 through the width contact results in nip load per unit width as given in Eqn. 5.22.

$$P = \int_{-a}^{a} K_1 \left[e^{\left[K_2 \left[\frac{a^2}{2Rb} \left(1 - \frac{x^2}{a^2} \right) \right] \right]} - 1 \right] dx = K_1 \left\{ \left[\left(\sqrt{\frac{2\pi R^* b}{K_2}} \right) e^{\frac{K_2 a^2}{2R^* b}} Erf \left(\sqrt{\frac{K_2 a^2}{2R^* b}} \right) \right] - 2a \right\} \qquad (5.22)$$

If the Pfeiffer coefficients 'K$_1$', 'K$_2$', the nip load per unit width 'P' and the layer thickness 'b' is known, the half width of contact 'a' can be iterated to arrive at the correct

57

value of 'a' for a given nip load 'P'. Once the contact width is determined, the pressure distribution through the contact zone is given by Eqn. 5.21. Using the average value of the contact pressure in Eqn. 5.10, the radial modulus can be computed for a nip load level and this value shall be used in both winding and flat bed analysis. The behavior of the half width of contact and radial modulus as a function of nip load is shown in Fig. 5.8. It should be noted that the wound roll radius was set to infinity while iterating on 'a' to compute radial modulus.
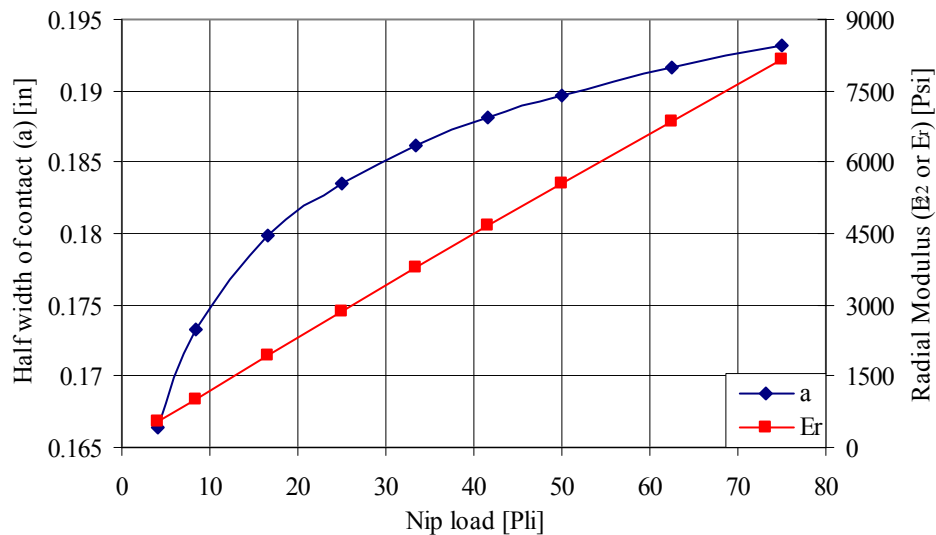
Figure 5.8: Radial modulus for a given nip load based on average contact pressure

The value of 'b' was set to 0.1 inches in both the flat bed and winding models while the radius of the nip roller was set at 4 inches in order to compute the radial modulus. In the winding model, a 10 inch diameter nip roller is used in order to study the effect of nip load on the WOT. Also, in the winding model only five layers are wound on top of the core. In the winding model, when the values of 'b' and nip roller diameter were set to the above values, they yielded values of 'E_r' comparable to that shown in Fig. 5.8.

at all nip loads. Hence 'E_r' shown in Fig. 5.8 is used in the winding model. Since 'v_{12}'

and 'E_1' are constants and Maxwell's relation is enforced by ABAQUS/Explicit®,

'v_{21}'depends on 'E_r'. The variation of 'v_{21}'with nip load is shown in Fig. 5.9. In general,

at all nip loads this value is very small compared to 'v_{12}'. Also, note that this value will

not affect the computation of 'G_{12}' as it is negligible in Eqn. 5.12.
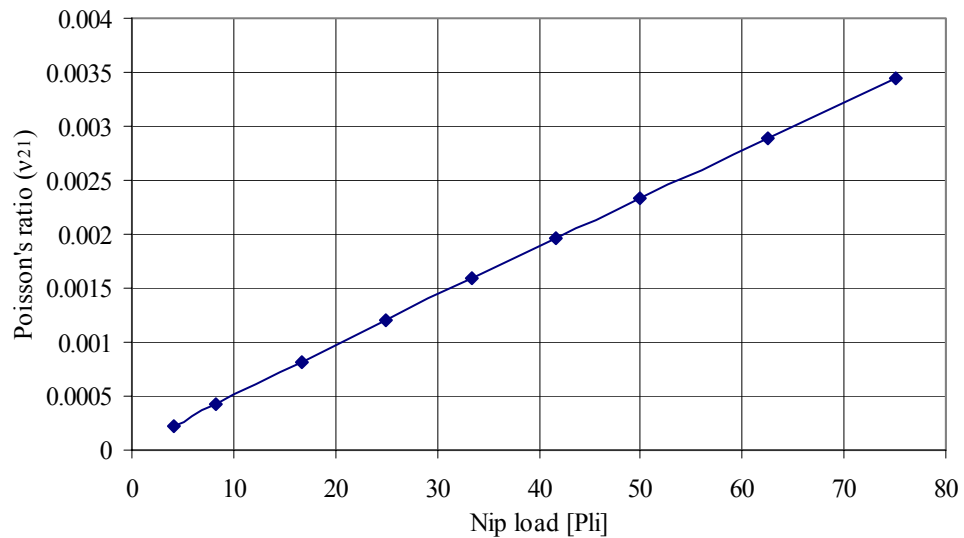
Figure 5.9: State dependency of out-of-plane Poisson's ratio (v_{21})

5.3.6 Coefficient of Friction

Typically the static and kinetic coefficient of friction values are measured using

ASTM D1894 standard test. This test is schematically described in Fig. 5.10. In this test,

a square puck of 2X2 in^2 area with a weight of 2.2 lb is used to measure the coefficient of

friction per the specifications. The puck is made of aluminum and has similar surface

characteristics as that of the rigid aluminum nip roller that shall be used in experiments.

One end of the puck is attached to a load cell through a flexible string. A single sheet of

web is placed on a rigid base that can traverse horizontally at a specified constant speed

of 6 in/min. The puck is placed on top of the web and as the rigid base starts traversing

from left to right, the weight of the puck keeps it in the same place and at the same time,

the force on the string is measured by the load cell fixed rigidly to the left end. The

friction coefficient is then calculated based on Amontons-Coloumb law of friction

($F=\mu N$). When a bare aluminum puck is used, the friction measured is equivalent to the

coefficient of friction between the nip roller and the web and when the aluminum puck is

covered with the web, the friction measured is equivalent to the coefficient of friction

between the web layers.
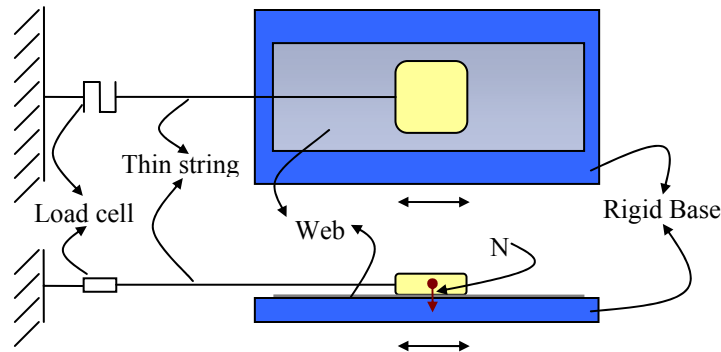
Figure 5.10: Schematic of the friction measurement set up per ASTM standards

In Fig. 5.11., the results of the ASTM standard test for measuring coefficient of

friction is shown. The static coefficient of friction is calculated as the maximum value of

the measured friction and the kinetic coefficient of friction is calculated as the average

value of the friction from Fig. 5.11. Based on ASTM measurements, the results show that

the values of the kinetic coefficient of friction '$\mu_{Nip/Web}$' and '$\mu_{Web/Web}$' are 0.18 and 0.22

respectively.
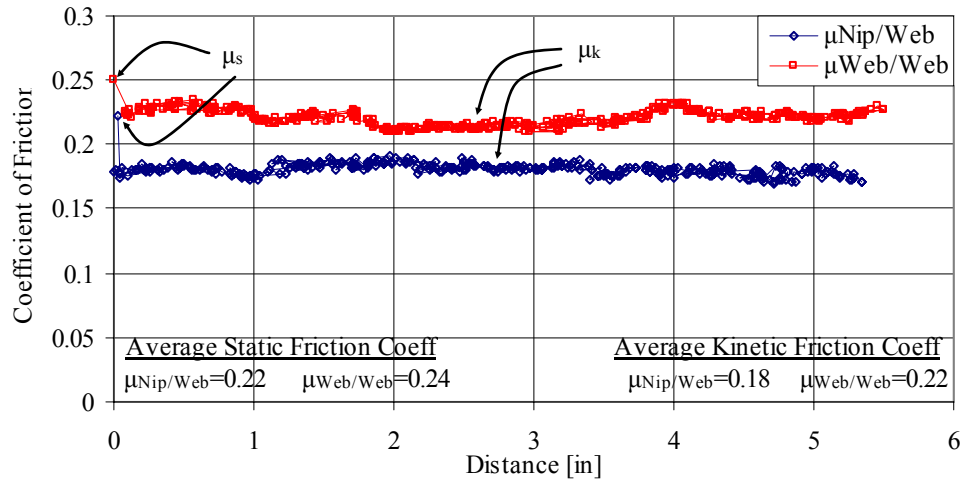
Figure 5.11: ASTM test measurements for coefficient of friction

The friction factors were also measured using an alternate method that involves a band-brake type set up as shown in Fig. 5.12. In this case the web wraps the nip roller at 90° or 180° with a force gage attached to one end. On the other end a known set of weights is hung. Using the force gage the web is pulled around the fixed nip roller while the force required to pull is recorded. The average values of the static and kinetic coefficients of friction '$\mu_{Nip/Web}$' are calculated at both wrap angles using the equation shown in Fig 5.12. For the measurement of '$\mu_{Web/Web}$', the test is conducted with the nip roller surface wrapped with the same type of web. Using this type of test, the static coefficient of friction values, namely, '$\mu_{Nip/Web}$' and '$\mu_{Web/Web}$' are measured at 0.23, 0.25 and the kinetic coefficient of friction values, namely, '$\mu_{Nip/Web}$' and '$\mu_{Web/Web}$' are measured at 0.18, 0.23 respectively.

Unless otherwise specified, a value of 0.18 will be used for the kinetic coefficient of friction '$\mu_{Nip/Web}$' in all the computations. Although both ASTM and the band-brake type friction tests yield a value of ≈0.22 for the kinetic coefficient of friction '$\mu_{Web/Web}$', a

value of 0.16 will be used in all the computations unless otherwise specified. This value was obtained from flat bed experimental measurements of NIT and the reason for using this value will be discussed in Chapter 7 (Experimental Verification).
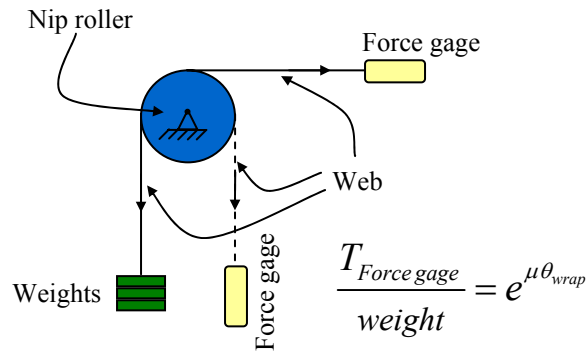
Figure 5.12: Band-brake type friction test

5.4 Interface Modeling

ABAQUS/Explicit[®] provides two algorithms for modeling contact and interaction problems: the general contact algorithm and the contact pair algorithm. The general or automatic contact algorithm allows for very simple definitions of contact with very few restrictions on the types of surfaces involved. The contact pair algorithm has more restrictions on the types of surfaces involved and often requires careful definition of contact; however, it allows for some interaction behaviors that are not available with the general contact algorithm. In general, the contact pair algorithm is computationally expensive compared to the general contact algorithm but is better suited when accurate contact definition is required and hence the contact pair algorithm will be used in this analysis.

5.4.1   Contact Formulation

By default, all contact pairs in an ABAQUS/Explicit® simulation use a kinematic predictor/corrector contact algorithm to strictly enforce contact constraints [60] (for example, no penetrations are allowed). However, in some situations, a penalty contact algorithm is needed. Both the kinematic and penalty methods are constraint enforcement methods and they conserve momentum between the contacting bodies. The following sections briefly describe these algorithms.

5.4.1.1   Kinematic Contact Algorithm

In a contact pair algorithm, there are two contact surfaces, a master surface and a slave surface. Typically rigid bodies act as master surfaces and elastic bodies act as slave surfaces. The kinematic contact algorithm uses a predictor/corrector algorithm. In each increment of the analysis, the kinematic state of the model is first advanced into a predicted configuration without considering the contact conditions. Then, in the predicted configuration, the slave nodes that penetrate the master surface are identified. The depth of each slave node's penetration, the mass associated with it, and the time increment are used to calculate the resisting force required to oppose the penetration. This is the force which, had it been applied using the increment, would have caused the slave node to exactly contact the master surface.

The resisting forces of all the slave nodes are then distributed to the nodes on the master surface as generalized forces. The mass of each contacting slave node is also distributed to the master surface nodes and added to their mass to determine the total

inertial mass of the contacting interfaces. These distributed forces and masses are used to calculate an acceleration correction for the master surface nodes. Acceleration corrections for the slave nodes are then determined using the predicted penetration for each node, the time increment, and the acceleration corrections for the master surface nodes. One set of corrections is calculated considering one surface as the master surface, and the other corrections are calculated considering that same surface as the slave surface. An average of the two values is then used to obtain a corrected configuration in which the contact constraints are enforced. However, after the initial correction is applied, it is possible to still have some penetration of the surfaces. Therefore, a second contact correction is used to resolve any remaining overclosure. Both master–slave assignment combinations are again considered to form the second applied acceleration correction.

5.4.1.2   Penalty Contact Algorithm

In situations where the master surface is a rigid surface with multi-point constraints defined, penalty contact method must be used (for example, an elastic layer tied to a rigid core). The penalty contact algorithm has a weaker enforcement of contact constraints but allows for treatment of more general types of contact. The penalty contact algorithm searches for slave node penetrations in the current configuration. Contact forces that are a function of the penetration distance are applied to the slave nodes to oppose the penetration, while equal and opposite forces act on the master surface at the penetration point. The "spring" stiffness that relates the contact force to the penetration distance is chosen automatically by ABAQUS/Explicit for hard penalty contact, such that

the effect on the time increment is minimal yet the allowed penetration is not significant in most analyses.

Although both kinematic and penalty contact methods conserve momentum between the contacting bodies, the kinematic contact model is advantageous to use due to computational time constraints. This is because the critical time increment is unaffected when kinematic contact method is used. In case of a penalty approach, the use of a large scale factor is likely to increase the computational time required for an analysis because of the reduction in the time increment that is necessary to maintain numerical stability. In general, a kinematic contact algorithm is used to define all contacting interfaces in the simulation model. The only exception is the interface between the rigid core and the incoming web wherein a part of the incoming web is tied to the core using a tie-type constraint. Self contact is used in the context of a surface folding and touching itself. Appropriate contact elements are generated internally for each node on the surface [61]. A node is allowed to contact all of the surface segments, with the exception of the segments that are adjacent to the node. Since a node is simultaneously a master and a slave (producing symmetric master-slave relationships), overconstraints would occur, for example, if the meshes on both sides of the interface matched exactly. If only a pair of nodes matches in two dimensions, no problem occurs due to the smoothing carried out on the master side of the interface. When two adjacent segments of the surface fold forming a sharp crack, the contact algorithm becomes pure master-slave instead of symmetric to prevent redundant contact constraints. It has been arbitrarily chosen that of these two segments the shortest is the slave and the longest is the master.

5.4.2 Contact Interaction: Normal and Tangential Behavior

The interaction between contacting surfaces consists of two components: one normal to the surfaces and one tangential to the surfaces. The tangential component consists of the relative motion of the surfaces and, possibly, frictional shear stresses and the normal component consist of the penetration between the surfaces. The normal contact is handled using hard contact model which assumes that the surfaces transmit no contact pressure unless the nodes of the slave surface contact the master surface. When in contact, there is no limit on the contact pressure that can be transmitted between the surfaces. The surfaces separate if the contact pressure reduces to zero and separated surfaces can come back into contact when the clearance between them reduces to zero. When surfaces are in contact they usually transmit shear as well as normal forces across their interface. The relationship between the two force components is expressed in terms of the stresses at the interface of the bodies. The tangential behavior between all contacting surfaces is modeled using a balanced kinematic master-slave contact algorithm [62] with finite sliding. The finite sliding formulation allows for any arbitrary motion between the surfaces involved.

5.4.3 Frictional Behavior

The friction between all contacting surfaces is modeled using the Coulomb's friction law provided by ABAQUS/Explicit, with a constant coefficient of friction. The basic concept of the Coulomb friction model is to relate the maximum allowable frictional (shear) stress across an interface to the contact pressure between the contacting bodies. In the basic form of the Coulomb friction model, two contacting surfaces can

carry shear stresses up to a certain magnitude across their interface before they start sliding relative to one another; this state is known as sticking. This is schematically represented in Fig. 5.13.
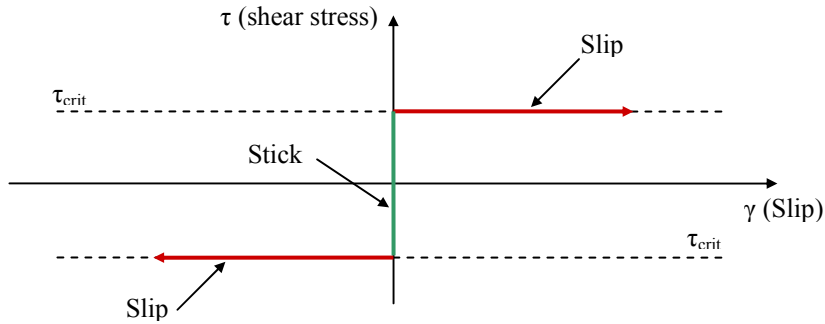
Figure 5.13: Schematic representation of a Coulomb friction model.

The Coulomb friction model defines this critical shear stress 'τ_{crit}' as the stress at which sliding of the surfaces starts as a fraction of the contact pressure '$p(x)$' between the surfaces as given in Eqn. 5.23. The stick/slip calculations determine when a point moves from sticking to slipping or from slipping to sticking.

$$\tau_{crit} = \mu\, p(x) \tag{5.23}$$

5.4.4 Constraints

Constraints are required to model the objects that are tied to each other. For instance, in the case of the contact between the incoming web sheet and the core during the start of the computational process requires at least a part of the web to be tied to the

core to prevent rigid body motion. This is handled using surface-based tie constraint in ABAQUS/Explicit®. A surface-based tie constraint ties the translational and rotational degrees of freedom between two surfaces. Typically the rigid surface is treated as the master surface and the elastic surface is treated as the slave surface.
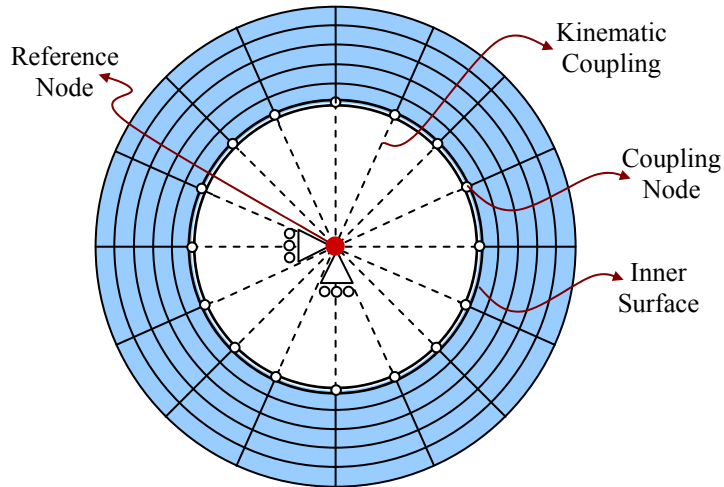
Figure 5.14: A Schematic representation of kinematic coupling constraints.

When nip rollers with compliant covers need to be modeled, surface based coupling constraints can be utilized. The surface based coupling provides coupling between a reference node and a group of nodes referred to as the 'coupling nodes'. The coupling constraint is useful when a group of coupling nodes is constrained to the rigid body motion of a single node. Kinematic coupling constraint can be applied to user specified degrees of freedom at the coupling nodes with respect to the global or local coordinate system. Kinematic constraints are imposed by eliminating the degrees of freedom of the coupling nodes. Thus in the case of nip rollers with compliant covers, the

inner surface of the compliant cover can be kinematically coupled to the center of rotation (called the reference node) of an imaginary rigid body of same inner radius and by imposing the boundary conditions on the reference node as shown in Fig. 5.14.

5.5   Loading rates and Damping

The actual time taken for a physical process is called its natural time. Generally, it is safe to assume that performing an analysis in the natural time for a quasi-static process will produce accurate static results. If the real-life event actually occurs in a natural time scale in which velocities are zero at the conclusion, a dynamic analysis should be able to capture the fact that the analysis has achieved a steady state. One can increase the loading rate so that the same physical event occurs in less time as long as the solution remains nearly the same as the true static solution and dynamic effects remain insignificant. In some cases damping can reduce these dynamic effects and with careful selection of the damping properties, the solution may not be significantly changed, yet facilitate faster computational times.

5.5.1   Loading Rates

For accuracy and efficiency, quasi-static analysis requires the application of loading that is as smooth as possible. Sudden, jerky movements cause stress waves, which can induce noisy or inaccurate solutions. Applying the load in the smoothest possible manner requires that the acceleration changes only a small amount from one

increment to the next. If the acceleration is smooth, it follows that the changes in velocity and displacement are also smooth. In order to reduce the oscillatory behavior of these parameters, the displacement and load boundary conditions are ramped to their final values smoothly. The amplitude of a given boundary condition at any given time during the ramping stage is calculated using Eqn. 5.24. The boundary conditions as a function of time in both the flat bed model and winding model are shown in Fig. 5.15.
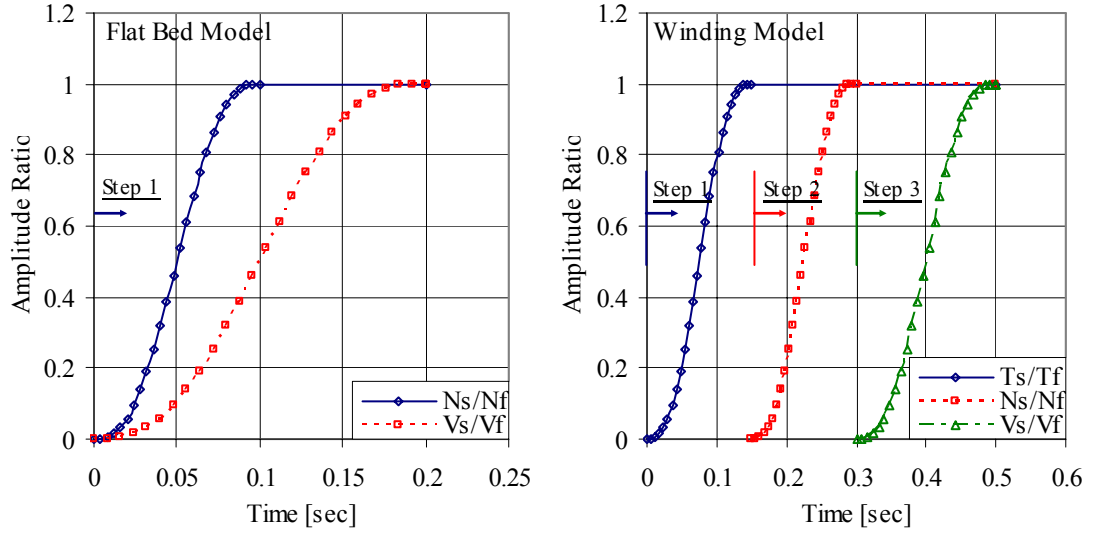
Figure 5.15: Loading rates in flat bed and winding models (Legend: s-start, f-final; N – Nip load, V – Velocity, T – Tension).

$$A(t) = A_s + (A_f - A_s)\,\xi(t)^3\,(10 - 15\,\xi(t) + 6\,\xi(t)^2) \;;\; \xi(t) = \frac{t - t_s}{t_f - t_s} \qquad (5.24)$$

5.5.2 Damping

Typically, damping is used for two reasons in dynamics analysis. One is to limit the numerical oscillations in the system and the other is when physical damping is

required. ABAQUS/Explicit adds a bulk viscosity damping to the model by default. The bulk viscosity introduces damping associated with the volumetric straining. Its purpose is to improve the modeling of high-speed dynamic events. There are two forms of bulk viscosity in ABAQUS/Explicit. The first is found in all elements and is introduced to damp the "ringing" in the highest element frequency. This damping is sometimes referred to as truncation frequency damping. It generates a bulk viscosity pressure, which is linear in the volumetric strain and is given in Eqn. 5.25.

$$p_l = b_1 \, \rho \, c_d \, L^e \, \dot{\varepsilon}_{vol} \tag{5.25}$$

The second form of bulk viscosity pressure is quadratic in the volumetric strain rate and is expressed as

$$p_q = \rho \left(b_2 L^e \right)^2 \left| \dot{\varepsilon}_{vol} \right| min(0, \dot{\varepsilon}_{vol}) \tag{5.26}$$

The quadratic bulk viscosity is applied only if the volumetric strain rate is compressive. The quadratic bulk viscosity pressure will smear a shock front across several elements and is introduced to prevent elements from collapsing under extremely high velocity gradients. The quadratic bulk viscosity pressure will introduce a resisting pressure that will prevent the element from collapsing. The bulk viscosity pressure is not included in the material point stresses because it is intended as a numerical effect only. It is not considered to be a part of the material's constitutive response.

The default values for 'b_1' and 'b_2' in ABAQUS/Explicit[®] are 0.06 and 1.2 respectively. Since the time period of loading is very long compared to the periods of the natural frequencies of the model, the damping factors do not affect the solution appreciably. Increasing or decreasing the damping factors by a factor of 10 did not change the solution appreciably and the error among different important parameters is shown in Table. 5.5 and 5.6. The tables compares the % error in the net 'σ_{11}', net integrated value of 'q', the penetration of the nip roller 'δ' and the surface velocity of the nip roller 'V_d' (reported in the table in the same order) between the values obtained for default values of bulk viscosity values and modified bulk viscosity values for both the flat bed and winding models.

Flat Bed Model		b_2		
		0.12	1.2	12
b_1	0.006	0.083, 0.473, 0.026, 0.004	0.095, 0.039, 0.026, 0.02	0.097, 0.057, 0.008, 0.027
	0.06	0.004, 0.03, 0.009, 0.002	-	0.001, 0.005, 0.0004, 0.002
	0.6	0.344, 0.687, 0.163, 0.008	0.34, 0.135, 0.157, 0.006	0.362, 0.129, 0.157, 0.004

Table 5.4: Effect of damping parameters 'b1' and 'b2' on flat bed model results

Winding Model		b_2		
		0.12	1.2	12
b_1	0.006	5.919, 5.560, 0.830, 0.005	1.719, 0.809, 0.666, 0.155	3.531, 4.164, 0.847, 0.186
	0.06	0.372, 0.028, 0.171, 0.130	-	0.244, 0.731, 0.327, 0.100
	0.6	0.066, 0.954, 0.069, 0.044	0.057, 1.394, 0.061, 0.069	0.033, 1.041, 0.052, 0.058

Table 5.5: Effect of damping parameters 'b1' and 'b2' on winding model results

In the flat bed model the maximum error was less than 1%. Although, the stable time increment did not change for changes in 'b_2', it increased for values of 'b_1=0.6'. For the winding model, the model results were compared after the acceleration phase for changes in viscosity parameters and the results are shown in Table. 5.5. The maximum error was observed when 'b_1' was 0.006. For values of 'b_1' greater than 0.006, the maximum error was less than 1%. Hence, for analysis purposes, the default values of 'b_1=0.06' and 'b_2=1.2' will be used.

5.6 Solution Accuracy

The analysis of winding process using explicit FEM procedure requires the treatment of the winding problem as a quasi-static problem in order to reduce the dynamic effects. However, the total computational time can be huge if the parameters that control the time increments and accuracies are not chosen carefully. The following sections describe how an optimum accuracy can be achieved yet keeping the computational time lower by changing these parameters.

5.6.1 Stability

Explicit dynamic FEM offers many advantages in treating severe nonlinearities such as nonlinear material, large deformation, instability and contact. The explicit procedure integrates through time by using many small time increments. The time increment is based on the central difference operator that is only conditionally stable. The stability limit is the largest time increment that can be used without generating large,

rapidly growing errors. It is closely related to the time required for a stress wave to cross the smallest element dimension in the model and is expressed in terms of the highest frequency of the system as given in Eqn. 5.27.

$$\Delta t \leq \frac{2}{\omega_{max}}$$ (5.27)

An approximation to the stability limit is written as the smallest transit time of a dilatational wave across any of the elements in the mesh as given in Eqn 5.28, where 'L_{min}' is the smallest element dimension in the mesh and 'C_d' is the dilatational wave speed expressed in terms of Lame's constant and material density. This estimate for 'Δt' is only approximate and is typically scaled by a factor between 1 and $1/\sqrt{2}$ for two dimensional analysis and between 1 and $1/\sqrt{3}$ for three dimensional analysis. Thus, the time increment in an explicit dynamic analysis can be very short if the mesh contains small elements or if the stress wave speed in the material is very high.

$$\Delta t \approx \frac{L_{min}}{C_d}; \ C_d = \sqrt{\frac{\lambda + 2\mu}{\rho}}; \ \lambda = \frac{E\nu}{(1+\nu)(1-2\nu)}; \ \mu = \frac{E}{2(1+\nu)}$$ (5.28)

5.6.2 Mass Scaling and Element Size

In commercial winding processes, winding of webs into wound rolls occur at very high speeds, typically, in the range of many thousands of feet per minute. Therefore when the explicit FEM procedure is used for winding analysis, it is necessary to convert the

real problem into a virtual problem with a different time scale. In this context time scaling and mass scaling techniques have been widely used in order to save computational time. Because the explicit central difference method is used to integrate the equations in time, the discrete mass matrix used in the equilibrium equations plays a crucial role in both computational efficiency and accuracy for both classes of problems [48].

Mass scaling is the procedure of increasing the mass of the entire or partial structure such that the smallest stable time increment can be increased to reduce the overall computational time. As can be inferred from Eqn. 5.28, the stable time increment is directly proportional to the square root of density. When a mass scaling factor of 'f' is used, the stable time increment increases by $\sqrt{f}$. When used appropriately, mass scaling can often improve the computational efficiency while retaining the necessary degree of accuracy required for a particular problem. Mass scaling for quasi-static analysis is usually performed on the entire model. A limited amount of mass scaling is usually possible for most quasi-static cases and will result in a corresponding increase in the time increment used by ABAQUS/Explicit and a corresponding reduction in computational time. It should be ensured that the changes in the mass and consequent increases in the inertial forces do not alter the solution significantly.

Since the stable time increment is also dependent on the smallest elemental dimension, choice of the elemental dimensions and mesh schemes can play an important role in both the accuracy and computational time. However, this can easily be performed

by experimenting with different element dimensions, mesh schemes and choosing an appropriate size based on the convergence of the results.

5.6.3 Mesh Convergence Analysis

Mesh refinement increases the computational cost by increasing the number of elements and reducing the smallest element dimension. To understand the contact mechanics, a proper description of the contact is required. Determination of the proper mesh definition requires setting correct values to both the length and thickness dimensions of an element. Intuitively, one can set the length of the element based on the contact width determined from the contact mechanics analysis for estimation of the radial modulus (section 5.3.5). In the flat bed model, an element length of 0.01 inches will provide adequate definition in the contact zone which was on the order of 0.17 inches in width. In the case of winding model, the length of the element was fixed at 0.0125 inches. Since reduced integration isoparametric quadrilateral solid elements are used to model the web, more than one element will be required to model the bending effects. The thickness of each element is then set based on mesh convergence studies conducted in both the flat bed and winding contact models as discussed below.

5.6.3.1 Flat Bed Nip Mechanics Model

The effect of the number of elements through the depth (automatically fixes the element thickness) of the web on the top, bottom and net σ_{11} stresses in the contact zone is shown in Figure 5.16. It should be noted that the top and bottom surface stresses were

linearly extrapolated to the surface based on the stresses at the integration points. When only 2 elements are used through the thickness of the web, the bending stresses are over-estimated. However the net σ_{11} stress in the trailing zone of contact is very similar. The use of 3 or more elements through the web thickness produces good convergence in the σ_{11} stresses. When the contact pressure values are compared, number of elements through the depth did not affect the normal pressure and hence the traction limits as shown in Fig. 5.17. Comparison of the top surface tractions showed some discrepancy in the results between the center and leading edge of contact as shown in Fig. 5.18. However, the overall agreement is good. In the case of the bottom surface tractions the agreement between the 3 cases was good. When the integrated value of the net traction was compared the results were within 3% of each other. It should be noted that a mass scaling factor of 75 was used in all three cases shown above. Although the convergence of the parameters investigated in all the three cases tested was good, the computational time is different.
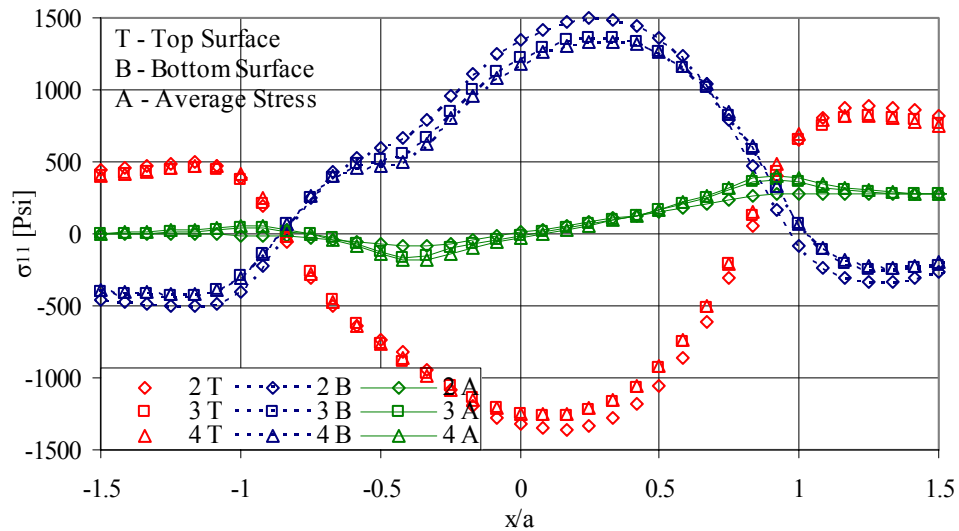
Figure 5.16: Effect of mesh density on the machine direction stresses in the nip contact zone. (Legend: Numbers indicate the number of elements used through the depth of the web)
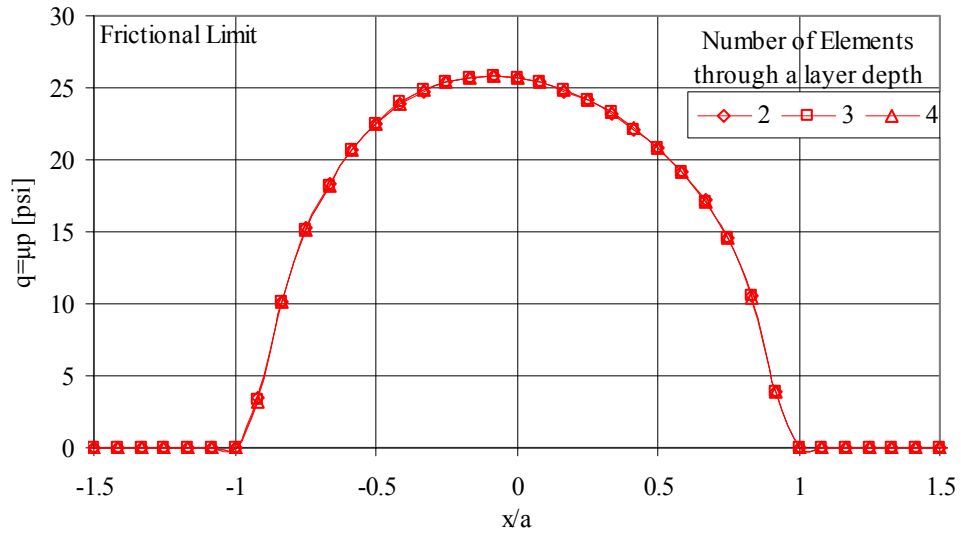
Figure 5.17: Effect of mesh density on nip contact pressure.

The stable time increment for each of the cases is 4.99×10^{-7}, 3.53×10^{-7}, 2.19×10^{-7} seconds in the order of 2, 3, 4 elements through the depth respectively. Thus it is very clear that the computational time increases almost linearly with increase in the number of elements.
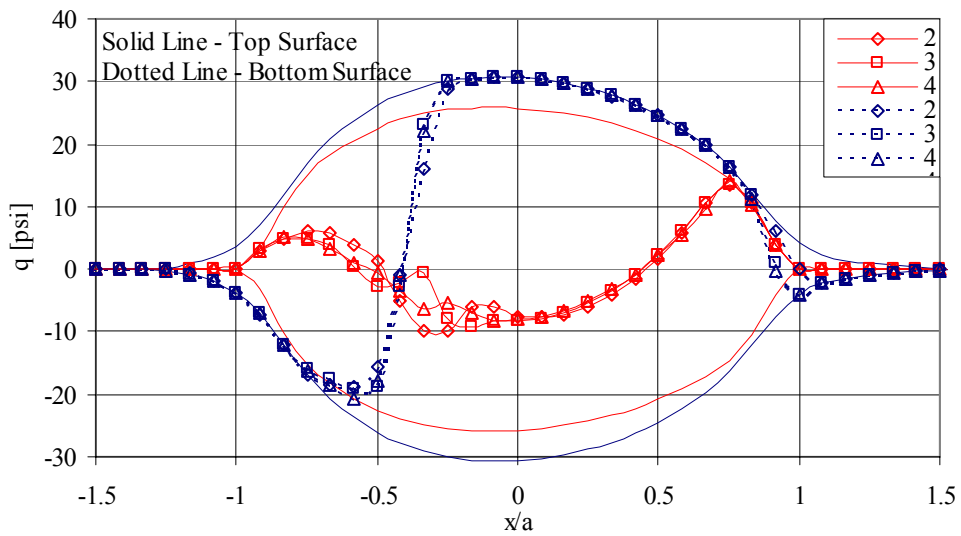
Figure 5.18: Effect of mesh density on contact shear tractions (Legend: Number of elements through the depth of a layer).

5.6.3.2 Winding Model

In the case of winding model, since the contact tractions are the most important parameters, one only has to perform the convergence analysis during the acceleration period of the winding problem. During the start of the winding problem, contact occurs between an elastic web and two rigid bodies and many iterations are required to achieve a reasonably well behaved contact profile. As the roll builds, the elastic cushion provided by the web layers beneath the top layer helps reduce the number of iterations required, thus justifying the mesh convergence analysis being performed only during the acceleration periods. The convergence analysis was carried out in center winding model only. When the 'σ_{11}' stresses in the contact zone were compared it is evident that atleast 3 or more elements are required to simulate the bending stresses within the contact zone as shown in Fig. 5.19. However, the 3 element case produced the same net 'σ_{11}' stress in the layer as compared to the case of 4 elements through the depth.
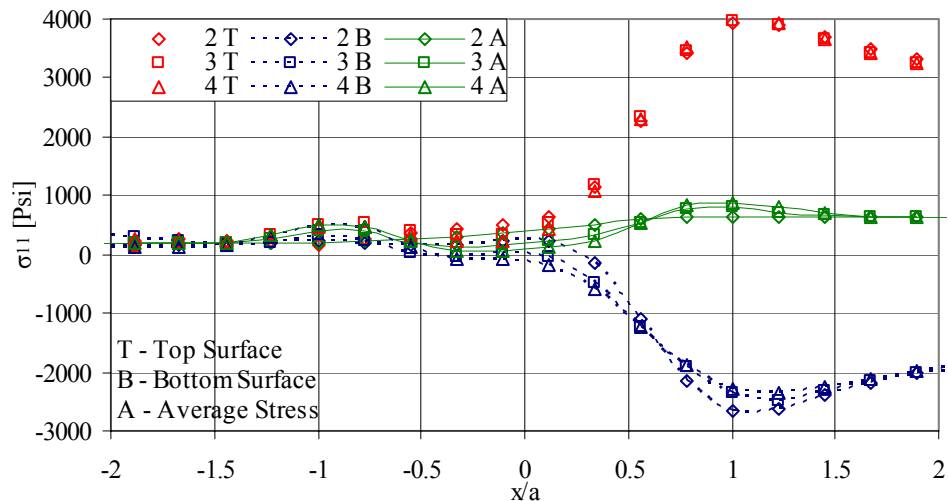
Figure 5.19: Effect of mesh density on the machine direction stresses in the nip contact zone (Legend: Number of elements through the depth of a layer).
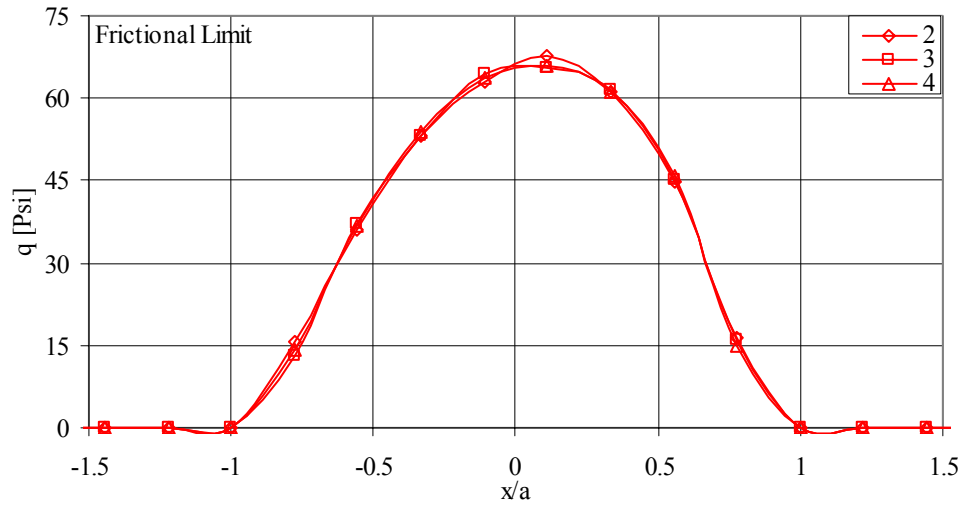
Figure 5.20: Effect of mesh density on nip contact pressure (Legend: Number of elements through the depth of a layer).
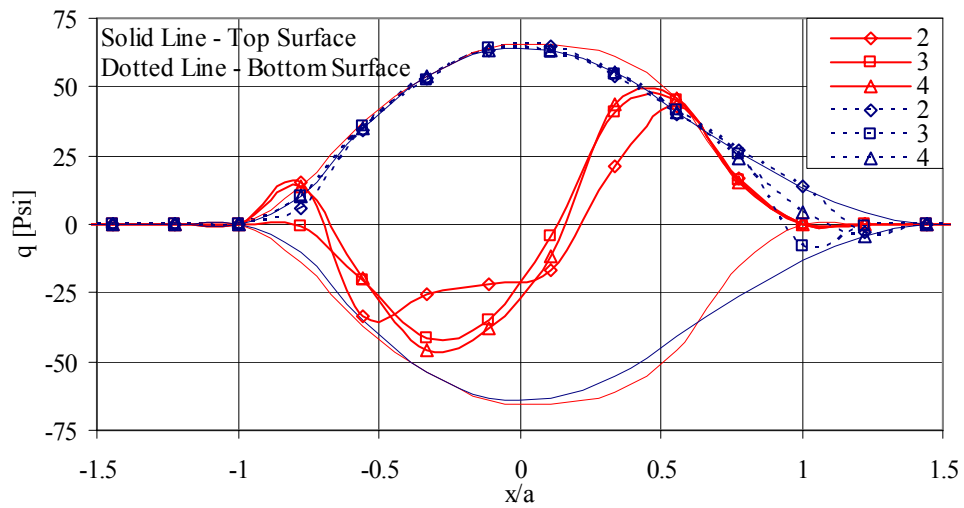
Figure 5.21: Effect of mesh density on contact surface tractions (Legend: Number of elements through the depth of a layer).

The contact pressure behavior remains the same for all the cases tested as shown in Fig. 5.20. The 2 element case was not accurate enough to model the top contact tractions correctly as shown in Fig. 5.21. Use of 3 or 4 elements through the depth

produced very similar results. Although there was some discrepancy in the bottom surface tractions at the trailing edge of contact, the overall behavior is very similar between the different cases as shown in Fig. 5.18. The stable time increment for each of the cases is 3.28×10^{-7}, 2.27×10^{-7}, 1.73×10^{-7} seconds in the order of 2, 3, 4 elements through the depth respectively. Thus the use of 3 elements through the depth offers significant computational advantages and hence will be used in winding analysis.

5.6.4 Effect of Mass Scaling

In the preceding section, it was mentioned that the computational time can be reduced by increasing the mass of the structure. However, too high a scaling factor will result in increasing the dynamic effects and may cause incorrect results, especially for the stresses. In this situation, it is difficult to figure out how large the scaling factor should be to reduce computational time. Due to the complex contact conditions involved and the lack of accurate reference solutions to choosing a mass scaling factor, estimating the correct mass scaling factor in this work was not a straight forward task. Several authors (for example [63]) have shown that the overall deformation and strain distribution can be predicted within acceptable accuracy if the chosen scaling factor yields a low ratio of the total kinetic energy to the total internal energy.

When the energy equation, Eqn. 5.3, is integrated from 0 to time t_i,

$$E_k = \frac{1}{2} m \, v_i^2 = W_{ext} - W_{int} \qquad (5.29)$$

For a static case,

$$0 = W_{ext} - W_{int} \tag{5.30}$$

where 'W_{int}' and 'W_{ext}' are the total internal and external energies and 'E_k' is the total kinetic energy respectively. If the dynamic process at 't_i' is close to a static one, the kinetic energy in Eqn. 5.29 should be small compared with the internal energy. Therefore, a common criterion for the acceptability of a solution to a quasi-static process is that

$$\frac{E_k(t)}{W_{int}(t)} < \varepsilon_0 \text{ for all '}t\text{'} \tag{5.31}$$

where 'ε_0' is a small constant. Belytschko [47] suggested an alternative error estimate, when significant plastic work is needed to be modeled. For a sheet metal forming process, the ratio of change in kinetic energy to plastic work was calculated at different sub domains and a value of less than 10% was shown to produce good results. This was confirmed by Kim et al [64]. In the sheet metal problem investigated by Belytschko, the ratio of the kinetic energy to elastic internal energy was much higher compared to the ratio of change in kinetic energy to plastic work and this value was around four.

5.6.4.1 Flat Bed Nip Mechanics Model

The only prior work in the FE analysis of winding problem using an explicit code was that of Ärölä and von Hertzen's work [42]. In their case, a mass scaling factor of 50

was used. When the ratio of kinetic energy to internal energy was computed in their case, the ratio was ≈ 15 at the end of the acceleration period.

In the flat bed and winding models, the effect of mass scaling factors of 75, 300 and 600 was studied for the case of 4 elements through the layer thickness. The 'σ_{11}' stresses in the contact zone do not change with increasing scaling factors. However, changing the mass scaling factor only had an effect on the top surface tractions as shown in Fig. 5.22. Although, the top surface tractions show some difference in behavior, this difference does not manifest itself in the integrated net traction and hence does not affect the average value of 'σ_{11}'.
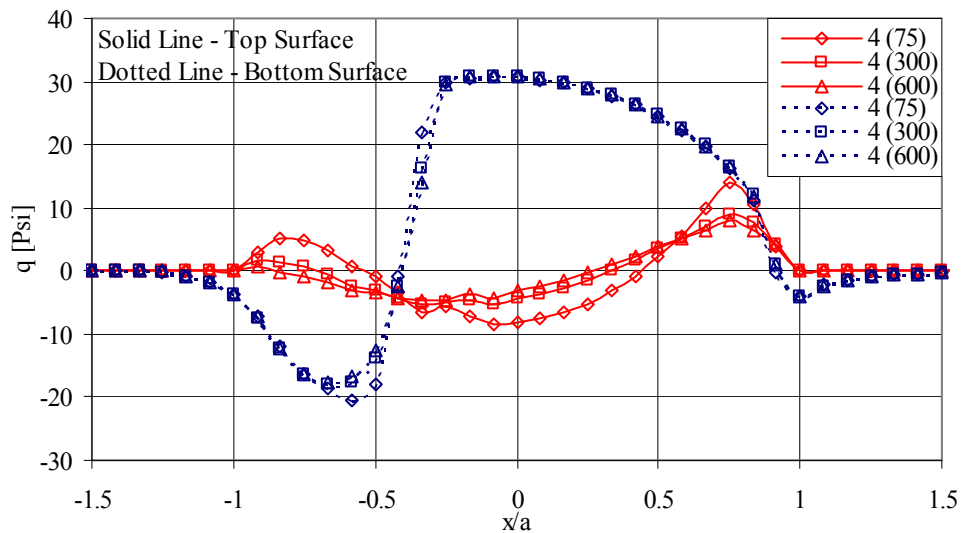
Figure 5.22: Effect of mass scaling on contact shear tractions (Legend: Number of elements through the depth (Mass scaling factor)).

Furthermore, the ratio kinetic energy to the internal energy was evaluated for all the different cases. Since the internal energy is based on the total strain, this value does not change appreciably for different mass scaling factors or for different elemental

dimensions. In the case of kinetic energy, the elemental dimensions do not affect the solution. However, change of mass will affect the total kinetic energy. The histories of internal and kinetic energies are shown in Fig. 5.23 for a mass scaling factor of 75. The ratio of the energies for different mass scaling factors is shown in Fig. 5.24.
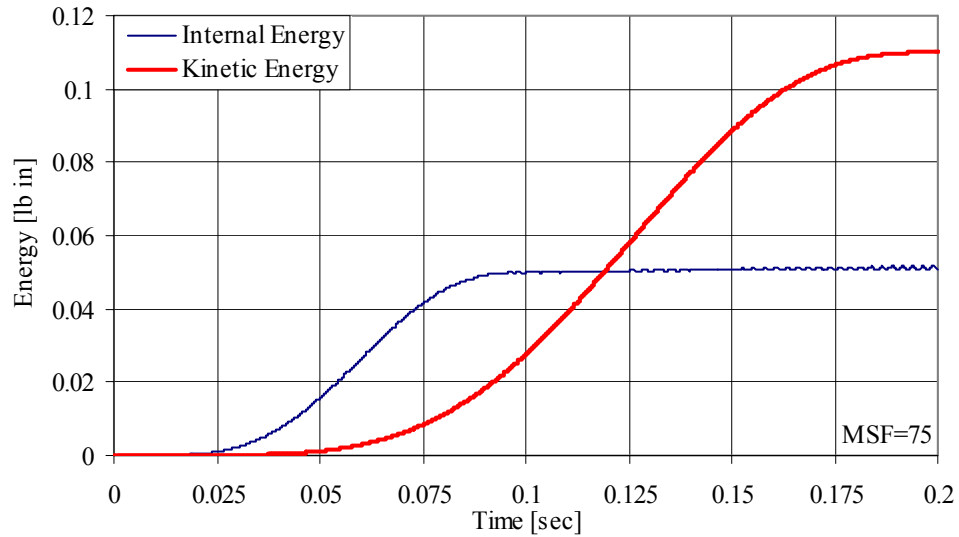
Figure 5.23: Energy history during the acceleration phase in the flat bed model.
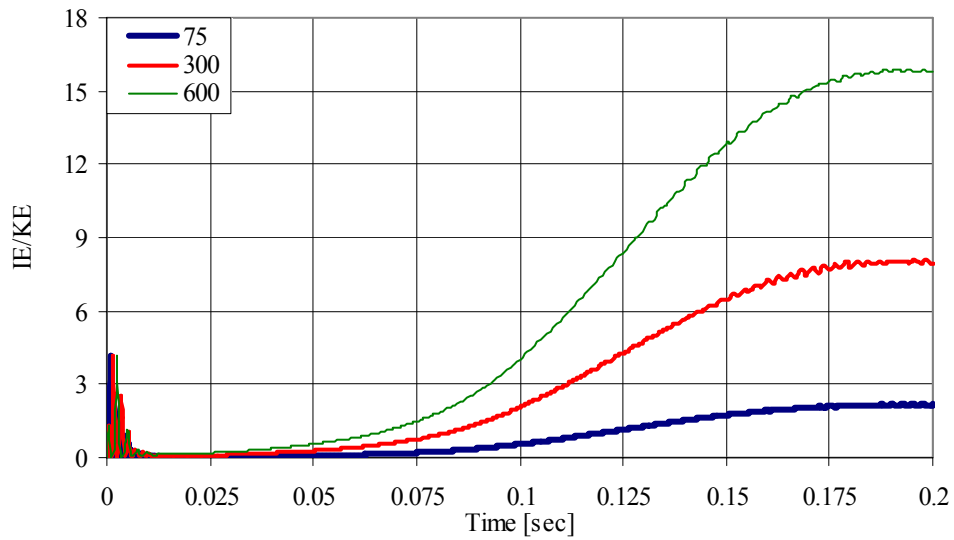
Figure 5.24: Effect of mass scaling on the ratio of internal and kinetic energy history (Legend: Mass scaling factor).

84

Although all the factors resulted in ratios comparable to or less than that was observed in Ärölä's case, only a factor of 75 resulted in energy ratios that was less than that was observed by Belytschko et al. Thus based on the mass scaling and mesh convergence analysis the elemental dimensions are set at 0.01 inches for length, 0.025 inches for depth and the mass scaling factor is set at 75.

5.6.4.2 Winding Model

Similar to the flat bed case, mass scaling factors of 75, 300 and 600 were used in the winding model and the results during the acceleration phase of the problem were compared. When the bottom surface contact tractions were compared, the overall behavior seemed to be unaffected by the mass scaling factors used for a given mesh as shown in Fig. 5.25. However there was some disagreement in the top surface contact traction values for different scaling factors; but the overall behavior was similar. When the 'σ_{11}' stresses in the contact zone were compared for these different mass scaling factors the results matched closely.

In addition, the ratios of energy histories were compared. The behavior of the internal and kinetic energy histories are shown in Fig. 5.26 for the case when mass scaling factor was 300. The internal energy is dependent on the total strain and hence it will not change for different mass scaling factors. On the otherhand, the kinetic energy is dependent on the mass of the bodies involved and hence increases with increase in mass scaling factor. The ratio of internal energy to kinetic energy for different mass scaling

factors is shown in Fig. 5.27. In all the cases the ratio is less than 4 and compare well to

Belytschko's error estimate.
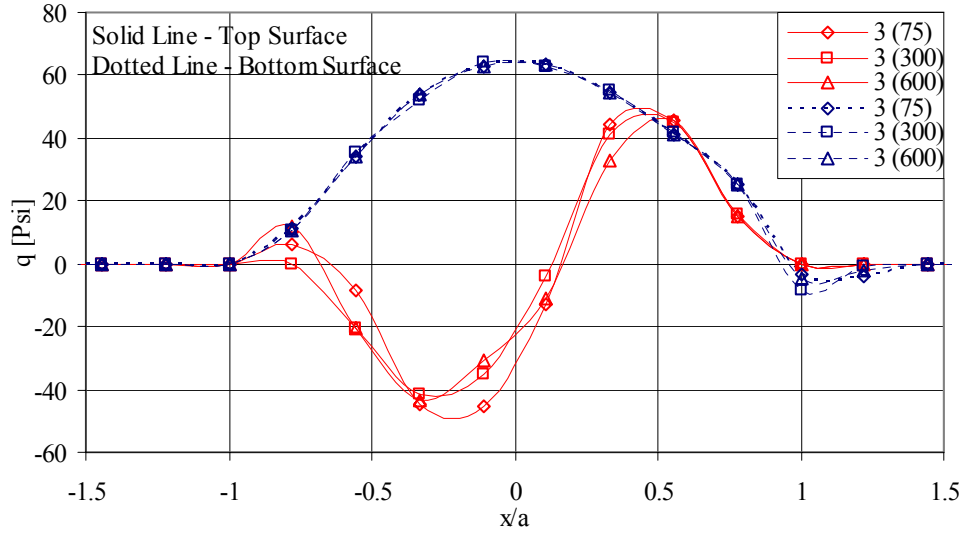
Figure 5.25: Effect of mass scaling on contact shear tractions (Legend: Number of elements through the depth (Mass scaling factor)).
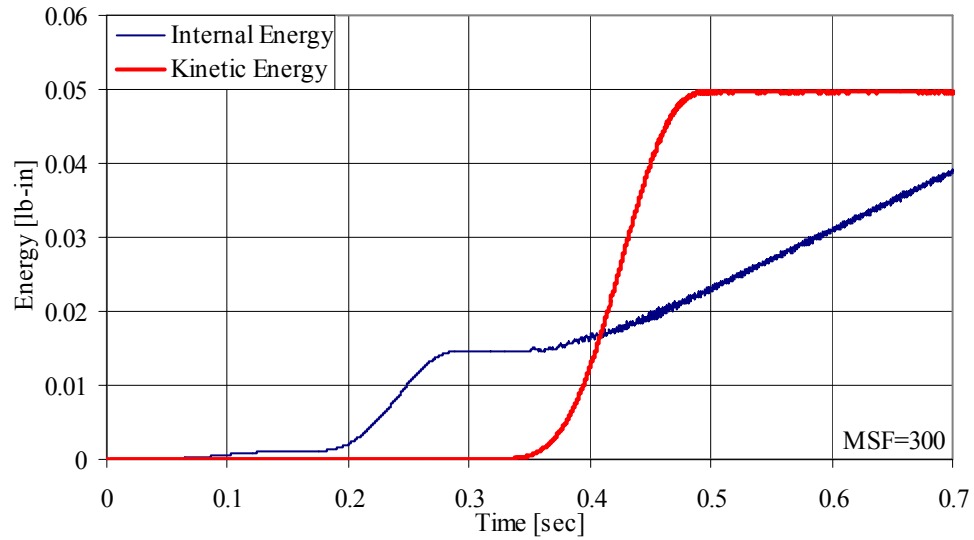
Figure 5.26: Energy history during the acceleration phase in the winding model.

When high loading rates/mass scaling factors are used, dynamic effects like wave propagation effects can affect the results. Hence a value of 300 was chosen for the mass scaling factor in the winding analysis without losing the accuracy of the results. When the energy ratios for the entire time period of the winding process were observed, the ratios were much less than Belytschko's estimate.
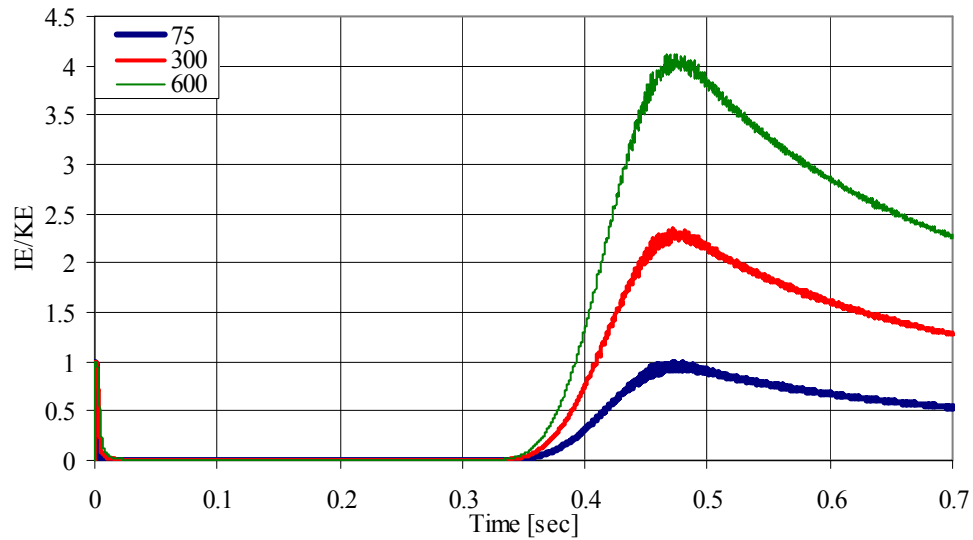
Figure 5.27: Effect of mass scaling on the ratio of internal and kinetic energy history.

5.6.5 Computational Aspects

The flat bed model consists of 50,002 nodes and 39,964 elements with 100,006 degrees of freedom. Off-the-shelf desktop computers with an average processing capabilities equivalent to that of an Intel Pentium IV® 3.0 GHz processor with 1 Megabyte of RAM were used for model simulations. On such computers, a single analysis takes on an average of 30 hours to complete. The winding model consists of 17,706 nodes and 13,279 elements with 35,414 degrees of freedom. Every single analysis takes on an average 240 hours to complete.

6 Numerical Results and Discussion

6.1 Flat Bed Nip Mechanics

In this section, the behavior of contact tractions and contact stresses in a static contact between a rigid nip roller and a stack of sheets is studied. The rolling contact mechanics between the nip roller and a stack of sheets is then studied. The development of wound-on-tension in a given web layer is observed and the basic phenomenon is presented. The effect of various parameters on the nip mechanics and the development of the wound-on-tension are also discussed.

6.1.1 Static Contact of a Nip Roller and a Stack of Web Layers

The behavior of the top surface tractions in the top layer is shown in Fig. 6.1. In the figure, the traction limits are represented by the envelopes that are calculated by multiplying the coefficient of friction and the contact pressure at that point. The traction values are then represented as data points on/between these envelopes. Since the strain field does not change with time, the velocities of micro-slip between the contacting points can be expressed as

$$\dot{s}_x = v_{x1} - v_{x2} \tag{6.1}$$

When the surface is under stick, it follows that the velocities at the contacting points between the two surfaces should be equal and hence, $\dot{s}_x$ is zero in a stick zone. In addition, the resultant tangential traction in the stick zone must not exceed the limiting value as given in Eqn. 6.2.

$$|q| \leq \mu p \qquad (6.2)$$

On the other hand, the surface is under complete slip when the resultant tangential traction in the slip zone equals the limiting value as given in Eqn. 6.3. In a slip region, the direction of the traction acts in a direction opposite to the slip direction/velocity.

$$|q| \leq \mu p \ \text{(or)} \ q \leq \pm \mu p \qquad (6.3)$$

The top surface tractions fall between the traction limits throughout the zone of contact indicating that the entire surface is under stick. Also, within the contact zone, the traction at the contacting points act anti-symmetric about the origin or the center of contact zone. Note that as the contact pressure becomes zero at x/a=±1, the tractions fall to zero. The bottom surface is under slip at the edges of contact and these slip zones act in opposite direction to each other as shown in Fig. 6.2. In the middle, the direction of slip reverses through a small stick zone. The net traction in any given layer is calculated by summing the top and bottom surface tractions. Since the top and bottom surface tractions are anti-symmetric in nature, the net traction is anti-symmetric about the center of contact as shown in Fig. 6.3.
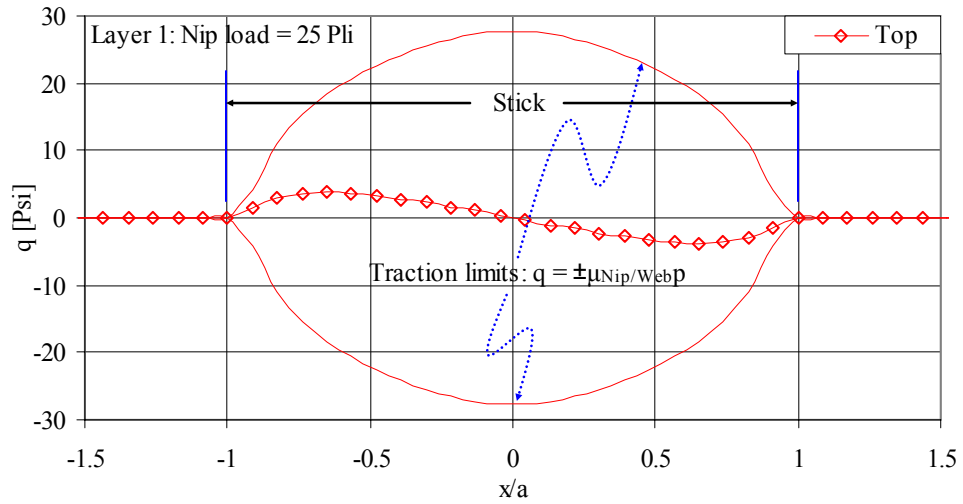
Figure 6.1: The behavior of top surface traction in the top layer in static contact between a rigid nip roller and a web stack.
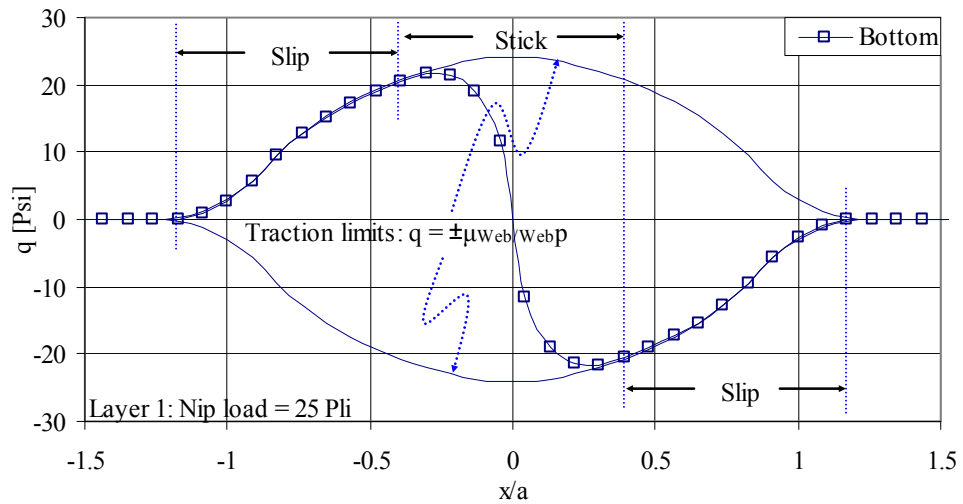
Figure 6.2: The behavior of bottom surface traction in the top layer in static contact between a rigid nip roller and a web stack.

Since the net traction is anti-symmetric about the center of contact zone, the integration of the net traction yields a value of zero for the total traction that is transmitted. As shown in Fig. 6.4., the top layer experiences significant bending stresses. The average stresses calculated as the sum of the top and the bottom bending stresses in

the layer represents the membrane stresses. In Fig. 6.4., within the contact zone, the average 'σ_{11}' stress is compressive and acts anti-symmetrically about the middle of contact. This stress is due to material being squished on either side due to the penetration of the nip roller into the web stack. However, the web layers are not constrained and hence, no net increase in stress can occur in any given layer in the case of a static contact.
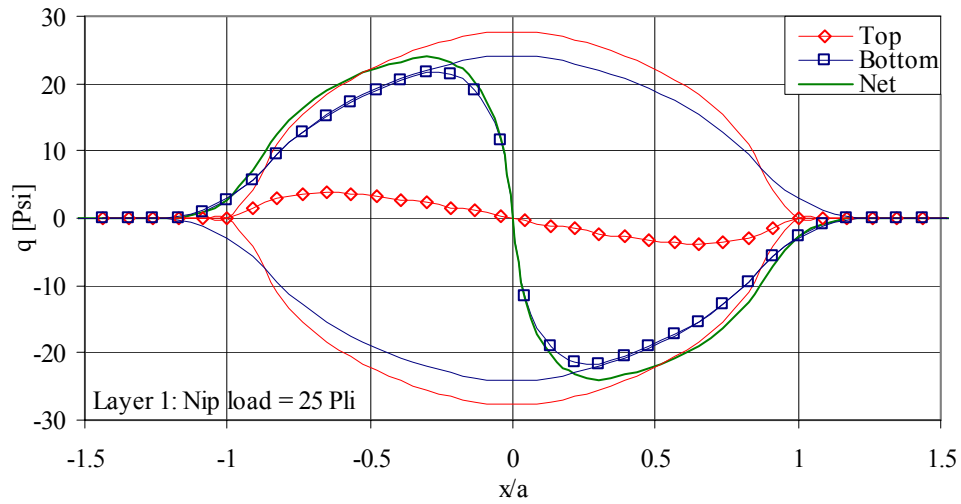
Figure 6.3: The behavior of net traction in the top layer in static contact between a rigid nip roller and a web stack.
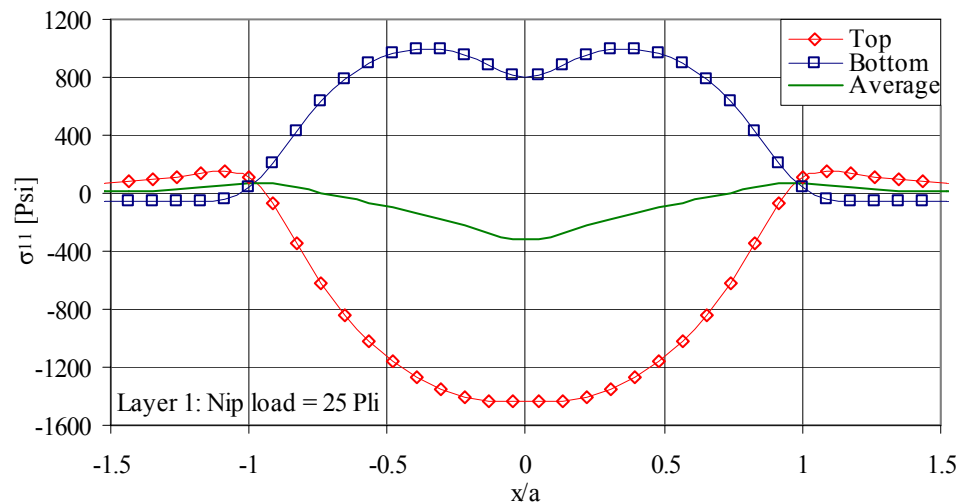
Figure 6.4: The behavior of σ_{11} stresses in the contact zone in the top layer in static contact between a rigid nip roller and a web stack.

6.1.2 Development of the Wound-on-Tension

In the case of a rolling contact between a nip roller and a stack of webs, as the nip roller rolls to the right, the machine direction stress 'σ_{11}' in the layers change as a function of nip rolling distance. The net increase in stress due to the rolling motion of the nip can be calculated by averaging the stresses in each layer at the left end of the sheet where the velocity boundary condition is prescribed. This stress in each layer as a function of the nip rolling distance for the case of nip load=25 Pli is shown in Fig. 6.5. It is evident that the stresses in each layer saturate after the nip has rolled some distance and this saturated value is commonly referred to as the nip-induced-tension (NIT). This saturated value or the NIT for each layer is shown in Fig. 6.6.
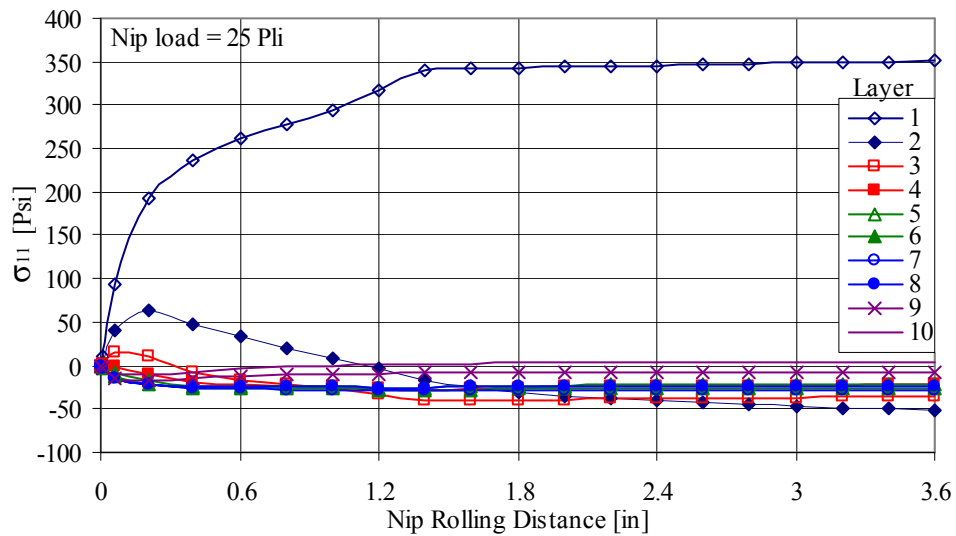
Figure 6.5: Development of the NIT as a function of nip rolling distance.

The topmost and bottommost layers are under tension while the other layers are under compression. This shows that, in this case, the instant center lies in the second layer. Pfeiffer reported the instant center to have existed many layers deep in the stack in

the tests he conducted. Ärölä's [42] simulations showed that the instant center existed in layer 4 in a stack of 10 layers. In both Pfeiffer's and Ärölä's case, the material used was paper and in each of their cases the thickness of the web was much smaller than the PET film thickness.
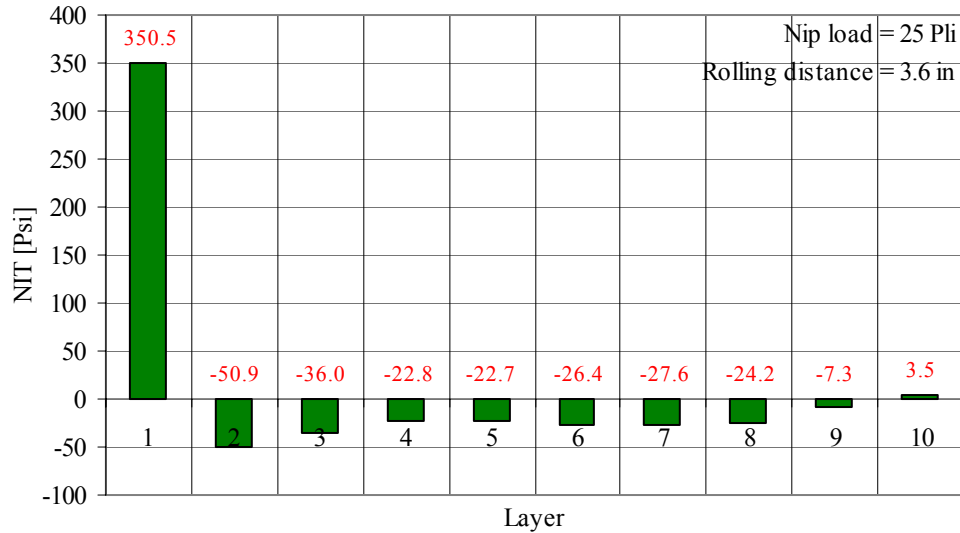
Figure 6.6: NIT in each layer in the stack.

6.1.3 Behavior of the Contact Stresses

The stresses in the contact zone (under the nip roller) when the nip had rolled 3.6 inches is shown in Fig. 6.7. for each layer. The top and bottom surface 'σ_{11}' stresses are obtained by extrapolating the 'Gauss' point stresses through the thickness of the layer to the surface. The top and bottom surface stresses under the nip represent both the bending and the membrane component of the nip-induced stress. The total stress in the layer is represented as the average of the top and bottom surface stresses and this stress represents the nip-induced stress. Away from the contact zone, the top and bottom surface stresses approach each other due to the absence of the bending stresses. The layers deeper into the

stack and near the base experience lesser bending stresses within the contact zone compared to the layers near the top and in contact with the nip roller. At the trailing edge (exit) of the contact zone, only the topmost layer (layer 1) experiences significant tension and hence the most important. In order to determine how and why this layer shows significant increase in tension one has to look at the behavior of the surface tractions in the contact zone.

The top and bottom surface tractions under the nip roller in the top layer are shown in Fig. 6.8 and Fig. 6.9 respectively. As was described in section 6.1.1., the maximum traction that can be sustained by any layer is equal to the coefficient of friction multiplied by the normal force. This limit is represented by the dotted envelopes (both for top and bottom surfaces) in each figure. When the shear traction at the surface of the web reaches the maximum traction value (data points fall on the envelope) the surface is under the condition of slip. If the traction value at the surface is lesser than the maximum traction value, the surface is under the condition of stick. In the topmost layer, the top surface traction exhibits very similar characteristics to tractions that exist in rolling contact of elastic cylinders. Near the leading edge ($x/a \approx -1$), the surface is under slip. In the middle of the contact ($-1 < x/a < 1$), the surface is under stick and at the trailing edge of the nip ($x/a \approx +1$), the surface is under slip. The bottom surface shows five distinct regions. Both the leading and trailing edges are under slip and act in the same direction and the slip zone in the middle acts in the opposite directions. Between the leading edge and the middle slip zone, the trailing edge and the middle slip zone, two stick zones exist.

94
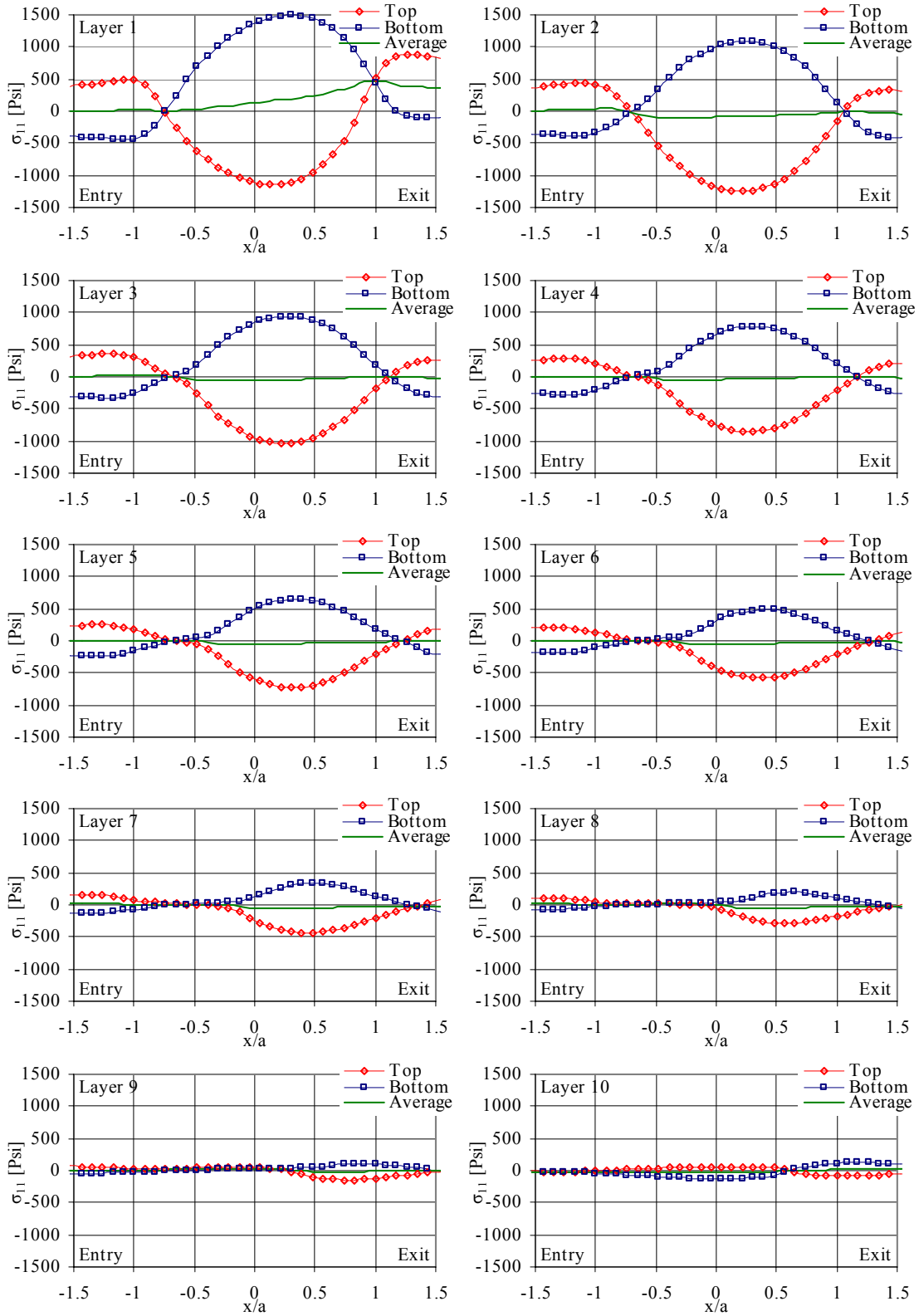
Figure 6.7: 'σ_{11}' stresses in the nip contact zone for the case of nip load=25 Pli.
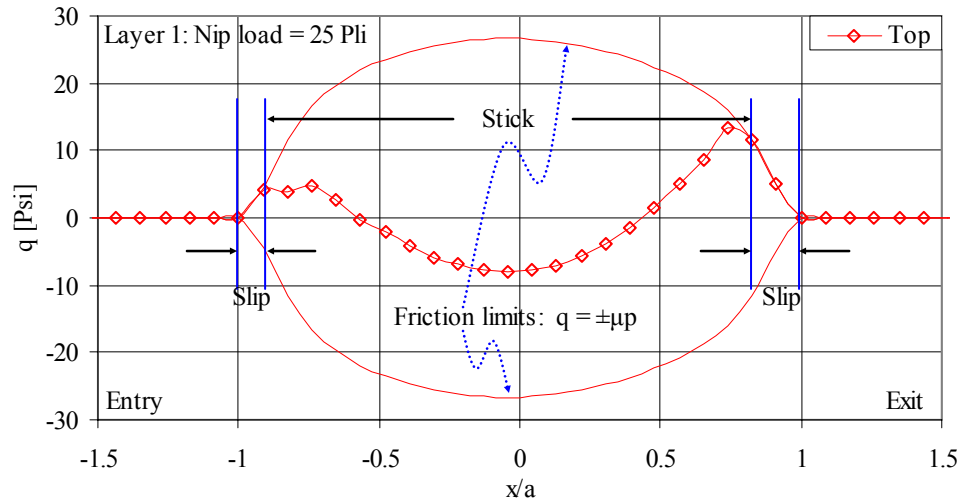
Figure 6.8: The behavior of top surface traction in the top layer in rolling contact between a rigid nip roller and a web stack.
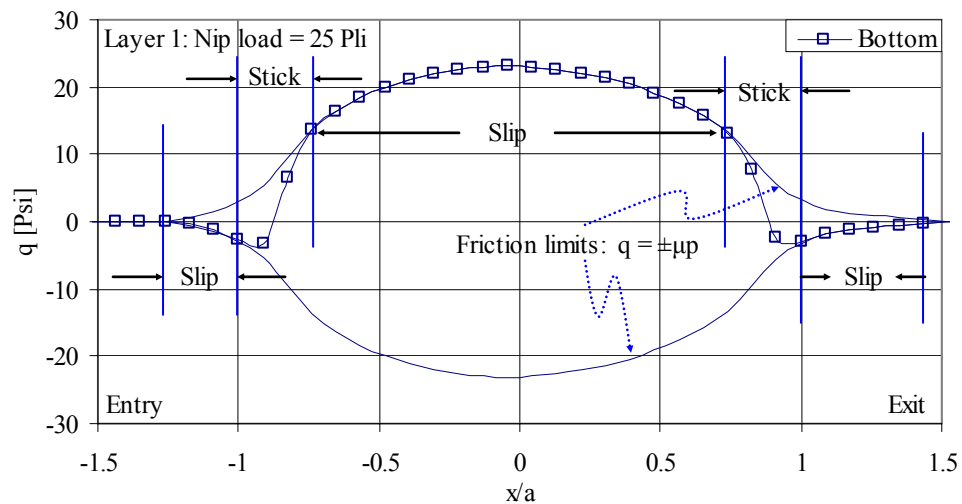
Figure 6.9: The behavior of the bottom surface traction in the top layer in rolling contact between a rigid nip roller and a web stack.

Although one can distinguish the stick, slip conditions in the nip contact zone, it would be instructive to understand the velocity conditions at the zone of contact to better understand the surface behavior. Let us consider a web layer as shown in Fig. 6.10. The notation for positive and negative surface tractions is as shown. Consider 'layer 1' moving at a velocity 'v_{1-1}' and 'layer 2' moving at velocity 'v_{2-1}' such that 'v_{2-1}' > 'v_{1-1}'.

Based on Fig. 6.10(a) and Fig. 6.10(b), it is clear that the bottom surface tractions of 'layer 1' will be negative and the top surface tractions of 'layer 2' will be positive and this is shown in Fig. 6.5(c).
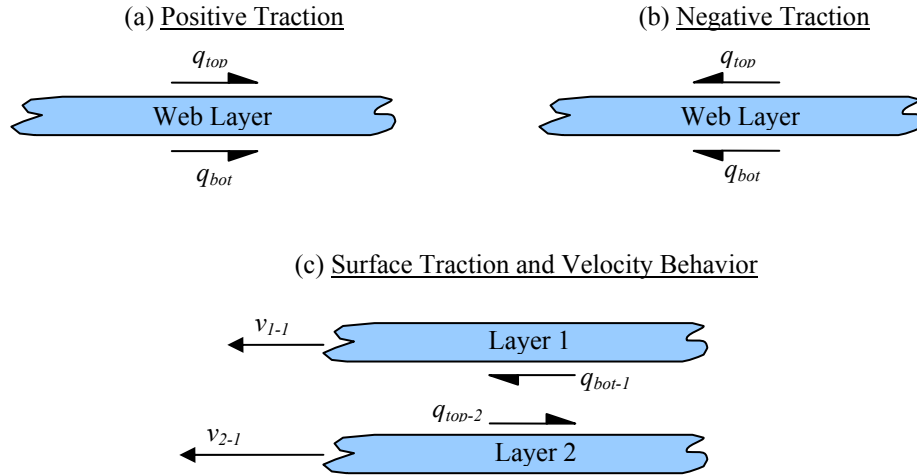
Figure 6.10: Direction of shear tractions and web velocities.

In Fig. 6.8., the top surface traction in 'layer 1' at the leading and trailing edges of contact is positive and is in a slip condition. This indicates that the top surface is moving faster than the nip roller in these slip zones. In the middle of the contact zone, the contact is under stick and hence the velocity of the nip roller and the top surface are equal. As shown in Fig. 6.9., on the bottom surface of 'layer 1', the surface traction is negative at the leading and trailing edges of contact and this indicates that the bottom surface of 'layer 1' moves slower than the top surface of 'layer 2' in these slip regions. In the middle of the contact zone, the bottom surface traction is positive and is in a condition of slip. This indicates that the bottom surface of 'layer 1' is moving faster than the top surface of 'layer 2'. Between the trailing edge and the middle of the contact zone and between the leading edge and the middle of contact zone, there exists stick zones. At the ends of these zones, the slip direction reverses. This is similar to what Johnson [41]

observed in the case of an elastic layer between rigid nips and is a classic example of micro-slip situation. In the stick zone the surface velocity of the bottom surface of 'layer 1' is equal to the surface velocity of the top surface of 'layer 2'.

The net traction in each layer is computed by summing the top and bottom surface tractions. The behavior of the top and bottom surface tractions along with the net traction in each layer is shown in Fig. 6.11. In 'layer 2', the behavior of both the top and bottom surface tractions is similar to that was observed in the bottom surface in 'layer 1'. Also, through most of the contact zone, the top and bottom surface tractions act in opposite directions. The behavior of both the top and bottom surface tractions in layers three through ten are very similar to the behavior of tractions observed in 'layer 2'. However, the intermediate stick zone near the leading edge of the contact grows in size as we go deeper into the stack and toward the base. When the net traction in each layer is compared, only the top layer exhibits any significant net traction. In layers one and two, the surface contact traction plots and their corresponding σ_{11}-stress plots are shown in Fig. 6.12. In 'layer 1', the net traction obtained by summing the top and bottom surface tractions is positive through most of the contact zone. Due to equilibrium of forces, this positive net traction results in a net increase in 'σ_{11}' stress as shown in the 'σ_{11}' plot. In 'layer 2', the net traction is negative near the leading edge and positive near the trailing edge of contact and zero elsewhere as the top and bottom surface tractions cancel each other. This produces a very small compressive stress in 'layer 2. This indicates that the net traction in a given layer controls the 'σ_{11}' stresses. The behavior of layers three through ten is similar to the behavior seen in layer two.
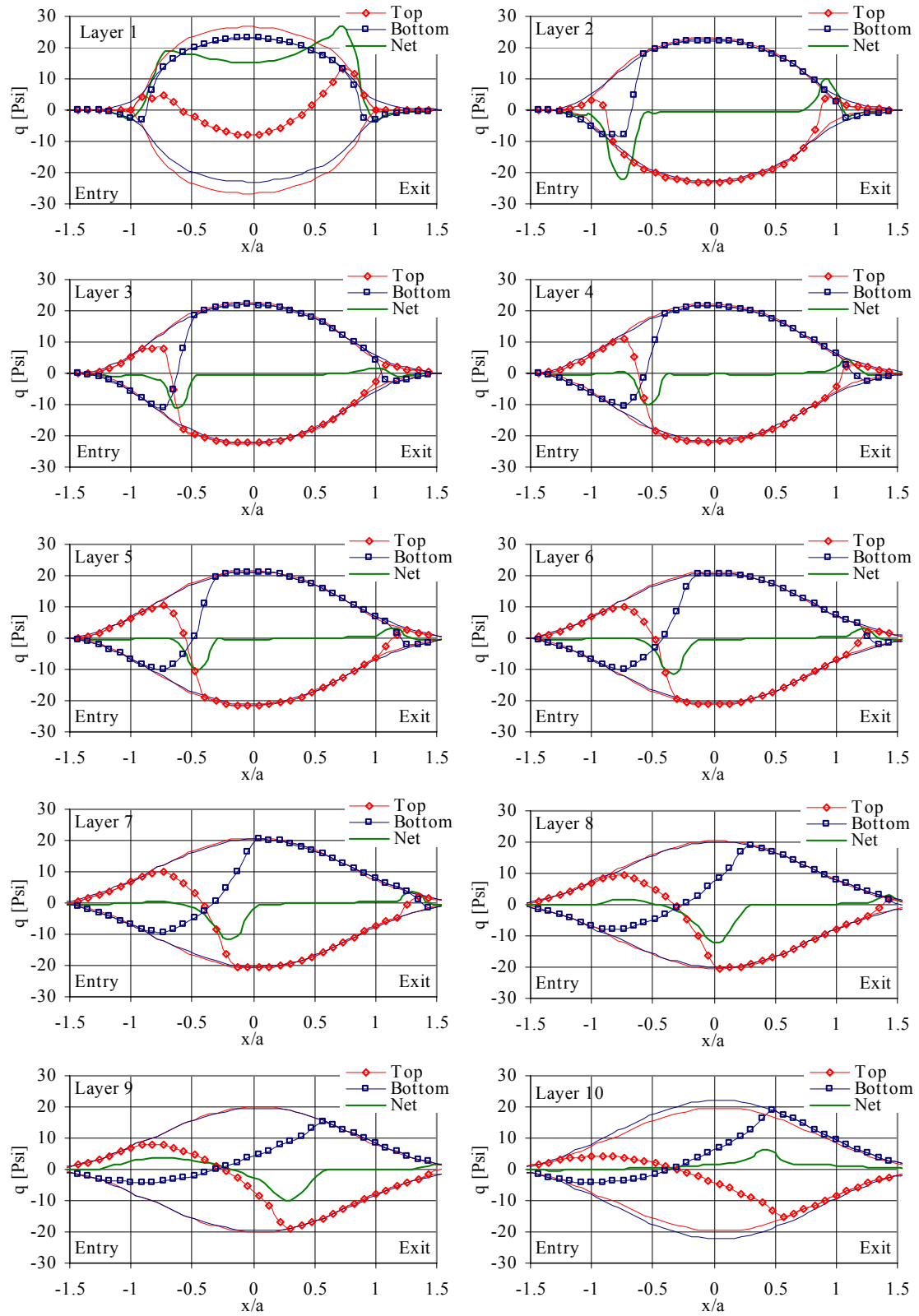
Figure 6.11: Contact shear tractions in web layers under the nip roller for the case of nip load=25 Pli.
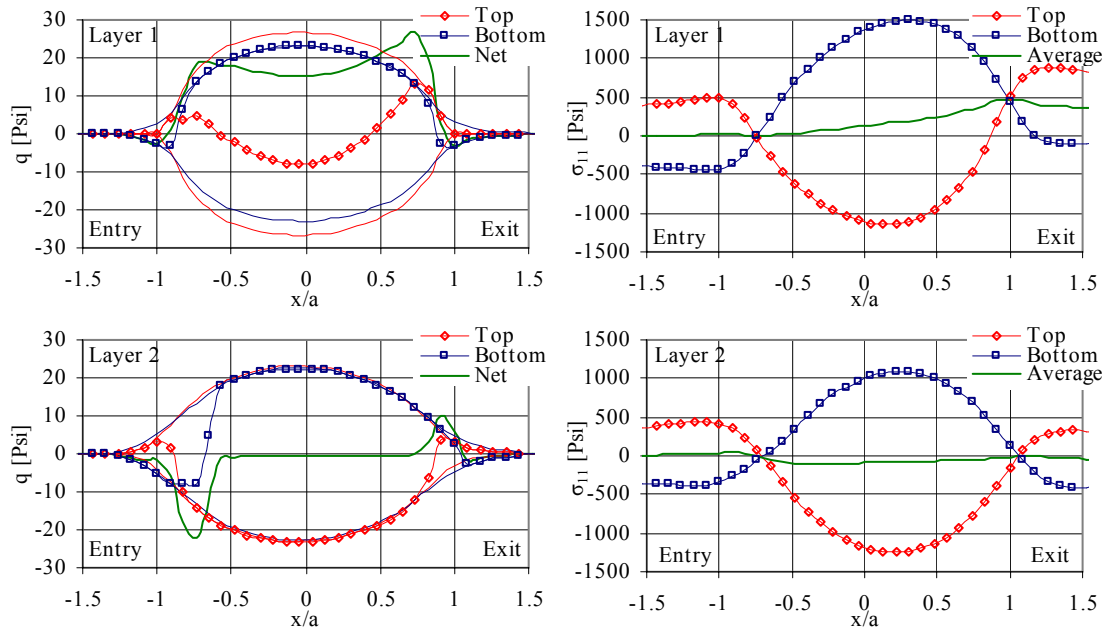
Figure 6.12: Contact shear tractions giving rise to machine direction stresses.

In Ärölä and von Hertzen's [42] case, they report only three distinct regions in both the top and bottom surface behavior. However, this is incorrect as there was a small micro-slip zone observed even in their case. Also, on the bottom surface of the topmost layer, a substantial stick zone that spans through most of the contact zone exists in their results. However, this was due to a significantly high value of nip load (55 Pli for paper material) and a low value of 'E_r' used in their case. This results in a large value for the half-width of contact and the rolling contact conditions exhibiting a substantial stick zone near the entry zone of contact.

In this case, the development of the NIT in terms of the contact tractions that exist in the top layer as a function of rolling distance is shown in Fig. 6.13. At the start of the rolling process (0.0057 in), the surface tractions behave very similar to that was observed

in the static contact case explained in section 6.1.1. When the nip rolls to about 0.063 in, the top surface traction behaves similar to that observed in rolling contact of elastic cylinders. At this instant, the bottom surface traction exhibits a significant amount of stick in the contact zone where $-0.5 < x/a < 0.2$. When the total rolling distance becomes 0.21 in, the stick zone in the bottom surface traction moves towards the leading edge of contact.

The slope of the NIT curve (refer to Fig. 6.5.) for the first layer changes gradually up to a rolling distance of 0.21 in. Beyond this the slope remains almost a constant till the rolling distance is about 1 in. The slope changes from that point onward till the rolling distance is about 1.4 inches and the slope remains a constant thereafter. This can be observed in the contact traction plots as very little difference is observed between the 1.6 in and 3.6 in.
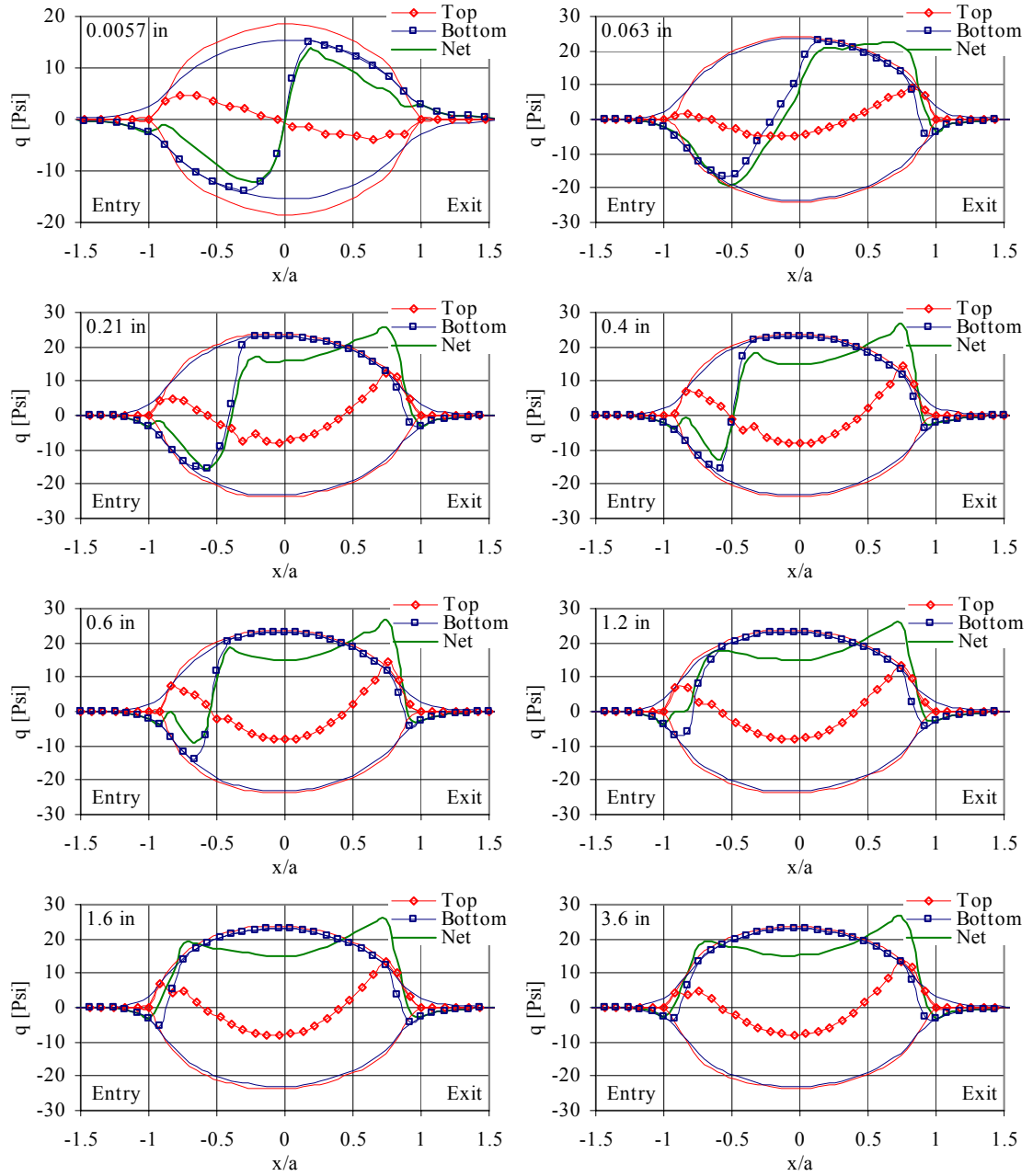
Figure 6.13: Contact shear tractions under the nip roller at different nip rolling distance.

6.1.4 Effect of Nip Load

The effect of nip load on the saturation rate of the NIT is shown in Fig. 6.14. As the nip load increases, the rolling distance for the saturation of NIT also increases. We

can observe that even at the highest nip load level, the saturation distance will be less than the circumference of a typical winding core (~3.4 inches diameter core). Observe that at low nip loads (≤25 Pli), the 'σ_{11}' stress reaches a constant saturated value for rolling distances less than 1.5 inches. At nip loads > 25 Pli, the 'σ_{11}' stress exponentially increases and appears to saturate at rolling distances greater than 1.5 inches. However, due to transient behavior in 'σ_{11}' stresses observed in layers beneath the top layer (predominantly in 'layer 2'), the 'σ_{11}' stress in the top layer increases after the initial saturation level to achieve the final saturated value during further rolling of the nip as shown in Fig. 6.14 (For example, observe 'σ_{11}' stress at a nip load of 41.67 Pli).
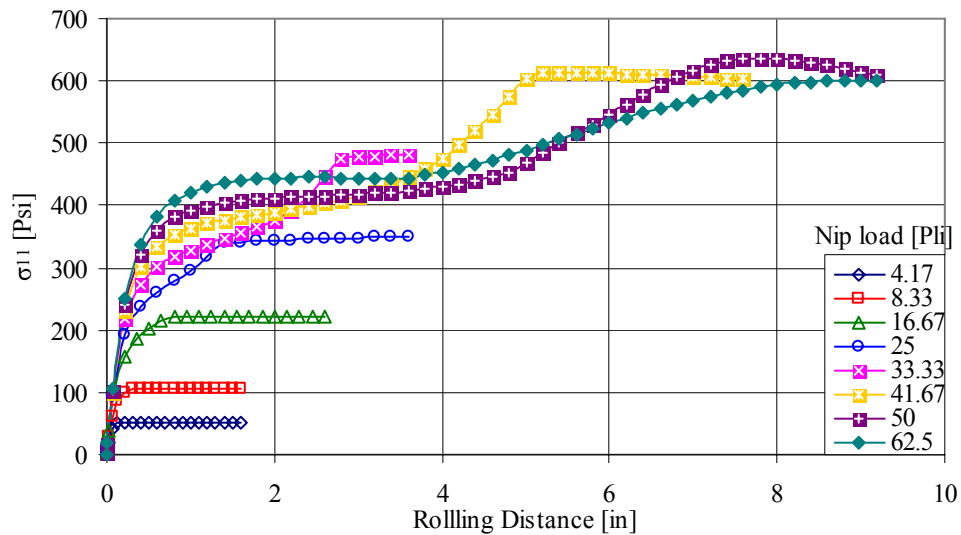
Figure 6.14: Effect of nip load on the nip-induced stress and saturation distance.

The NIT at a given nip load is calculated as the average value at the saturated level. The effect of the nip load on the NIT is shown in Fig. 6.15. As the nip load increases, the NIT increases linearly up to a certain level of nip load. Beyond this nip

load, the NIT levels out very quickly and start to decrease with further increase in nip load. The slope of the NIT curve in the linear region is approximately equal to the coefficient of friction between the web layers. In this case, at all nip loads, a value of 0.16 was used as an input for '$\mu_{Web/Web}$'. This behavior has been previously observed by Good et al [25]. Good, however, observed a much slower leveling out of the NIT tension with increase in nip load.
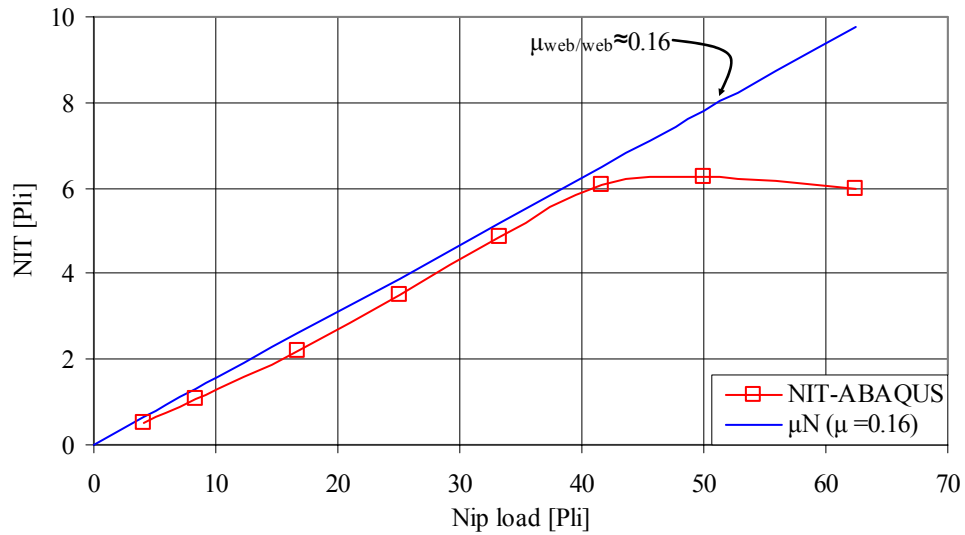
Figure 6.15: Effect of nip load on the NIT.

The half width of contact and the penetration of the nip roller at different nip loads is shown in Fig. 6.16. Both the nip roller penetration and half width of contact increases and asymptotically saturates with nip load. This is mainly due to the nonlinear contact of a cylinder with a half-space and also due to the increase in radial modulus that occurs with increase in nip load. This is also one of the reasons why at higher nip loads, the NIT begins to level off. The main reason why the NIT is much less than μN at higher

nip loads is the traction behavior in the contact zone and this is discussed in the following section.
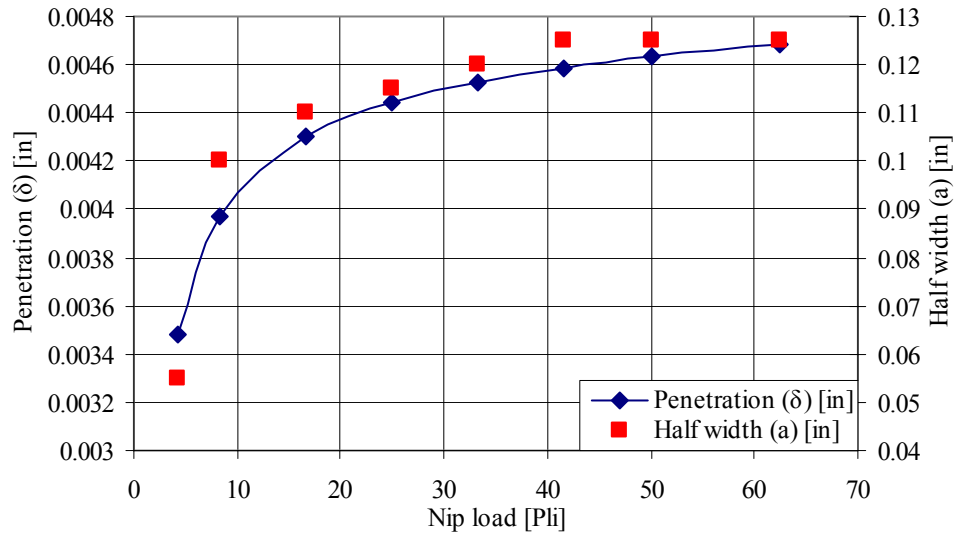
Figure 6.16: Effect of nip load on penetration and half width of contact.

The behavior of the top surface tractions in the top layer at different nip loads is shown in Fig. 6.17. At all nip loads, three distinct regions exist within the nip contact zone. At the leading edge of the nip there exists a slip zone where in the traction values are positive indicating that the top surface of the sheet is moving faster than the nip roller surface. The middle region of contact is in stick and in this region, the surface velocity of the top surface of the web and the nip roller are equal. In the trailing edge of the nip, where the web experiences tension increase, the top surface is under slip. The traction values are positive indicating that the top surface of the web is moving faster than the drum. With increase in nip load, the magnitude of total slip decreases near the leading edge and increases near the trailing edge, thus more or less offsetting each other.
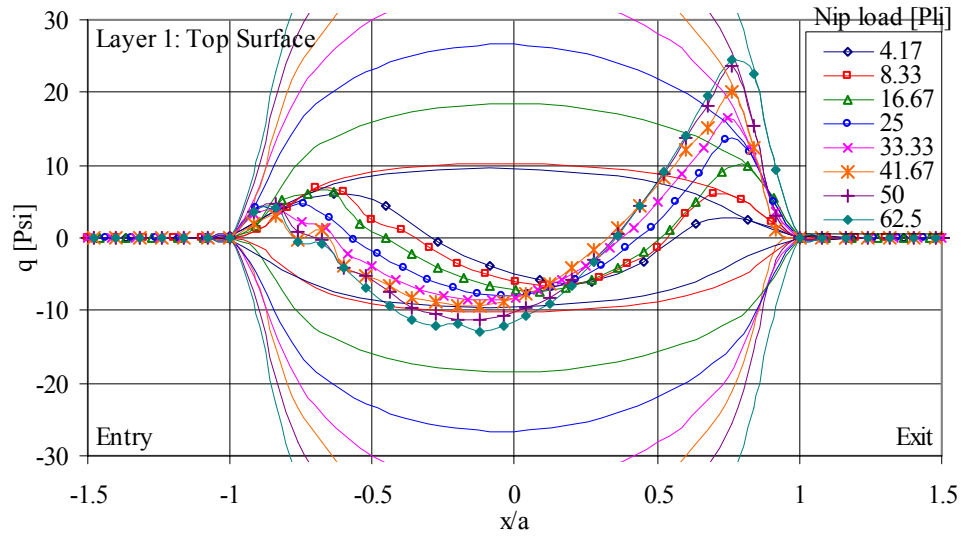
Figure 6.17: Effect of nip load on the top surface tractions in the top layer that contacts the nip roller.

The tractions in the bottom surface of the top layer in the nip contact zone is shown for different nip loads in Fig. 6.18. As explained in section 6.1.3. five distinct regions exist within the zone of contact. The tractions at the leading (entry) and trailing (exit) edges of contact act in the same direction and are under slip. In this zone, the web slips in a direction opposite to the direction of the web travel. Also, the velocity of the bottom surface of the top layer is lower than the top surface of the second layer. In the middle, at low nip loads, the slip reverses direction and the traction becomes positive. In this region, the velocity of the bottom surface of the top layer is greater than the velocity of the top surface of the second layer. Between these opposing slip zones near both ends of contact, the bottom surface is under stick.

At low nip loads, the slip zones at either ends of contact are tiny and so are the intermediate stick zones. This means that, at low nip loads, most of the bottom surface is

under complete slip. The traction in the slip zone acts in the direction of the web travel indicating that the traction is positive. Most of this traction manifests itself into the net traction at low nip loads. As the nip load increases, the stick region near the entry zone of the contact becomes large and grows with further increase in nip load. The slip region at the exit zone also grows with increase in nip load.
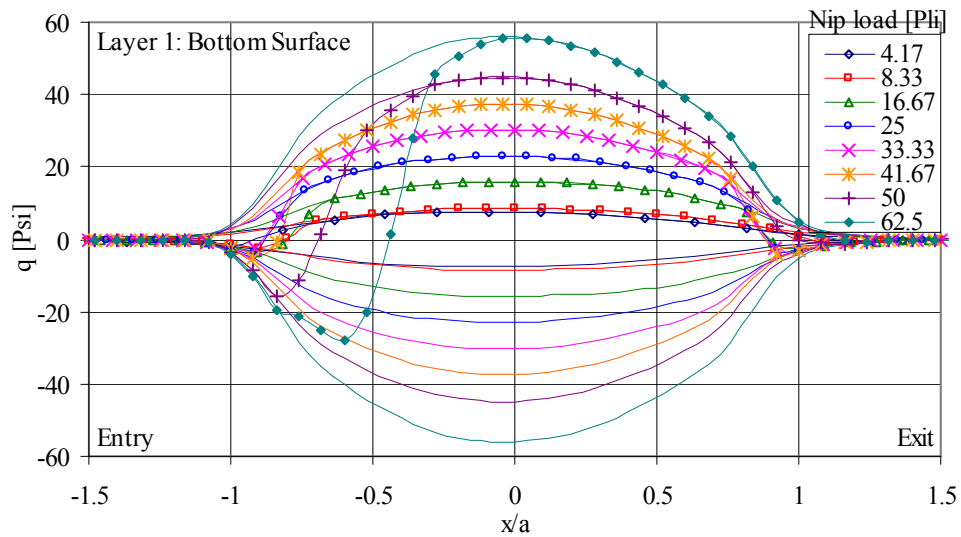
Figure 6.18: Effect of nip load on the bottom surface tractions in the top layer that contacts the nip roller.

The net traction expressed as the sum of the top and bottom surface tractions in the top layer is shown in Fig. 6.19. At the highest nip load, significant amount of net traction is negative due to the increase in the amount of slip and stick in the leading zone of contact in the bottom surface of the top layer. The total traction is the integrated value of the net traction curve and should be equal to the NIT based on the equilibrium of forces given in Eqn. 4.6, 4.7. The net traction is numerically integrated using the trapezoidal rule and is compared to the total NIT developed at the left end of the top layer

in Fig. 6.2. The average error between the total traction values and NIT values was less than 3.5% indicating that the total traction is the most important parameter in determining the NIT developed in the top layer. At high nip loads, the total traction decreases from the maximum possible value and hence the NIT is much less than $\mu_{web/web}N$.
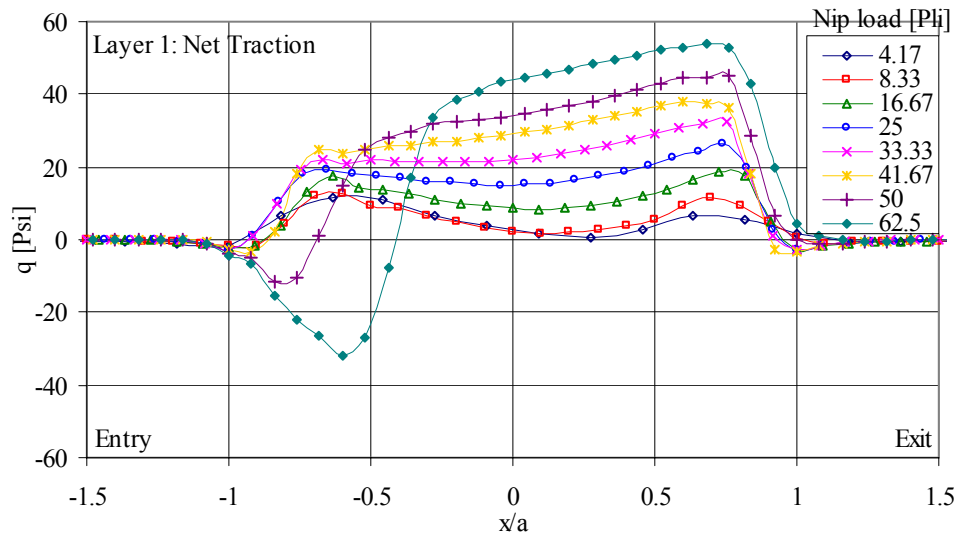
Figure 6.19: Effect of nip load on net traction in the top layer that contacts the nip roller.
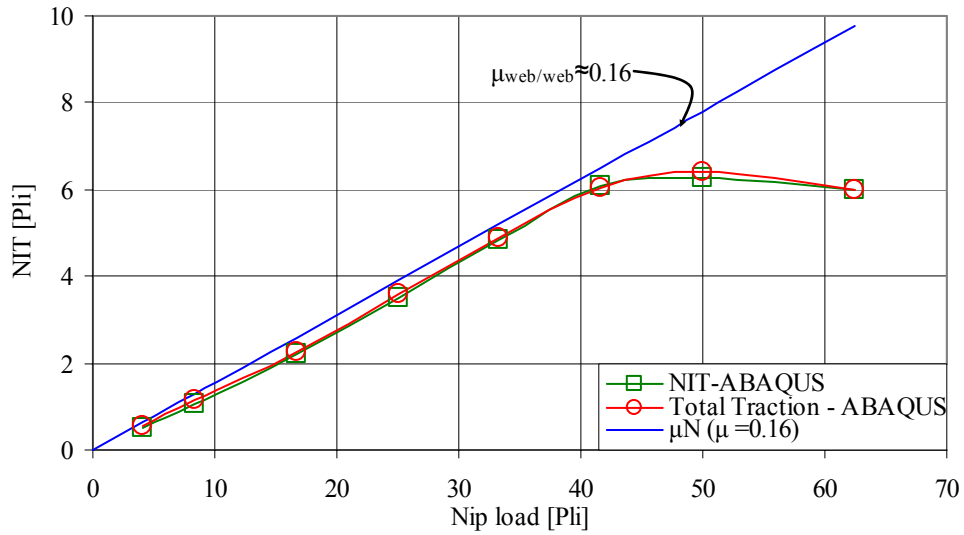
Figure 6.20: Importance of total traction in computing the NIT.

6.1.5 Behavior of the surface velocities

The model is set up in such a way that a velocity boundary condition is prescribed at the left end of the sheets and to the rigid base. Due to this the surface velocity of the rigid nip roller (drum) has to be inferred from the angular velocity as given in Eqn. 6.4. When the surface velocity of the drum was computed, it was less than the velocity of the rigid base (also, the left end of the sheets). This is due to the indentation of the rigid nip roller into the layers within the contact zone and due to the contact mechanics between the nip roller and the layers. The surface strains and the deformation of the top surface in the topmost layer are shown in Fig. 6.21. Within the contact zone, when the top surface is under stick, the top surface strains are compressive. Hence a certain surface element under the nip is shorter than the same surface element behind the nip. This indicates that as the nip roller rolls over this compressed element, it covers a longer distance due to the element being stretched behind the nip.
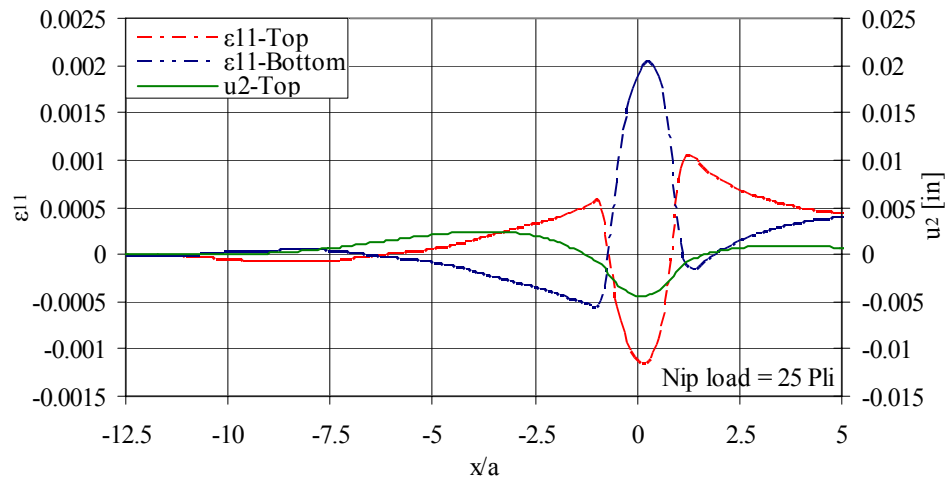
Figure 6.21: The behavior of the surface strains and deformations in the top layer

$$v_d = \omega_d . R_d \qquad (6.4)$$

The relative difference in the surface velocities between the nip roller and the top surface of the topmost layer and between the bottom surface of the topmost layer and the top surface of the second layer is shown in Fig. 6.22 for a nip load of 25 Pli. For the top surface, the velocity difference was calculated using the nodal velocity outputs. However, for the bottom surface, the velocities were calculated from the surface strains as the nodal velocity output was noisy. Ärölä and von Hertzen [42] also calculate the surface velocity from surface strains due to the same reason. The data in the Fig. 6.22 shows that the velocity difference between the nip roller surface and the top surface is negative near the edges of contact. Recalling the discussion on the notation of the velocities from section 6.1.3., we can observe that the top surface moves faster than the nip roller surface at the edges of contact. In the middle of the contact zone, the top surface is under stick and hence the velocity difference is zero. This is consistent with the behavior of the surface tractions observed in Fig. 6.17.
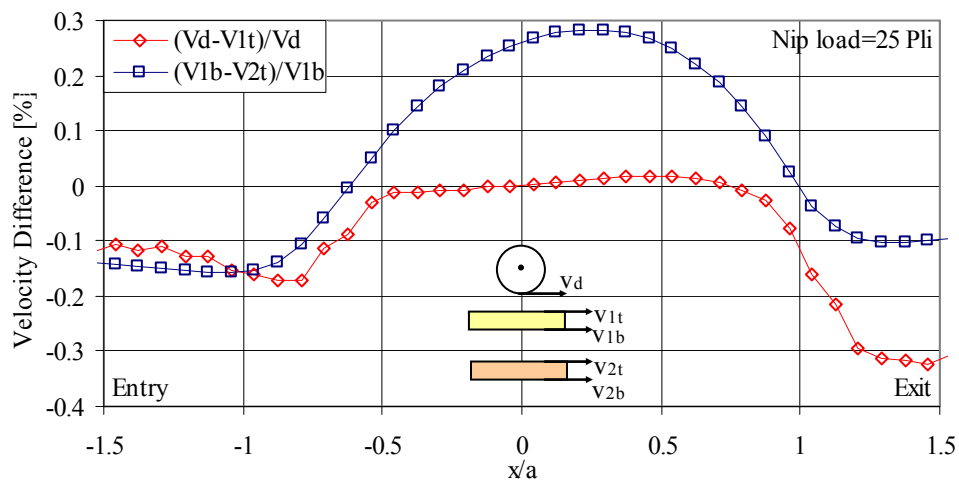
Figure 6.22: Behavior of the top and bottom surface velocities in the top layer at a nip load of 25 Pli.

110

The velocity difference between the bottom surface of the top layer and the top surface of the second layer indicates that the bottom surface is almost under complete slip. In the middle of contact, the velocity difference is positive indicating that the top surface of the second layer is moving faster than the bottom surface of the topmost layer. At the edges of contact, the velocity difference becomes negative indicating that the bottom surface of the topmost layer moves faster than the top surface of second layer. Recall that the bottom surface traction exhibited five distinct regions. Since the intermediate stick zones are small, the stick behavior is not observed in the velocity difference plots.

For the case when the nip load is 62.5 Pli, the velocity differences are shown in Fig. 6.23. In this case, the behavior of the surface velocity in the top surface compared to the nip roller is similar to that was observed for the case of nip load=25 Pli. In the bottom surface, at either ends of contact the bottom surface of the top layer moves faster than the top surface of the second layer. Near the entry zone of contact, the velocity difference becomes zero. This indicates that the bottom surface of the top layer exhibits significant stick zone in this region. This is consistent with the traction behavior observed in section 6.1.4. In the middle of the contact zone, the top surface of the second layer moves faster than the bottom surface of the top layer. A very small stick zone that exists at the exit zone of the contact as observed from the traction plots is not observed in the velocity difference plots.
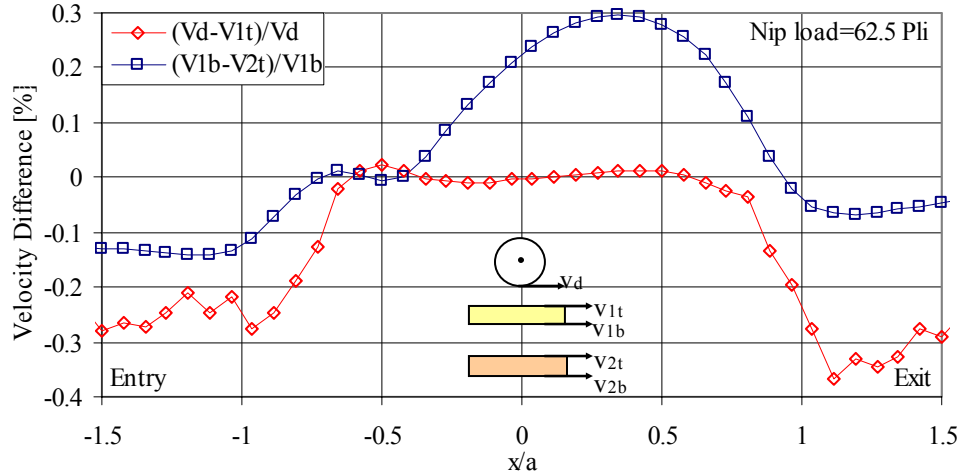
Figure 6.23: Behavior of the top and bottom surface velocities in the top layer at a nip load of 62.5 Pli.

6.1.6 Effect of Physical and Material Properties

In the preceding section, the influence of the total traction was discussed. The total traction will be affected by both the frictional conditions that exist at the contact zone and the material properties. The influence of the friction coefficients along with the effect of the radial modulus, out-of-plane Poisson's ratio, out-of-plane shear modulus and nip roller diameter on the NIT is discussed in the following section.

6.1.6.1 Effect of the coefficient of friction between the nip roller and web layer ($\mu_{Nip/Web}$)

The effect of '$\mu_{Nip/Web}$' on the σ_{11} stresses in the layer as a function of nip rolling distance is shown in Fig. 6.24. When the friction coefficient was increased from 0.18 to 1.0, there was no noticeable difference in the behavior of NIT. The difference in NIT was much less than 0.1% at different values of $\mu_{Nip/Web}$. When the top and bottom surface tractions were compared at different values of $\mu_{Nip/Web}$ as shown in Fig. 6.25, the behavior

remains the same. Due to this, given a nip load, the net traction remains the same at all values of $\mu_{Nip/Web}$. Also, the top surface tractions indicate that most of the surface is under stick. Increasing the values of $\mu_{Nip/Web}$ when the surface is under stick does not change the stick behavior. Hence the NIT remains the same.
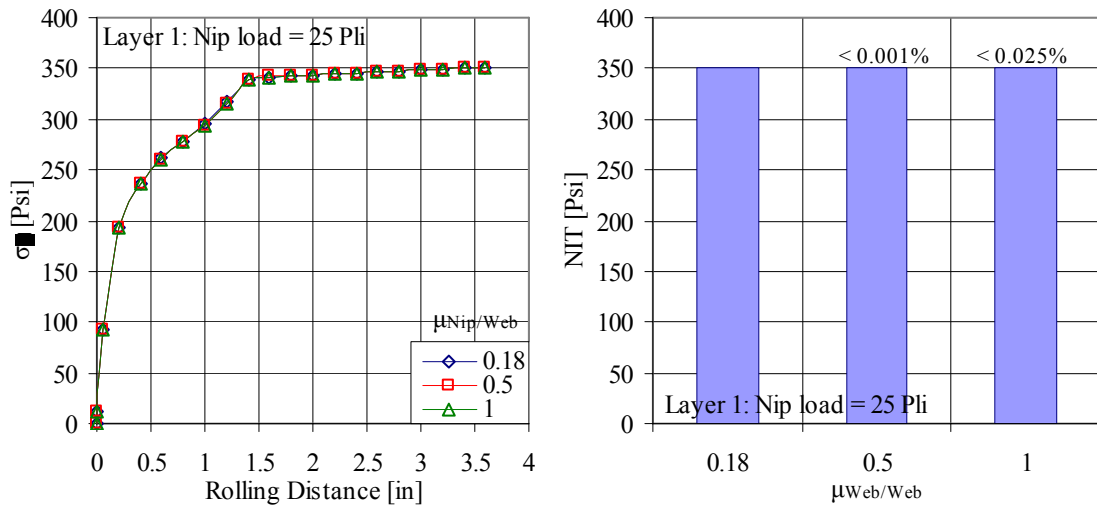
Figure 6.24: Behavior of the $\sigma 11$ stresses and the NIT in the top layer for different values of $\mu_{Nip/Web}$ and at a constant nip load of 25 Pli.
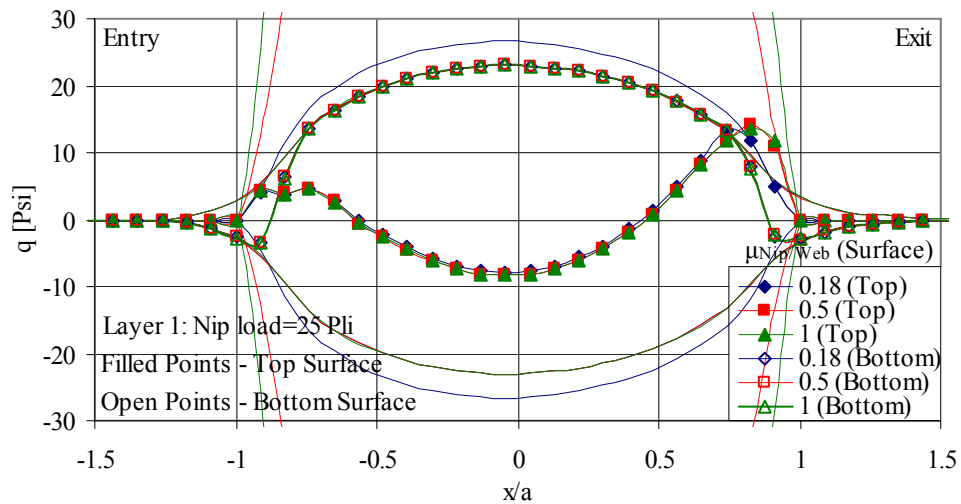
Figure 6.25: Effect of $\mu_{Nip/Web}$ on top and bottom surface traction in the top layer.

113

This type of flat bed nip mechanics analysis resemble closely to center winding process with an undriven nip roller. Hence, '$\mu_{Nip/Web}$' will not affect the NIT in a center winding process. However, one should realize that '$\mu_{Nip/Web}$' can affect the behavior of NIT in surface winding process.

6.1.6.2 Effect of Coefficient of Friction between Web Layers ($\mu_{Web/Web}$)

The effect of coefficient of friction between the web layers on the NIT is shown in Fig. 6.26. In this case, the nip load was fixed at a constant value of 25 Pli and the behavior in NIT was observed. For initial increase in the value of $\mu_{Web/Web}$, the NIT increases almost linearly. For these values of $\mu_{Web/Web}$, the NIT is approximately equal to $\mu_{Web/Web}N$. Further increase in values of $\mu_{Web/Web}$ (>0.3) results in decrease of NIT. This threshold value of $\mu_{Web/Web}$, beyond which the NIT starts to decrease, will depend both on the material used and on the winding conditions.

When the top surface tractions were observed, the behavior was unaffected for different values of '$\mu_{Web/Web}$'. The bottom surface tractions in the top layer for different values of '$\mu_{Web/Web}$' are shown in Fig. 6.27. For values less than 0.3, the bottom surface tractions are almost under complete slip (as explained in section 6.1.3). As the friction increases beyond 0.3, pronounced stick appears near the leading edge of contact. When the coefficient of friction is 1.0, most of the bottom surface is under stick. Although five distinct regions exist in the bottom surface tractions at all values of '$\mu_{Web/Web}$', at high values of '$\mu_{Web/Web}$', the slip and stick zones at the exit zone of contact become vanishingly small.
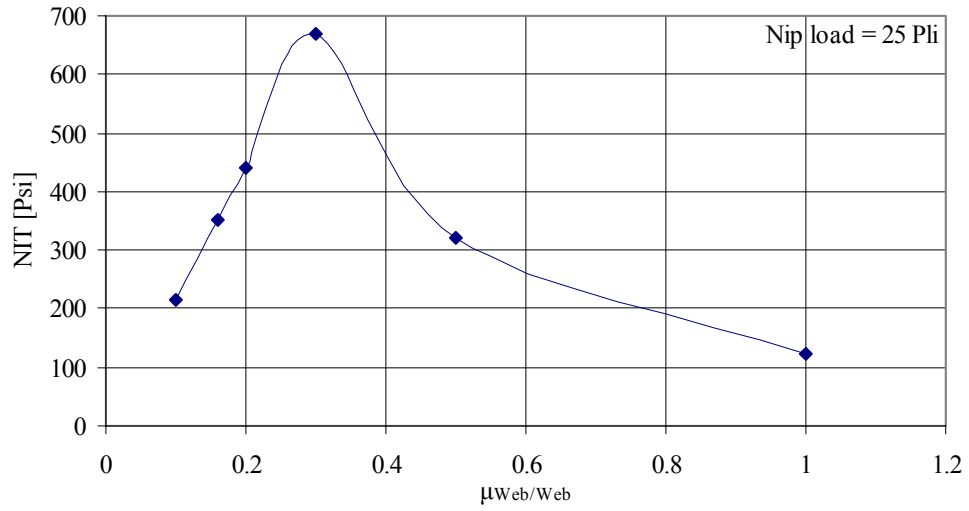
Figure 6.26: Effect of the coefficient of friction between web layers on the NIT.
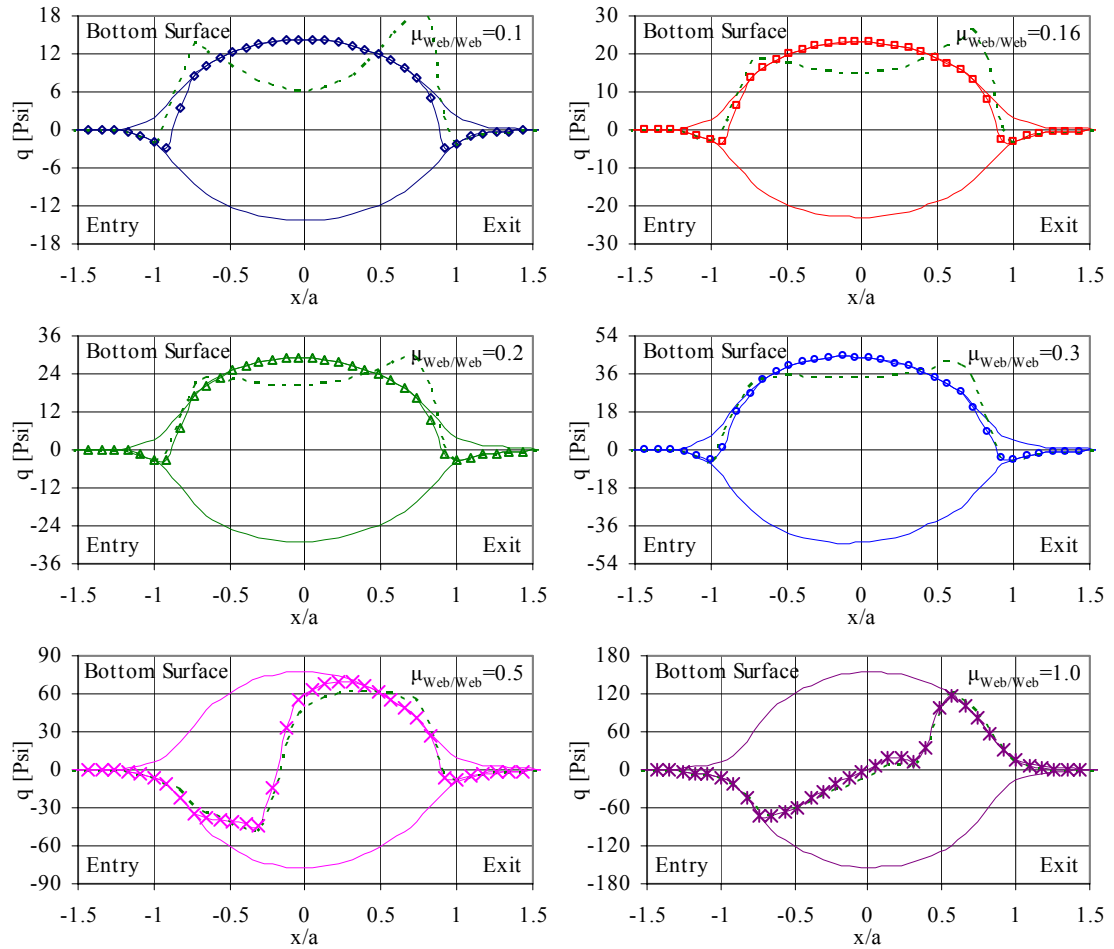
Figure 6.27: Effect of $\mu_{Web/Web}$ on the bottom surface tractions for the case of nip load=25 Pli.

The behavior observed in Fig. 6.27 is very similar to what Johnson [41] observed in the behavior of surface tractions in a calendaring process. Also, increasing '$\mu_{Web/Web}$' increases the traction limits and hence the traction in the bottom surface becomes much higher than the traction in the top surface. Due to this reason, the net traction represented using dotted lines in the bottom surface traction plots becomes almost equal to the bottom surface traction at high values of '$\mu_{Web/Web}$'.

The 'σ_{11}' stresses in the contact zone are shown in Fig. 6.28. When the bottom surface is almost under complete slip, the stresses through the contact zone monotonically increase. This behavior is seen in cases wherein the value of '$\mu_{Web/Web}$' was less than 0.3. However, when substantial stick zone exists in the contact zone in the bottom surface, the stresses behave differently. At higher values of '$\mu_{Nip/Web}$', the bottom surface tractions act in opposing directions at either ends of contact. Due to this, the σ_{11} stress in the contact zone becomes compressive near the leading edge when the bottom surface traction is negative and becomes tensile near the trailing edge as the bottom surface tractions become positive. Due to this, at higher values of '$\mu_{Nip/Web}$', the NIT is less compared to the NIT at lower values of '$\mu_{Nip/Web}$'. This behavior is also seen in Fig. 6.26.
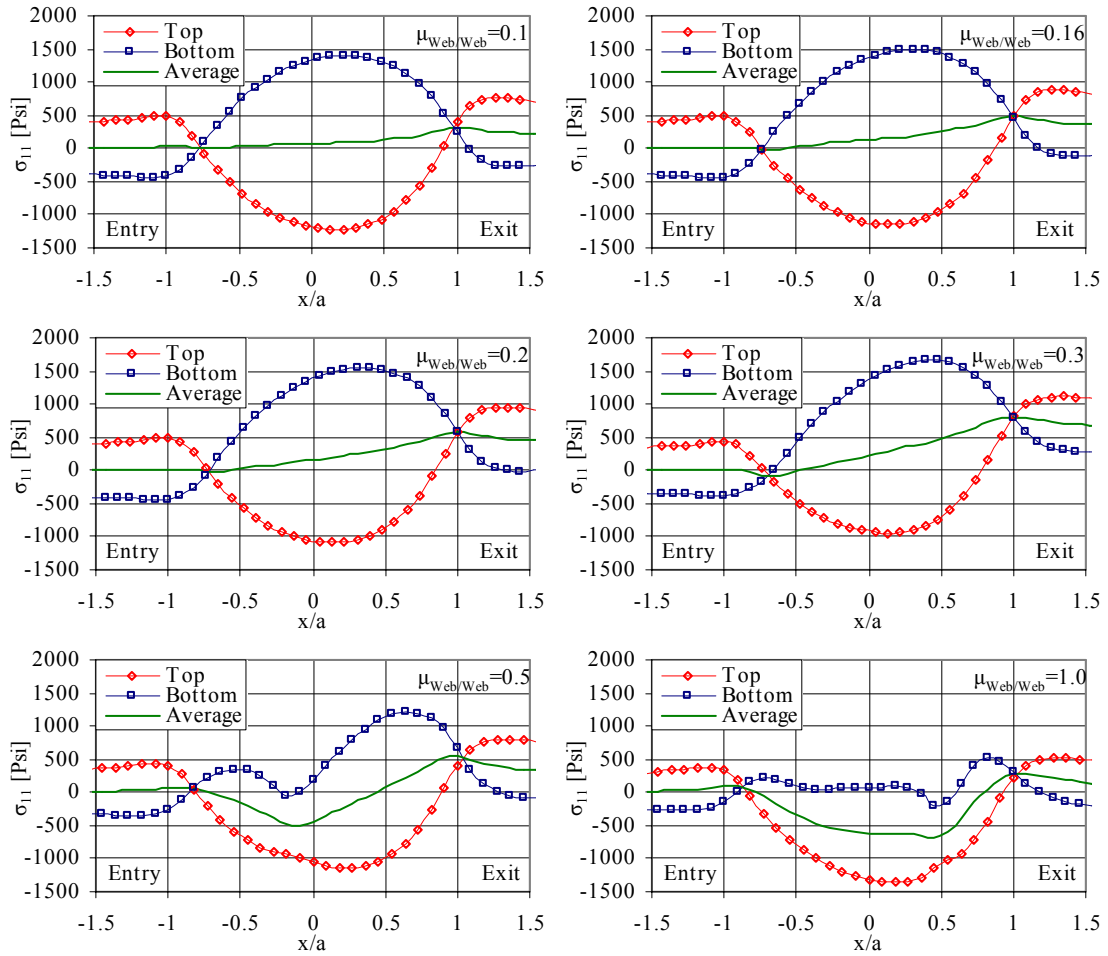
Figure 6.28: Effect of $\mu_{Web/Web}$ on the σ_{11} stress through the contact zone for the case of nip load=25 Pli.

6.1.6.3   Effect of Radial Modulus (E_r)

For nip load=25 Pli, the effect of radial modulus on the NIT and the half width of contact 'a' is shown in Fig. 6.29. For initial increase in radial modulus, the NIT more or less remains the same even though the half width of contact decreases very rapidly. The half width of contact asymptotically decreases with increase in 'E_r'. At high values of 'E_r', the NIT decreases rapidly while the change in 'a' becomes much less.
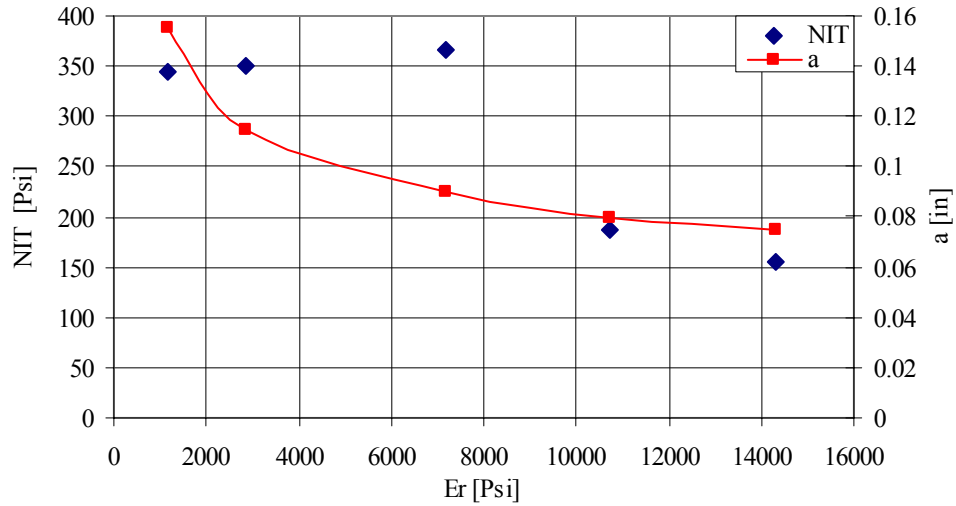
Figure 6.29: Effect of radial modulus on the NIT and the half width of contact 'a'.

Although the traction limits increase with increase in radial modulus, the top surface tractions remained unaffected. On the other hand, the bottom surface tractions are affected by radial modulus as shown in Fig. 6.30. In this case, for radial modulus values less than 7163 Psi, most of the bottom surface is under slip. Since the frictional envelopes increase with increase in radial modulus, the bottom surface tractions also increase when the surface is almost under complete slip. At higher values of 'E_r' (> 7163 Psi), the behavior of the bottom surface traction changes. At the entry zone, the bottom surface starts to stick and this stick zone increases with increase in radial modulus. Although, the bottom surface traction appears to increase for increase initial increase in 'E_r', it does not explain why the NIT remains almost the same as shown in Fig. 6.29. The reason can be deduced from the net traction plots expressed as a function of the half-width of contact as shown in Fig. 6.31.
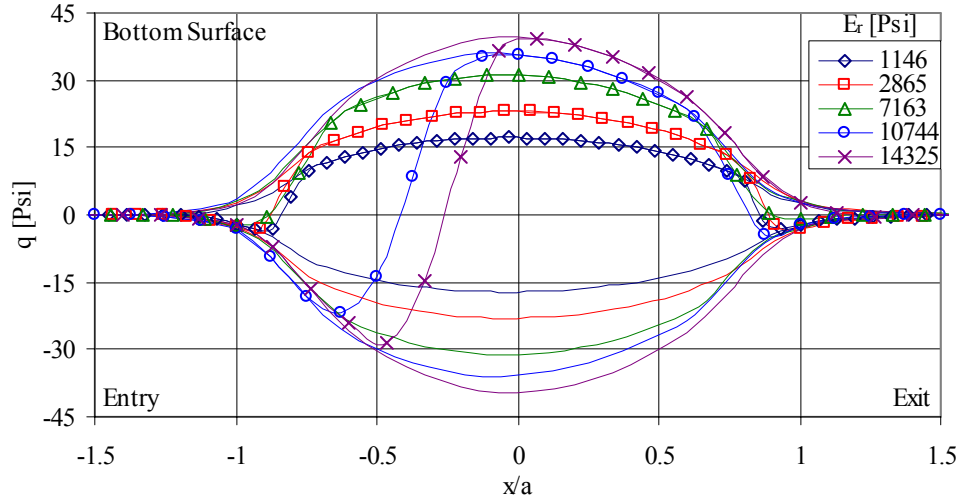
Figure 6.30: Effect of radial modulus on the bottom surface tractions at a nip load of 25 Pli.
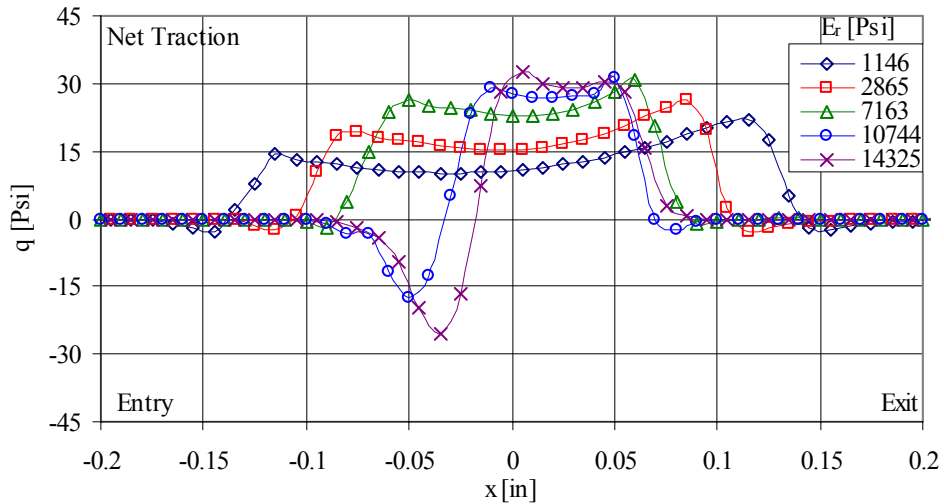
Figure 6.31: Behavior of the net traction due to change in radial modulus 'E$_r$'.

Since the top surface tractions remain unchanged with increase in radial modulus, the net traction is only affected by the bottom surface tractions. At low values of 'Er', the half width of contact decreases very rapidly. Although the net traction within the contact increases, the decrease in the contact width makes the NIT remain almost the same. At higher values of 'E$_r$', the change in width of contact is much less. So a significant

119

increase in stick-zone in the bottom surface traction reduces the net traction and hence the NIT. This behavior is analogous to the behavior of the NIT with respect to nip load. At low nip loads, the value of 'E_r' is low and the NIT is approximately equal to '$\mu_{Web/Web}.N$'. As the nip load increases, the NIT remains approximately equal to '$\mu_{Web/Web}.N$' till the stick zone near the entry zone of contact starts to grow at very high nip loads.

6.1.6.4 Effect of Out-of-Plane Shear Modulus (G_{12} or $G_{r\theta}$)

The behavior of the NIT for two different values of the out-of-plane shear modulus 'G_{12}' (also denoted as $G_{r\theta}$) is shown in the Fig. 6.32. At low nip loads, a tenfold increase in G_{12} does not affect the NIT. However, at high nip loads, a tenfold increase in shear modulus increases the NIT. Even at high nip loads, the NIT becomes approximately equal to $\mu_{Web/Web}.N$.
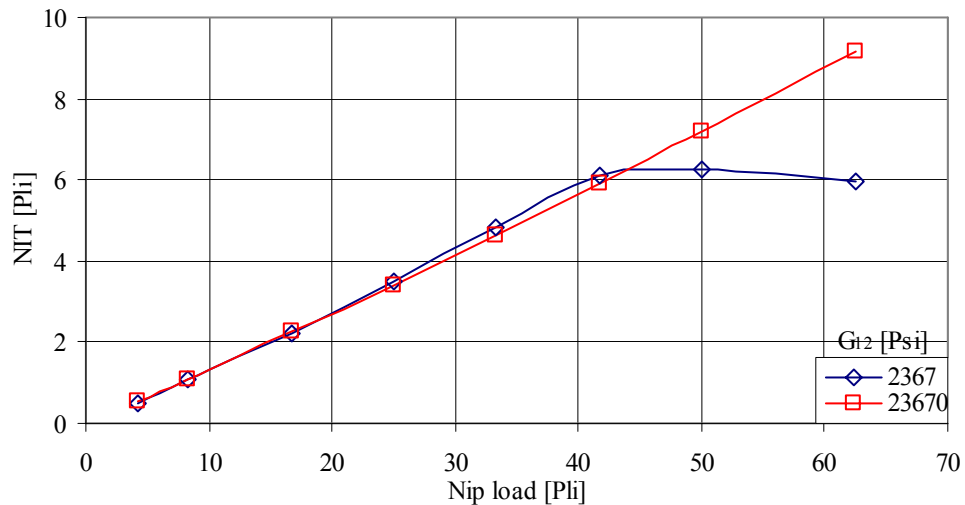
Figure 6.32: The behavior of the NIT for a tenfold increase in the out-of-plane shear modulus 'G_{12}'.

Although the top surface tractions were unaffected by increasing 'G_{12}', the effect on the bottom surface tractions is shown in Fig. 6.33. At low nip loads, the bottom surface tractions do not differ much for the two different 'G_{12}' values. This indicates that the shearing deformations that occur at low nip loads are limited by the frictional forces since the surface is under total slip. At high nip loads, the stick zone near the entry of the contact decreases significantly when 'G_{12}' is changed from 2367 to 23670 Psi. The bottom surface is almost under complete slip even at high nip loads causing the net traction to increase. This is the reason why the NIT becomes $\approx \mu_{Web/Web}$. N. This indicates that, at high nip loads, when stick begins to occur, the shearing deformations and the associated surface tractions are governed by the shear modulus and the shear strains. Hence, 'G_{12}' becomes an important parameter after the onset of stick but it may also dictate the point of departure of the NIT from the '$\mu_{Web/Web}$. N' behavior.
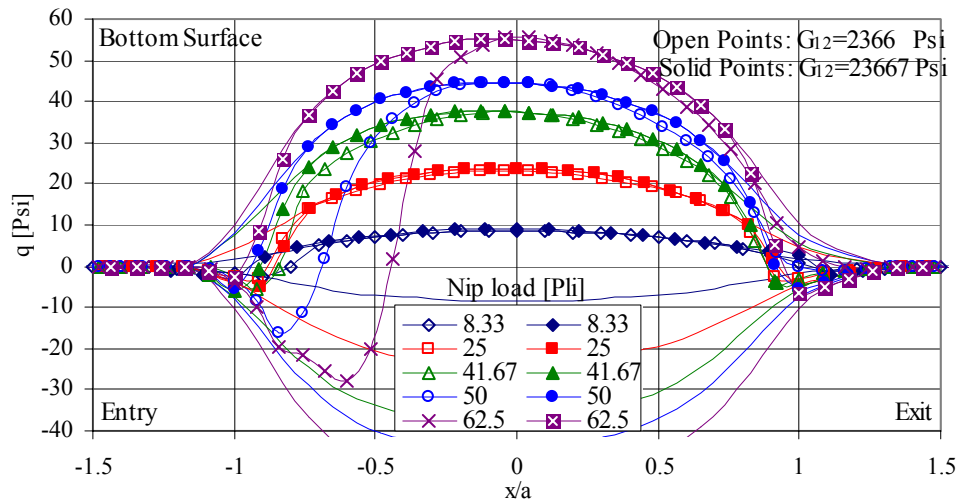
Figure 6.33: Effect of the out-of-plane shear modulus 'G_{12}' on the bottom surface tractions.

6.1.6.5 Effect of Out-of-Plane Poisson's ratio (ν_{12} or $\nu_{r\theta}$)

Changing the out-of-plane Poisson's ratio '$\nu_{r\theta}$' from 0.3 to 0.01 did not significantly change the NIT as shown in Fig. 6.34. At a given nip load, both the top and bottom surface tractions were similar for different values of Poisson's ratio. This indicated that the net traction and hence the NIT would remain unaffected. In this case a rigid nip roller was used and hence the shearing deformations and the resulting surface tractions are controlled more by the rigid nip roller. As a result the top and the bottom surface tractions are unaffected by changing the value of '$\nu_{r\theta}$'. This behavior is analogous to the behavior of the NIT with respect to '$\mu_{Nip/Web}$' as the top surface is predominantly under stick for different values of '$\mu_{Nip/Web}$'.
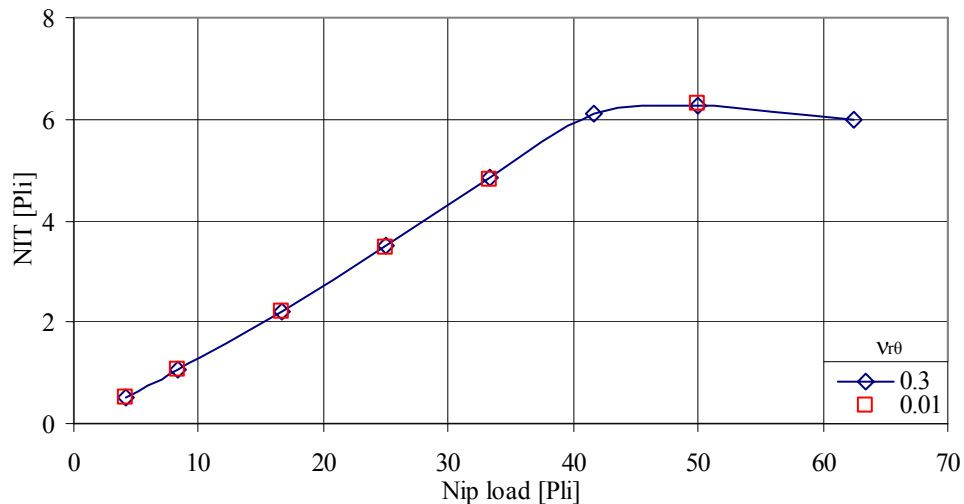
Figure 6.34: Effect of the out-of-plane Poisson's ratio $\nu_{r\theta}$ on the NIT.

6.1.6.6 Effect of Nip Roller Diameter

The effect of the nip roller diameter on the NIT and half width of contact is shown in Fig. 6.35. As the nip roller diameter increases, the contact width increases and the NIT

decreases. The effect of nip roller diameter on the top surface tractions of the topmost layer at a nip load of 25 Pli is shown in Fig. 6.36. Increase of nip diameter increases the nip contact width thus decreasing the contact pressure. Hence the frictional limit envelopes reduce as a result of increasing the nip diameter as shown in the figure. The slip at the leading and trailing edges of the nip roller decreases with increase in nip diameter and the top surface goes into complete stick.
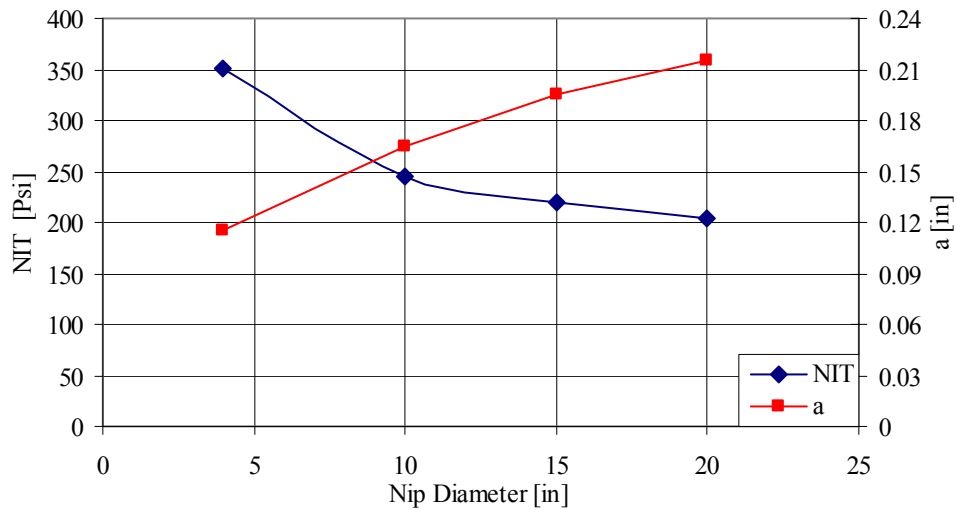
Figure 6.35: Effect of nip roller diameter on the NIT and half width of contact 'a'.
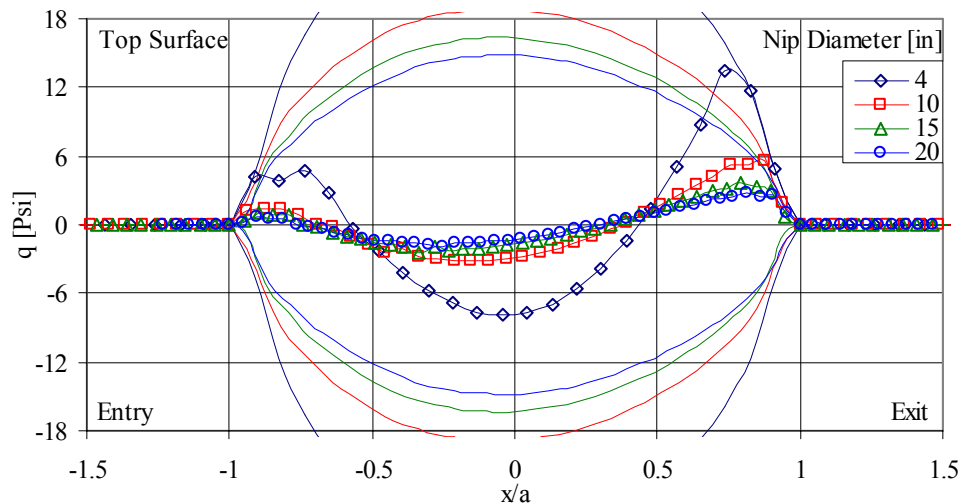
Figure 6.36: Effect of the nip roller diameter on the top surface tractions at nip load of 25 Pli.

123

In the case of the bottom surface, as the nip diameter increases, the leading edge starts to exhibit substantial stick zone. This is illustrated in Fig. 6.37. As a result, the net traction decreases due to both the contact pressure becoming less and the bottom surface experiencing significant stick conditions as the nip diameter increases as shown in Fig. 6.38. As a result of this, the total traction and hence the NIT reduces. This behavior has also been observed by Good [8] and Jorkama [10].
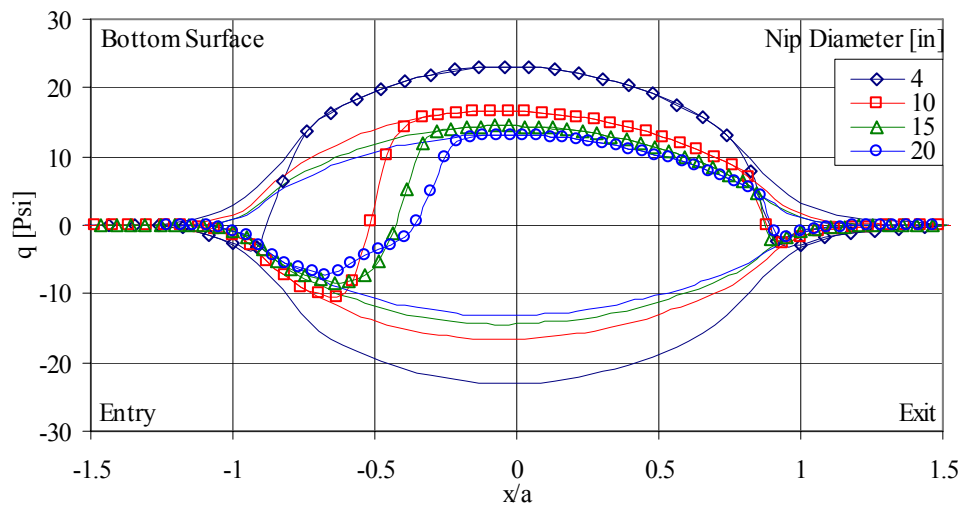
Figure 6.37: Effect of the nip roller diameter on the top surface tractions at nip load of 25 Pli.
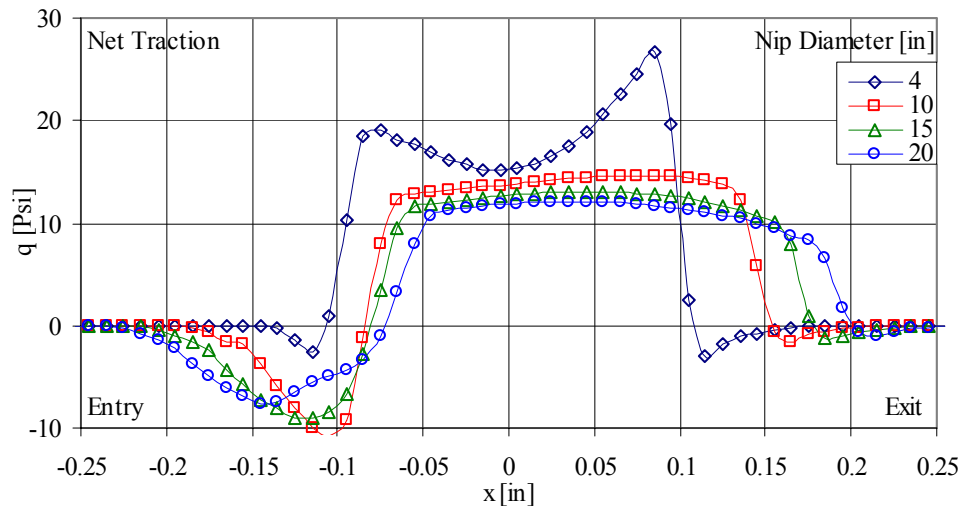
Figure 6.38: Effect of the nip roller diameter on the top surface tractions at nip load of 25 Pli.

6.1.6.7 Effect of Nip Cover Compliancy

The effect of the compliancy of the nip roller cover on the σ_{11} stresses at the left end of the topmost layer is shown in Fig. 6.39. The nip rollers with compliant covers produce much lesser NIT compared to the rigid nip roller. The cover is modeled using an isotropic material with properties of E=700 Psi, ν=0.46 representing a solid urethane material (rubber) and with properties of E=700 Psi, ν=0.01 representing a cellular urethane material (foam). The top and bottom surface tractions are shown in Fig. 6.40.
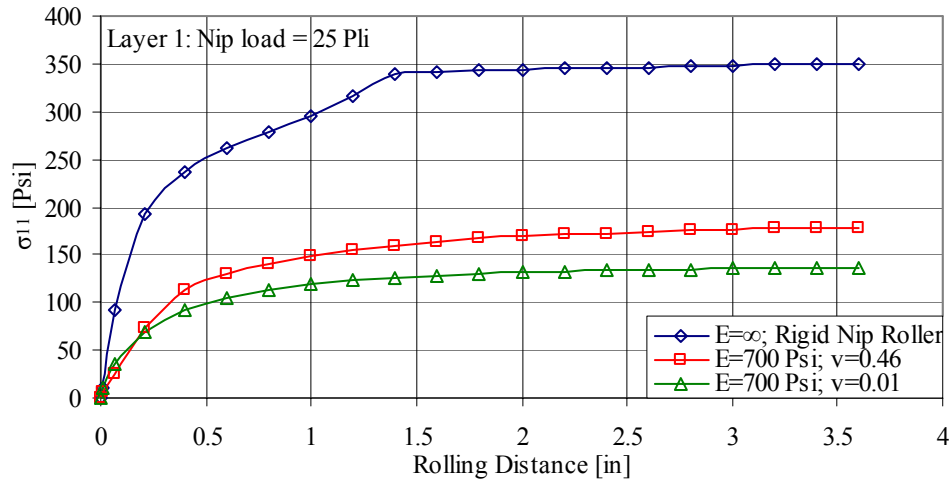
Figure 6.39: Effect of the nip roller compliancy on the σ_{11} stress in the topmost layer at a nip load of 25 Pli.

The half width of contact increases substantially for the nip roller with a compliant cover as given in each of the traction plots. Observe that the traction limits reduce significantly compared to the rigid nip roller case. In the case of a rubber cover, the top surface is under complete stick. Note that the oscillations in the top surface traction at the exit zone are due to numerical oscillations due to high mass scaling factors although the mass scaling factor was reduced from 25 to 3. In the case of the bottom

surface traction, a substantial stick exists near the entry zone causing the net traction to reduce significantly. This reduces the overall stresses in the contact zone as shown in the σ_{11} stress plot.
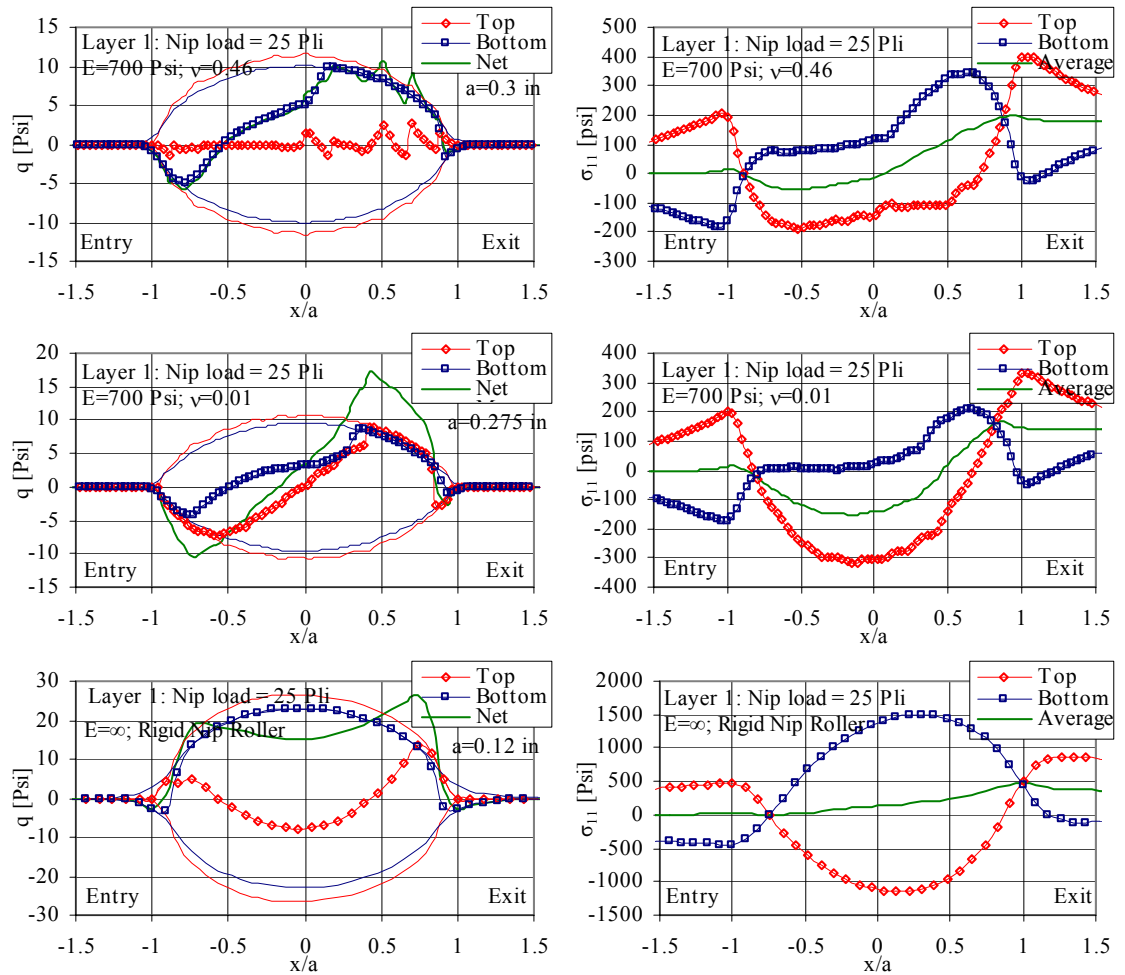
Figure 6.40: The effect of the nip roller compliancy on the behavior of the contact tractions and σ_{11} stresses in the contact zone for a nip load of 25 Pli

In the case of the foam covered nip roller, the top surface tractions behave very similar to the bottom surface traction. The top surface is under micro-slip exhibiting five distinct regions. Also, the two largest slip zones, one at the entry zone and one near the exit zone act in opposite directions. The bottom surface tractions also behave in the same

manner. Due to this the slip zones act additively at either ends although at either ends they act opposite to each other. This is also seen in the σ_{11} stress plot as the σ_{11} stress is compressive near the entry zone and is tensile near the exit zone. The behavior of the surface tractions in all the layers beneath the topmost layer is qualitatively similar to the behavior observed in the top layer. Also, since the nip roller cover is compliant, the bending stresses within the contact zone are significantly less compared to that generated for a rigid nip roller.

The % difference in velocities between the surface of the nip roller and the top surface of the topmost layer and between the bottom surface of the topmost layer and the top surface of the second layer in the contact zone are compared for different nip rollers in Fig. 6.41, 6.42 for rubber and foam covered nip rollers respectively. In the case of a rubber covered nip roller, the top surface of the sheet moves at the same velocity as the nip roller through the entire contact zone. The bottom surface of the topmost layer moves faster than the top surface of the second layer near the edges of contact. In the region wherein -0.75<x/a<0.2, the velocity difference is zero indicating that the region is under stick. In the region wherein 0.2<x/a<0.8, the bottom surface of the topmost layer moves slower than the top surface of the second layer indicating that the slip direction is opposite to that observed at the edges of the contact. This is consistent with the behavior observed in the contact tractions shown in Fig. 6.40. In the case of the foam covered nip roller, when the % difference in velocities between the surface of the nip roller and the top surface of the topmost layer is observed, it indicates that the layer surface moves faster compared to the nip roller surface at the edges of contact. In the region wherein -

127

0.75<x/a<0.42 the surface velocities are equal. In the region 0.42<x/a<0.78 the top surface of the topmost layer moves slower than the surface velocity of the nip roller. The qualitative behavior of the surface velocities between the bottom surface of the topmost layer and the top surface of the second layer are similar to that was observed for the case when the nip roller cover was rubber. This is consistent with the behavior observed in the contact tractions shown in Fig. 6.41.
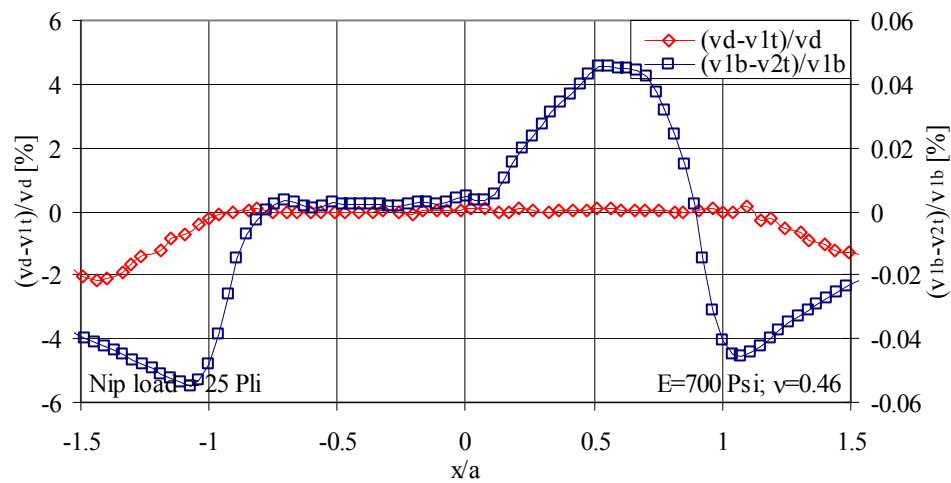
Figure 6.41: Behavior of the top and bottom surface velocities in the top layer at a nip load of 25 Pli for a rubber covered nip roller.
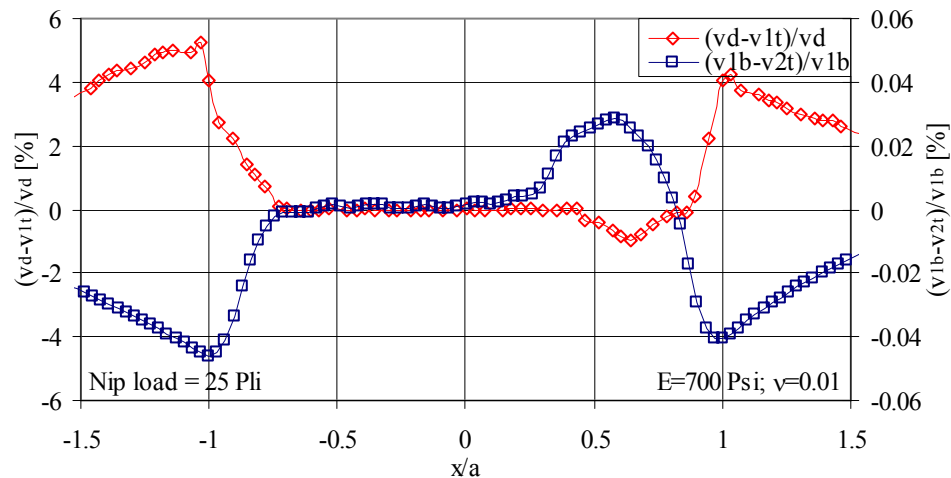
Figure 6.42: Behavior of the top and bottom surface velocities in the top layer at a nip load of 25 Pli for a foam covered nip roller.

When the absolute values of the surface velocities for different nip rollers are compared, as shown in Fig. 6.43, an important observation can be made. When the nip roller is rigid, the surface velocity is constant and this indicates that the bottom surface tractions will be very important. When the material of the nip roller cover is comparable to rubber, the velocity of the nip roller exhibits local speeding near the entry of the contact zone. This also shows that at high nip loads, this phenomenon can increase the NIT beyond what a rigid nip roller can produce and shows the importance of the top surface behavior. When the material of the nip roller cover is comparable to foam, the velocity of the nip roller slows down prior to the contact zone. This behavior can cause the web to lose almost all the web tension. Given that the surface tractions almost cancel each other between the entry and exit zones of the contact, very little NIT is generated.
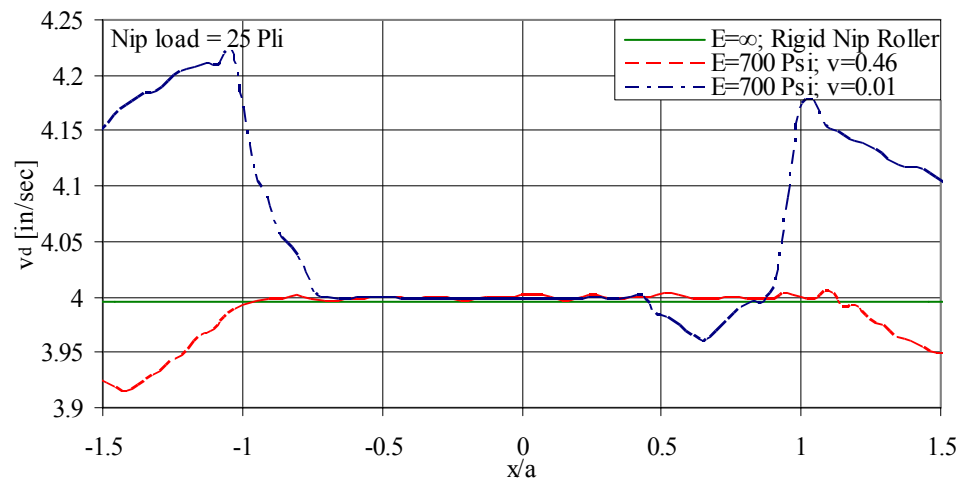
Figure 6.43: Behavior of the surface velocities of different nip rollers.

Jorkama [10] reports a similar behavior for compliant nip covers based on his nip contact model. Although the magnitudes are different, the general trends are similar when

compared with experimental measurements of Santhanakrishnan [30]. In his case, the Poisson's ratio of the nip cover affected the NIT more than the modulus of the nip cover. In this case, since a general behavior due to the use of compliant nip cover was sought, the nip cover was modeled as an isotropic body. However, sophisticated material laws should be used to correctly define the material behavior of rubber, foam nip covers in order to compare the NIT model results to experimental results.

6.2   Winding Mechanics

The contact mechanics between a nip roller and a winding roll is studied in detail in this section. The development of wound-on-tension in the outermost layer is observed and the basic phenomenon is presented. The effect of various parameters on the nip mechanics and the development of the wound-on-tension are also discussed.

6.2.1   Development of the Wound-on-Tension

A schematic of the winding process and the notation for the analysis of results is shown in Fig. 6.44. Observe that the layer on top of the core is represented as 'layer 5' and the layer in contact with the nip roll is represented as 'layer 1'. As the layer enters the winding roll it is bent about the axis of the nip roller in the contact zone and then bent around the winding roll about the centroidal axis of the winding roll. Due to this the layer experiences significant bending stresses along with the NIT. Given a layer, the top and the bottom surfaces exhibit both the bending and the membrane components. The WOT is the membrane component of the σ_{11} stress and is calculated by averaging the top and bottom surface stresses.
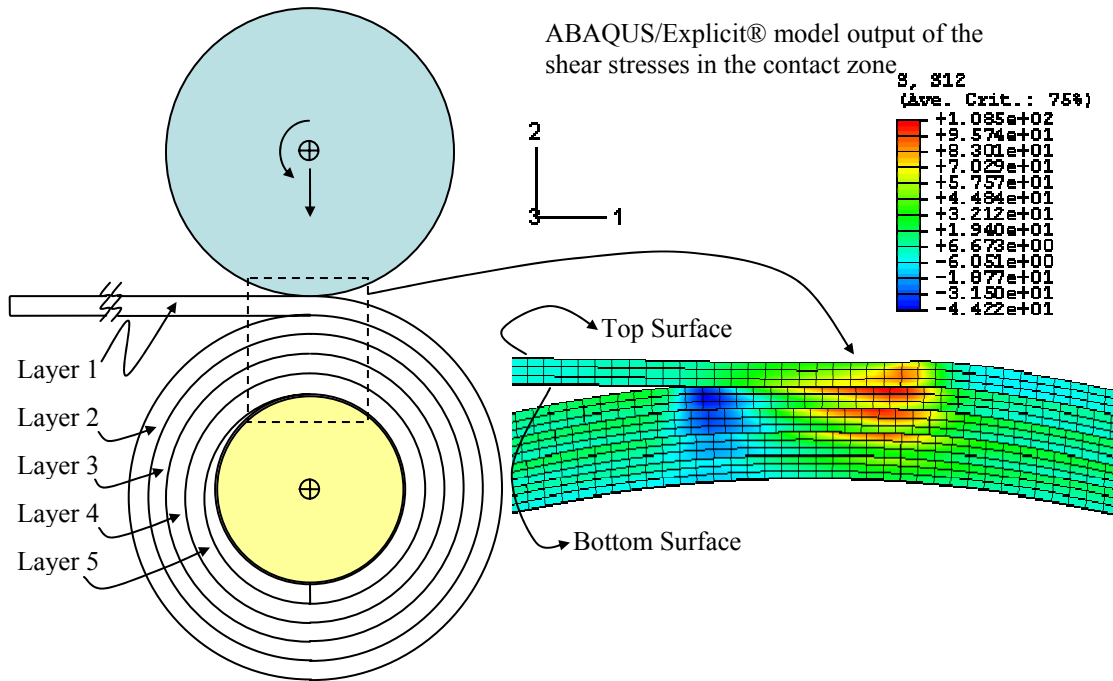
Figure 6.44: Schematic of the winding process, the notations used and ABAQUS/Explicit[®] output of shear stresses 'σ$_{12}$' in the nip contact zone.

The behavior of the machine direction stresses (σ$_{11}$) stresses in a center wound roll without an undriven nip roller at a given instant of time as a function of the total length of the web material is shown in Fig. 6.45. In this case, the roll is center wound at a constant web tension of 3 Pli. In the figure, the region wherein the total web length is less than 3 inches (free span), the web is under the prescribed value of web tension (3 Pli). Beyond this region, the web becomes part of the wound roll. In the free span, the bending stresses in the web are much less when compared to the bending stresses in the layers in the wound roll. Since the roll is center wound without the presence of a nip roller, the membrane stresses in the outermost layer must be equal to the web tension in the free span and this can be observed in Fig. 6.45.

Observe that the average value of 'σ$_{11}$' is constant through the outermost layer
and the average value of this stress in the outermost layer is calculated as the WOT. In
the winding case, significant tension exists in layers below the topmost layer. Addition of
each layer causes significant radial pressures in the layers beneath the outermost layer. In
this case, this pressure inhibits slip between the layers and due to this the WOT is
constant through the outermost layer. The theoretical bending stress in the layer
calculated using Eqn. 6.5. is ≈2035 Psi. Although the bottom surface stress is equal to the
theoretical value of the bending stress, the top surface stresses are offset by twice the
value of the web tension so that the average of the top and bottom stresses is equivalent
to the value of the web tension.

$$\sigma_{Bending} = E_{md}\frac{u}{r}$$ (6.5)
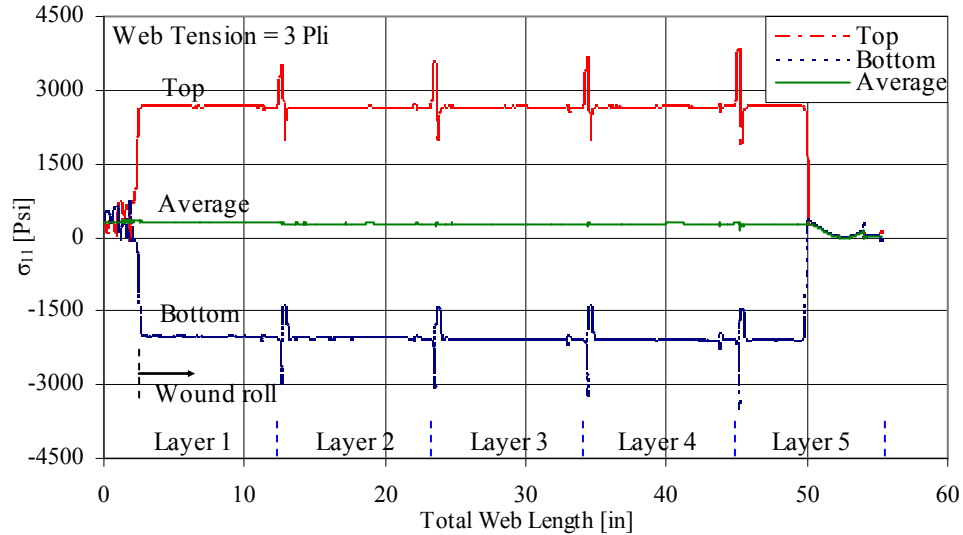
Figure 6.45: Behavior of the top, bottom and average 'σ$_{11}$' stresses in a center wound roll at Tw=3 Pli.

In Fig. 6.45., the σ$_{11}$ stresses in the wound roll show period peaks in every layer.
These peaks are caused as a result of the stress concentration that occurs due to the start

132

up of the wound roll as shown in Fig. 6.46. In this region, the bending stresses are significant compared to the overall value of WOT as represented by the peaks in Fig. 6.45.
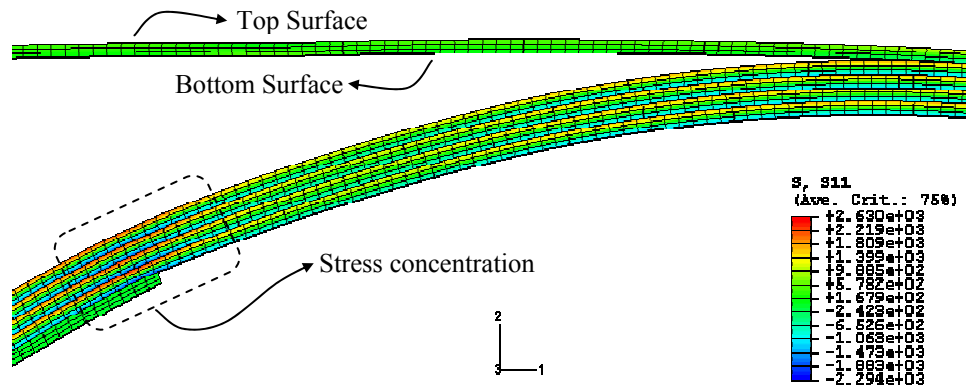
Figure 6.46: Effect of the start up of the wound roll on the bending stresses.

When an undriven nip roller is used in a center winding process, the nip roller increases the tension in the outermost layer beyond the web line tension. For a case of nip load = 25 Pli, he behavior of the 'σ_{11}' stresses at a given instant of time as a function of the total length of the web material in the model is shown in Fig. 6.47. The web enters the nip contact zone from the free span at an average 'σ_{11}' stress of 300 Psi which is equivalent to the prescribed web tension. As it passes under the nip roller, the tension in the web increases due to the nip action. The final value of the WOT is much higher than the web line tension. In the Fig. 6.47, in each layer, two peaks can be observed. One of the peaks is due to the stresses caused as a result of stress concentration and the other is due to the bending of the web due to the nip roller in the contact zone.
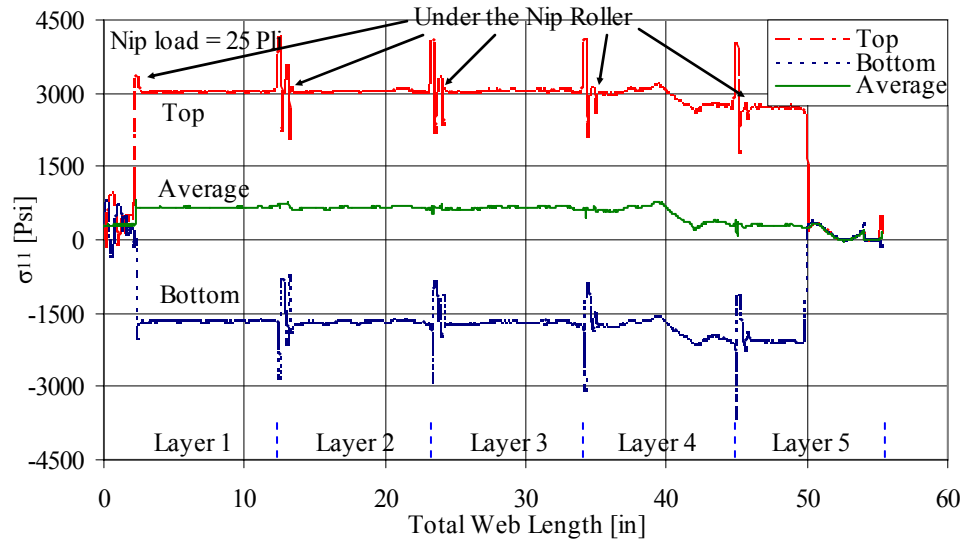
Figure 6.47: Behavior of the top, bottom and average 'σ11' stresses in a center wound roll at Tw=3 Pli and a nip load of 25 Pli

6.2.2   Behavior of the Contact Stresses

The behavior of the surface tractions and 'σ11' stresses in the contact zone in a center wound roll with an undriven nip roller at a web tension of 3 Pli and a nip load of 25 Pli are shown for each layer in Fig. 6.48. The behavior of the surface tractions is very similar to that was observed in the flat bed nip mechanics problem. Also, the directional notation and the behavior of the surface velocities is similar to that given in Fig. 6.10. In the topmost layer, the top surface tractions exhibit three distinct regions; slip at both ends of contact and a large stick zone in the middle. This indicates that the top surface of the incoming sheet moves faster at the edges of contact zone and at the same speed as the nip roller surface in the middle of the contact zone. The bottom surface is under micro-slip and exhibits five distinct regions. The edges of contact are under slip and although the middle of the contact slips, it slips in a direction opposite to the slip at the ends. Between

134

each of these slip zone, a stick zone exists. The behavior of the surface tractions indicate that the bottom surface of the topmost layer moves slower compared to the top surface of the second layer at the edges of the contact. In the two intermediate stick zones, the surface velocities of the bottom surface of the topmost layer and the top surface of the second layer are equal. In the middle slip zone, the direction of the surface traction is opposite compared to the ones at the edges. This indicates that the velocity of the bottom surface of the topmost layer in this region is faster than the top surface of the second layer.

An unbalanced net traction that is calculated as the sum of the top and bottom surface tractions exists in the topmost layer. This net traction when integrated through the contact zone gives rise to the NIT as explained in the flat bed nip mechanics section and this can be observed in the 'σ_{11}' stress plot. The qualitative behavior of the surface traction in layers below the topmost layer is similar to the behavior observed in the topmost layer. Compared to the flat bed case, the traction and 'σ_{11}' stresses in the layers below the topmost layer in the winding case are significantly different. In the case of surface winding, the behavior of the surface tractions and the '$\sigma11$' stresses are similar. However, the final value of the WOT differs by the value of web tension as discussed in the following section.
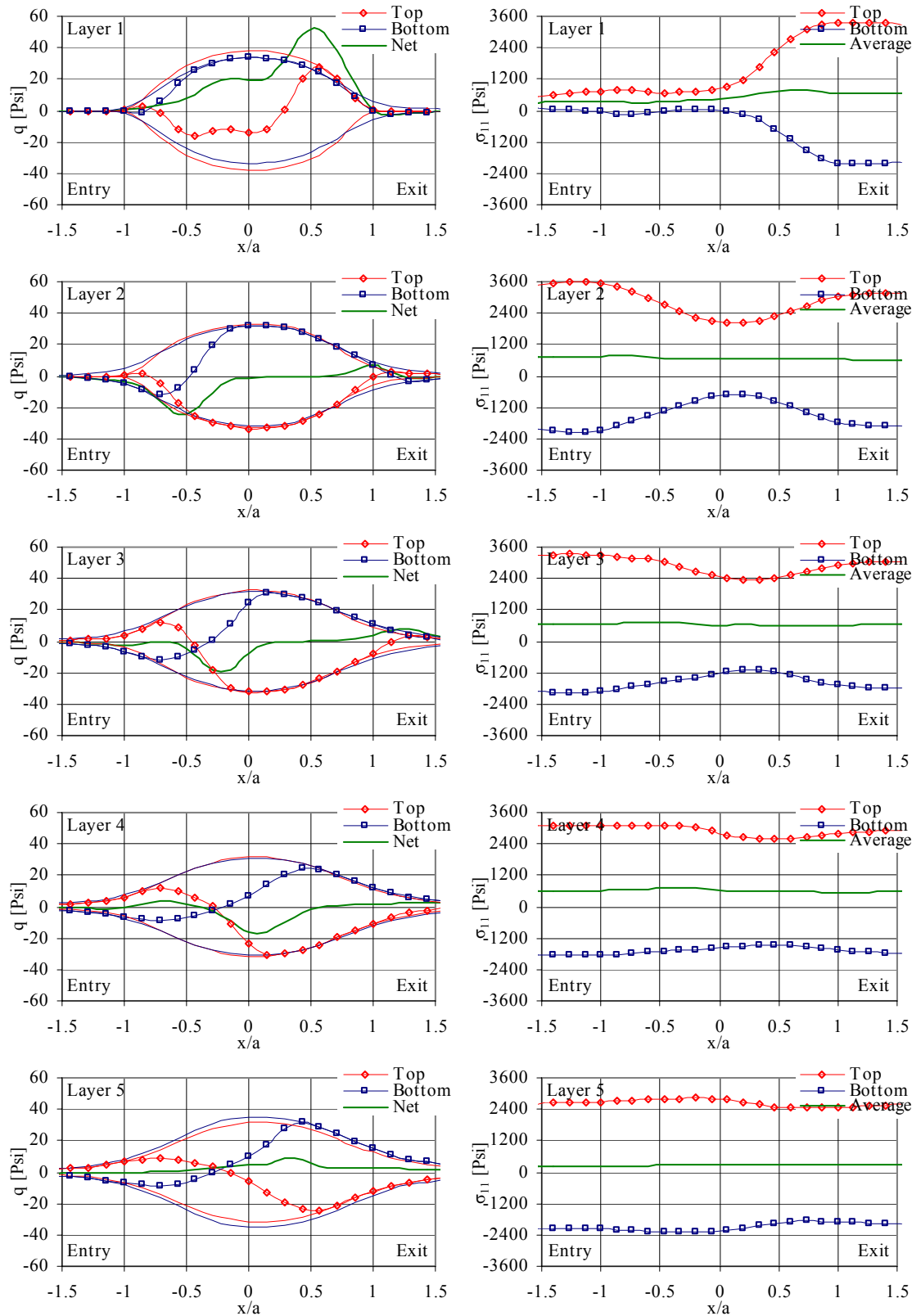
Figure 6.48: Behavior of the surface tractions and the 'σ_{11}' stresses in the nip contact zone in a center winding process with an undriven nip roller at a web tension of 3 Pli and a nip load of 25 Pli.

136

6.2.3 Effect of Nip Load in Center and Surface Winding

The effect of nip load on the WOT in center and surface winding is shown in Fig. 6.49. In the figure, the WOT is expressed in units of Pli and is calculated by multiplying the average value of 'σ_{11}' stresses (membrane only) in the outermost layer with the web thickness. As the nip load increases, the WOT increases linearly in both center and surface winding. At the highest nip load, the WOT begins to taper off in center winding. This behavior is very similar to that observed in the flat bed nip mechanics section. At all nip loads, the difference between center and surface winding is equivalent to web tension.
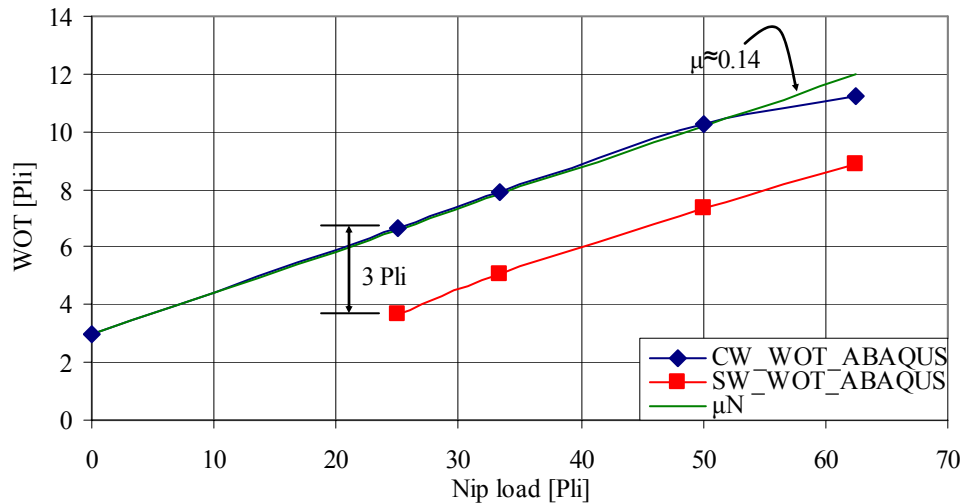
Figure 6.49: Effect of nip load on the WOT in center and surface winding.

The difference in behavior between top and bottom surface tractions in center and surface winding at different nip loads is shown in Fig. 6.50. The primary difference lies in the behavior of the top surface tractions while the difference in bottom surface tractions is very small. In surface winding, part of the top surface traction in the outermost layer (incoming web) is expended in overcoming web tension and in driving

137

the winding roll. Hence at all nip loads, the difference between center and surface winding is approximately the web tension.
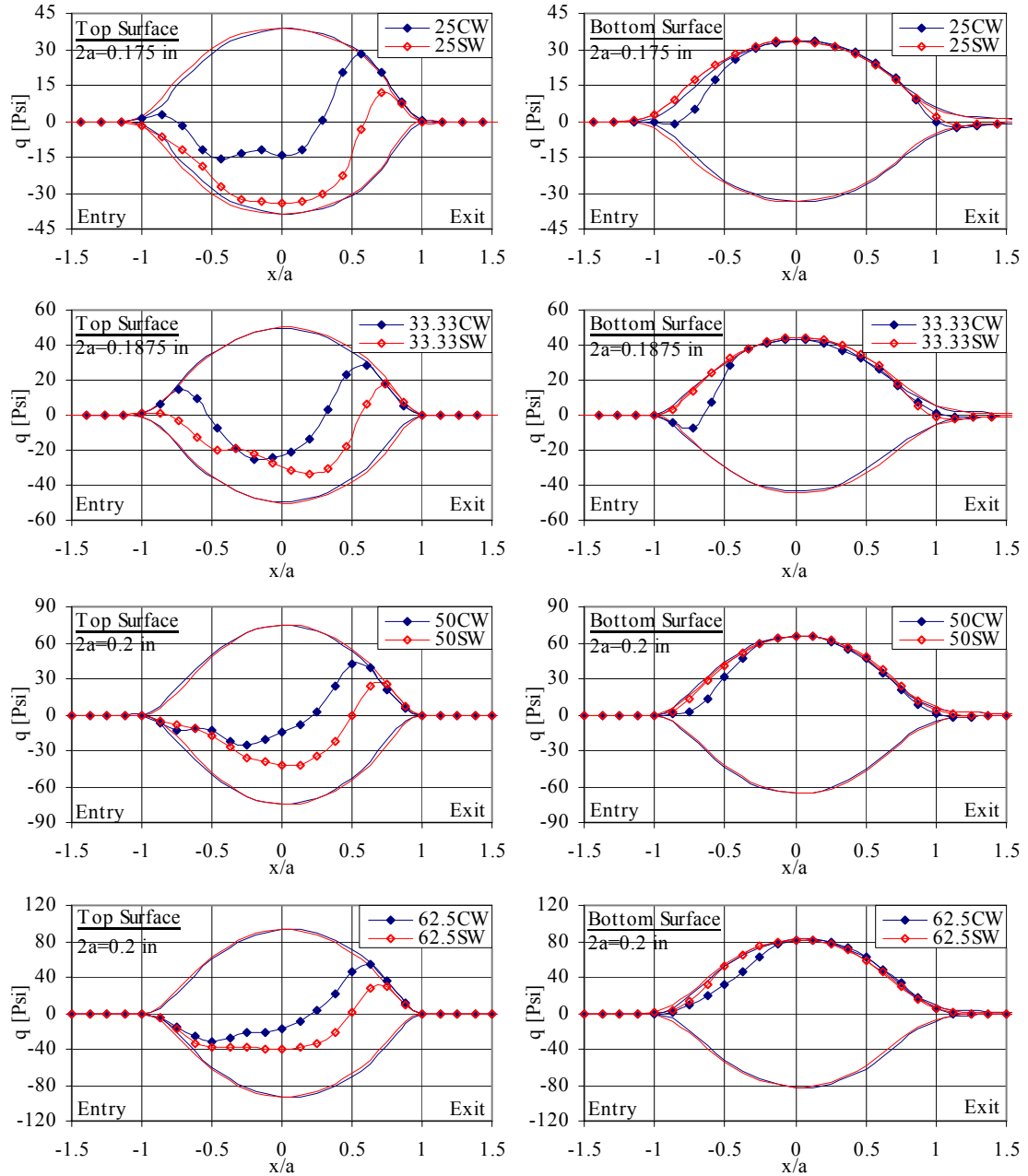
Figure 6.50: Difference in the behavior of the surface tractions between center and surface winding (Legend: Number - value of nip load [Pli], CW/SW - Center Winding/Surface Winding).

Given a winding process, the top, bottom and the net tractions are compared at different nip loads in Fig. 6.51. In both center and surface winding, as the nip load increases, the contact pressure increases and as a result the traction limits increase. At all nip loads, the top surface traction exhibit similar behavior to that explained in the previous section. In center winding, in the bottom surface tractions, the stick zone near the entry grows with increase in nip load as indicated in the figure. Although this behavior is similar in surface winding, the size of the stick zone is much smaller at high nip loads. The net tractions increase with increasing nip load in both center and surface winding process. This behavior is very similar to that was observed in flat bed rolling nip mechanics analysis (section 6.1.4). From Eqn. 4.6, in center winding, the NIT can be calculated as the value that is obtained by subtracting the web tension from the WOT. Also, this value of the NIT should be equal to the total traction that is obtained by numerical integration of the net traction over the contact width in center winding. In surface winding, the top surface traction is expended in overcoming the web tension. This was confirmed when the value obtained by the numerical integration of the top surface traction curve yielded a value equal to that of the web tension at all nip loads. This indicates that the WOT is largely independent of the web tension in surface winding. Hence, all the WOT produced in surface winding is nip induced as the WOT is largely independent of the web tension. The NIT computed in center and surface winding as described above is shown in Fig. 6.52. The data in the figure show that the NIT is similar in center and surface winding at a given nip load and hence, independent of the winding process. This is consistent with the observations of Good et al. [25] in center and surface wound rolls of newsprint.
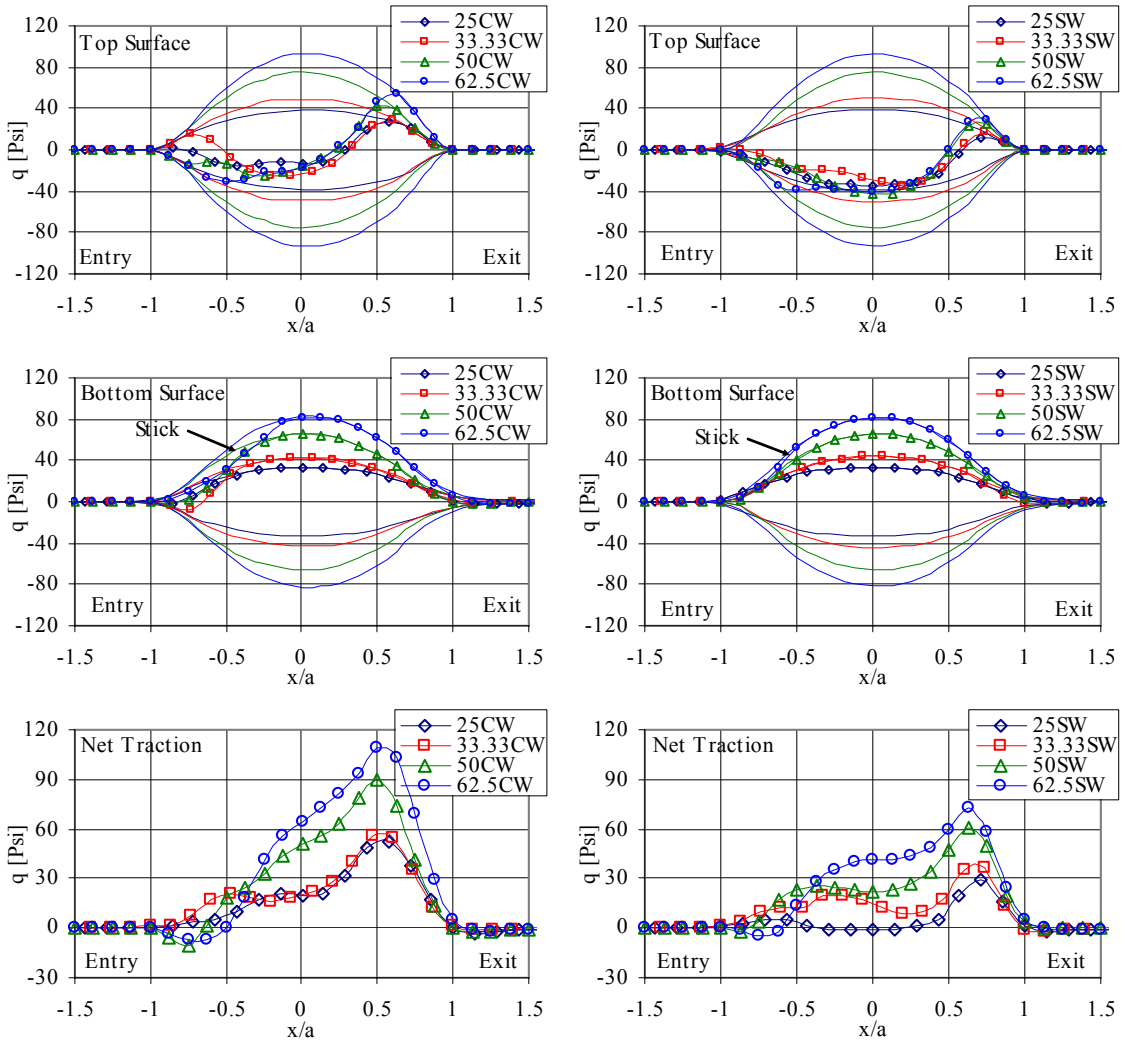
Figure 6.51: Behavior of the top, bottom and net tractions in center and surface winding at different nip loads (Legend: Number - value of nip load [Pli], CW/SW - Center Winding/Surface Winding).

The behavior of the nodal velocities in the contact zone was very noisy and hence the velocity ratios between surfaces were not computed. However, based on the surface traction behavior shown in Fig. 6.51 we can realize that the velocity difference behavior would be very similar to that was observed in the results of flat bed rolling nip mechanics analysis discussed in section 6.1.5.
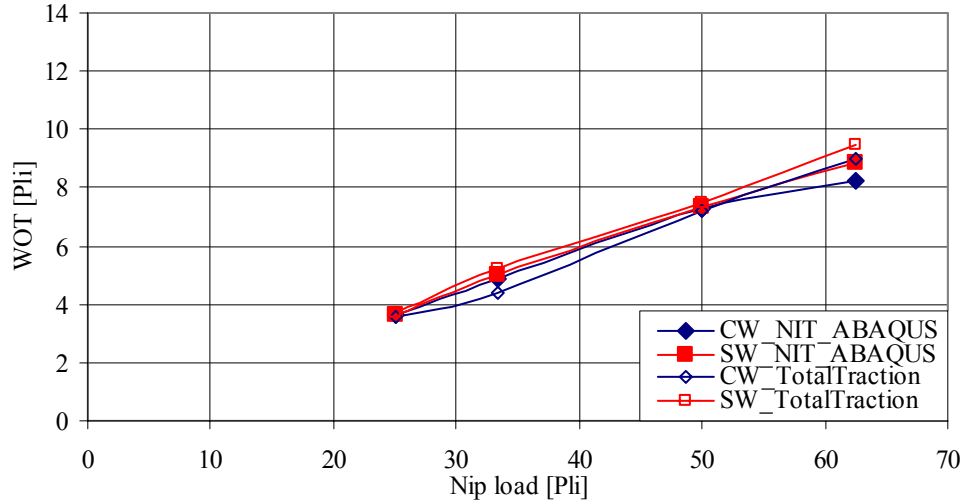
Figure 6.52: Comparison of the NIT computed by two different methods.

6.2.4 Effect of Physical and Material Properties

In the preceding section we observed that the behavior of the total traction, WOT with nip load in a winding problem is very similar to that was observed in the flat bed section. Hence, not all the properties discussed in the parametric study section 6.1.6 are analyzed in the winding problem. In the winding problem, the influence of the friction coefficients along with the effect of the radial modulus, out-of-plane Poisson's ratio and out-of-plane shear modulus on the WOT is studied and all the relevant details are discussed in the following section.

6.2.4.1 Effect of the coefficient of friction between the nip roller and the web layer ($\mu_{Nip/Web}$)

The effect of nip to web coefficient of friction '$\mu_{Nip/Web}$'on the WOT in center and surface winding is shown in Fig. 6.53. In center winding, increasing '$\mu_{Nip/Web}$' from 0.05 to 1.0 does not affect the WOT. This behavior is very similar to that was observed in the

flat bed model. Good [8] observed similar behavior of the WOT in center winding experiments wherein the aluminum nip roller was covered with friction tapes that exhibited friction coefficients greater than one. In surface winding the WOT remains the same for $\mu_{Nip/Web} \geq 0.1$. However, when '$\mu_{Nip/Web}$' was equal to 0.05 winding was not possible. This indicates that there is a minimum threshold for '$\mu_{Nip/Web}$' in surface winding process for a given nip load. As explained in the preceding section, this value is determined by setting the value of '$\mu_{Nip/Web}.N$' equal to that of the incoming web tension.
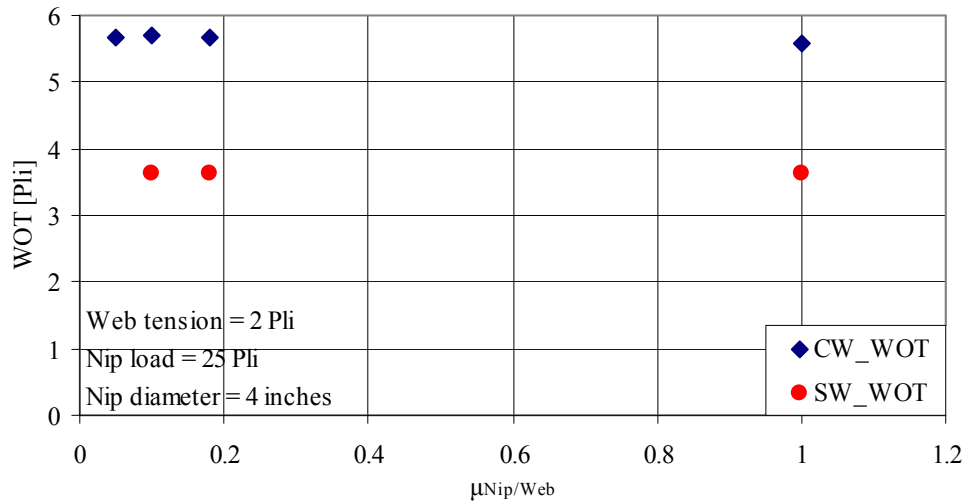
Figure 6.53: Effect of nip to web coefficient of friction ($\mu_{Nip/Web}$) on the WOT in center and surface winding at a nip load of 25 Pli and web tension of 2 Pli

The surface tractions in the contact zone for different $\mu_{Nip/Web}$ in both center and surface winding are shown in Fig. 6.54. Observe that in both center and surface winding, the bottom surface tractions do not change much for increase in '$\mu_{Nip/Web}$'. Increasing '$\mu_{Nip/Web}$' increases the traction limits in the top surface in both center and surface winding. Except at the lowest '$\mu_{Nip/Web}$', the top surface is almost under complete stick in center winding. At the lowest value of '$\mu_{Nip/Web}$' the bottom surface is under significant

slip at either ends of contact. Although some difference in behavior is observed in the top surface tractions for different '$\mu_{Nip/Web}$', the changes do not affect the total traction and hence the WOT remains constant.
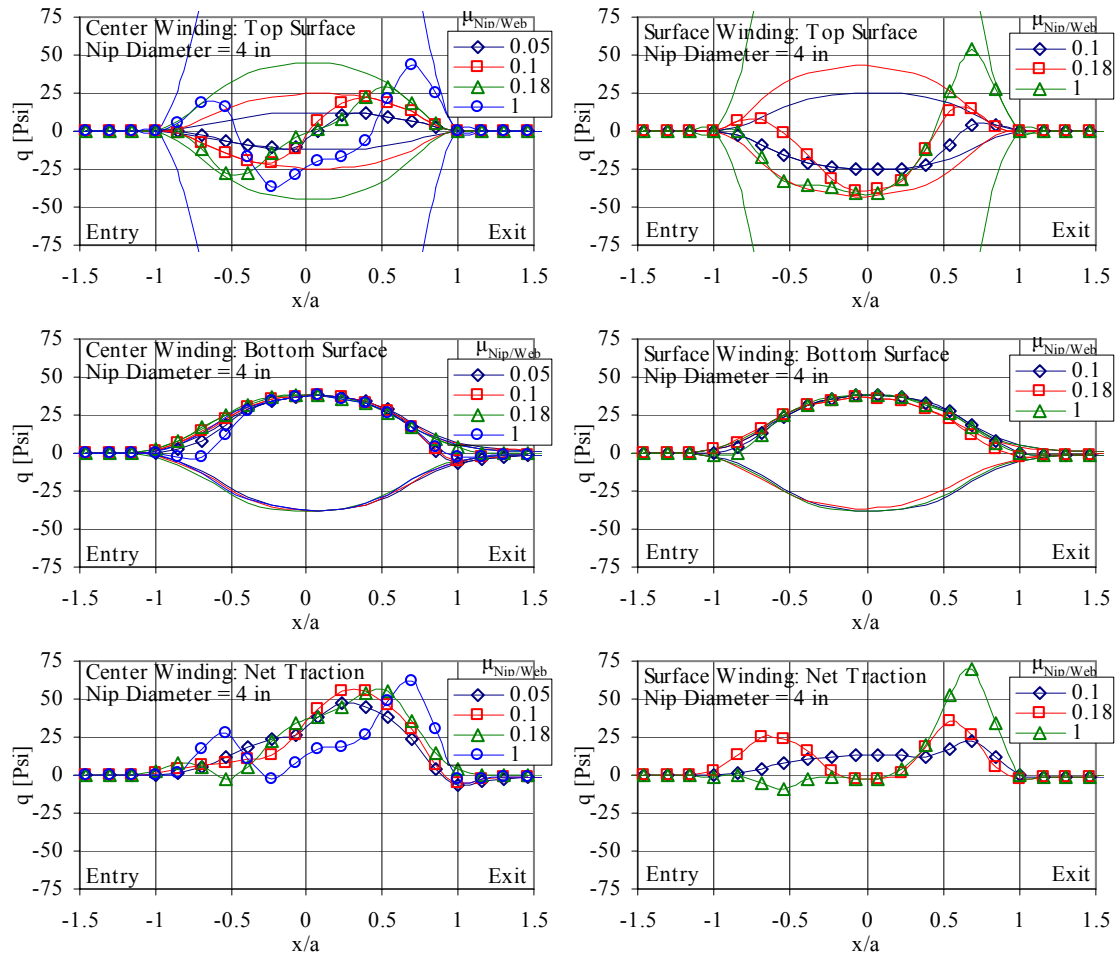
Figure 6.54: Behavior of the surface tractions for different '$\mu_{Nip/Web}$' in both center and surface winding at a nip load of 25 Pli and web tension of 2 Pli

In surface winding, when $\mu_{Nip/Web}$=0.1, the top surface is almost under complete slip. Beyond '$\mu_{Nip/Web}$ = 0.1', the top surface is almost under complete stick similar to that was observed in the center winding case. The total traction remains the same due to this and hence the WOT is not affected for $\mu_{Nip/Web} \geq 0.1$. When $\mu_{Nip/Web}$=0.05, the top surface

is under complete slip and in such a situation the total traction is much less than the web tension. Hence, winding cannot be accomplished. This region is typically referred to as the 'stall' region in surface winding process.

6.2.4.2 Effect of the coefficient of friction between the web layers ($\mu_{Web/Web}$)

The effect of the coefficient of friction between the web layers '$\mu_{Web/Web}$' on the WOT in center and surface winding is shown in Fig. 6.55. In both center and surface winding, as '$\mu_{Web/Web}$' increases, the WOT initially increases almost proportional to '$\mu_{Web/Web}.N$'. At really high values of '$\mu_{Web/Web}$' the WOT tapers off in both center and surface winding and in this region the WOT is much less than '$\mu_{Web/Web}. N$'.
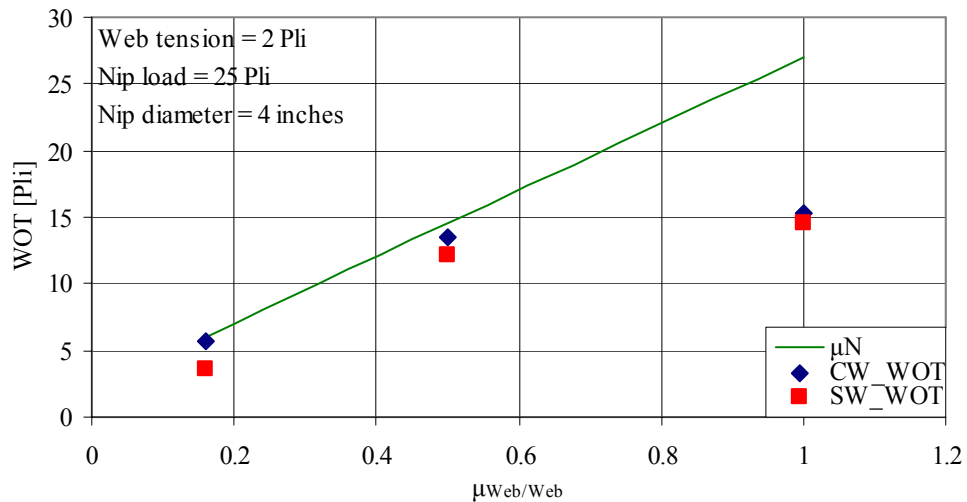
Figure 6.55: Effect of nip to web coefficient of friction ($\mu_{Web/Web}$) on the WOT in center and surface winding at a nip load of 25 Pli and web tension of 2 Pli

The behavior of the surface tractions in the contact zone for increasing values of '$\mu_{Web/Web}$' in both center and surface winding is shown in Fig. 6.56. For all values of

'$\mu_{Web/Web}$', the top surface tractions remain almost the same in both center and surface winding. This behavior is similar to that was seen in the flat bed model.
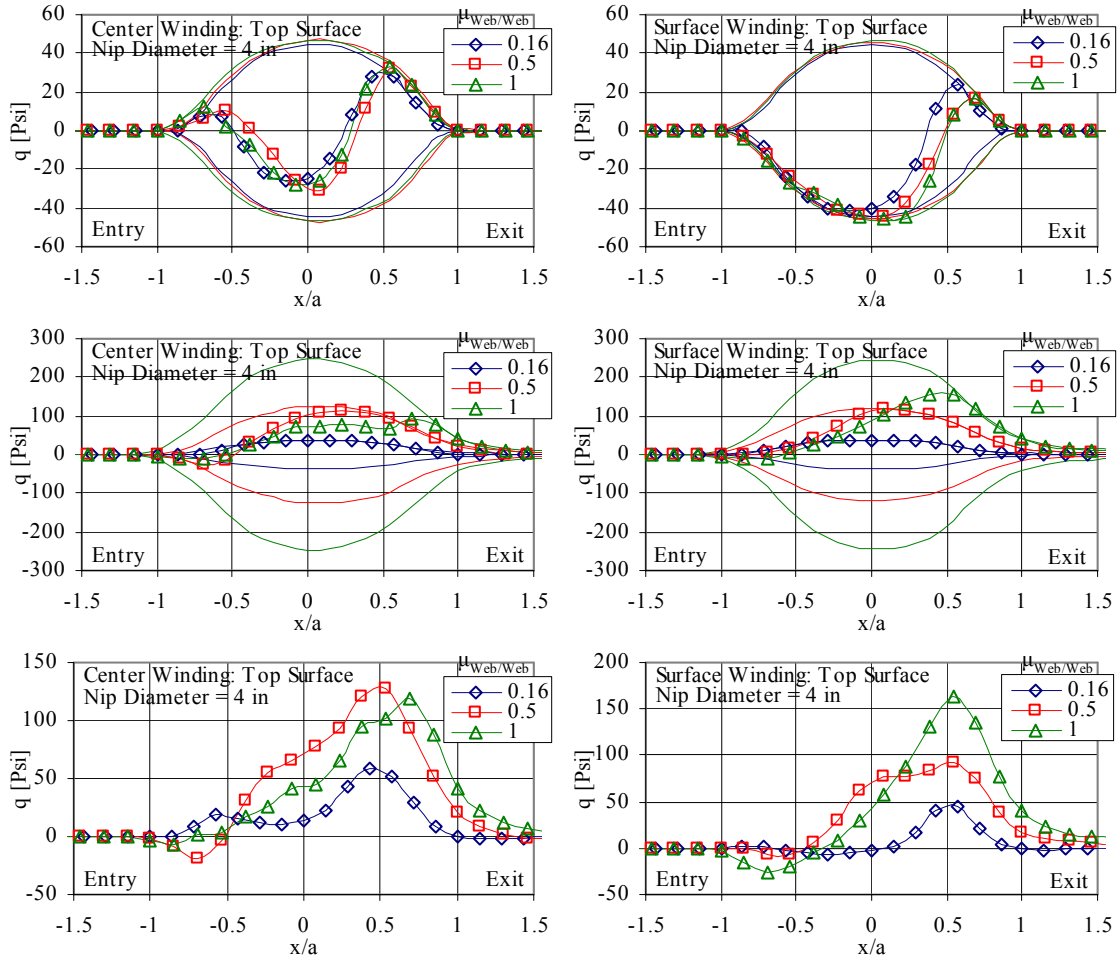
Figure 6.56: The behavior of the surface tractions for different '$\mu_{Web/Web}$' in both center and surface winding at a nip load of 25 Pli and web tension of 2 Pli

The traction limits in the bottom surface increases with increasing values of '$\mu_{Web/Web}$'. At low values of '$\mu_{Web/Web}$' the bottom surface is almost under complete slip in both center and surface winding. As '$\mu_{Web/Web}$' increases, the bottom surface starts to stick near the entry zone of contact and this stick zone spans through most of the contact at very high values of '$\mu_{Web/Web}$'. Due to this, the total traction becomes similar at high

145

values of '$\mu_{Web/Web}$'. Hence, the WOT is much lower than '$\mu_{Web/Web}$. N' and begins to taper off at high value of '$\mu_{Web/Web}$'.

6.2.4.3   Effect of Radial Modulus (E_r)

The effect of radial modulus 'E_r' on the WOT and half width of contact 'a' in both center and surface winding is shown in Fig. 6.57. As 'E_r' increases, the WOT in both center and surface winding remains more or less the same. Observe that the half width of contact 'a' rapidly decreases with increase in 'E_r'. The top, bottom surface tractions and the net traction are shown in Fig. 6.58. As 'E_r' increases, the contact pressure increases causing the traction limits to increase. Although some difference in behavior in the top surface tractions can be observed in both center and surface winding for increasing 'E_r', the difference is less and the total traction remains unaffected by this.
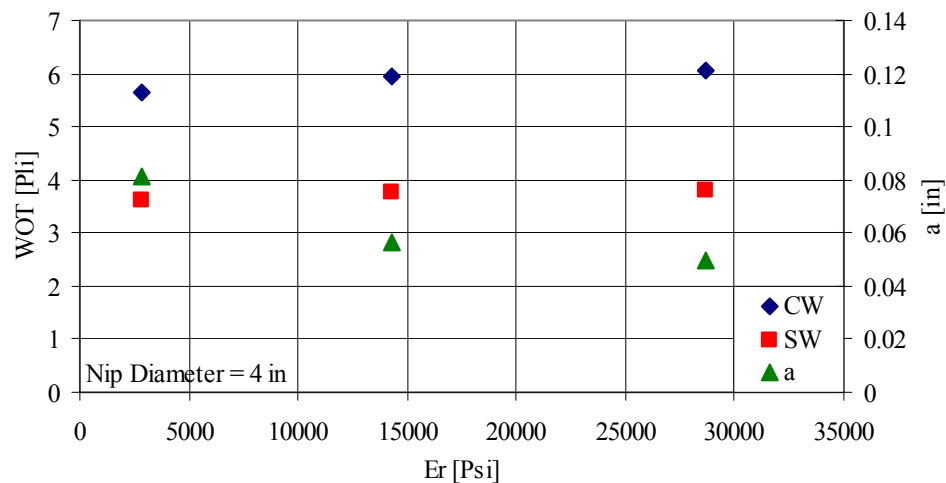
Figure 6.57: Effect of radial modulus 'E_r' on the WOT in center and surface winding at a nip load of 25 Pli and web tension of 2 Pli.

The bottom surface is almost under complete slip in both center and surface winding. The reduction in contact width compensates for the increase in traction limits and hence the total traction remains the same. As observed in the flat bed nip mechanics section 6.1.6.3., further increase in 'E_r' should decrease the WOT in both center and surface winding. However, in the winding model, further increase in 'E_r' beyond 28650 Psi will decrease the contact width significantly. In such a case, the contact definition in terms of the number of nodes present will not be adequate and hence not attempted.
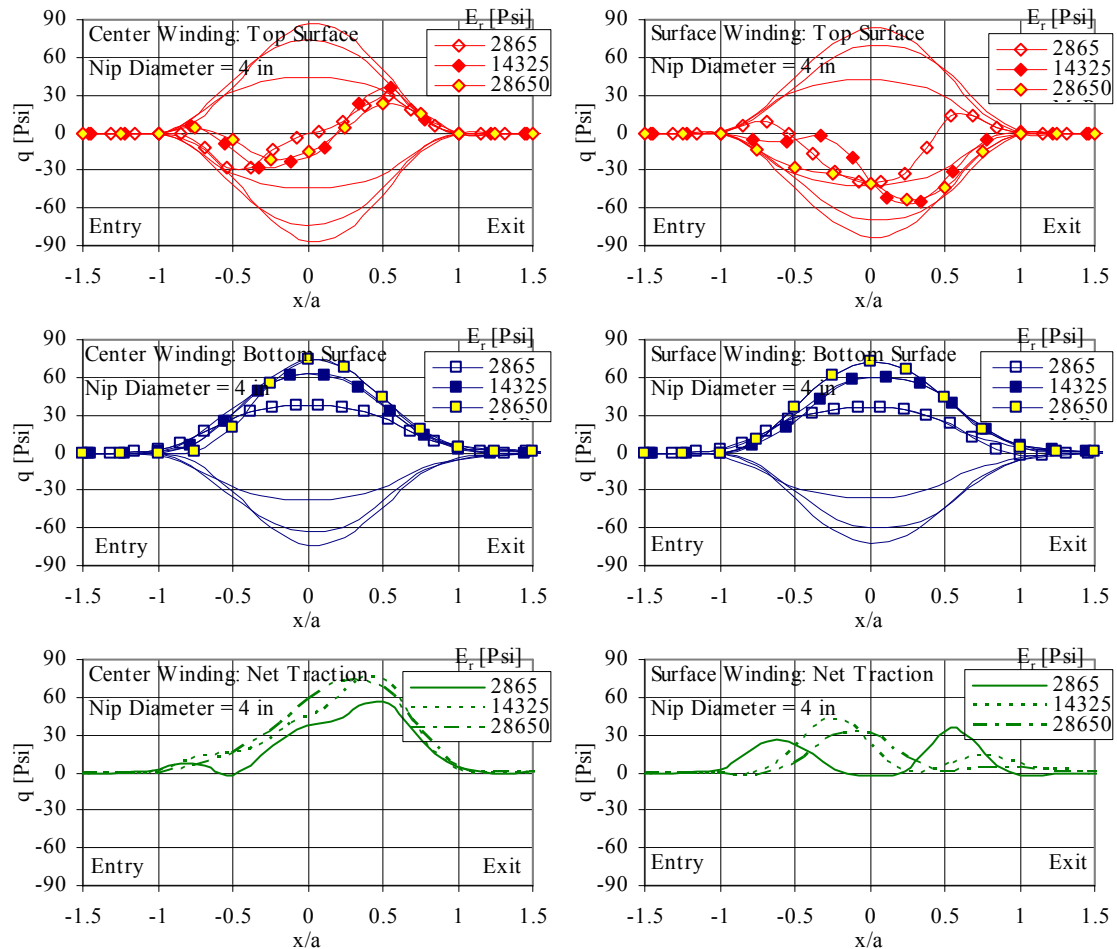
Figure 6.58: The behavior of the surface tractions for different 'E_r' in both center and surface winding at a nip load of 25 Pli and web tension of 2 Pli

6.2.4.4 Effect of Out-of-Plane Shear Modulus (G_{12} or $G_{r\theta}$)

The effect of out-of-plane shear modulus 'G_{12}' on the WOT in both center and surface winding is shown in Fig. 6.59. In this case, the effect of 'G_{12}' at two different nip loads is observed. Similar to the behavior observed in flat bed nip mechanics section 6.1.6.4, 'G_{12}' does not affect the WOT at low nip loads wherein the NIT is approximately equal to '$\mu_{Web/Web}$. N'. In section 6.2.3, the behavior of WOT with nip load was discussed and it was shown that at the high nip loads, the WOT begins to taper off. When 'G_{12}' is increased, the WOT becomes approximately equal to '$\mu_{Web/Web}$. N' even at high nip loads as shown in Fig. 6.59.
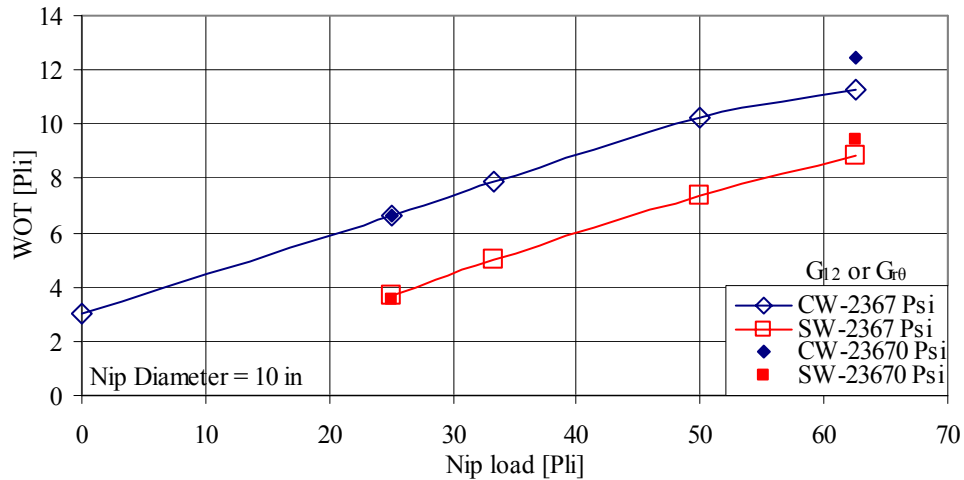
Figure 6.59: Effect of the out-of-plane shear modulus '$G_{r\theta}$ or G_{12}' on the WOT in both center and surface winding at a web tension of 3 Pli and at different nip loads.

Since the difference in surface tractions at a low nip load of 25 Pli for increase in 'G_{12}' is negligible, the behavior surface tractions at nip load of 62.5 Pli is also shown in Fig. 6.60. In this case observe that the top surface tractions remain the same in both center and surface winding for increase in 'G_{12}'. In the bottom surface tractions,

significant stick zone exists near the entry zone when 'G_{12}=2367 Psi'. This stick zone becomes very small when 'G_{12}=23670 Psi.' Due to this the bottom surface is almost under complete slip even at high nip loads. Hence the net traction increases in both the center and surface winding. This causes the total traction to increase and the NIT becoming approximately equal to '$\mu_{Web/Web}$. N'.
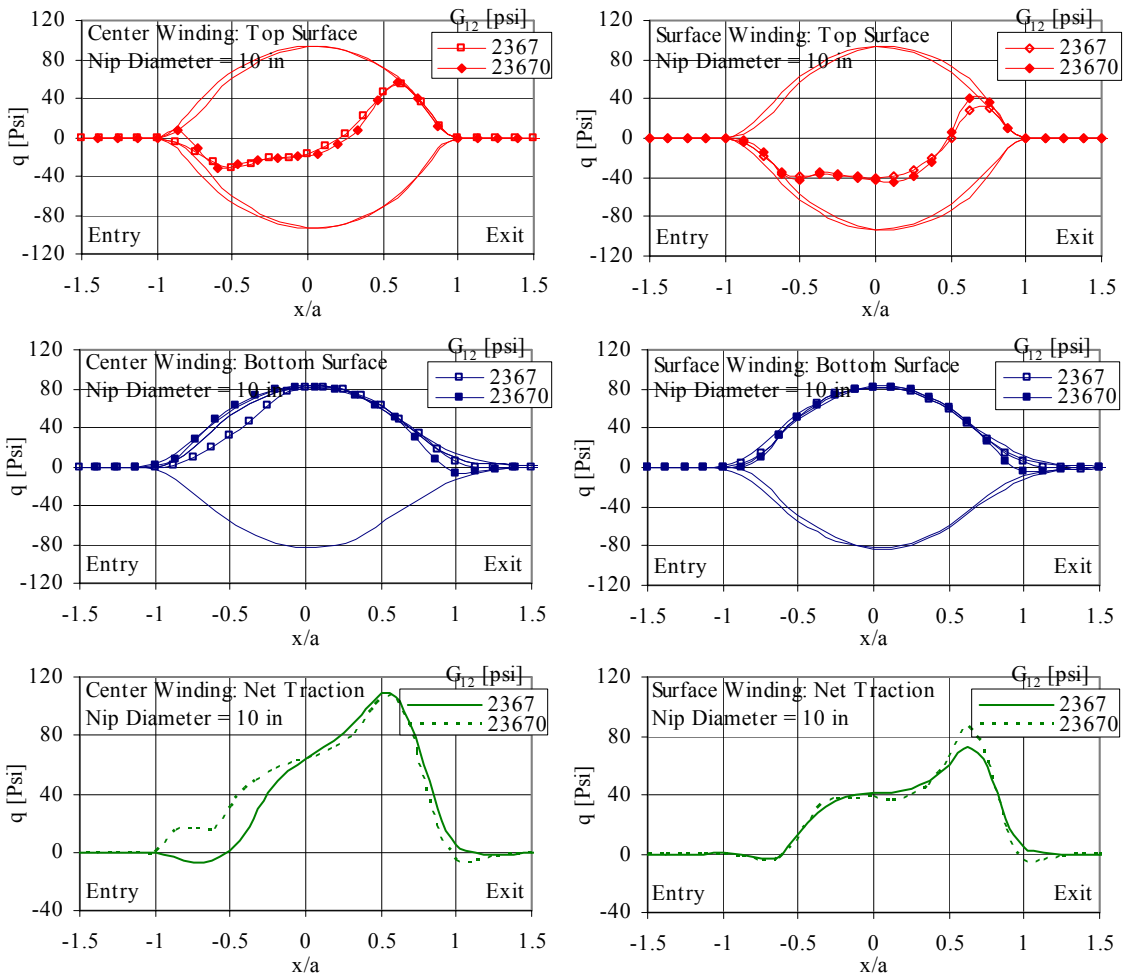
Figure 6.60: The behavior of the surface tractions for different 'G_{12}' in both center and surface winding at a web tension of 3 Pli.

6.2.4.5 Effect of Out-of-Plane Poisson's Ratio (ν_{12} or $\nu_{r\theta}$)

The effect of the out-of-plane Poisson's ratio '$\nu_{r\theta}$ or ν_{12}' on the WOT in both center and surface winding is shown in Fig. 6.61. At all nip loads, changing '$\nu_{r\theta}$' from 0.3 to 0.01 does not affect the WOT in both center and surface winding. When the contact tractions were observed, no noticeable difference was observed in any of the surface tractions for the different Poisson's ratio's used. This is consistent with what is observed in Fig. 6.61 and also with what was observed in the flat bed nip mechanics section 6.1.6.5.
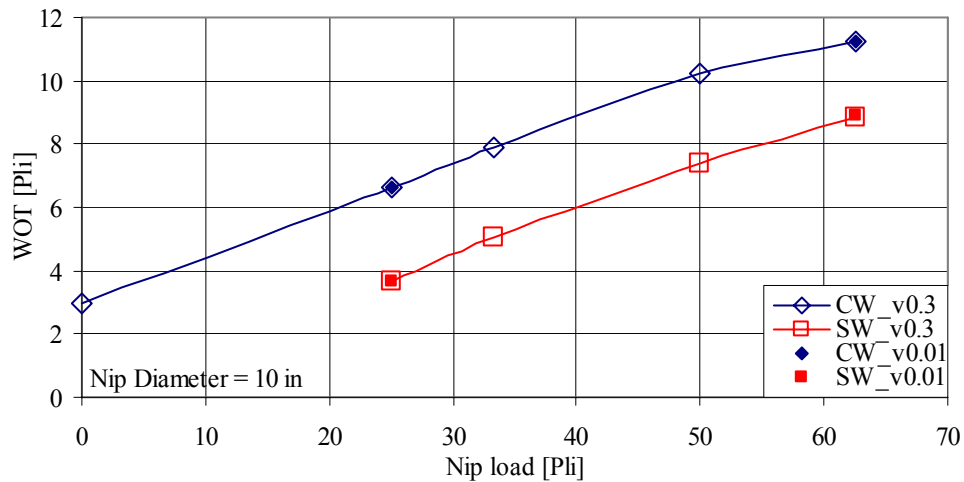
Figure 6.61: Effect of the out-of-plane Poisson's ratio $\nu_{r\theta}$ or ν_{12} on the WOT in center and surface winding at a web tension of 3 Pli and at different nip loads

7 Experimental Verification

The results from ABAQUS/Explicit$^{®}$ are verified using experimental measurements of the NIT and WOT and the following section describes in detail the different types of verification carried out.

7.1 Verification of the Flat Bed Model

In section 6.1.4, the effect of nip load on the NIT in a flat bed model was discussed. In that case, the NIT was calculated as the saturated average 'σ_{11}' stress at the left end of the topmost layer. A flat bed rolling nip test bed as shown in Fig. 7.1. was designed to verify the model results of NIT.
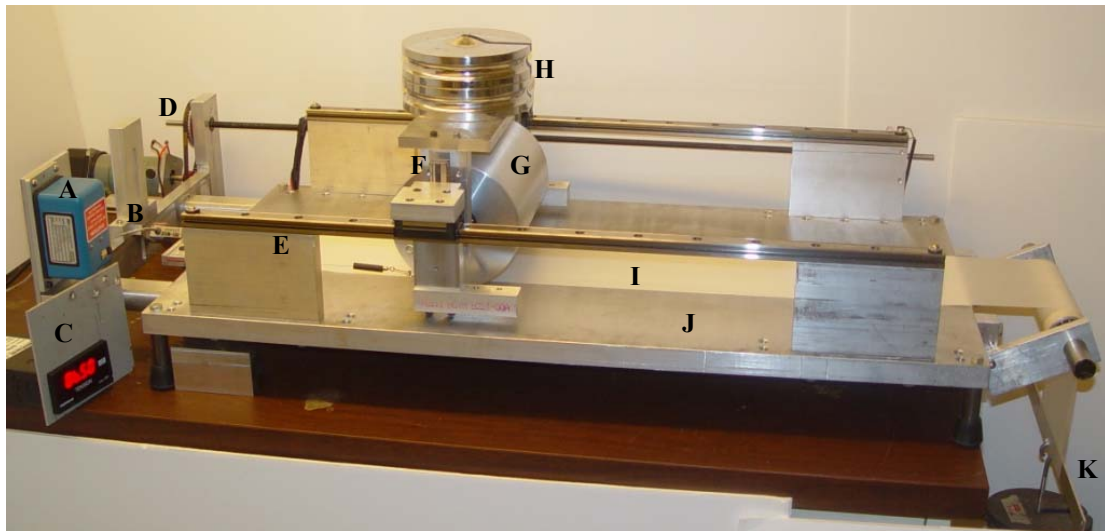
Figure 7.1: Flat bed rolling nip test bed (Legend: A-Linear potentiometer, B-Tension load cell, C- Tension indicator, D-Motor-lead screw assembly, E-Horizontal linear rail, F-Vertical linear rail, G-4 inches diameter rigid Aluminum nip roller, H-Weights for nip load, I- Web stack with top layer connected to load cell at one end and weights for tension at the other, J-Rigid base, K-Weights for web tension).

The test bed consists of a rigid base (J) on top of which a 10 sheet stack of web (I) rests. The topmost layer is connected to a load cell at the left end (B). A set of weights (K) hanging from the right end simulates web tension as shown in the figure. This tension helps keep the web stack in its place during the nip rolling process. The rigid base has supports at each corner and two linear rails (E) parallel to each other run along the length of the base on top of these supports. A nip roller assembly (G) is connected to the vertical linear rails (F) that are attached to horizontal linear bearings at either end. A motor-lead screw assembly (D) connected to one of the linear bearings ensures that the nip roller assembly can traverse on top of the rigid base in either direction. The nip roller assembly is also attached to a linear potentiometer (A) that accurately measures the given position of the nip roller. A set of weights placed on top of the nip roller (H) simulates nip load. The total nip load is calculated as the sum of the dead weight of the nip roller assembly and the amount of weights placed on the assembly.

As the nip roller rolls from left to right from a stationary starting position, the tension in the topmost layer (behind the nip) as measured by the load cell increases. At the same time the linear potentiometer accurately records the position of the nip roller. Using a data acquisition system and a program written in LabVIEW®, the position of the nip roller along with the load cell output is simultaneously recorded while the nip rolls on top of the stack. As a function of the rolling distance and at different nip loads, the behavior of the tension in topmost layer is shown in Fig. 7.2. Although a web tension of 2 Pli was used during tests to keep the web stack in place, this value was subtracted from the load cell output to get the correct value of the NIT.
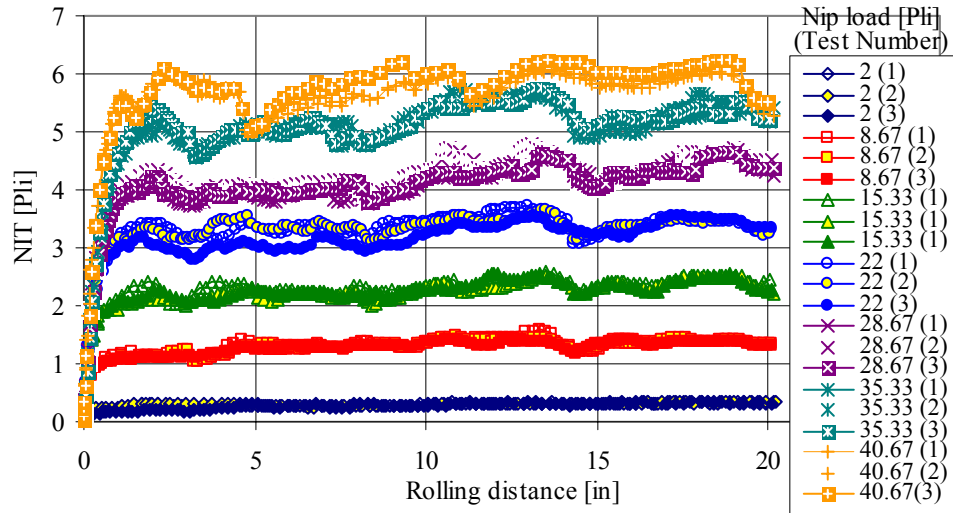
Figure 7.2: Behavior of the NIT in the topmost layer as a function of rolling distance and at different nip loads.

As the nip rolls from left to right, the tension in the sheet behind the nip increases exponentially and saturates after the nip has traveled some distance. The saturated value of this tension is commonly referred to as the NIT. This behavior is very similar to that was observed in the model results shown in Fig. 6.5 for the topmost layer. Observe that the behavior of the sheet tension is very noisy at high nip loads. This is due to the inability of the sheet to sustain such high tensions without some slip and also due to the jerky motion of the nip roller. The highest nip load that could be achieved with this test set up was ≈42 Pli. Observe that the Fig.7.2. shows the NIT behavior in three different tests at each nip load level. The average value of the saturated value of the tension in the topmost layer at a given nip load represents the NIT and this value as a function of nip load is shown in Fig. 7.3. As the nip load increases, the NIT increases linearly up to ≈30 Pli and then starts to taper off only at very high nip loads (≈42 Pli.). The slope of the linear region represents the value of the coefficient of friction between the web layers. In this case $\mu_{Web/Web}$ is approximately equal to 0.16.
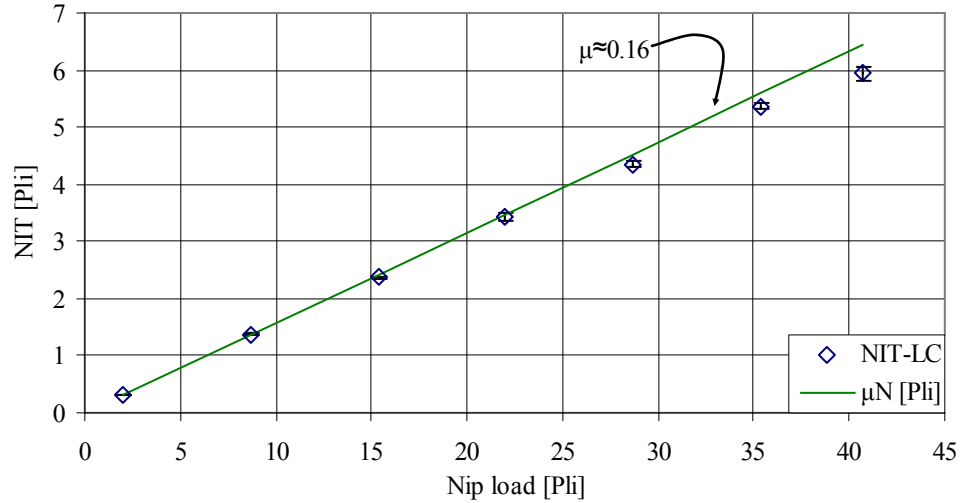
Figure 7.3: Effect of nip load on the NIT.

Recall from section 5.3.6, both the ASTM standard test measurements and band-brake type measurements of kinetic coefficient of friction yield a value of ≈ 0.22 for $\mu_{Web/Web}$. When this value (0.22) was used for $\mu_{Web/Web}$, the model results do not agree well with the experimental results as shown in Fig. 7.4.
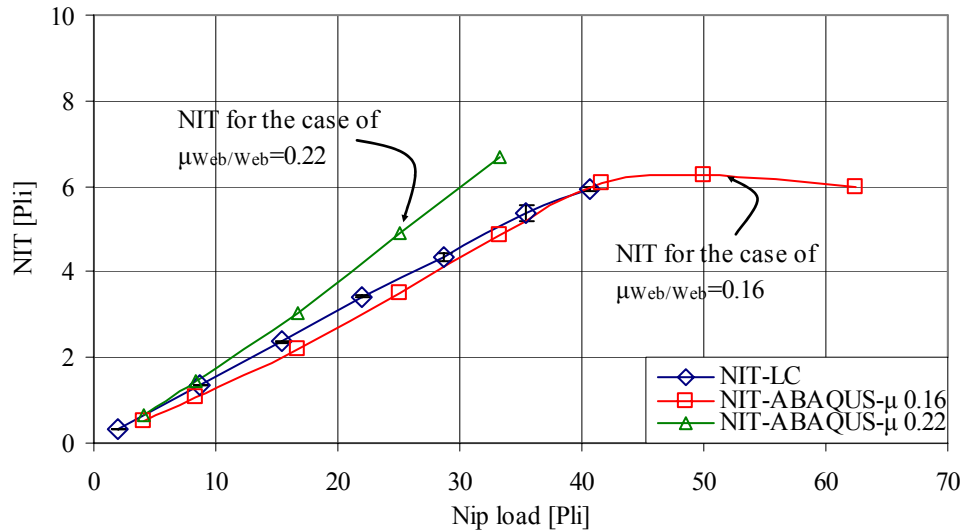
Figure 7.4: NIT comparison between experimental and model results.

Johnson [41] describes that the coefficient of friction that exist in rolling contact conditions cannot be measured using standard tests. This is because of the existence of micro-slip in rolling contact. As a result one has to obtain the friction coefficient by measuring it in similar rolling contact conditions. This suggests that a coefficient of friction of 0.16 that was measured using the flat bed rolling test bed should be used in the model in order to get correct results. When a value of 0.16 was used for '$\mu_{Web/Web}$', the model results compare well to the experimentally measured NIT as shown in Fig. 7.4. This concludes the verification of the NIT results from flat bed nip mechanics ABAQUS/Explicit$^{®}$ model.

7.2   Verification of the Winding Model

One of the ways in which the WOT in a winding process can be measured is by using the load cell method as discussed in section 2.2. A winder that is capable of running at very high speeds ($\approx$5000 Fpm) and at very low speeds ($\approx$1 Fpm) as shown in Fig. 7.5[1]. is used for experiments. The control system in the web line is such that the tension in the web can be held a constant at zero velocity. For the measurement of the WOT, this machine was instrumented with a WOT load cell assembly as shown in Fig. 7.5[2]. A schematic of the WOT load cell system is described in Fig. 7.6. The web from the unwind station passes through a sequence of nip stands that maintain constant web velocity and idlers that support the web between different spans involved. Before entering the rewind station, the web passes through a web guide and through an idler mounted on a load cell. This load cell measures the tension in the web upstream of the rewinder. Also, the signal from this load cell is used in a tension feed back system that maintains a constant web tension.
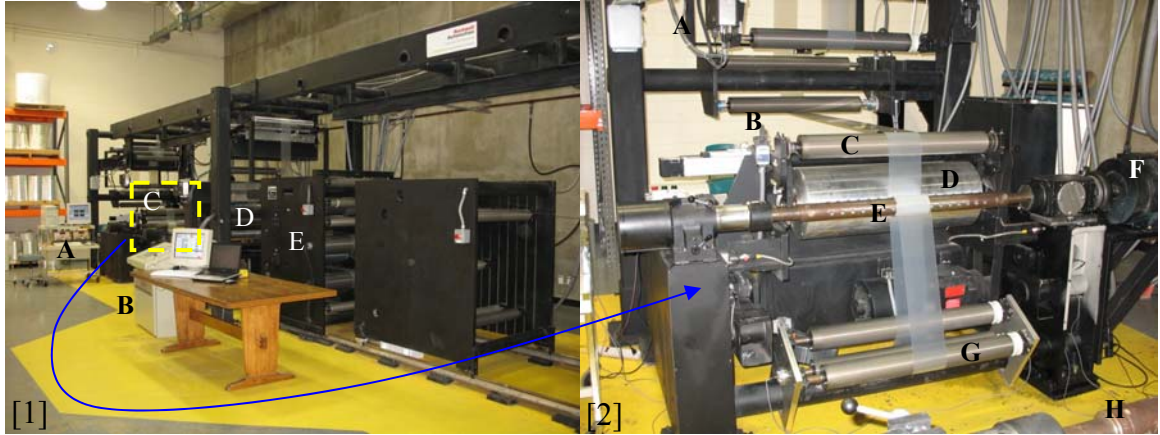
Figure 7.5: [1] High Speed Winding Machine (Legend: A-LabVIEW® Data acquisition system, B-Winder control stand, C-Rewind assembly with WOT load cell arrangement, D-Unwind station, E-Intermediate nip stands for velocity control) [2] Close-up of the WOT load cell arrangement (A-Upstream web guide, B-Upstream tension load cell, C-Idler that controls nip roller web wrap, D-10 inches diameter nip roller, E-rewind core shaft, F-Rewind motor, G-WOT LC assembly, H-Unwind shaft).
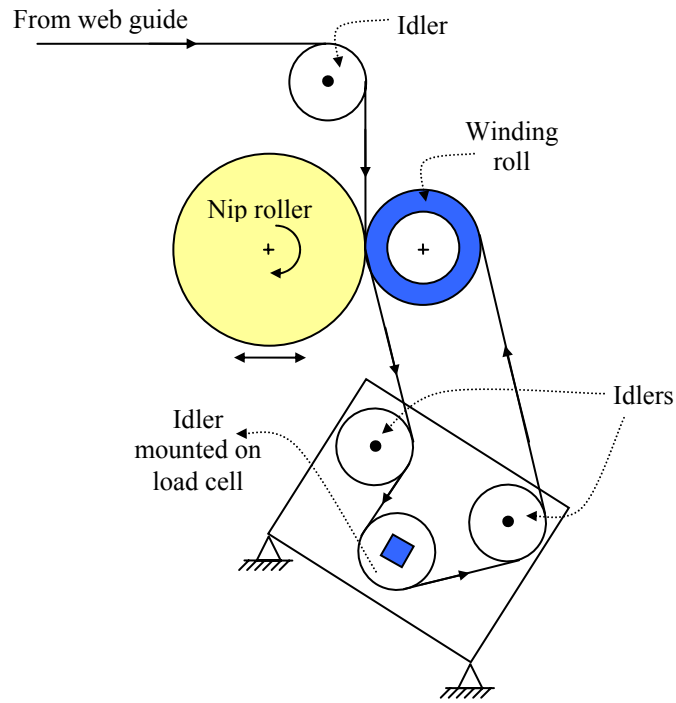
Figure 7.6: Schematic of the WOT load cell assembly.

The web then wraps around an idler at 90° angle before entering the nip contact zone. The purpose of this idler is to ensure that the web enters the nip contact zone

156

without wrapping the nip roller. Normally, the web would enter the winding roll beyond the nip contact zone. However, in order to measure the WOT, the web is peeled away from the winding roll as shown in Fig. 7.6. and passed through an idler that is mounted on a load cell that measures the WOT. The web is then returned to the winding roll as shown in Fig. 7.6. Two idlers, one upstream and one downstream of the roller mounted on a load cell that measures the WOT ensures that a constant wrap angle is maintained throughout the winding process. A data acquisition system acquires the tension, nip load and WOT signals and a program written in LabVIEW® continuously records the data as the roll is being wound. The data from a typical experimental run is shown in Fig. 7.7. Observe that the roll is center wound at a web tension of 3 Pli and a nip load of 9 Pli at 25 Fpm. The WOT, tension and nip load remains constant with wound roll radius and the average of each of these parameters constitute one data point.
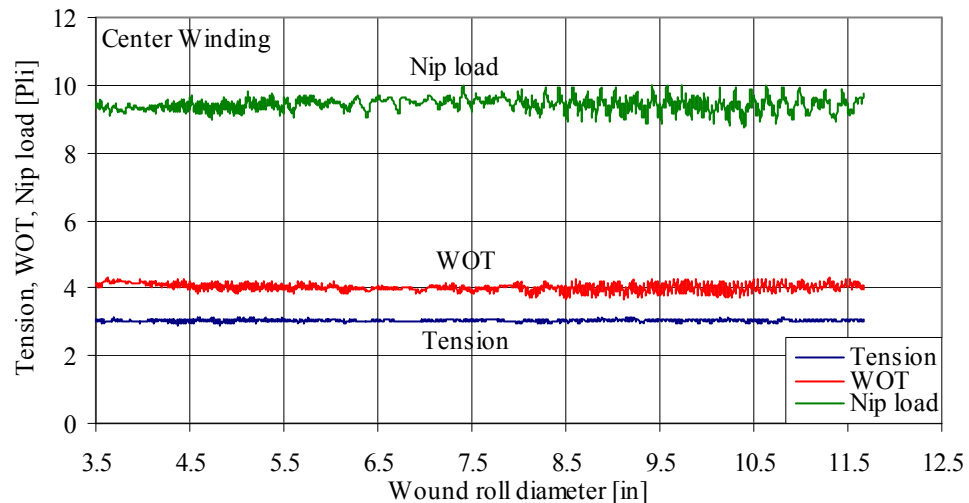
Figure 7.7: Behavior of web tension, nip load and the WOT in center winding.

In most rolling contact problems [41] an equivalent radius is involved in the computations of the tractions and the stresses in the contact zone. This would indicate

157

that the stresses (WOT in this case) would be dependent on the equivalent radius. From the parametric studies discussed in chapters 6 and 7 one can infer that the properties like 'G$_{12}$' and 'E$_r$' affect the WOT only when the bottom surface of the contact starts to go into stick conditions. Similarly one can say that when the contact surface is slipping and the WOT is ≈ 'μ$_{Web/Web}$. N' the wound roll radius may not have an effect. Since the web tension, nip load and WOT remain constant as a function of wound roll radius, the WOT at different nip loads can be measured in a single test as shown in Fig. 7.8. In this test, the nip load is decreased in a sequence of steps during the course of winding the roll. At each step the nip load is maintained constant until at least some amount of material is wound at that nip load level. The data in Fig 7.8 represents the behavior of the WOT in center winding at a constant web tension of 3 Pli and at different nip loads.
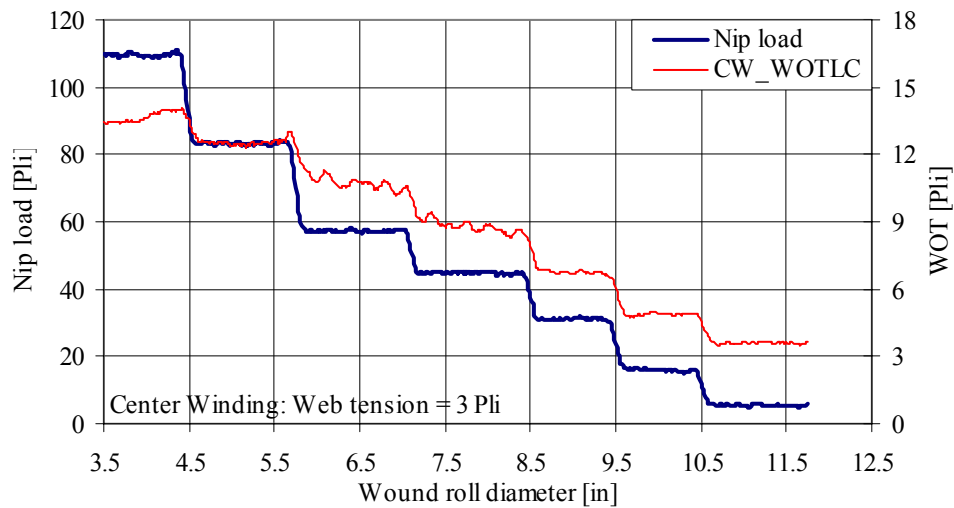
Figure 7.8: Behavior of the WOT at different nip load levels.

At each nip load step in Fig. 7.8., the average value of both the nip load and the WOT is calculated and the WOT as a function of nip load is shown in Fig. 7.9. In this

case, the WOT initially increases linearly for nip loads less than ≈60 Pli and starts to taper off beyond this level. Observe that the slope of the linear part is approximately equal to 0.14. In the same figure, the experimental WOT results are compared to the winding model results. Recall that the winding model results for the NIT were explained in section 6.2.3 and the WOT values were obtained in a center winding case for $\mu_{Web/Web}$ = 0.16. This value of 0.16 was obtained from the NIT results in a rolling nip test bed that approximates the winding contact conditions than an ASTM measurement method. The winding model results compare well with the experimental measurements of the WOT and this indicates that the coefficient of friction in winding contact conditions is similar to that obtained from the flat bed rolling nip tests. There is some disagreement between the results but one must recall that the load cell method can be an interfering method since the path of the web is different from that used in the model.
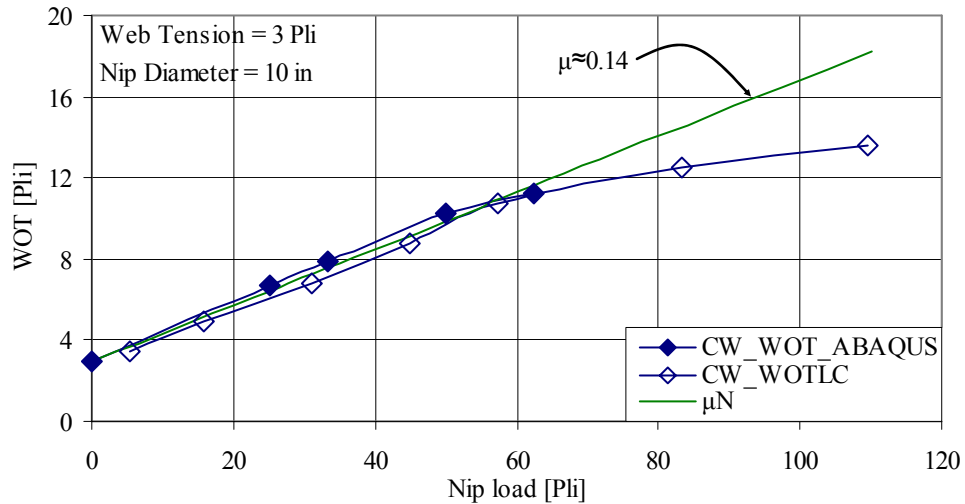
Figure 7.9: Comparison between experimental and model results of WOT in center winding.

7.3 Verification of the contact stresses

In the preceding sections we showed that the model results agree with macro stress measurements in the form of the NIT and the WOT. In this section the behavior of the stresses in the contact zone between the winding roll and the nip roller is discussed and compared to the model results. Stain gages have been used to measure the WOT by Rand and Eriksson [3]. However they used the strain gages to measure the overall WOT in the incoming web. Strain gages that have sensing area much less than the contact width are commercially available. A schematic of the strain gage that is used to measure the contact strains and, hence the stresses is shown in Fig. 7.10.
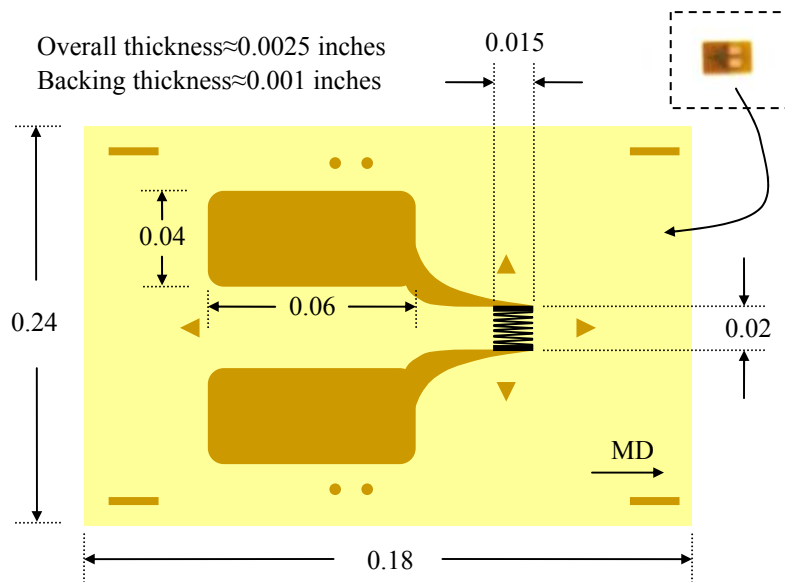
Figure 7.10: A schematic of the contact strain gage.

The gage consists of a constantan grid completely encapsulated in polyimide, with large, rugged copper-coated tabs. This type of gage is primarily used for general-purpose static and dynamic stress analysis when the normal operating temperatures of the strain

gage is between -100° F and 400° F. The resistance of the strain gage is 120±0.3% ohms and has a gage factor of 2.085. The strain gage has a range of ±3% and has a fatigue life of 10^5 cycles at ±1500 microstrain (μin/in). Observe that the sensing length of the strain gage is 0.015 inches and when compared to the contact width shown in Fig. 6.50. (as text), the length of the sensing area is significantly less.

When strain gages are used for strain measurements in thin films, the effect of reinforcement caused by the strain gage needs to be evaluated and this factor is referred to as the reinforcement factor. The PET film used in experiments is 0.01 inches thick and is four times thicker than the web. The reinforcement factor is calculated as the ratio of the measured strain compared to theoretical strain and for this web it was equal to one.

Measurement of the strain in the web in the free span and on the wound roll is achieved using the following steps:

1. The surface of the web is prepared and conditioned such that a strain gage can be glued on. The location for the strain gage along the web length is chosen such that the strain gage will enter the wound roll as the fifth lap is laid on. This ensures that the comparison with model results will be made for the same lap. Recall that the WOT is calculated as the average 'σ_{11}' stress in the fifth lap from ABAQUS model results.

2. The strain gage is then glued on to the web surface and 30 AWG wires are soldered to the copper tabs with minimal solder such that the solder joints do not

protrude significantly on top of the strain gage surface. These wires are connected to a strain indicator.

3. Before the winding process is started, the tension level in the web is brought to the desired level using the winder controls. The winding process is then started and as the strain gage passes beyond the idler and enters the span between the idler and the winding roll as shown in Fig. 7.11., the winding process is temporarily halted. During this time, the web tension is held constant.

4. The strain gage output is balanced to read zero such that the effect of web tension is cancelled.

5. The winding process is then continued and the strain in the web is monitored and recorded continuously using a data acquisition system.
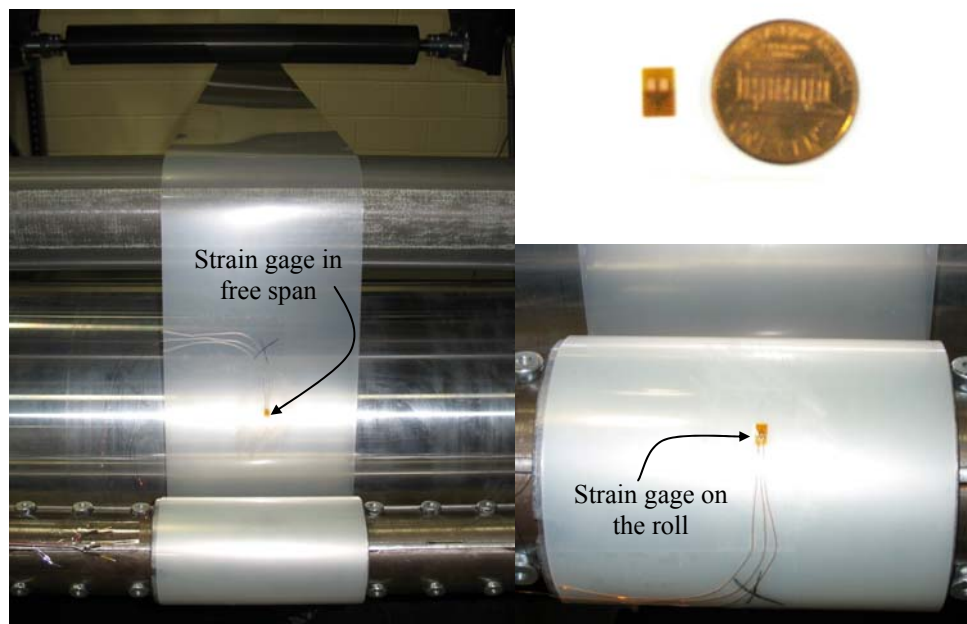
Figure 7.11: Strain gage on the web in the free span and on the wound roll.

Firstly, the strain gage output is recorded in a center winding process wherein the nip roller is not used and at a constant web tension of 3 Pli. The behavior of the strain in the free span and on the wound roll is shown in Fig. 7.12. Note that the results of three different tests under the same winding conditions are shown in Fig. 7.12. Observe that the strain measurements are very repeatable and compare well to theoretical bending strain calculated using linear bending theory as given in Eqn. 7.1. Also, the tension in the web remains constant through the winding process even through the halt period when the strain gage output is balanced.

$$\varepsilon_{Bending} = \frac{u}{r} \tag{7.1}$$
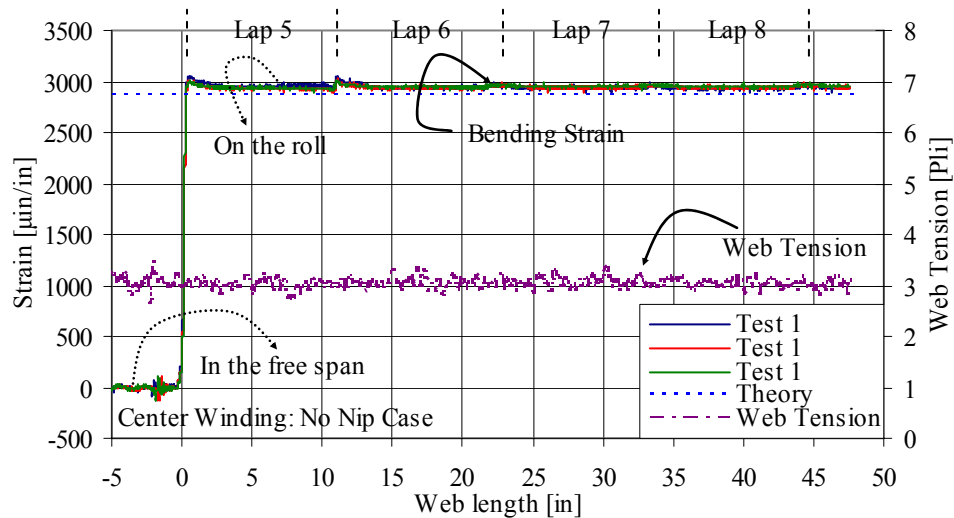
Figure 7.12: Behavior of web tension and strain in the web measured using the contact strain gage as a function of web length.

When a nip roller is used and a nip load of 25 Pli is applied during the winding process, the behavior of the stresses on the wound roll is shown in Fig. 7.13. Since a nip

163

roller is used in this case, the strain in the web measured using the strain gage includes both the bending component as well as the nip induced component of the strain. Also, the top and the bottom surface strains need to be measured in order to accurately compute the WOT. Figure 7.13 shows both the top and bottom surface stresses in the web on the wound roll and the stresses are calculated as the measured strain multiplied by the machine direction modulus.
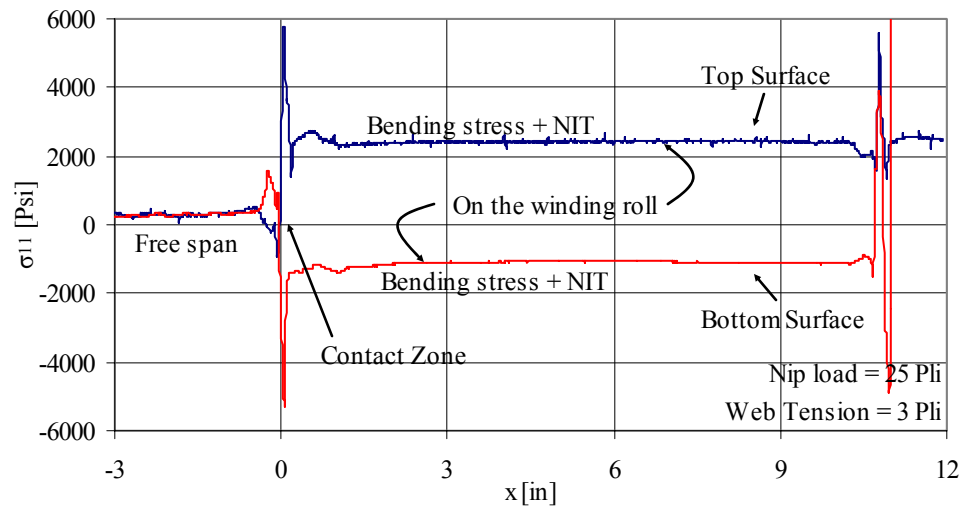
Figure 7.13: Behavior of the top and bottom surface stresses in the web in a center winding process at a web tension of 3 Pli and a nip load of 25 Pli.

The measured stresses in a center wound roll with an undriven nip roller at a nip load of 25 Pli and a web tension of 3 Pli is compared to the model results for the top and bottom surface stresses in Fig. 7.14 and Fig. 7.15 respectively. In the free span the average value of the stresses compare well to the model results. In the contact zone, the overall behavior of the contact stresses is very similar between the model results and the experimental measurements. The peak stresses in both the figures between the model

results and experimental measurements do not match and this can be due to the solder joints. As the nip roller rolls on top of the solder joints in the strain gage the bending stresses become very high as seen in the figures. Also, the contact widths are comparable between experimental values and model results.
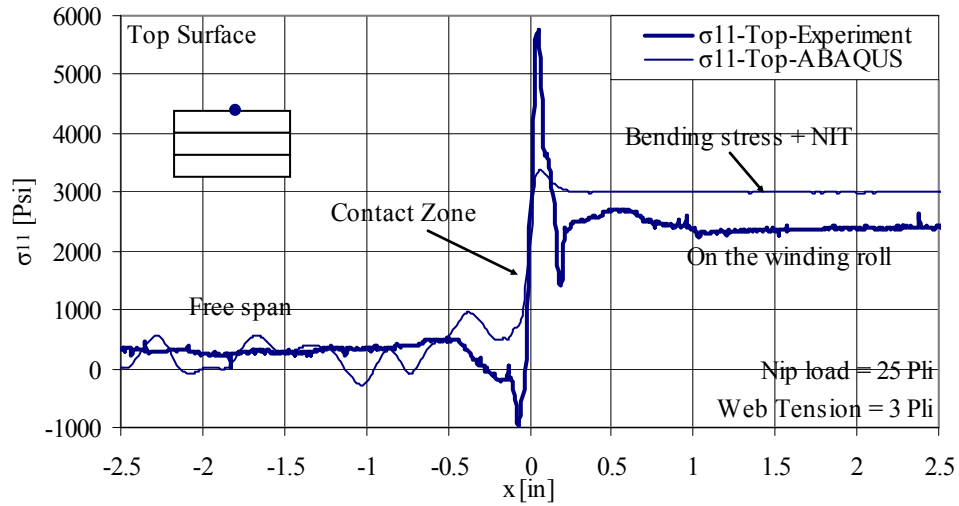
Figure 7.14: Comparison of the top surface stresses in the free span, contact zone and on the wound roll between the model results and experimental measurements.
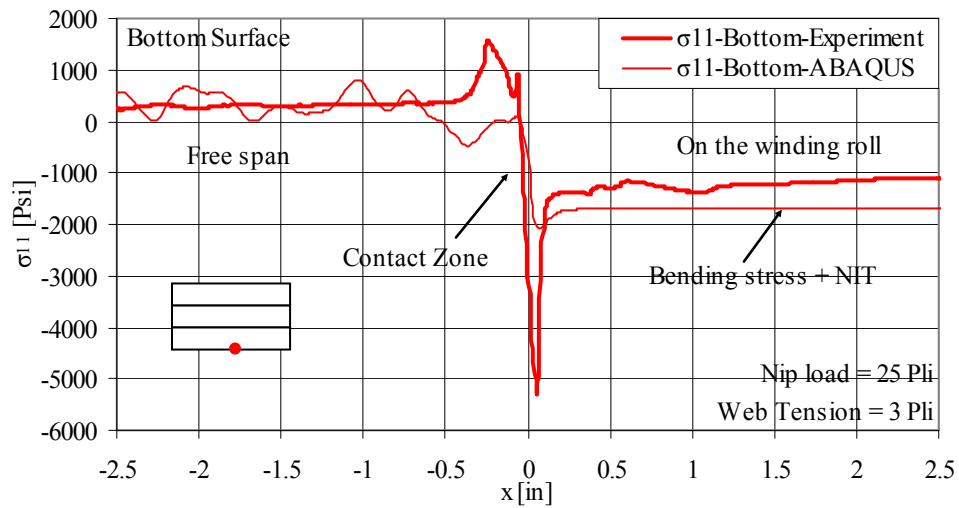
Figure 7.15: Comparison of the bottom surface stresses in the free span, contact zone and on the wound roll between the model results and experimental measurements.

165

When the top and bottom surface stresses are compared on the wound roll, they differ considerably between model and experimental values. However when the average of the top and bottom surface stresses are compared to the model results, they agree well as shown in Fig. 7.16. The results of the surface stresses do not compare well because of many factors like effect of backing thickness, significant bending and unbending of the web experienced in and beyond the contact zone. The average stresses compare well because, the effects explained above cancel each other between the top and the bottom surface stresses to leave the membrane stresses unaffected.
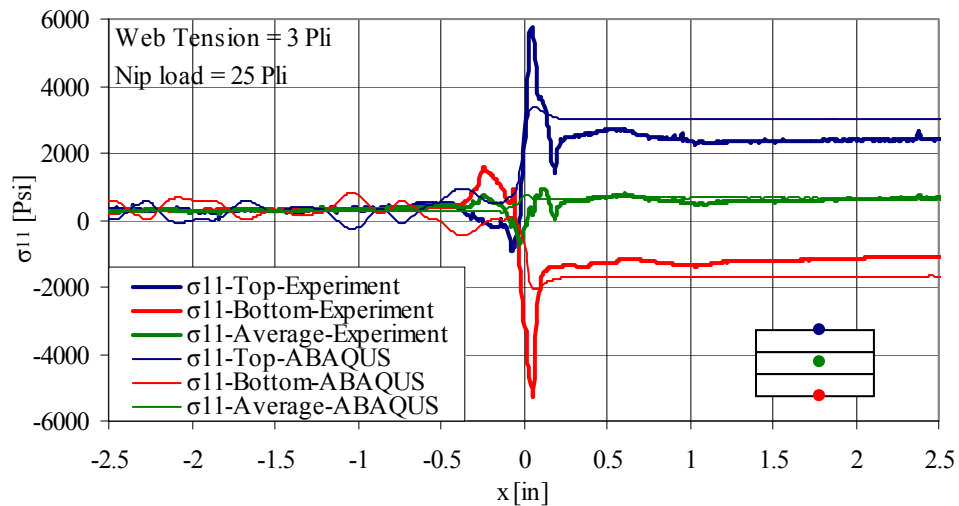
Figure 7.16: Comparison of the top, bottom and average stresses in the free span, contact zone and on the wound roll between the model results and experimental measurements.

The membrane stresses computed as an average of the top and bottom surface stresses is averaged and is represented as the WOT in the outermost layer of a winding roll. This value is compared to the model WOT results and to the WOT measured using the load cell method as shown in Fig. 7.17. Note that the measurement of WOT using this method is very difficult and only two different nip loads of 25 Pli and 50 Pli respectively

166

were attempted. The figure shows that the measurement of WOT using the strain gage compares well with the model output. The verification efforts discussed thus far show that the model results compare well with experimental measurements.
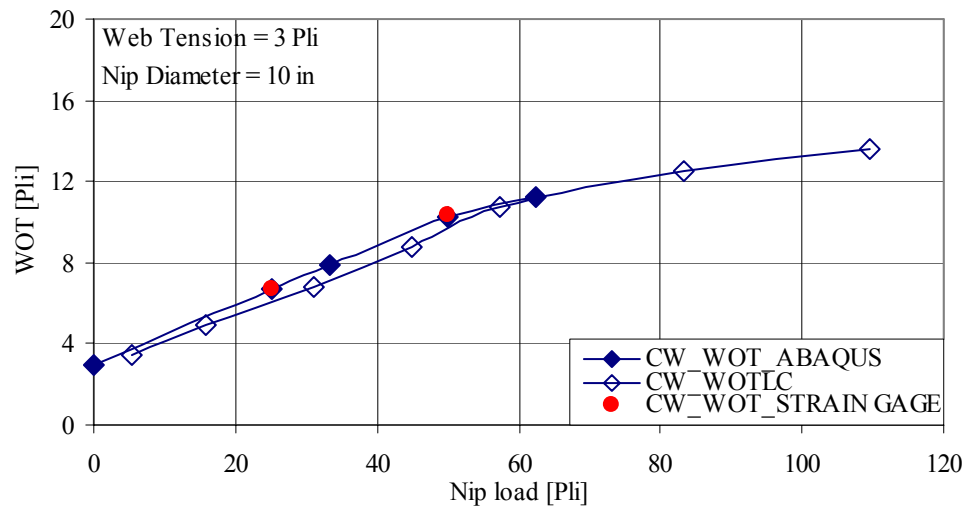
Figure 7.17: Comparison between WOT from model output, load cell method and strain gage measurements.

8 Conclusions

The objective of this research is to analyze the development of the Wound-on-Tension in a winding process without imposing any of the assumption used by previous researchers like Good and Jorkama. The analysis of the problem is carried out such that it focused on answering the following questions:

- How the WOT is developed in a web wound into a roll?

- How do the winding parameters affect the behavior of the WOT?

- How do the material properties affect the development of the WOT? and

- What is the effect of a compliant nip roller cover on the WOT?

Some general conclusions drawn from the results of this effort for the case when the incoming web does not wrap the nip roller have been summarized as follows:

- A first of kind approach has been developed such that the winding contact problem shall be analyzed using commercial finite element tools like ABAQUS/Explicit$^®$.

- In the presence of a nip roller, the numerical results show that the WOT is developed due to the existence of a net traction in the outermost layer of a winding roll as a result of the rolling contact mechanics. This net traction, when

integrated through the contact zone results in the NIT and when added with the web tension results in the WOT. In the absence of the nip roller, the WOT is equal to the tension in the incoming web.

- The net traction is calculated as the sum of the top and bottom surface tractions in the topmost layer. The top surface tractions exhibit three distinct regions. At the edges of the contact, the surface is under slip and the surface velocity of the web is higher than the velocity of the drum. In the middle of the contact, the top surface is under stick and in this zone, the surface velocities are equal.

- The bottom surface of the topmost layer is under micro-slip and exhibits five distinct regions. The surface is under slip at the edges of contact and in these zones, the bottom surface of the web moves slower than the top surface of the second layer. In the middle of the contact, another slip zone exists and in this zone the bottom surface moves faster than the top surface of the second layer. Between these slip zones, two intermediate stick zones exist wherein the surface velocities are equal.

In the following section, specific conclusions based on the parametric studies wherein the wrap angle of the web around the nip roller is zero are summarized.

- In both center and surface winding, at low nip loads, the numerical results show that the NIT is approximately equal to '$\mu_{Web/Web.}$ N'. At high nip loads, the NIT starts to taper off and decreases from the maximum possible value of '$\mu_{Web/Web.}$N'.

In surface winding, the numerical results show that the integrated value of the top surface traction is equal to the web tension so long as winding is possible.

- The numerical results show that the NIT is similar in both center and surface winding for a given level of nip load. This is consistent with the observations of Good et al [25].

- The numerical results show that the coefficient of friction between the nip roller and the winding roll does not affect the WOT in a center winding process. In surface winding, the smallest value of the nip load that can be used in order to wind the roll is determined as the value of '$\mu_{Nip/Web}.N$' that offsets the web tension. The results also indicate that the material can be surface wound at a given nip load if the '$\mu_{Nip/Web}$' is high enough such that '$\mu_{Nip/Web}.N$' offsets the value of web tension. This behavior is consistent with experimental observations of Kandadai and Good [29].

- In both center and surface winding, the numerical results show that the WOT is much less than '$\mu_{Web/Web}.N$' at very high values of '$\mu_{Web/Web}$' as the bottom surface of the topmost layer exhibits significant stick near the entry zone causing the net traction to reduce. The results indicate that the slippage on the bottom surface of the outermost layer is necessary in the development of the WOT. Due to this, webs like adhesive tapes or any web coated with a pressure sensitive adhesive will develop little WOT due to nip induced slippage.

- The results of the flat bed rolling nip model indicate that the WOT decreases with increase in nip roller diameter. As the nip roller diameter increases, the contact pressure decreases and the contact width increases. This causes the traction limits

to decrease. A significant stick zone exists in the bottom surface near the entry zone for larger diameter nips and combined with increase in the contact width causes the total traction to decrease. Hence the WOT decreases. This behavior is consistent with experimental observations of Good [8].

- The numerical results show that at high values of radial modulus ('E_r') the contact width reduces substantially and along with significant stick exhibited by the bottom surface causes the WOT to decrease. At lower values of 'E_r', the WOT appears to be independent of 'E_r'

- The numerical results show that the out-of-plane Poisson's ratio '$\nu_{r\theta}$' of the web does not affect the final value of the WOT in both center and surface winding for the cases observed. This is in agreement with what Jorkama [10] observed; However this behavior disagrees with the WOT model proposed by Good [8]. Although this observation is true, one should note that the model did not allow '$\nu_{r\theta}$' to be a truly independent parameter as '$\nu_{r\theta}$' is coupled to 'E_r' and '$\nu_{\theta r}$' through Maxwell's relation. Also, the web stiffness properties in the model only apply to a few types of webs. One has to study different webs that encompass a wide range of web stiffness in order to understand the effect of '$\nu_{r\theta}$'.

- The numerical results show that the out-of-plane shear modulus '$G_{r\theta}$' is an important parameter at high nip loads when the bottom surface of the outer layer starts exhibiting significant stick zone. The results also indicate that '$G_{r\theta}$' can affect the point at which the NIT starts to deviate from '$\mu_{Web/Web}$. N'. At high nip loads, increasing '$G_{r\theta}$' results in an increase in the WOT. At a given nip load,

Jorkama [10] observed that the NIT and hence the WOT increases with increase in '$G_{r\theta}$'.

- When a compliant nip roller is used, the numerical results show that the WOT can be affected by changing both the modulus and the Poisson's ratio of the nip cover. When a soft rubber cover was used, the WOT was significantly less than that produced for a rigid nip roller. When a foam-type nip cover is used, very little WOT is produced. Although the magnitudes were different, the general trends show similar behavior to that observed by Jorkama [10]. The experimental measurements of Santhanakrishnan [30] show that the compliancy of the nip cover had a much less effect on the WOT compared to the Poisson's ratio. However, in this research, the nip cover was not modeled adequately and hence only the trends could be compared.

Based on the experimental results, the following conclusions shall be drawn

- The experimental measurements of the WOT measured using the load cell method agrees well with the model results when the coefficient of friction between web layers input to the model is measured in rolling contact conditions. In this context, measurement of coefficient of friction using a rolling nip test bed is much more representative of the frictional conditions that exist in the winding contact zone than the ASTM measurements.
- The strain gage measurements show that the overall behavior of the stresses in the contact zone compare well to the model results.

9   Future Work and Recommendations

From the parametric studies discussed in sections 6.1.6 and 6.2.4, it is evident that some of the material properties can be extremely important. Although, one can attempt 'what if' scenarios with this model, it is not ideally suited for industrial applications as some of these analyses can take 10 days to run. In order to develop accurate models that can predict the behavior of the WOT in a given material and a winding process it is necessary to understand the material parameters that affect the model results.

One set of future work should focus on understanding the state dependency of some of the material properties. The parametric studies in both the flat bed and winding models showed that the out-of-plane shear modulus 'G_{12}' can be an important parameter. In this dissertation, the value of this parameter is set based on Eqn 5.12. Note that Eqn. 5.12. includes a radial modulus term in it. The state dependency of the radial modulus on radial pressure is well understood. Due to this, Eqn. 5.12 would indicate that the value of 'G_{12}' is also state dependent on pressure. However, the validity of this equation in the out-of-plane direction of the web is not yet proven. So, it is necessary to first understand the behavior of this parameter. Also, the state dependency of the out-of-plane Poisson's ratio needs to be better understood.

The other set of future work should focus on model development based on contact mechanics formulations. Boundary element formulations similar to that used by Soong and Li [38] and Jorkama [10] need to be explored further. Soong and Li use an isotropic material model and Jorkama uses a linear orthotropic material model for modeling the web material property. However webs are nonlinearly anisotropic and the model development should focus on correct material definition and better solution schemes than that has been employed previously.

ABAQUS/Explicit$^{®}$ is a very powerful tool as has been shown in this dissertation. There are several areas in web handling that can be explored with the help of this model and with some modifications to this model. Some of the recommendations include the following:

- Study of calendaring problems

    Typically webs are crushed between nip rollers for many purposes including densification, caliper reduction, etc. This process can be analyzed successfully with some modifications to the flat bed model.

- Study of roll cover designs

    Adding another dimension to the 2D flat bed model, the behavior of different types of nip roller/calendar roller covers can be studied and better roll cover designs can be achieved.

- Study of web caliper variations, axial stresses and WOT behavior

    Although, a 3D winding model would be ideally suited for the analysis of this type of problem it will be computationally huge. However a flatbed 3D model shall be ideally suited for the analysis of this type of problem.

174

- Web transport studies

  The focus of this dissertation has been on nip mechanics and wound roll mechanics using a FE tool. The problems and defects caused due to the wound roll structure forms one end of the spectrum. The other end of the spectrum consists of web transport problems that include wrinkling, roll storage, etc. The versatility of the explicit code can be put to good use in studying the troughing and wrinkling behaviors in webs due to roller misalignment and roller designs. Also, the effect of roll weight in storage of highly compressible webs can also be studied.

Bibliography

1. Z. Hakiel, "Nonlinear Model for Wound Roll Stresses," *TAPPI Journal*, vol. 70, pp. 113-117, 1987.

2. J. D. Pfeiffer, "Mechanics of a Rolling Nip on Paper Webs," *TAPPI Journal*, vol. 51, pp. 77A-85A, 1968.

3. T. Rand and L. G. Eriksson, "Physical Properties of Newsprint Rolls during Winding," *TAPPI Journal*, vol. 56, pp. 153-156, 1973.

4. J. K. Good and Z. Wu, "The Mechanism of Nip Induced Tension in Wound Rolls," *Journal of Applied Mechanics, Transactions ASME*, vol. 60, pp. 942-947, 1993.

5. J. K. Good, Z. Wu, and M. W. R. Fikes, "The Internal Stresses in Wound Rolls with the Presence of a Nip Roller," *Journal of Applied Mechanics, Transactions ASME*, vol. 61, pp. 182-185, 1994.

6. "ASTM D1894-05: Standard Test Method for Static and Kinetic Coefficients of Friction of Plastic Film and Sheeting," *Annual Book of ASTM Standards*, vol. 08.01.

7. E. G. Welp and B. Gueldenberg, "Analysis of the Kinematic and Dynamic Process during Winding based on a Systematology of Models for Winding Mechanics," *Proceedings of the Fourth International Conference on Web Handling, Web Handling Research Center, Oklahoma State University, Stillwater, Oklahoma*, pp. 71-89, 1997.

8. J. K. Good, "Modeling Nip Induced Tension in Wound Rolls," *Proceedings of the Sixth Interntational Conference on Web Handling, Web Handling Research Center, Oklahoma State University, Stillwater, Oklahoma*, pp. 103-122, 2001.

9. M. Jorkama and R. von Hertzen, "The Mechanism of Nip Induced Tension in Winding," *Journal of Pulp and Paper Science*, vol. 28, pp. 280-284, 2002.

10.   M. Jorkama, "Contact Mechanical Model for Winding Nip," *Doctoral Thesis, Helsinki University of Technology*, 2001.

11.   J. K. Good, "The Abilities and Inabilities of Wound Roll Models to Predict Winding Defects (Keynote Speech)," *Proceedings of the Eight International Conference on Web Handling, Web Handling Research Center, Stillwater, Oklahoma*, 2005.

12.   P. Hoffecker and J. K. Good, "Tension Allocation in Three Dimensional Axisymmetric Wound Roll Model," *Proceedings of the Eighth International Conference on Web Handling, Web Handling Research Center, Oklahoma State University, Stillwater, Oklahoma*, 2005.

13.   Y. M. Lee and J. A. Wickert, "Stress Field in Finite Width Axisymmetric Wound Rolls," *ASME Journal of Applied Mechanics*, vol. 69, pp. 130-138, 2002.

14.   P. Smolinski, C. S. Miller, R. D. Marangoni, and D. Onipede, "Modeling the collapse of coiled material," *Finite Elements in Analysis and Design*, vol. 38, pp. 521-535, 2002.

15.   H. C. Altmann, "Formulas for Computing Stress in Center-Wound Rolls," *TAPPI Journal*, vol. 51, pp. 176, 1968.

16.   O. C. Zienkiewicz and G. N. Pande, "Time-dependent multilaminate model of rocks - a numerical study of deformation and failure of rock masses," *International Journal for Numerical and Analytical Methods in Geomechanics*, vol. 1, pp. 219-247, 1977.

17.   S. Li and J. Cao, "A hybrid approach for quantifying the winding process and material effects on sheet coil deformation," *Journal of Engineering Materials and Technology, Transactions of the ASME*, vol. 126, pp. 303-313, 2004.

18.   R. C. Benson, "A Nonlinear Wound Roll Model Allowing for Large Deformation," *Journal of Applied Mechanics*, vol. 62, pp. 853-859, 1995.

19.   J. D. Pfeiffer, "Nip Forces and their Effect on Wound-In-Tension," *TAPPI Journal*, vol. 60, pp. 115-117, 1977.

20.   J. D. Pfeiffer, "Wound-Off Tension Measurement in Paper Rolls," *TAPPI Journal*, vol. 60, pp. 106-108, 1977.

21.   J. D. Pfeiffer and Beloit Corporation, "Measuring and Controlling Wound-in-Tension for Web Winding Machines," *United States Patent 3687388*, 1972.

22.   J. K. Good and M. W. R. Fikes, "Predicting the Internal Stresses in Center-wound Rolls with an Undriven Nip Roller," *TAPPI Journal*, vol. 74, pp. 101-109, 1991.

23. N. Cai, "The Effects of Nip Roller Compliancy upon Center and Surface Winding," *M.S. Thesis, Oklahoma State University*, 1992.

24. R. E. Steves, "The Effect of Nip Load on Wound-On-Tension in Surface Winding," *M.S. Thesis, Oklahoma State University*, 1995.

25. J. K. Good, J. Hartwig, and R. Markum, "A Comparison of Center and Surface Winding Using the Wound-In-Tension Method," *Proceedings of the Fifth International Conference on Web Handling, Web Handling Research Center, Stillwater, Oklahoma*, pp. 87-104, 1999.

26. B. Gueldenberg, "Quantitative Analysis of Nip Induced Tension by use of Digital Image Processing," *Proceedings of the Fifth International Conference on Web Handling, Web Handling Research Center, Oklahoma State University, Stillwater, Oklahoma*, pp. 19-38, 1999.

27. E. P. Laumer, "Minimizing 'Wound-In' Paper Defects within Shipping Rolls," *TAPPI Journal,*, vol. 49, pp. 127 A, 1966.

28. B. Kandadai, "A Study of the Wound-On-Tension Measurement Method in Surface Winding Condition on TYVEK Webs," *M.S. Thesis, Oklahoma State University*, 2001.

29. B. Kandadai and J. K. Good, "Wound-in-Tension in a Non-Woven Web," *Proceedings of the Eighth International Conference on Web Handling, Web Handling Research Center, Oklahoma State University, Stillwater, Oklahoma*, 2005.

30. N. Santhanakrishnan, "Effect of Rubber Covered Nip Rollers on Wound-on-Tension in Center and Surface Winding," *M.S. Thesis, Oklahoma State University*, 2002.

31. E. M. J. Jalkanen, "Influence of Certain Winding Parameters on the Formation and Structure of Newsprint Paper Rolls (In Finnish)," *M.S. Thesis, Helsinki University of Technology*, 1968.

32. R. H. Bentall and K. L. Johnson, "Slip in the rolling contact of two dissimilar elastic rollers," *International Journal of Mechanical Sciences*, vol. 9, pp. 389-404, 1967.

33. R. H. Bentall and K. L. Johnson, "An elastic strip in plane rolling contact," *International Journal of Mechanical Sciences*, vol. 10, pp. 637-663, 1968.

34.   J. J. Kalker, "On the Rolling Contact of Two Elastic Bodies in the Presence of Dry Friction " in *Department of Mechanical Engineering*: Technische Hogeschool, Delft, 1968.

35.   P. D. Panagiotopoulos, "A Nonlinear Programming Approach to the Unilateral Contact and Friction-Boundary value Problem in Theory of Elasticity," *Ingenieur-Archiv*, vol. 44, pp. 421-432, 1975.

36.   T.-C. Soong and C. Li, "On the Unbounded Contact Between Plates and Layered Cylinders," *ASME Journal of Applied Mechanics*, vol. 47, pp. 841-846, 1980.

37.   T.-C. Soong and C. Li, "The steady rolling contact of two elastic layer bonded cylinders with a sheet in the nip," *International Journal of Mechanical Sciences*, vol. 23, pp. 263-273, 1981.

38.   T.-C. Soong and C. Li, "Rolling Contact of Two Elastic Layer Covered Cylinders Driving a Loaded Sheet in the Nip," *ASME Journal of Applied Mechanics*, vol. 48, pp. 889-894, 1981.

39.   H. Hertz, "Über die Berührung fester elastischer Körper," *J. reine und angewandte Mathematik*, vol. 92, pp. 156-171, 1882.

40.   S. G. Lekhnitskii, "Theory of Elasticity of an Anisotropic Elastic Body," *Holden-Day, San Francisco*, 1963.

41.   K. L. Johnson, "Contact Mechanics," *Cambridge University Press*, 1985.

42.   K. Arola and R. von Hertzen, "Development of Sheet Tension under a Rolling Nip on a Paper Stack," *International Journal of Mechanical Sciences*, vol. 47, pp. 110-133, 2005.

43.   O. Kaya, "Wound-on-Tension in Surface Winding," *M.S. Thesis, Oklahoma State University*, 1999.

44.   "ASTM D2240-05: Standard Test Method for Rubber Property - Durometer Hardness," *Annual Book of ASTM Standards*, vol. 09.01.

45.   W. K. Chung, S. K. Choi, and P. F. Thomson, "Three Dimensional simulation of the Edge Rolling Process by the Explicit Finite Element Method," *Journal of Materials Processing Technology*, vol. 38, pp. 85-102, 1993.

46.   Ghosh. S., M. Li, and D. Gardiner, "A Computational and Experimental Study of Cold Rolling of Aluminum Alloys with Edge Cracking," *Journal of Manufacturing Science and Engineering*, vol. 126, pp. 74-82, 2004.

47.	T. Belytschko, W. J. Chung, and J. W. Cho, "On the dynamic effects of explicit FEM in sheet metal forming analysis," *Engineering Computations*, vol. 15, pp. 750-776, 1998.

48.	T. Belytschko, W. K. Liu, and B. Moran, "<u>Nonlinear Finite Elements for Continua and Structures</u>," *John Wiley & Sons, Ltd.*, 2000.

49.	D. P. Flanagan and T. Belytschko, "A Uniform Strain Hexahedron and Quadrilateral with Orthogonal Hourglass Control," *International Journal for Numerical Methods in Engineering*, vol. 17, pp. 679-706, 1981.

50.	"ASTM D882-05: Test Method for Tensile Properties of Thin Plastic Sheeting (strip tensile)," *Annual Book of ASTM Standards*, vol. 08.01.

51.	J. K. Good and B. Kandadai, "Private Communication," 2000.

52.	J. D. Pfeiffer, "Measurement of the K2 Factor for Paper," *TAPPI Journal*, pp. 139-141, 1980.

53.	R. Feng and J. R. Farris, "Linear Thermoelastic Characterization of Anisotropic Poly(ethylene terephthalate) Films," *Journal of Applied Polymer Science*, vol. 86, pp. 1937-1947, 2001.

54.	Y. Okabe, N. Takeda, M. Yanaka, and Y. Tsukahara, "Determination of the Orthotropic Elastic Constants of Thin PET Film by an Ultrasonic Micro-Spectrometer," *IEEE Transactions on Ultrasonics, Ferroelectrics, and Frequency Control*, vol. 46, pp. 1269-1275, 1999.

55.	S. L. Zhang and J. C. M. Li, "Anisotropic Elastic Moduli and Poisson's Ratios of a Poly(ethylene terephthalate) Film," *Journal of Polymer Science: Part B: Polymer Physics*, vol. 42, pp. 260-266, 2004.

56.	M. S. Willett and W. L. Poesch, "Determining the Stress Distributions in Wound Reels of Magnetic Tape using a Nonlinear Finite Difference Approach," *Journal of Applied Mechanics, Transactions ASME*, vol. 55, pp. 365-371, 1988.

57.	M. Jorkama and R. von Hertzen, "Contact Mechanical Approach to the Winding Nip," *Proceedings of the Fifth International Conference on Web Handling, Web Handling Research Center, Oklahoma State University, Stillwater, Oklahoma*, pp. 39-49, 1999.

58.	S. Cheng and C. C. Cheng, "Relation between E, ν, G and Invariants of the Elastic Coefficients for an Orthotropic Body," *The Winter Annual Meeting of the American Society of Mechanical Engineers, Dallas, Texas, Applied Mechanics Division and the Materials Division, ASME*, vol. 112, pp. 63-65, 1990.

59. E. P. Saliklis, "Empirical Prediction of Shear Modulus and Young's Modulus of Plywood Panels," *CD-ROM Proceedings of the 14th ASCE Engineering Mechanics Division Conference, The University of Texas, Austin, Texas*, 2000.

60. ABAQUS Inc., "Getting Started with ABAQUS Manual," 2005.

61. ABAQUS Inc., "ABAQUS Theory Manual," 2005.

62. ABAQUS Inc., "ABAQUS Analysis User's Manual," 2005.

63. E. Nakamachi and T. Huo, "Dynamic-explicit elastic plastic finite-element simulation of hemispherical punch-drawing of sheet metal," *Engineering Computations*, vol. 13, pp. 327-337, 1996.

64. J. Kim, S. J. Kang, and B. S. Kange, "A comparitive study of implicit and explicit FEM for the wrinkling prediction in the hydroforming process," *International Journal for Advanced Manufacturing Technology*, vol. 22, pp. 547-552, 2003.

APPENDIX A

Input file template for the flat bed model with a rigid nip

```
**----------------------------------------------------------------------
**          PLANE STRAIN LINEAR FLAT BED NIP MECHANICS FEM MODEL
**              INPUT FILE CREATED BY BALAJI KOVIL KANDADAI
**                    CREATED 08/06/2005 - PROPERTY OF WHRC
**
**                      THICKNESS OF LAYER=0.01 IN
**                     RIGID ALUMINUM NIP = 4 IN DIA
**            ELEMENTAL DIMENSIONS = 0.01 X 0.0025 (L X H)
**                    TOTAL LAYER LENGTH = 10 IN
**----------------------------------------------------------------------
*HEADING
            FLAT BED NIP MECHANICS - NIP LOAD = 25 PLI
**----------------------------------------------------------------------
**                                      PARTS
**----------------------------------------------------------------------
**----------------------------------------------------------------------
**          PART: 10 WEB LAYERS; NODE, ELEMENT, SET DEFINITIONS
**----------------------------------------------------------------------
*PART, NAME=WEBSTACK
*NODE, NSET=NLEFT
     1,  0.000000000, 0.100000000
  1001,  0.000000000, 0.097500000
  2001,  0.000000000, 0.095000000
** CONTINUED FROM 3001 TO 47001
 48001,  0.000000000, 0.002500000
 49001,  0.000000000, 0.000000000
*NODE, NSET=NRIGHT
  1000, 10.000000000, 0.100000000
  2000, 10.000000000, 0.097500000
  3000, 10.000000000, 0.095000000
** CONTINUED FROM 4000 TO 47000
 48000, 10.000000000, 0.005000000
 49000, 10.000000000, 0.002500000
 50000, 10.000000000, 0.000000000
*NGEN, NSET=NLAYER1
     1,    1000
  1001,    2000
  2001,    3000
  3001,    4000
  4001,    5000
** REPEAT FOR LAYERS 2 THROUGH 9
*NGEN, NSET=NLAYER10
 45001,   46000
 46001,   47000
 47001,   48000
 48001,   49000
 49001,   50000
*NSET, NSET=NLAYER1_TOP
     1,    1000
*NSET, NSET=NLAYER1_BOT
  4001,    5000
** REPEAT FOR LAYERS 2 THROUGH 9
*NSET, NSET=NLAYER1_TOP
 45001,   46000
*NSET, NSET=NLAYER1_BOT
 49001,   50000
*NSET, NSET=NSTACK
```

```
 NLAYER1
** REPEAT FOR LAYERS 2 THROUGH 9
 NLAYER10
*ELEMENT, TYPE=CPE4R
      1,   1001,   1002,      2,      1
  4001,   6001,   6002,   5002,   5001
** REPEAT FOR LAYER 3 THROUGH 8
 32001,  41001,  41002,  40002,  40001
 36001,  46001,  46002,  45002,  45001
*ELGEN, ELSET=ELAYER1
      1, 999, 1, 1, 4, 1000, 1000
*ELGEN, ELSET=ELAYER2
  4001, 999, 1, 1, 4, 1000, 1000
** REPEAT FROM ELAYER3 TILL ELAYER9
*ELGEN, ELSET=ELAYER10
 36001, 999, 1, 1, 4, 1000, 1000
*ELSET, ELSET=ESTACK
 ELAYER1
** REPEAT FOR LAYERS 2 THROUGH 9
 ELAYER10
*ELSET, ELSET=ELAYER1_TOP, GENERATE
      1,    999
*ELSET, ELSET=ELAYER1_BOT, GENERATE
  3001,   3999
** REPEAT FOR LAYERS 2 THROUGH 9
*ELSET, ELSET=ELAYER10_TOP, GENERATE
 36001, 36999
*ELSET, ELSET=ELAYER10_BOT, GENERATE
 39001, 39999
*SURFACE, TYPE=ELEMENT, NAME=SLAYER1_TOP
 ELAYER1_TOP, S3
*SURFACE, TYPE=ELEMENT, NAME=SLAYER1_BOT
 ELAYER1_BOT, S1
** REPEAT FOR LAYERS 2 THROUGH 9
*SURFACE, TYPE=ELEMENT, NAME=SLAYER10_TOP
 ELAYER10_TOP, S3
*SURFACE, TYPE=ELEMENT, NAME=SLAYER10_BOT
 ELAYER10_BOT, S1
**---------------------------------------------------------------------
**                        SECTION PROPERTIES
**---------------------------------------------------------------------
*ORIENTATION, NAME=MATCORD
1.0, 0.0, 0.0, 0.0, 1.0, 0.0
1, 0.0
*SOLID SECTION, ELSET=ESTACK, ORIENTATION=MATCORD, MATERIAL=LORTHO
 1.0,
**---------------------------------------------------------------------
**                      END SECTION PROPERTIES
**---------------------------------------------------------------------
*END PART
**---------------------------------------------------------------------
**                      END PART: 10 WEB LAYERS
**---------------------------------------------------------------------
**---------------------------------------------------------------------
**           PART:  RIGID NIP; NODE ELEMENT, SECTION DEFINITIONS
**---------------------------------------------------------------------
*PART, NAME=NIP
```

```
*NODE, NSET=NIPNODE
 200000, 1.500000000, 2.100000000
*SURFACE, TYPE=SEGMENTS, NAME=SNIP
START,  1.500000000, 0.100000000
CIRCL, -0.500000000, 2.100000000, 1.50000000, 2.10000000
CIRCL,  1.500000000, 4.100000000, 1.50000000, 2.10000000
CIRCL,  3.500000000, 2.100000000, 1.50000000, 2.10000000
CIRCL,  1.500000000, 0.100000000, 1.50000000, 2.10000000
*RIGID BODY, ANALYTICAL SURFACE=SNIP, REFNODE=NIPNODE
*MASS, ELSET=ROLM_N
 0.001
*ROTARY INERTIA, ELSET=ROLI_N
 0.0010, 0.0010, 0.0010, 0.0000, 0.0000, 0.0000
*ELEMENT, TYPE=MASS, ELSET=ROLM_N
 200000, 200000
*ELEMENT, TYPE=ROTARYI, ELSET=ROLI_N
 200001, 200000
*END PART
**-----------------------------------------------------------------------
**                          END PART:  RIGID NIP
**-----------------------------------------------------------------------
**-----------------------------------------------------------------------
**          PART:  RIGID BASE; NODE ELEMENT, SECTION DEFINITIONS
**-----------------------------------------------------------------------
*PART, NAME=BASE
*NODE, NSET=BASENODE
 300000, 0.00000000, 0.00000000
*SURFACE, TYPE=SEGMENTS, NAME=SBASE
 START, -0.500000000, 0.0000000000
 LINE,  11.000000000, 0.0000000000
*RIGID BODY, ANALYTICAL SURFACE=SBASE, REFNODE=BASENODE
*MASS, ELSET=ROLM_B
 0.001
*ROTARY INERTIA, ELSET=ROLI_B
 0.0010, 0.0010, 0.0010, 0.0000, 0.0000, 0.0000
*ELEMENT, TYPE=MASS, ELSET=ROLM_B
 300000, 300000
*ELEMENT, TYPE=ROTARYI, ELSET=ROLI_B
 300001, 300000
*END PART
**-----------------------------------------------------------------------
**                          END PART:  RIGID BASE
**-----------------------------------------------------------------------
**-----------------------------------------------------------------------
**                              END PARTS
**-----------------------------------------------------------------------
**-----------------------------------------------------------------------
**                              ASSEMBLY
**-----------------------------------------------------------------------
*ASSEMBLY, NAME=FBR
*INSTANCE, NAME=IWEBSTACK, PART=WEBSTACK
*END INSTANCE
*INSTANCE, NAME=INIP, PART=NIP
*END INSTANCE
*INSTANCE, NAME=IBASE, PART=BASE
*END INSTANCE
*END ASSEMBLY
```

```
**----------------------------------------------------------------------
**                              END ASSEMBLY
**----------------------------------------------------------------------
**----------------------------------------------------------------------
**                         AMPLITUDE DEFINITIONS
**----------------------------------------------------------------------
*AMPLITUDE, NAME=LOADING, DEFINITION=SMOOTH STEP
0.0, 0.0, 0.1, 1.0
*AMPLITUDE, NAME=ROLLING, DEFINITION=SMOOTH STEP
0.0, 0.0, 0.2, 1.0
**----------------------------------------------------------------------
**                       END AMPLITUDE DEFINITIONS
**----------------------------------------------------------------------
**----------------------------------------------------------------------
**                          MATERIAL PROPERTIES
**----------------------------------------------------------------------
*MATERIAL, NAME=LORTHO
*DENSITY
 0.0001553
*ELASTIC, TYPE=ENGINEERING CONSTANTS
 710000, 2865, 740000, 0.3, 0.36, 0.01, 2367, 1000
   1000
**----------------------------------------------------------------------
**                        END MATERIAL PROPERTIES
**----------------------------------------------------------------------
**----------------------------------------------------------------------
**                         INTERACTION PROPERTIES
**----------------------------------------------------------------------
*SURFACE INTERACTION, NAME=FNIP_WEB
*FRICTION
 0.18,
*SURFACE INTERACTION, NAME=FBASE_WEB
*FRICTION
 0.18,
*SURFACE INTERACTION, NAME=FWEB_WEB
*FRICTION
 0.16,
**----------------------------------------------------------------------
**                       END INTERACTION PROPERTIES
**----------------------------------------------------------------------
**----------------------------------------------------------------------
**                    INITIAL BCS - LOAD & DISPLACEMENT
**----------------------------------------------------------------------
*BOUNDARY, OP=NEW, TYPE=DISPLACEMENT
 INIP.NIPNODE, 1, 1
*BOUNDARY, OP=NEW, TYPE=DISPLACEMENT
 IBASE.BASENODE, 2, 2
 IBASE.BASENODE, 6, 6
**----------------------------------------------------------------------
**                    END INITIAL BCS:LOAD & DISPLACEMENT
**----------------------------------------------------------------------
**----------------------------------------------------------------------
**                 STEP: DYNAMIC EXPLICIT: STEP 1 NIP&ROLLING
**----------------------------------------------------------------------
*STEP, NAME=NIP_ROLLING, NLGEOM=YES
*DYNAMIC, EXPLICIT
 ,1.0
```

```
*FIXED MASS SCALING, FACTOR = 75.0, ELSET=IWEBSTACK.ESTACK
*BULK VISCOSITY
 0.06, 1.2
**----------------------------------------------------------------------
**               MODIFIED BCS: LOAD, DISPLACEMENT & VELOCITY
**----------------------------------------------------------------------
*BOUNDARY, OP=NEW, TYPE=DISPLACEMENT
 IBASE.BASENODE, 2, 2
 IBASE.BASENODE, 6, 6
*BOUNDARY, OP=NEW, TYPE=DISPLACEMENT
 INIP.NIPNODE, 1, 1
*BOUNDARY, OP=NEW, TYPE=VELOCITY, AMPLITUDE=ROLLING
 IWEBSTACK.NLEFT, 1, 1, -4.00
 IBASE.BASENODE,  1, 1, -4.00
*DLOAD
 IWEBSTACK.ESTACK, GRAV, 386.4, 0.0, -1.0, 0.0
*CLOAD, , AMPLITUDE=LOADING
 INIP.NIPNODE, 2, -25.0
**----------------------------------------------------------------------
**               END MODIFIED BCS: LOAD, DISPLACEMENT & VELOCITY
**----------------------------------------------------------------------
**----------------------------------------------------------------------
**                         INTERACTION PROPERTIES
**----------------------------------------------------------------------
*CONTACT PAIR, CPSET=N_W, INTERACTION=FNIP_WEB
 IWEBSTACK.SLAYER1_TOP, INIP.SNIP
*CONTACT PAIR, CPSET=W_W12, INTERACTION=FWEB_WEB
 IWEBSTACK.SLAYER1_BOT, IWEBSTACK.SLAYER2_TOP
*CONTACT PAIR, CPSET=W_W23, INTERACTION=FWEB_WEB
 IWEBSTACK.SLAYER2_BOT, IWEBSTACK.SLAYER3_TOP
** REPEAT FOR LAYERS 3 THROUGH 9
*CONTACT PAIR, CPSET=W_W910, INTERACTION=FWEB_WEB
 IWEBSTACK.SLAYER9_BOT, IWEBSTACK.SLAYER10_TOP
*CONTACT PAIR, CPSET=B_W, INTERACTION=FBASE_WEB
 IWEBSTACK.SLAYER10_BOT, IBASE.SBASE
*CONTACT CONTROLS, CPSET=N_W, GLOBTRKINC=99999
*CONTACT CONTROLS, CPSET=W_W12, GLOBTRKINC=99999
*CONTACT CONTROLS, CPSET=W_W23, GLOBTRKINC=99999
** REPEAT FOR LAYERS 3 THROUGH 9
*CONTACT CONTROLS, CPSET=W_W910, GLOBTRKINC=99999
*CONTACT CONTROLS, CPSET=B_W, GLOBTRKINC=99999
**----------------------------------------------------------------------
**                         END INTERACTION PROPERTIES
**----------------------------------------------------------------------
**----------------------------------------------------------------------
**                              OUTPUT REQUESTS
**----------------------------------------------------------------------
*RESTART, WRITE, NUMBER INTERVAL=2, OVERLAY
*OUTPUT, FIELD, NUMBER INTERVAL=20, TIME MARKS=YES
*ELEMENT OUTPUT
 S, LE, EMSF, EDT, DENSITY
*NODE OUTPUT
 U ,V, A, RF
*CONTACT OUTPUT
 CSTRESS
*OUTPUT, HIST, FREQUENCY=200
*ENERGY OUTPUT
```

```
 ALLAE, ALLCD, ALLDMD, ALLFD, ALLIE, ALLKE, ALLPD, ALLSE, ALLVD, ALLWK,
ETOTAL
*INCREMENTATION OUTPUT
 DMASS, DT
**----------------------------------------------------------------------
**                          END OUTPUT REQUESTS
**----------------------------------------------------------------------
*END STEP
**----------------------------------------------------------------------
**            END STEP: DYNAMIC EXPLICIT: STEP 1 NIP&ROLLING
**----------------------------------------------------------------------
```

APPENDIX B

Input file template for the flat bed model with a compliant nip cover

In the input file given in Appendix A the elastic cover definition replaces the entire part definition for the rigid nip as shown below.

```
**----------------------------------------------------------------------
**              PART:  RIGID NIP; NODE ELEMENT, SECTION DEFINITIONS
**----------------------------------------------------------------------

                    Copy the elastic nip cover definition here

**----------------------------------------------------------------------
**                            END PART:  RIGID NIP
**----------------------------------------------------------------------
```

<u>ELASTIC COVER DEFINITION</u>

```
**----------------------------------------------------------------------
**                        PART:  ELASTIC NIP
**----------------------------------------------------------------------
*PART, NAME=NIP
*NODE, NSET=NIPNODE
 200000, 1.500000000, 2.100000000
*NODE, NSET=START
 100001, 1.500000000, 0.100000000
 101001, 1.500000000, 0.150000000
 102001, 1.500000000, 0.200000000
 103001, 1.500000000, 0.250000000
 104001, 1.500000000, 0.300000000
 105001, 1.500000000, 0.350000000
 106001, 1.500000000, 0.400000000
 107001, 1.500000000, 0.450000000
 108001, 1.500000000, 0.500000000
 109001, 1.500000000, 0.550000000
 110001, 1.500000000, 0.600000000
*NODE, NSET=END
 101000, 1.512566288, 0.100039478
 102000, 1.512252131, 0.150038491
 103000, 1.511937974, 0.200037504
 104000, 1.511623816, 0.250036517
 105000, 1.511309659, 0.300035530
 106000, 1.510995502, 0.350034544
 107000, 1.510681345, 0.400033557
 108000, 1.510367188, 0.450032570
 109000, 1.510053030, 0.500031583
 110000, 1.509738873, 0.550030596
 111000, 1.509424716, 0.600029609
*NGEN,LINE=C,NSET=N1
 100001, 101000,1,200000,,,,0.0,0.0,-1.0
*NGEN,LINE=C,NSET=N2
 101001, 102000,1,200000,,,,0.0,0.0,-1.0
** REPEAT TILL NEXT LINE
*NGEN,LINE=C,NSET=N11
 110001, 111000,1,200000,,,,0.0,0.0,-1.0
*ELEMENT, TYPE=CPE4R, ELSET=ESTART
 100001, 101001, 101002, 100002, 100001
```

190

```
 101001, 102001, 102002, 101002, 101001
** REPEAT TILL NEXT LINE
 109001, 110001, 110002, 109002, 109001
*ELEMENT, TYPE=CPE4R, ELSET=EEND
 101000, 102000, 101001, 100001, 101000
 102000, 103000, 102001, 101001, 102000
** REPEAT TILL NEXT LINE
 110000, 111000, 110001, 109001, 110000
*ELGEN, ELSET=E1
 100001, 999, 1, 1, 1
*ELGEN, ELSET=E2
 101001, 999, 1, 1, 1
**REPEAT TILL NEXT LINE
*ELGEN, ELSET=E10
 109001, 999, 1, 1, 1
*ELSET, ELSET=ENIP
 E1, E2, E3, E4, E5, E6, E7, E8, E9, E10, EEND
*ELSET, ELSET=ERIM
 E10, 110000
*ELSET, ELSET=EOUTER
 E1,  101000
*SURFACE, TYPE=ELEMENT, NAME=SRIM
 ERIM, S1
*SURFACE, TYPE=ELEMENT, NAME=SOUTER
 EOUTER, S3
*MASS, ELSET=ROLM_N
 0.001
*ROTARY INERTIA, ELSET=ROLI_N
 0.0010, 0.0010, 0.0010, 0.0000, 0.0000, 0.0000
*ELEMENT, TYPE=MASS, ELSET=ROLM_N
 200000, 200000
*ELEMENT, TYPE=ROTARYI, ELSET=ROLI_N
 200001, 200000
**----------------------------------------------------------------------
**                     SECTION PROPERTIES
**----------------------------------------------------------------------
*SOLID SECTION, ELSET=ENIP, MATERIAL=ELASTIC
 1.0,
**----------------------------------------------------------------------
**                  END SECTION PROPERTIES
**----------------------------------------------------------------------
*END PART
**----------------------------------------------------------------------
**                  END PART:  ELASTIC NIP
**----------------------------------------------------------------------
```

In addition, the following lines are added between *END INSTANCE and *END ASSEMBLY commands in the input file shown in Appendix A.

```
**----------------------------------------------------------------------
**                  CONSTRAINTS: COUPLING
**----------------------------------------------------------------------
*COUPLING, CONSTRAINT NAME=JOIN_RIM, REF NODE=INIP.NIPNODE,
SURFACE=INIP.SRIM
*KINEMATIC
```

```
**-------------------------------------------------------------------
**                  END CONSTRAINTS: COUPLING
**-------------------------------------------------------------------
```

Also, the following lines are added before the END MATERIAL PROPERTIES comment.

```
*MATERIAL, NAME=ELASTIC
*DENSITY
 0.0001
*Elastic
 700.0, 0.01
```

The interaction definition between the top surface of 'layer 1' and the outer surface of the elastic nip is defined by replacing the first two command lines in the interaction module as shown below.

```
*CONTACT PAIR, CPSET=N_W, INTERACTION=FNIP_WEB
 IWEBSTACK.SLAYER1_TOP, INIP.SNIP
```

The above lines are changed to the ones shown below.

```
*CONTACT PAIR, CPSET=N_W, INTERACTION=FNIP_WEB
 IWEBSTACK.SLAYER1_TOP, INIP.SOUTER
```

The rest of the input file given in Appendix A is left unchanged.

APPENDIX C

Input file template for the winding model

```
**----------------------------------------------------------------------
**           PLANE STRAIN LINEAR WINDING MECHANICS
**                       FEM MODEL
**      INPUT FILE CREATED BY BALAJI KOVIL KANDADAI
**          CREATED 08/06/2005 - PROPERTY OF WHRC
**               ADVISOR : DR. J. K. GOOD
**
**              THICKNESS OF LAYER=0.01 IN
**            CORE=3.4 IN OD, NIP = 10 IN OD
**      ELEMENTAL DIMENSIONS = 0.0125 X 0.00333 (L X H)
**               TOTAL LENGTH = 55.34 IN
**----------------------------------------------------------------------
*HEADING
  CENTER WINDING WOT MODEL -  NIP LOAD = 25 PLI
**----------------------------------------------------------------------
**                         PARTS
**----------------------------------------------------------------------
**----------------------------------------------------------------------
**                    PART: WEB LAYER
**----------------------------------------------------------------------
*PART, NAME=WEB
*NODE, NSET=WEBREF
 100001,    0.000000000,  1.700000000
*NODE, NSET=NSL1
      1, -50.000000000,  3.400000000
   4001,   0.000000000,  3.400000000
   4213,   1.700000000,  1.700000000
   4426,   0.000000000,  0.000000000
** REPEAT FOR INTERMEDIATE NODES
*NODE, NSET=NSL4
  30001, -50.000000000,  3.410000000
  34001,   0.000000000,  3.410000000
  34213,   1.710000000,  1.700000000
  34426,   0.000000000, -0.010000000
*NGEN
      1,  4001
  10001, 14001
  20001, 24001
  30001, 34001
*NGEN, LINE=C
   4001,  4213, 1, 100001
   4213,  4426, 1, 100001
** REPEAT FOR INTERMEDIATE NODES
  34001, 34213, 1, 100001
  34213, 34426, 1, 100001
*NSET, NSET=NL1, GENERATE
      1,  4426
** REPEAT FOR INTERMEDIATE NODES
*NSET, NSET=NL4, GENERATE
  30001, 34426
*NSET, NSET=NLOADEND
      1, 10001, 20001, 30001
*NSET, NSET=NALL, GENERATE
      1,  4426
  10001, 14426
  20001, 24426
  30001, 34426
```

```
*ELEMENT, TYPE=CPE4R
      1,      1,      2, 10002, 10001
  10001, 10001, 10002, 20002, 20001
  20001, 20001, 20002, 30002, 30001
*ELGEN, ELSET=EL1
      1,  4425, 1, 1, 1
*ELGEN, ELSET=EL2
  10001,  4425, 1, 1, 1
*ELGEN, ELSET=EL3
  20001,  4425, 1, 1, 1
*ELSET, ELSET=WEB
  EL1
  EL2
  EL3
*ELSET, ELSET=ELOADEND
      1
  10001
  20001
*ELSET, ELSET=ERIGHTEND
   4425
  14425
  24425
*ELSET, ELSET=ECORECONTACT, GENERATE
      1,  4319
*ELSET, ELSET=ECORETIE, GENERATE
   4320,  4425
*ELSET, ELSET=ENIPCONTACT, GENERATE
  20001, 24425
*SURFACE, TYPE=ELEMENT, NAME=SLOADEND
  ELOADEND, S4
*SURFACE, TYPE=ELEMENT, NAME=SCORETIE
  ECORETIE, S1
*SURFACE, TYPE=ELEMENT, NAME=SCORECONTACT
  ECORECONTACT, S1
*SURFACE, TYPE=ELEMENT, NAME=SNIPCONTACT
  ENIPCONTACT, S3
*SURFACE, TYPE=ELEMENT, NAME=SSELFCONTACT
  ECORECONTACT, S1
  ELOADEND, S4
  ENIPCONTACT, S3
**----------------------------------------------------------------------
**                    SECTION PROPERTIES
**----------------------------------------------------------------------
*ORIENTATION, NAME=MATCORD
1.0, 0.0, 0.0, 0.0, 1.0, 0.0
1, 0.0
*SOLID SECTION, ELSET=WEB, ORIENTATION=MATCORD, MATERIAL=LORTHO
 1.0,
**----------------------------------------------------------------------
**                    END SECTION PROPERTIES
**----------------------------------------------------------------------
*END PART
**----------------------------------------------------------------------
**                    END PART: WEB LAYER
**----------------------------------------------------------------------
**----------------------------------------------------------------------
**                      PART:  RIGID CORE
```

```
**------------------------------------------------------------------------
*PART, NAME=CORE
*NODE, NSET=CORENODE
  120000, 0.00000000, 1.70000000
*SURFACE, TYPE=SEGMENTS, NAME=SCORE
 START,  0.00000000, 0.00000000
 CIRCL, -1.70000000, 1.70000000, 0.00000000, 1.70000000
 CIRCL,  0.00000000, 3.40000000, 0.00000000, 1.70000000
 CIRCL,  1.70000000, 1.70000000, 0.00000000, 1.70000000
 CIRCL,  0.00000000, 0.00000000, 0.00000000, 1.70000000
*RIGID BODY, ANALYTICAL SURFACE=SCORE, REFNODE=CORENODE
*MASS, ELSET=ROLM_C
 0.001
*ROTARY INERTIA, ELSET=ROLI_C
 0.0010, 0.0010, 0.0010, 0.0000, 0.0000, 0.0000
*ELEMENT, TYPE=MASS, ELSET=ROLM_C
 120000, 120000
*ELEMENT, TYPE=ROTARYI, ELSET=ROLI_C
 120001, 120000
*END PART
**------------------------------------------------------------------------
**                  END PART:  RIGID CORE
**------------------------------------------------------------------------
**------------------------------------------------------------------------
**                    PART:  RIGID NIP
**------------------------------------------------------------------------
*PART, NAME=NIP
*NODE, NSET=NIPNODE
  130000, 0.00000000, 8.41000000
*SURFACE, TYPE=SEGMENTS, NAME=SNIP
 START,  0.00000000, 3.41000000
 CIRCL, -5.00000000,  8.41000000, 0.00000000, 8.41000000
 CIRCL,  0.00000000, 13.41000000, 0.00000000, 8.41000000
 CIRCL,  5.00000000,  8.41000000, 0.00000000, 8.41000000
 CIRCL,  0.00000000,  3.41000000, 0.00000000, 8.41000000
*RIGID BODY, ANALYTICAL SURFACE=SNIP, REFNODE=NIPNODE
*MASS, ELSET=ROLM_N
 0.001
*ROTARY INERTIA, ELSET=ROLI_N
 0.0010, 0.0010, 0.0010, 0.0000, 0.0000, 0.0000
*ELEMENT, TYPE=MASS, ELSET=ROLM_N
 130000, 130000
*ELEMENT, TYPE=ROTARYI, ELSET=ROLI_N
 130001, 130000
*END PART
**------------------------------------------------------------------------
**                  END PART:  RIGID NIP
**------------------------------------------------------------------------
**------------------------------------------------------------------------
**                     END PARTS
**------------------------------------------------------------------------
**------------------------------------------------------------------------
**                      ASSEMBLY
**------------------------------------------------------------------------
*ASSEMBLY, NAME=WINDING
*INSTANCE, NAME=IWEB, PART=WEB
*END INSTANCE
```

```
*INSTANCE, NAME=ICORE, PART=CORE
*END INSTANCE
*INSTANCE, NAME=INIP, PART=NIP
*END INSTANCE
**---------------------------------------------------------------------------
**                       CONSTRAINTS: TIE
**---------------------------------------------------------------------------
*TIE, NAME=TIE_WEB_CORE, ADJUST=YES
 IWEB.SCORETIE, ICORE.SCORE
**---------------------------------------------------------------------------
**                       END CONSTRAINTS: TIE
**---------------------------------------------------------------------------
*END ASSEMBLY
**---------------------------------------------------------------------------
**                       END ASSEMBLY
**---------------------------------------------------------------------------
**---------------------------------------------------------------------------
**                   AMPLITUDE DEFINITIONS
**---------------------------------------------------------------------------
*AMPLITUDE, NAME=LOAD, DEFINITION=SMOOTH STEP
0.0, 0.0, 0.15, 1.0
*AMPLITUDE, NAME=WIND, DEFINITION=SMOOTH STEP
0.0, 0.0, 0.20, 1.0
**---------------------------------------------------------------------------
**                   END AMPLITUDE DEFINITIONS
**---------------------------------------------------------------------------
**---------------------------------------------------------------------------
**                   MATERIAL PROPERTIES
**---------------------------------------------------------------------------
*MATERIAL, NAME=LORTHO
*DENSITY
 0.0001553
*ELASTIC, TYPE=ENGINEERING CONSTANTS
 710000, 2865, 740000, 0.3, 0.36, 0.01, 2367, 1000
   1000
**---------------------------------------------------------------------------
**                   END MATERIAL PROPERTIES
**---------------------------------------------------------------------------
**---------------------------------------------------------------------------
**                   INTERACTION PROPERTIES
**---------------------------------------------------------------------------
*SURFACE INTERACTION, NAME=FCORE_WEB
*FRICTION
 0.18,
*SURFACE INTERACTION, NAME=FNIP_WEB
*FRICTION
 0.18,
*SURFACE INTERACTION, NAME=FWEB_WEB
*FRICTION
 0.16,
**---------------------------------------------------------------------------
**                   END INTERACTION PROPERTIES
**---------------------------------------------------------------------------
**---------------------------------------------------------------------------
**    STEP: DYNAMIC EXPLICIT: STEP 1 TENSION
**---------------------------------------------------------------------------
*STEP, NAME=TENSION, NLGEOM=YES
```

```
*DYNAMIC, EXPLICIT
 ,0.15
*FIXED MASS SCALING, FACTOR = 300.0, ELSET=WINDING.IWEB.WEB
*BULK VISCOSITY
 0.06, 1.2
**----------------------------------------------------------------------
**          MODIFIED BCS: LOAD & DISPLACEMENT
**----------------------------------------------------------------------
*BOUNDARY, TYPE=DISPLACEMENT
 ICORE.CORENODE, 1, 1
 ICORE.CORENODE, 2, 2
 ICORE.CORENODE, 6, 6
*BOUNDARY, TYPE=DISPLACEMENT
 INIP.NIPNODE, 1, 1
 INIP.NIPNODE, 2, 2
 INIP.NIPNODE, 6, 6
*BOUNDARY, TYPE=DISPLACEMENT
 IWEB.NLOADEND, 2, 2
 IWEB.NLOADEND, 6, 6
*DSLOAD, AMPLITUDE=LOAD
 IWEB.SLOADEND, P, -300
**----------------------------------------------------------------------
**          END MODIFIED BCS: LOAD & DISPLACEMENT
**----------------------------------------------------------------------
**----------------------------------------------------------------------
**                  INTERACTION PROPERTIES
**----------------------------------------------------------------------
*CONTACT PAIR, INTERACTION=FNIP_WEB, MECHANICAL CONSTRAINT=KINEMATIC,
CPSET=W_N
 IWEB.SNIPCONTACT, INIP.SNIP
*CONTACT PAIR, INTERACTION=FCORE_WEB, MECHANICAL CONSTRAINT=PENALTY,
CPSET=W_C
 IWEB.SCORECONTACT, ICORE.SCORE
*CONTACT PAIR, INTERACTION=FWEB_WEB, MECHANICAL CONSTRAINT=KINEMATIC,
CPSET=W_W
 IWEB.SSELFCONTACT
*CONTACT CONTROLS, CPSET=W_N, GLOBTRKINC=10000
*CONTACT CONTROLS, CPSET=W_C, GLOBTRKINC=10000
*CONTACT CONTROLS, CPSET=W_W, GLOBTRKINC=10000
**----------------------------------------------------------------------
**                  END INTERACTION PROPERTIES
**----------------------------------------------------------------------
**----------------------------------------------------------------------
**                      OUTPUT REQUESTS
**----------------------------------------------------------------------
*RESTART, WRITE, NUMBER INTERVAL=2, OVERLAY
*OUTPUT, FIELD, NUMBER INTERVAL=20, TIME MARKS=YES
*ELEMENT OUTPUT
 S, LE, EMSF, EDT, DENSITY
*NODE OUTPUT
 U ,V, A, RF
*CONTACT OUTPUT
 CSTRESS
*OUTPUT, HIST, FREQUENCY=200
*ENERGY OUTPUT
 ALLAE, ALLCD, ALLDMD, ALLFD, ALLIE, ALLKE, ALLPD, ALLSE, ALLVD, ALLWK,
ETOTAL
```

```
*INCREMENTATION OUTPUT
 DMASS, DT
**----------------------------------------------------------------------
**                   END OUTPUT REQUESTS
**----------------------------------------------------------------------
*END STEP
**----------------------------------------------------------------------
**   END STEP: DYNAMIC EXPLICIT: STEP 1 TENSION
**----------------------------------------------------------------------
**----------------------------------------------------------------------
**     STEP: DYNAMIC EXPLICIT: STEP 300 NIP
**----------------------------------------------------------------------
*STEP, NAME=NIP, NLGEOM=YES
*DYNAMIC, EXPLICIT
 ,0.15
*FIXED MASS SCALING, FACTOR = 300, ELSET=WINDING.IWEB.WEB
*BULK VISCOSITY
 0.06, 1.2
**----------------------------------------------------------------------
**            MODIFIED BCS: LOAD & DISPLACEMENT
**----------------------------------------------------------------------
*BOUNDARY, OP=NEW, TYPE=DISPLACEMENT
 ICORE.CORENODE, 1, 1
 ICORE.CORENODE, 2, 2
 ICORE.CORENODE, 6, 6
*BOUNDARY, OP=NEW, TYPE=DISPLACEMENT
 INIP.NIPNODE, 1, 1
 INIP.NIPNODE, 6, 6
*BOUNDARY, OP=NEW, TYPE=DISPLACEMENT
 IWEB.NLOADEND, 2, 2
 IWEB.NLOADEND, 6, 6
*CLOAD, AMPLITUDE=LOAD
 INIP.NIPNODE, 2, -25
**----------------------------------------------------------------------
**         END MODIFIED BCS: LOAD & DISPLACEMENT
**----------------------------------------------------------------------
** REPEAT OUTPUT REQUESTS AS IN STEP 1
*END STEP
**----------------------------------------------------------------------
**   END STEP: DYNAMIC EXPLICIT: STEP 2 NIP
**----------------------------------------------------------------------
**----------------------------------------------------------------------
**   STEP: DYNAMIC EXPLICIT: STEP 3 ANGULAR VELOCITY
**----------------------------------------------------------------------
*STEP, NAME=WINDING, NLGEOM=YES
*DYNAMIC, EXPLICIT
 ,8.0
*FIXED MASS SCALING, FACTOR = 300, ELSET=WINDING.IWEB.WEB
*BULK VISCOSITY
 0.06, 1.2
**----------------------------------------------------------------------
**     MODIFIED BCS: LOAD, DISPLACEMENT & VELOCITY
**----------------------------------------------------------------------
*BOUNDARY, OP=NEW, TYPE=DISPLACEMENT
 ICORE.CORENODE, 1, 1
 ICORE.CORENODE, 2, 2
*BOUNDARY, OP=NEW, TYPE=DISPLACEMENT
```

```
 INIP.NIPNODE, 1, 1
*BOUNDARY, OP=NEW, TYPE=DISPLACEMENT
 IWEB.NLOADEND, 2, 2
 IWEB.NLOADEND, 6, 6
*BOUNDARY, OP=NEW, AMPLITUDE=WIND, TYPE=VELOCITY
 ICORE.CORENODE, 6, 6, -3.53
** IN SURFACE WINDING CHANGE THE ABOVE LINE TO THE FOLLOWING
** INIP.NIPNODE, 6, 6, 3.0
**------------------------------------------------------------------
**  END MODIFIED BCS: LOAD, DISPLACEMENT & VELOCITY
**------------------------------------------------------------------
** REPEAT OUTPUT REQUESTS AS IN STEP 1
*END STEP
**------------------------------------------------------------------
**END STEP: DYNAMIC EXPLICIT: STEP 3 ANGULAR VELOCITY
**------------------------------------------------------------------
```

VITA

Balaji Kovil Kandadai

Candidate for the Degree of

Doctor of Philosophy

Thesis: THE DEVELOPMENT OF WOUND-ON-TENSION IN WEBS WOUND INTO
ROLLS

Major Field: Mechanical Engineering

Biographical:

Personal Data: Born in Chennai, Tamilnadu, India, On March 4, 1978, the son of
Krishnaswamy Kovil Kandadai and Pitchammal Ananthanpillai.

Education: Graduated from N.S.N Higher Secondary School, Chennai, India in
May 1995; received Bachelor of Engineering in Mechanical Engineering
from University of Madras, Chennai, India in May 1999; received Master
of Science in Mechanical Engineering from Oklahoma State University,
Stillwater, Oklahoma in August 2001. Completed the requirements for the
Doctor of Philosophy degree with a major in Mechanical Engineering at
Oklahoma State University, Stillwater, Oklahoma in December 2006.

Experience: Employed by Department of Mechanical Engineering at Oklahoma
State University, Stillwater as a graduate teaching and research assistant,
1999 to present. Employed by Kimberly-Clark Corporation., as a summer
intern, May '04-August '04 and May '05-August-'05.

Professional Memberships: American Society of Mechanical Engineers (ASME).
Technical Association of Pulp and Paper producing Industries (TAPPI).

Name: Balaji Kovil Kandadai   Date of Degree: December, 2006

Institution: Oklahoma State University   Location: Stillwater, Oklahoma

Title of Study: THE DEVELOPMENT OF WOUND-ON-TENSION IN WEBS
                WOUND INTO ROLLS

Pages in Study: 200   Candidate for the Degree of Doctor of Philosophy

Major Field: Mechanical Engineering

Scope and Method of Study: The Wound-on-Tension (WOT) is the tension in the outermost layer of a winding roll. The WOT controls the stresses in the wound roll and hence, the defects that can arise due to these stresses. Typically, rolls are wound with impinged nip rollers that exude air that might otherwise get entrained in the rolls. The nip rollers introduce tension in the web that is beyond the web line tension. Depending on the type of winding process, the WOT may have two components: one due to the nip roller and the other due to the web tension. In this thesis, the analysis of how the WOT is developed has been carried out. A first of a kind approach using the principles of contact mechanics and using a finite element tool has been attempted to model the nip mechanics. The surface tractions in the contact zone and the resulting behavior of slip and stick have been studied and their effect on the WOT is addressed.

Findings and Conclusions: The numerical model shows that three distinct regions of contact exist in the top surface of the outer layer. At the edges of the contact zone, the top surface is under slip and travels faster than the nip roller. In the middle of the contact zone, the top surface is under stick and moves at the same velocity as the nip roller. The bottom surface of the outer layer is under micro-slip. At the edges of the contact zone, the surface is under slip and moves slower compared to the top surface of the layer beneath it. These slip zones reverse direction in the middle and between these three slip zones, two stick zones exist. In the slip zone in the middle, the bottom surface moves faster than the top surface of the layer beneath it and in the stick zones, the surface velocities are equal. Due to this differential behavior in the tractions between the top and the bottom surface, a net traction exists in the top layer. This net traction when integrated through the contact width and summed with the web tension produces the WOT in center winding. In surface winding all the WOT is nip induced and hence, the WOT is equal to the nip-induced-tension (NIT). At low nip loads, the numerical results show that the WOT is approximately equal to '$\mu_{Web/Web}.N$' and at high nip loads, the WOT is much less than '$\mu_{Web/Web}.N$' where, '$\mu_{Web/Web}$' is the coefficient of friction between the web layers and 'N' is the nip load. Also, the results indicate that the NIT is independent of the type of winding process. The results of the parametric studies show that the model results agree with previous works. Also, the model results for the WOT and for the stresses in the contact zone were verified using experimental measurements.

ADVISER'S APPROVAL:_____Dr. J. K. Good_____